Tampere University

VALENTINA DONADEI

Icephobicity of Flame-Sprayed Polymer Coatings

Tampere University Dissertations 683

Tampere University Dissertations 683

VALENTINA DONADEI

Icephobicity of Flame-Sprayed Polymer Coatings

ACADEMIC DISSERTATION
To be presented, with the permission of
the Faculty of Engineering and Natural Science
of Tampere University,
for public discussion in the auditorium K1702
of the Konetalo Building, Korkeakoulunkatu 6, Tampere,
on 9 December 2022, at 12 o'clock.

ACADEMIC DISSERTATION
Tampere University, Faculty of Engineering and Natural Sciences
Finland

Responsible supervisor and Custos	Professor Emeritus Petri Vuoristo Tampere University Finland	
Supervisors	Associate Professor Essi Sarlin Tampere University Finland	Doctor Heli Koivuluoto Tampere University Finland
Pre-examiners	Professor Ali Dolatabadi University of Toronto Canada	Associate Professor Reza Jafari Aminabadi University of Québec at Chicoutimi Canada
Opponents	Professor Ali Dolatabadi University of Toronto Canada	Associate Professor Carlo Antonini University of Milano-Bicocca Italy

The originality of this thesis has been checked using the Turnitin OriginalityCheck service.

Cover design: Roihu Inc.

ISBN 978-952-03-2597-8 (print)
ISBN 978-952-03-2598-5 (pdf)
ISSN 2489-9860 (print)
ISSN 2490-0028 (pdf)
http://urn.fi/URN:ISBN:978-952-03-2598-5

HIILINEUTRAALI PAINOTUOTE
ClimateCalc CC-000025/FI
PunaMusta Printing

Carbon dioxide emissions from printing Tampere University dissertations have been compensated.

PunaMusta Oy – Yliopistopaino
Joensuu 2022

In memory of Anthony Toma

PREFACE

The work presented in this doctoral thesis was carried out in the Surface Engineering Research Group of the Faculty of Engineering and Natural Sciences at Tampere University (formerly Tampere University of Technology) during the years 2017-2022. The supervisors of the thesis were Professor Petri Vuoristo, Dr Heli Koivuluoto and Associate Professor Essi Sarlin. The research work was funded in the years 2017-2021 by the LubISS (Lubricant Impregnated Slippery Surfaces) project, which has received funding from the European Union's Horizon 2020 research and innovation programme under the Marie Skłodowska-Curie Grant Agreement No. 722497. In addition, the Faculty of Engineering and Natural Sciences of Tampere University is gratefully acknowledged for the financial support of the research work during the years 2021-2022.

I am grateful to my supervisor Prof. Petri Vuoristo for guiding me in this challenging and satisfying journey of becoming an independent researcher. His wisdom and experience have helped me to understand that research is not only made of innovative and successful outputs. Failures are also valuable because, after all, we are all human beings who make mistakes. I am grateful I learned to follow his motto, "*Don't worry, be happy!*" which has been helpful in stressful work and personal situations. I also want to thank Dr Heli Koivuluoto for her invaluable support and guidance throughout the journey, both on sunny and less sunny days. Finally, this work could not have been completed without the expertise of Associate Professor Essi Sarlin, who encouraged me when I was stuck.

I was lucky to share my time with exceptional colleagues in Konetalo room K3242. Thank you, Ville, Jarkko and Davide, for our shared moments. You will always be part of my Finnish chapter, despite our short time together. A special thanks goes to my dear colleague and friend Henna, the *"Ice Queen"*. Thank you for being such a thoughtful friend in this cold place far from home. Thank you, Enni, Kaisa, Niklas, Karoliina, Matteo, Ruqaya and Jari, for being kind and supportive. I am grateful for your help. Thank you, Davide B., for our collaboration and constant support in research and life. I have lovely memories of our time in Tampere, which I will never forget!

I want to thank all my colleagues from the LubISS project. All of you, my big research family, made this work journey unforgettable. Thank you for our unique trips, conferences, meetings, holidays and laughs during these years. I want to thank Associate Professor Doris Vollmer and the Physics at Interfaces Research group for warmly welcoming me during my research visit to the Max Planck Institute for Polymer Research in Mainz. The research visit would not have been the same without Maria, Emanuela, William, Lukas, Philipp, Abhinav, Katharina, Srinath, Diana and Azadeh. Thank you for the active working days at the office and the relaxing evenings spent along the Rhine river.

I want to thank my colleagues at the Surface Engineering Research group and the technicians at the thermal spray laboratory for their contribution to my work. Thank you, Kati M., Merja, Jarmo, Leo, Kati V. and Mari H., for your precious time supporting me with exciting science and, on most occasions, helping to solve setbacks. Some people I met at university are now friends I can count on in life. Thank you, Naiara, Maria, Guilherme, Angela, Michele and Federica. Thank you Teemu…for our fun evenings. Thank you all again for being my family in Finland.

Ringrazio i miei genitori per ogni sacrificio fatto e i loro insegnamenti, che mi hanno fatto diventare la persona che sono oggi. Grazie per esservi fidati di me quando decisi di intraprendere questo percorso lontano da voi. Ringrazio mio fratello, per l'amore e la complicità che ci lega. Ringrazio i miei familiari per essermi stati sempre vicini, dimostrandomi tutto l'amore e la stima cha hanno per me. Ringrazio gli amici di sempre, che sono stati lì ad ascoltarmi in questo percorso difficile e alle volte interminabile.

Ik bedank mijn Nederlandse familie die mijn manier van denken heeft veranderd en me heeft geleerd geduld te hebben in het leven, omdat elk doel en verlangen in het leven, indien sterk gewenst, werkelijkheid zal worden. Bedankt, Maarten, om altijd in mij te geloven. Bedankt dat je me hebt aangemoedigd om nooit op te geven. Bedankt dat je me het positieve standpunt van alle situaties hebt laten zien en dat je voor me hebt gezorgd. Bedankt dat je hier bent, nog steeds naast me, na deze vijf jaar op afstand. Dank je!

Finally, I want to thank myself for the discipline and willingness to challenge myself in different situations, countries and cultures; always exploring the world with the curious eyes of an *"eterna bambina"*.

9th September 2022, Velp, The Netherlands

Valentina Donadei

ABSTRACT

Atmospheric ice accretes and accumulates outdoors on the surfaces of several engineering applications, representing a hazard for various industrial sectors, including power transmission, renewable energy, telecommunication and transportation (ground, sea and air). For instance, ice accumulation on power lines can compromise operational performance and mechanical stability, thus ultimately causing their collapse. Moreover, ice accretion on aircraft surfaces can alter aerodynamics, endangering flight operations and, most importantly, human life. Current methods to mitigate icing problems include manual operations, mechanical vibrations, compressed air, thermal heating and chemical fluids. However, these methods, known as active anti-icing and deicing methods, are not durable and cause additional costs, energy consumption and environmental pollution. Considering these drawbacks, passive methods, which can remove ice without external energy input, have been developed as more sustainable alternatives to active methods. These passive strategies mainly consist of coatings, which reduce ice adhesion and facilitate passive ice removal.

The work presented in this thesis aims at fabricating novel polymer composite coatings with icephobic properties using flame spray technology. Flame spraying allows the fast processing of materials, fed in powder form, heated to a melt or semi-molten state using a combustive flame, and accelerated towards a substrate to form a coating. As a result, coatings can be produced on large surfaces using a single fabrication step. The first stage of the research focused on fabricating plain low-density polyethylene (LDPE) coatings. The flame spraying parameters were varied to study their effect on the properties and icephobic behaviour of coatings. Coatings were characterised by measuring thickness, roughness, surface chemical composition, wetting behaviour and thermal properties. In addition, the icephobicity of coatings was evaluated by accreting ice using an icing wind tunnel and measuring ice adhesion using a centrifugal ice adhesion test. The results showed that the selected process parameters and resulting heat input transferred to the polymer significantly affected the icephobicity of coatings. In particular, the higher the heat input, the higher the oxidation produced in the polymer and the lower was the icephobic behaviour of coatings. The second stage of the research aimed at

developing novel composite coatings, named lubricated icephobic coatings (LICs), by adding a solid lubricating additive to the LDPE material. To produce the composite coatings, the flame spray process was modified to feed the additive and simultaneously spray it with LDPE. The modified flame spray process was named flame spraying with hybrid feedstock injection. The results demonstrated that the addition of lubricating additives improved the icephobic behaviour of plain flame-sprayed LDPE coatings. The third stage of the research focused on assessing the durability of LICs under various environmental stresses, such as exposure to repeated icing/deicing cycles, different corrosive media and ultraviolet radiation on laboratory scale. The results showed that stable icephobic behaviour could be obtained for LICs over the icing/deicing cycles. Moreover, the lubricated coatings demonstrated good chemical resistance in the studied corrosive environments and limited photo-oxidation during exposure to ultraviolet radiation.

This research demonstrated the potential of lubricated icephobic coatings, which could be used as anti-icing solutions in the future. In addition, flame spraying allows the fast deposition of coatings on large surfaces, and these advantages are relevant to many industrial sectors facing icing problems. Therefore, further research is needed on the potential application of these coatings in various industrial sectors to limit the current inconveniences caused by ice formation.

SOMMARIO

Il ghiaccio atmosferico cresce e si accumula nell'ambiente esterno sulle superfici di numerose applicazioni ingegneristiche, rappresentando un pericolo per vari settori industriali, tra cui trasmissione energetica, energia rinnovabile, telecomunicazioni e trasporti (terra, mare e aria). Ad esempio, l'accumulo di ghiaccio sulle linee elettriche può comprometterne le prestazioni operative e la stabilità meccanica e, alla fine, provocarne il crollo. Inoltre, l'accumulo di ghiaccio sulle superfici degli aerei può alterarne l'aerodinamicità, mettendo in pericolo le operazioni di volo e, quel che più importa, la vita umana. Gli attuali metodi per ridurre i problemi causati dalla formazione di ghiaccio sono vari: rimozione mediante operazioni manuali, vibrazioni meccaniche, aria compressa, scioglimento tramite riscaldamento termico o con prodotti chimici specifici. Tuttavia, questi metodi, noti come metodi attivi antighiaccio, non sono durevoli e sono causa di costi aggiuntivi, di consumo di energia e di inquinamento ambientale. Considerando questi inconvenienti, i metodi passivi, che possono rimuovere il ghiaccio senza l'input di una energia esterna, sono stati sviluppati come alternative più sostenibili ai metodi attivi. Queste strategie passive consistono principalmente in rivestimenti, che riducono l'adesione del ghiaccio e ne facilitano la sua rimozione passiva.

Lo studio presentato in questa tesi ha avuto come obiettivo la realizzazione di nuovi rivestimenti compositi polimerici con proprietà ghiacciofobiche (dall'inglese, "icephobic") utilizzando il metodo della spruzzatura a fiamma. La spruzzatura a fiamma consente una rapida lavorazione dei materiali, che vengono alimentati sotto forma di polvere, riscaldati allo stato fuso o semifuso utilizzando una fiamma comburente e accelerati verso un substrato per formare un rivestimento. Di conseguenza, i rivestimenti possono essere prodotti su grandi superfici utilizzando un'unica fase di fabbricazione. La prima fase della ricerca si è focalizzata sulla fabbricazione di rivestimenti in polietilene a bassa densità (LDPE). I parametri di spruzzatura a fiamma sono stati variati per studiarne l'effetto sulle proprietà e sul comportamento ghiacciofobico dei rivestimenti. I rivestimenti sono stati caratterizzati misurando lo spessore, la rugosità, la composizione chimica superficiale, il comportamento di bagnatura e le proprietà termiche. Inoltre, il comportamento ghiacciofobico dei rivestimenti è stato valutato accrescendo il

ghiaccio in una galleria del vento e misurando la sua adesione con una prova di adesione centrifuga. I risultati hanno dimostrato che i parametri di processo selezionati e il conseguente apporto di calore trasferito al polimero hanno influenzato in modo significativo il comportamento ghiacciofobico dei rivestimenti. In particolare, in presenza di un maggiore apporto di energia termica, sono stati osservati una maggiore ossidazione nel polimero e un ridotto comportamento ghiacciofobico dei rivestimenti. La seconda fase della ricerca ha avuto come obiettivo lo sviluppo di nuovi rivestimenti compositi, denominati rivestimenti ghiacciofobici lubrificati (LICs), aggiungendo un additivo lubrificante solido al materiale LDPE. Per produrre i rivestimenti compositi, il processo di spruzzatura a fiamma è stato modificato per aggiungere l'additivo e spruzzarlo contemporaneamente con il LDPE. Il processo di spruzzatura a fiamma modificato è stato denominato spruzzatura a fiamma con iniezione ibrida di materia prima. I risultati hanno dimostrato che l'aggiunta di additivi lubrificanti ha migliorato il comportamento ghiacciofobico dei rivestimenti in LDPE spruzzati a fiamma. La terza fase della ricerca si è incentrata sullo studio della durabilità dei LICs sottoposti a vari fattori di stress ambientali, come ad esempio l'esposizione a cicli ripetuti di accrescimento e rimozione del ghiaccio, a diversi ambienti corrosivi e a radiazioni ultraviolette su scala di laboratorio. I risultati hanno mostrato che è stato possibile ottenere un comportamento ghiacciofobico stabile per i LICs durante i cicli di accrescimento e rimozione del ghiaccio. Inoltre, i rivestimenti lubrificati hanno dimostrato una buona resistenza chimica negli ambienti corrosivi esaminati e una limitata foto-ossidazione durante l'esposizione ai raggi ultravioletti.

Questa ricerca ha dimostrato il potenziale dei rivestimenti ghiacciofobici lubrificati, che potrebbero essere utilizzati come soluzioni antighiaccio in futuro. Inoltre, la spruzzatura a fiamma consente una rapida deposizione di rivestimenti su grandi superfici e questi vantaggi sono rilevanti per molti settori industriali che devono affrontare i problemi legati alla formazione del ghiaccio. Pertanto, si rendono necessarie ulteriori ricerche per una potenziale applicazione di tali rivestimenti in vari settori industriali per limitare gli attuali inconvenienti causati dalla formazione di ghiaccio.

CONTENTS

SYMBOLS AND ABBREVIATIONS

a	Length of the crack [m]
A	Contact area [m²]
a^*	Red/green coordinate [-]
a_1^*	Red/green coordinate of the pristine sample [-]
a_2^*	Red/green coordinate of the aged sample [-]
B	Experimental constant [-]
b^*	Yellow/blue coordinate [-]
b_1^*	Yellow/blue coordinate of the pristine sample [-]
b_2^*	Yellow/blue coordinate of the aged sample [-]
E^*	Apparent bulk Young's modulus of the solid [Pa]
F	Force [N]
$F_{centrif}$	Centrifugal force [N]
F_{max}	Maximum force measured at ice detachment [N]
G	Shear modulus of the solid [Pa]
h	Height of the ice block [m]
L	Length of the ice block [m]
L^*	Colour lightness [-]
L_1^*	Colour lightness of the pristine sample [-]
L_2^*	Colour lightness of the aged sample [-]
m	Mass of the ice block [kg]
r	Radius of rotation [m]
Ra	Arithmetic mean deviation of selected profile [µm]
Sa	Average height of selected area [µm]
Sdr	Developed interfacial area ratio [-]
Sq	Root-Mean-Square height of selected area [µm]
Sz	Maximum height of selected area [µm]
t	Time [s]
t_c	Thickness of the coating [m]

T_{deg}	Thermal degradation temperature [°C]
T_g	Glass transition temperature [°C]
T_m	Melting temperature [°C]
w	Width of the ice block [m]
W_a	Thermodynamic work of adhesion [J/m^2]
W_p	Practical work of adhesion [J/m^2]

α	Angular acceleration [rad/s^2]
γ_I	Surface free energy at the ice-vapour interface [mN/m]
γ_S	Surface free energy at the solid-vapour interface [mN/m]
γ_{SI}	Interfacial free energy at the solid-ice interface [mN/m]
γ_{SW}	Interfacial tension at the solid-water interface [mN/m]
γ_W	Surface tension at the water-vapour interface [mN/m]
δ	Removal distance between the ice and surface [m]
ΔE^*_{ab}	Colour difference between the pristine and aged samples [-]
ΔH	Enthalpy of fusion [J/g]
$\Delta H_{100\%}$	Enthalpy of fusion of the fully crystalline material [J/g]
θ_{adv}	Advancing contact angle [°]
θ_e	Young's contact angle or equilibrium contact angle [°]
θ_{rec}	Receding contact angle [°]
Λ	Non-dimensional constant [-]
ρ	Density of the ice block [kg/m^3]
τ_{ice}	Ice adhesion strength [Pa]
χ	Degree of crystallinity [-]
ω	Angular velocity [rad/s]

ACA	Advancing Contact Angle
APS	Air Plasma Spraying
ASTM	American Society for Testing and Materials
ATR	Attenuated Total Reflectance

BEAMS	Buckling Elastomer-like Anti-icing Metallic Surfaces
CAH	Contact Angle Hysteresis
CAT	Centrifugal Adhesion Test
CTE	Coefficient of Thermal Expansion
DAIS	Dynamic Anti-Icing Surfaces
DSC	Differential Scanning Calorimetry
EMAA	Ethylene Methacrylic Acid Copolymer
FS	Flame Spraying
FTIR	Fourier Transform Infrared
HVAF	High-Velocity Air Fuel
HVOF	High-Velocity Oxygen Fuel
I	Ice
ISO	International Organization for Standardization
IWiT	Icing Wind Tunnel
LDPE	Low-Density Polyethylene
LIC	Lubricated Icephobic Coating
LWC	Liquid Water Content
MACI	Macro-Crack Initiator
MVD	Median Volume Diameter
PDMS	Polydimethylsiloxane
PE	Polyethylene
PEEK	Polyetheretherketone
PEI	Polyether Imide
PET	Polyethylene Terephthalate
PHBV	Poly(3-hydroxybutyrate-co-3-hydroxyvalerate)
PMMA	Polymethylmethacrylate
PP	Polypropylene
PTFE	Polytetrafluoroethylene (Teflon)
PTS	Polymer Thermal Spraying
RCA	Receding Contact Angle
RoA	Roll-off Angle
S	Solid
SA	Sliding Angle
SFE	Surface Free Energy
SHS	Superhydrophobic Surface
SLIPS	Slippery Liquid-Infused Porous Surface

TGA	Thermogravimetric Analysis
UV	Ultraviolet
UVA	Ultraviolet A
VOC	Volatile Organic Compound
W	Water
WCA	Water Contact Angle
WORK	Owens-Wendt-Rabel-Kaelble
WS	Warm Spraying

ORIGINAL PUBLICATIONS

Publication I V. Donadei, H. Koivuluoto, E. Sarlin, and P. Vuoristo. Icephobic behaviour and thermal stability of flame-sprayed polyethylene coating: the effect of process parameters. *Journal of Thermal Spray Technology*, 29.1 (2020), 241-254. DOI: 10.1007/s11666-019-00947-0.

Publication II V. Donadei, H. Koivuluoto, E. Sarlin, and P. Vuoristo. Lubricated icephobic coatings prepared by flame spraying with hybrid feedstock injection. *Surface and Coatings Technology*, 403 (2020),126396. DOI: 10.1016/j.surfcoat.2020.126396.

Publication III V. Donadei, H. Koivuluoto, E. Sarlin, and P. Vuoristo. Durability of lubricated icephobic coatings under various environmental stresses. *Polymers*, 14.2 (2022), 303. DOI: 10.3390/polym14020303.

Publication IV V. Donadei, H. Koivuluoto, E. Sarlin, H. Niemelä-Anttonen, T. Varis, and P. Vuoristo. The effect of mechanical and thermal stresses on the performance of lubricated icephobic coatings during cyclic icing/deicing tests. *Progress in Organic Coatings*, 163 (2022), 106614. DOI: 10.1016/j.porgcoat.2021.106614.

AUTHOR'S CONTRIBUTION

The author is responsible for the planning, experimental work, analysis of the results and writing the original manuscripts of all publications. All the co-authors participated in planning the experiments and commenting on the manuscripts. The author deposited all the coatings analysed in this work with the support of the laboratory staff. Dr Heli Koivuluoto supervised the deposition process of coatings in Publication I. Henna Niemelä M.Sc. and Dr Tommi Varis actively contributed to discussing and explaining the experimental results in Publication IV, giving insightful comments. In addition, Henna Niemelä instructed the author how to operate the icing facilities in the Ice Laboratory and helped to perform the icing experiments with the support of the laboratory staff in all publications.

The author wrote the compendium of this work, and the doctoral dissertation was commented on and reviewed by the supervisors Prof Petri Vuoristo, Associate Prof Essi Sarlin and Dr Heli Koivuluoto. Moreover, the author presented the main results of this dissertation at the International Thermal Spray Conference (ITSC 2019) in Yokohama, Japan (conference paper), at the Wetting Dynamics Conference (2020) in Bonn, Germany (abstract-only presentation), and at the International Thermal Spray Conference (ITSC 2021) in Quebec City, Canada (conference paper).

1 INTRODUCTION

The issues related to the undesired formation and accumulation of ice on outdoor structures are well known to those who live in the coldest regions of the world. Ice adhesion and accumulation on exposed surfaces can compromise the operational performance of several applications, cause their malfunctioning or reduced efficiency in operations and even endanger human life [1–3]. Icing problems are faced in various engineering fields, such as aviation, maritime and ground transportation, power transmission and renewable energy sectors [2, 4–8]. For example, ice accretion and accumulation on the wings and surfaces of an aircraft can result in loss of lift, increase in drag, grave danger of stalling and even fatal accidents [9–12]. To address these issues, the aviation industry uses several deicing and anti-icing methods to ensure safe flight operations. These methods mainly consist of chemical deicing fluids sprayed onto the aircraft surfaces, electrical heating, vibrations and compressed air, which are used to prevent or delay ice formation and remove the ice that may accumulate in flight [13, 14]. These active methods, which require energy input to function, are also employed in other applications facing icing problems [15, 16]. The active methods currently employed effectively remove the ice accumulated on functional surfaces, and they are therefore widely used. However, their use is always related to energy waste, time-consuming operations and environmental pollution [17–19]. These drawbacks have strongly motivated the scientific community to find more sustainable and efficient deicing and anti-icing methods.

Passive anti-icing methods represent a promising alternative to current active methods. Passive methods consist of ice-repellent surfaces, such as paints, coatings and surface modifications, which reduce ice adhesion or even avoid ice formation on surfaces, thus passively mitigating icing problems [20]. Passive methods are known as icephobic coatings. Icephobic coatings represent an efficient and innovative approach to solving icing problems since the coatings act against ice with no need for an energy input or time-consuming operations.

The main objective of this thesis is to develop a novel icephobic polymer coating, which can be fabricated using flame spray technology. This method was selected owing to its advantages of a one-step process and large-scale production, which are

specifically relevant for most industrial sectors facing icing problems. In the first stage of the research, the author investigated the effect of the employed process parameters on the properties and icephobicity of flame-sprayed low-density polyethylene (LDPE) coatings. In the second stage, a polymeric lubricating additive was added to the structure of plain LDPE coatings to develop novel lubricated composite coatings. The effect of lubricant addition on the properties and icephobic behaviour of coatings was studied. In the last stage, lubricated composite coatings were exposed to various environmental stresses, such as repeated icing/deicing cycles, immersion in various corrosive media and exposure to ultraviolet radiation. Their durability was investigated under these conditions. This thesis introduces both scientific and technological novelties. For the first time, the flame spray process has been implemented to fabricate a novel design of icephobic coating, termed here lubricated icephobic coating (LIC). The traditional flame spray method has been modified to co-spray both LDPE and lubricating additive materials in order to fabricate LICs in one step. In this dissertation, this modified method is named the flame spray process with hybrid feedstock injection.

The thesis comprises eight chapters, including this introduction. Chapters 2-4 provide the reader with the theoretical background of the present study. Chapter 2 introduces the concept of icephobicity and ice adhesion together with the factors affecting the adhesion between ice and a solid surface. Chapter 3 summarises the passive anti-icing and deicing methods presented in the literature. Chapter 4 introduces the principles of thermal spray technologies, focusing on the fabrication of polymeric coatings. Moreover, the effect of the selected process parameters on the properties of polymer coatings is discussed. Chapter 5 states the detailed aims of the present study and defines the investigated research questions. Chapter 6 starts with the experimental part of the thesis and introduces the feedstock materials, the modified coating technology and the characterisation methods used in this study. Chapter 7 reports the main results of this work together with the discussion. Finally, Chapter 8 describes the scientific contributions of this thesis and suggests future work on the topic. The appendix includes the four original publications that comprise this thesis.

2 ICEPHOBICITY AND ICE ADHESION

In the last few decades, the term "icephobicity" (from ice and Greek φόβος phobos "fear") has been commonly used by the research community to describe the ability of surfaces to repel ice or retard ice formation [20–23]. Icephobicity is described based on the anti-icing mechanism of the surface [21, 24]. A surface is considered icephobic if it can repel incoming water droplets in cold environments. This condition assumes that theoretically no ice can form without water depositing and adhering to surfaces [25–28]. Moreover, the surface is icephobic if it can delay or prevent ice nucleation and formation by keeping water in the liquid phase as long as needed for the concerned application [29–32]. Finally, the surface is considered icephobic if it can reduce the adhesion strength to ice [33–36] and maintain this value below 100 kPa [21, 37]. However, the latter is not an absolute value. It depends on several factors, such as the employed ice adhesion test method, ice type and other variables, which will be described later in this chapter. This thesis describes the development of icephobic coatings that can reduce ice adhesion strength, and therefore the icephobicity of such surfaces is characterised by measuring ice adhesion.

In engineering applications, the aim of adhesion to surfaces is commonly to form a firm bond between the parts. However, when ice adheres to surfaces, the situation is reversed. All forces responsible for adhesion must be decreased to weaken the bond strength between the ice (adhesive) and the solid (adherend). Therefore, identifying the adhesion forces responsible for the ice-solid bond is important when designing coatings with enhanced icephobicity. Several studies have found that intermolecular interactions and mechanical interlocking between ice and the solid surface significantly influence icephobicity [38–41]. Moreover, this property is affected by ice formation conditions and test-related factors [42, 43]. This chapter presents an overview of the literature on ice adhesion. The first part introduces the definition of adhesion and describes the adhesion mechanisms in the case of ice. The second part discusses the main factors influencing ice adhesion.

2.1 Ice adhesion mechanisms

The term "adhesion" commonly describes the phenomenon or condition in which two bodies, the adhesive and the adherend, come into contact and stick together [44]. This term is used both for the fundamental atomic and molecular forces that hold two phases together, known as "fundamental" adhesion, and the numerical values obtained from an adhesion test, known as "practical" adhesion [44, 45]. Concerning fundamental adhesion, different intermolecular adhesion forces are present between the two parts that come into contact [46]. The principal intermolecular interactions responsible for the adhesion mechanisms are covalent forces, non-covalent forces, diffusion forces and friction forces [44, 47, 48]. Moreover, these forces are classified as strong or weak and short- or long-range forces based on the strength and scale of interaction [46]. Several theories have been developed to describe the different mechanisms leading to adhesion [45], such as 1) electrostatic, 2) adsorption, 3) mechanical, 4) diffusion theories and, more recently, 5) pressure-sensitive theories [44, 45]. Electrostatic theories state that adhesion results from electrostatic interactions between the adhesive and the adherend (surfaces in contact form an electrical double layer [45]). Adsorption theories define the adhesion phenomena in terms of intermolecular forces (mainly van der Waals forces and acid-base interactions) acting between the adhesive and the adherend molecules [45]. This phenomenon is known as physisorption when adsorption occurs due to solely physical interactions. However, if covalent bonds form between the molecules of adhesive and adherend after adsorption, the phenomenon is known as chemisorption [45]. Mechanical theories state that adhesion occurs when the adhesive penetrates the cavities of the rough and porous adherend surface, thus forming hooks that hold the phases together [45]. This adhesion phenomenon is known as mechanical keying or mechanical interlocking [44, 49]. Diffusion theories define the adhesion phenomena as occurring due to the intermixing of two materials at the molecular level. This adhesion phenomenon requires sufficient mobility of molecules at the interface to occur. Moreover, the adhesive and adherend should have similar solubility parameters and high compatibility to allow interdiffusion [49]. Pressure-sensitive theories describe the adhesion phenomena as resulting from the viscous forces of the adhesive, which adheres to the surfaces upon applied pressure [44].

Considering fundamental adhesion between ice and a solid surface, ice adhesion on a solid surface can be described at the molecular level as attractive forces (non-covalent interactions) between the molecules of water in the ice crystal and the

molecules of the solid surface [39–41, 50]. On a larger scale, the surface roughness of the solid becomes an important factor in understanding ice adhesion. The presence of surface roughness on the solid surface can increase the interfacial contact area with ice, thus leading to more non-covalent interactions and mechanical interlocking, contributing to ice adhesion [51]. Therefore, the ice adhesion force mainly depends on electrostatic forces, hydrogen bonding, van der Waals forces and mechanical interlocking [40, 41, 50]. A schematisation of these adhesion forces between ice and a solid surface is presented in Figure 1.

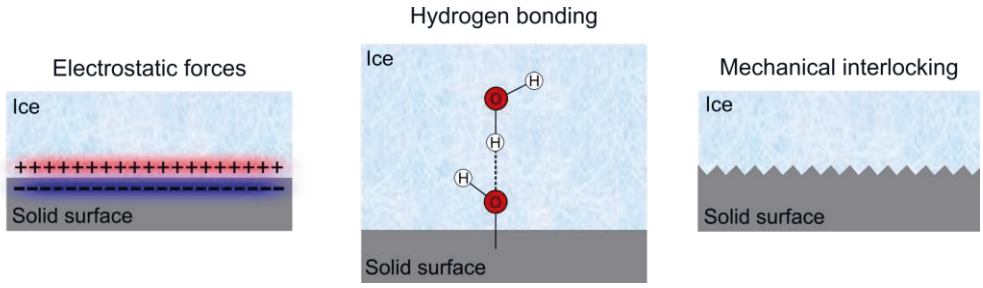

Figure 1. Schematic illustration of the adhesion forces between ice and a solid surface, such as electrostatic forces, hydrogen bonding and mechanical interlocking.

Electrostatic forces at the ice-solid interface

Electrostatic forces occur between two electrically charged entities with a transfer of electrons between the atoms and molecules at the interface [40, 46, 52]. Electrostatic forces are attractive if the two bodies have a charge of opposite signs and are based on Coulomb's law and acceptor-donor interactions [52, 53]. Petrenko and Ryzhkin [50] have claimed that electrostatic forces are always present at the ice-solid interface and play an essential role in ice adhesion. They have supposed that an electric charge is present at the ice surface due to the presence of charge defects in the ice crystal [39, 50, 53]. This charge at the ice surface may induce an opposite charge on the solid surface in contact with ice, thus forming an electrical double-layer structure at the ice-solid interface [39]. Petrenko and Ryzhkin [39, 50] have modelled that the force of this electrostatic interaction depends on the dielectric permittivity of the solid. The lower the dielectric permittivity of the solid material, the lower may be the contribution of electrostatic forces to adhesion [39, 40]. The authors have considered the example of Teflon in contact with ice as a solid material with low dielectric permittivity. This property may lower the contribution of electrostatic forces to ice adhesion, thus justifying the potential icephobic character of this material [39, 41].

Hydrogen bonding and van der Waals forces at the ice-solid interface

Hydrogen bonding is an attractive electrostatic interaction between an electronegative atom and a hydrogen atom covalently bonded to another electronegative atom (e.g. nitrogen, oxygen or fluorine) [54]. In the case of ice, a hydrogen atom can form a hydrogen bond with an electronegative atom. Petrenko and Peng [55] have shown that the strength of the hydrogen bond depends on the adherend chemical composition and its affinity with water, which determine the adherend wetting properties [55]. The higher the chemical affinity of the solid surface with water, the higher is the degree of hydrogen bonding formed at the ice-solid interface, resulting in increased values of ice adhesion strength [55, 56]. Van der Waals forces consist of attractive and repulsive interactions, always present between atoms and molecules [46]. Van der Waals forces include different contributions, such as London dispersion forces, Keesom forces and Debye forces [45, 46]. London forces are generated from the interaction between a fluctuating dipole and an induced dipole in atoms and molecules. Keesom forces arise from the attraction between permanent dipoles, and Debye forces originate from the interaction between a permanent dipole and an induced dipole [45, 46]. Van der Waal forces are also present between the atoms and molecules at the ice-solid interface [40, 41, 57]. However, a few studies have concluded that these interactions may not be dominant in determining the adhesion to ice [38, 41, 57, 58].

Mechanical interlocking at the ice-solid interface

Mechanical interlocking occurs between ice and the solid at the nano-micrometre scale, which is larger than the atomic and molecular scale of electrostatic interactions and hydrogen bonding [57]. Solid surfaces are rarely ideally smooth. A certain level of irregularities (i.e. asperities and cavities) and pores is always present. Water can penetrate the cavities and pores of surfaces before it solidifies to become ice. Once water solidifies, ice can anchor itself with the surface irregularities, thus establishing adhesion via mechanical interlocking [40, 41, 57]. Surface roughness contributes to mechanical interlocking by increasing the contact surface area between the ice and the solid surface, and its effect has been estimated by measuring the values of ice adhesion strength [56, 59, 60]. Chen et al. [56] have measured the ice adhesion strength of smooth and textured silicon surfaces. They have found that textured surfaces have ice adhesion strength 4.5 times higher than flat surfaces, on which almost no mechanical interlocking formed. Moreover, Hassan et al. [60] have found that ice adhesion strength increases from 0.142 MPa to 2.279 MPa for surface roughness Ra from 0.47 μm to 1.65 μm on aluminium surfaces. However, the degree

of mechanical interlocking on rough surfaces depends on other factors, such as the ice formation method, icing conditions and the chemical composition of the solid surface [56, 61]. These aspects will be discussed in the following Section 2.2.1.

In addition to molecular interactions and mechanical interlocking, an amorphous ice layer, known as the liquid-like layer or quasi-liquid layer, can be present between the ice crystal and the solid surface, which can influence ice adhesion [41, 53, 62]. Several studies have evidenced that the test temperature affects the physical properties of the liquid-like layer (in particular, its viscosity). The physical properties of this layer determine the fracture mode at the ice-solid interface, thus influencing the obtained ice adhesion value [35, 53, 62]. More information on the liquid-like layer and its effect on ice adhesion can be found in the following studies [38, 40, 53, 63–65].

Concerning practical adhesion, the value of ice adhesion is obtained using an ice adhesion test. Ice represents the adhesive material, which is formed through water freezing or accretion from supercooled droplets in the ice adhesion tests. In general, ice adhesion strength τ_{ice}[Pa] is calculated as the ratio between the maximum force F_{max} [N] required to detach the ice from the solid surface and the contact area A [m²] at the ice-solid interface, given by Equation 1 [22, 66–69]:

$$\tau_{ice} = \frac{F_{max}}{A} \tag{1}$$

Ice detachment can occur at the ice-solid interface (interfacial failure or adhesive failure), within the ice material and/or the solid material (cohesive failure) or partially at the interface and partially in the materials (mixed adhesive/cohesive failure). However, the discussion in this section is limited to the scenario of interfacial failure. Moreover, different loading modes, which determine the type of ice adhesion test, can be used to detach ice. For example, if a tensile load is applied to detach ice, the test is called a tensile ice adhesion test. The most common loading modes and corresponding ice adhesion tests will be described briefly in Section 2.2.3 below.

2.2 Factors influencing practical ice adhesion

Factors influencing ice adhesion have been classified into three main categories: 1) the solid surface to which ice adheres, 2) the ice formation and meteorological conditions, and 3) the test apparatus and related experimental conditions [69].

However, several factors from the same or different categories can influence each other, and it is complex to distinguish or separate the effect of single factors on ice adhesion. The following sections will describe the influence of the most well-known factors affecting ice adhesion strength, referring to the experimental results presented in the literature. The discussion will mainly focus on the properties of the solid surface directly in contact with ice. Other factors related to ice formation and test apparatus are presented more briefly, as these aspects are relevant for the state of the art but beyond the scope of this thesis.

2.2.1 Factors related to solid surfaces

Ice adhesion is influenced by the surface properties of a solid in contact with ice, such as topography and chemical composition [70]. Concerning surface topography, a rough surface allows an increased contact area with ice compared to a smooth surface. If ice perfectly adheres to the surface features, increased surface roughness results in a higher contact area between ice and surface, which can increase ice adhesion strength [51, 71–73]. However, if air pockets are stably present at the ice-solid interface, no intimate contact exists between the ice and the valleys and peaks of the solid surface [74]. In that case, the contact area is lower compared to a smooth surface. Air pockets at the interface can act as stress concentrators, promoting crack formation at the ice-solid interface during ice removal [59, 75]. The crack formation allows debonding of ice at lower stresses, which may result in reduced ice adhesion strength [61, 75–77]. Furthermore, the effect of surface roughness on ice adhesion varies depending on the chemical composition of the solid surface, which affects the wetting properties of the solid surface [78]. For example, ice adhesion can increase with increased roughness when the water repellence of the surface is low. Conversely, ice adhesion can decrease with increased roughness when the water repellence of the surface is high [69, 79, 80]. However, these correlations between roughness, water repellence and ice adhesion of surfaces are not always verified. Other factors (e.g. ice accretion parameters, ice type, which could penetrate more or less into the surface features, and scale of investigation) need to be considered when establishing relationships between these properties [56, 61, 81–83].

Considering now the case of an ideally smooth surface, the chemical composition of the solid surface has been shown to influence ice adhesion [84–86]. Ice adhesion strength is affected by a property of the solid surface known as surface free energy (SFE) [87]. SFE represents the work required to form a unit area of a solid surface.

This property can be indirectly evaluated by measuring the contact angle of different liquids on a solid surface using models suitable for the solid material [88–91]. Several models have been developed from the theories on intermolecular interactions between an ideal solid surface and a liquid (dispersion and polar interactions, such as van der Waals and hydrogen bond intermolecular forces) [87]. In laboratory-scale ice adhesion tests, the lower the SFE of smooth surfaces, the lower is the reported ice adhesion strength [85–87, 92–94]. The chemical composition of the surface can also be affected by the presence of contaminants, which have been shown to influence ice adhesion strength [95]. For example, Raraty and Tabor [95] have measured that greasy contaminants, i.e. a monolayer of stearic acid, on a steel surface reduce the ice adhesion strength by ten times compared to a clean steel surface. Therefore, ensuring the cleanliness of the solid surface before the ice adhesion test is essential to obtain reliable and reproducible results.

Considering that icing phenomena involve the interaction of surfaces with water molecules, the water contact angle and other related wetting properties have been extensively studied in correlation with ice adhesion strength [22, 68, 84, 96–98]. When a droplet of water (W) is deposited on an ideal solid surface (S), the water droplet forms an equilibrium contact angle θ_e with the solid surface, as presented schematically in Figure 2. The equilibrium contact angle, also known as Young's contact angle or static water contact angle (WCA), is defined for an ideal surface, which is a smooth, inert and chemically homogeneous solid surface [99, 100]. However, this angle is referred to as the apparent contact angle when real surfaces are considered, which are characterised by local topographical and chemical inhomogeneities. When the apparent contact angle lies between 0° and 90°, the surface is called hydrophilic (the surface attracts water). When this angle is higher than 90° or even greater than 150°, the surface is referred to as hydrophobic or superhydrophobic, respectively (the surface repels water). For ideal surfaces, the equilibrium contact angle is derived from the equilibrium of three tension or energy components acting at the point of contact between the water-vapour, solid-vapour and solid-water interfaces. These components are the surface tension at the water-vapour interface γ_W, the surface free energy at the solid-vapour interface γ_S and the interfacial tension between the solid and water γ_{SW}, as illustrated in Figure 2. The energies at the equilibrium condition are described by Young's equation [78, 99] (Equation 2) as follows:

$$\gamma_{SW} + \gamma_W \cos\theta_e = \gamma_S \tag{2}$$

According to Young's equation, a solid surface with high surface energy (i.e. high γ_S) exhibits a low contact angle, whereas a surface with low surface energy (i.e. low γ_S) exhibits a high contact angle [101].

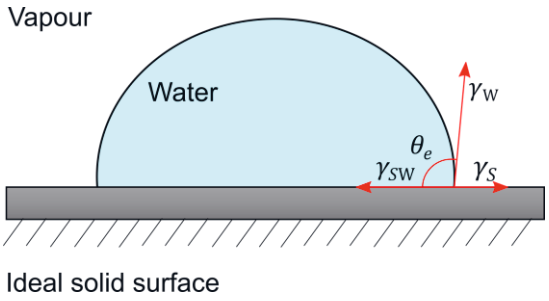

Figure 2. Water droplet on an ideal solid surface and the definition of Young's equilibrium contact angle.

When the water droplet solidifies, the solid surface (S) is now in contact with a droplet of ice (I) and a new solid-ice interface is formed (SI)[84]. The work required to separate the solid-ice interface (SI) to create two new surfaces (S and I) is known as the thermodynamic work of adhesion (W_a). The thermodynamic work of adhesion is defined here as the reversible work to separate a unit area of the solid-ice interface. Assuming that no deformations occur in the solid or the ice during separation, W_a is measured using the Dupré equation [102] (Equation 3) as follows:

$$W_a = \gamma_S + \gamma_I - \gamma_{SI} \tag{3}$$

where γ_S and γ_I represent the surface free energies of the solid and the ice, respectively, and γ_{SI} indicates the interfacial free energy between the solid and the ice. By inserting the definition of γ_S from Equation 2 in Equation 3, W_a can be expressed by Equation 4 as follows:

$$W_a = \gamma_{SW} + \gamma_W \cos\theta_e + \gamma_I - \gamma_{SI} \tag{4}$$

Assuming that the surface tension of water is similar to the surface free energy of ice [65] and that the solid-water interfacial tension is similar to the solid-ice interfacial free energy [84], W_a can be approximated using the following Equation 5 [84]:

$$W_a \approx \gamma_W(1 + \cos\theta_e) \tag{5}$$

According to Equation 5, when the contact angle of water approaches 180°, the work of adhesion to an ideal surface approaches zero. In other words, as the contact angle between the water and solid rises (i.e. as the surface becomes more and more hydrophobic), the work of adhesion decreases [36, 68, 84]. Makkonen [84] has stated that deviation in macro-scale experiments from the relationship expressed in Equation 5 may imply that some work is spent on material deformation or that the solid-ice contact is complex or incomplete [84]. Considering that Equation 1 describes ice adhesion as a measure of pressure and Equation 5 expresses the work of adhesion as a measure of energy [68], a relationship can be found between these two quantities by multiplying the ice adhesion by the surface contact area of the ice and a measure of distance, as defined in the following Equation 6:

$$W_a = \tau_{ice} A \delta \tag{6}$$

where δ is a characteristic measure of the removal distance between the ice and surface [68]. Therefore, combining Equations 5 and 6 results in Equation 7:

$$\tau_{ice} \approx \frac{\gamma_W}{A\delta}(1 + \cos\theta_e) \tag{7}$$

According to Equation 7, a dependence exists in theory between ice adhesion and the water surface tension and water contact angle on the surface in question [68].

Additionally to the static contact angle, other wetting properties have been studied to find a correlation with ice adhesion, such as advancing contact angle (θ_{adv} or ACA) and receding contact angle (θ_{rec} or RCA), roll-off angle (RoA), also known as sliding angle (SA), and contact angle hysteresis (CAH) [22, 68, 94, 103, 104]. ACA and RCA represent the maximum and minimum angles in the hysteresis range, as determined by increasing and decreasing the water droplet volume [101]. RoA corresponds to the inclination angle at which the water droplet rolls off the solid surface. CAH, which is crucial for determining the mobility of water droplets on surfaces, is described as the difference between ACA and RCA or their cosines [101]. Figure 3 presents a schematisation of the advancing contact angle, receding contact angle, roll-off angle or sliding angle.

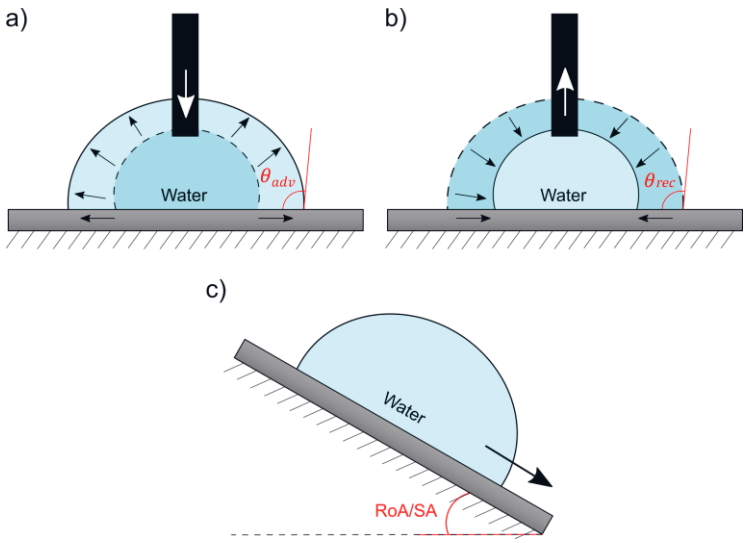

Figure 3. Schematic representation of a) advancing water contact angle (θ_{adv}), b) receding water contact angle (θ_{rec}) and c) roll-off angle (RoA) or sliding angle (SA). Adapted from [101].

When the contact angle θ_e in Equation 5 is replaced by the receding contact angle θ_{rec}, the work of adhesion is known as the practical work of adhesion W_p, thus resulting in Equation 8 [22, 94]:

$$W_p \approx \gamma_W(1 + \cos\theta_{rec}) \tag{8}$$

The same reasoning may be applied to Equation 8 as was applied to Equation 5 to derive Equation 7, with an analogous result [68]. As a result, both static and receding contact angles can correlate with ice adhesion following a cosine function. Several studies have demonstrated a correlation between ice adhesion and the receding contact angle [22, 94, 103]. However, other works discard such a relation [37] or consider this valid for surfaces with ice adhesion strengths above 160 kPa (transverse shear ice adhesion test with moulded ice) [22, 96]. Moreover, researchers have demonstrated that wetting properties vary with temperatures (due to water condensation phenomena on cold surfaces) and a better correlation can be found with ice adhesion if the wetting properties are evaluated at the icing test temperature and conditions [85, 105, 106]. Additionally, the effect of surface roughness on wetting properties needs to be considered. Young's equation is modified based on different wetting states, which are presented in Figure 4. If the water wets the actual solid surface thoroughly, the water droplet is in a Wenzel wetting state. However, if

the water droplet partially wets the surface features and stable air pockets are present beneath the droplet, the water droplet is in a Cassie-Baxter wetting state [107].

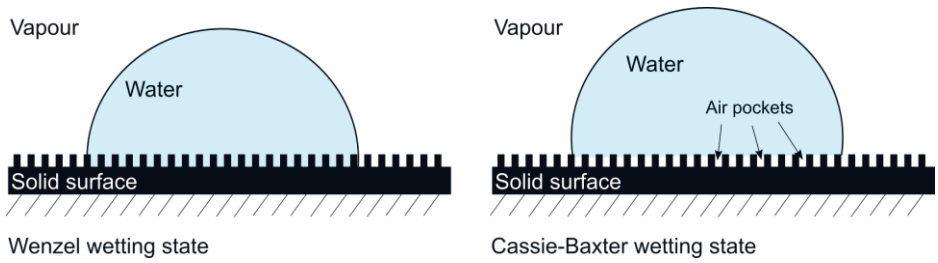

Figure 4. Schematic representation of a water droplet in a Wenzel wetting state (on the left) and a Cassie-Baxter wetting state (on the right).

In summary, the thermodynamic theory predicts a cosine relationship between ice adhesion strength, water contact angle and receding contact angle. However, the experimentally measured ice adhesion strength depends on other factors related to the solid surface in contact with ice, icing formation and test conditions. Therefore, these factors should be considered in the theoretical models and additional fundamental and experimental studies are needed to validate this relationship.

In addition to surface properties, the bulk properties of the solid material to which ice adheres have been shown to affect the ice adhesion strength [37, 84, 86]. The ice adhesion strength has been found to depend on the mechanical properties of the solid material, such as Young's modulus and shear modulus [37, 75, 86, 108, 109]. Young's modulus, also referred to as elastic modulus, is a measure of the stiffness of the solid material under tensile or compressive stresses, while the shear modulus measures the stiffness under shear stress. In theory, ice adhesion strength τ_{ice}, can be approximated using the following Equation 9 [75, 86, 110]:

$$\tau_{ice} = \sqrt{\frac{E^* \gamma_S}{\pi a \Lambda}} \tag{9}$$

where E^* represents the apparent bulk Young's modulus of the solid material, γ_S is the surface free energy of the solid surface, a is the length of the crack and Λ is a non-dimensional constant [86]. According to Equation 9, ice adhesion strength can be decreased by reducing the Young's modulus of the solid to which ice adheres. Several studies have demonstrated that when ice is removed from a solid with low Young's modulus, the formation of macroscopic crack is promoted at the ice-solid

interface, thus lowering the ice adhesion strength [86, 109, 111]. This mechanism of crack formation at the ice-solid interface depends on the property mismatch and deformation incompatibility between the ice and the solid [86]. However, He et al. [96] have examined the relationship between ice adhesion strength and elastic modulus of different solid surfaces. They have found that not all solid surfaces with low elastic modulus demonstrate low ice adhesion strength, whereas all solids with low ice adhesion always show low elastic modulus [96, 112]. Therefore, the relationship in Equation 9 has not always been verified in the direction of low elastic modulus resulting in low ice adhesion strength. Furthermore, Golovin et al. [113] have demonstrated that coatings with a high elastic modulus might be more effective at removing ice on large areas due to a mechanism known as low interfacial toughness. A direct correlation between the ice adhesion strength and the shear modulus G has been found for soft solid materials, such as elastomers [37, 114, 115]. The stress required to shear a block of ice from a soft film (such as an elastomeric coating) is given by the following Equation 10:

$$\tau_{ice} = B\sqrt{\frac{W_a G}{t_c}} \tag{10}$$

where B is an experimental constant, W_a is the work of adhesion and t_c is the thickness of the soft coating [37, 114, 115]. According to Equation 10, the lower the shear modulus (for example, obtained by reducing the cross-link density of the elastomer [37]), the lower is the obtained ice adhesion strength. Moreover, solid surfaces with alternating low and high shear moduli areas have been proposed to simultaneously promote low ice adhesion (low shear moduli areas) and ensure the durability (high shear moduli areas) of the solid material [116]. Additionally, the higher the thickness of the elastomeric coating, the lower may be the measured ice adhesion [117, 118]. However, the effect of thickness on ice adhesion has been found to be negligible for rigid polymeric solids (which are in a glassy state, i.e. below the glass transition temperature at the ice adhesion test temperature) [117].

In addition to mechanical properties, the thermal properties of the solid material have been found to influence the measured ice adhesion strength [72, 84, 119, 120]. One thermal property of the solid material is the coefficient of linear thermal expansion (CTE), which describes how the dimensions of the material change with a temperature variation. Makkonen [84] has claimed that when the solid material is in contact with ice and cooled down to the test temperature, thermal contraction always occurs for both the ice and the solid material. If the CTE of the solid differs

from the CTE of ice, stresses can be induced at the interface during cooling with possible formation of fractures at the ice-solid interface and ice cracking, thus weakening the ice adhesion strength [72, 84]. Moreover, the solid material and ice may also have a different heat capacity and coefficient of thermal conduction, resulting in different cooling rates, thus causing additional stress at the interface [84]. However, when the solid material remains elastic down to the test temperature, the effect of CTE mismatch is absent [84]. Another thermal property affecting ice adhesion strength is the glass transition temperature (T_g) of the polymeric solid [119, 120]. T_g is the temperature range where an amorphous or semicrystalline polymer changes from a rigid glassy material (below T_g) to a soft or rubbery (not melted) material (above T_g), and this property is usually measured in terms of the stiffness or modulus [121]. If the T_g of the solid polymer is lower than the temperature of the ice adhesion test, the polymer is in a rubbery state (the polymer behaves like a rubbery material) when ice is detached. Murase et al. [119, 120] have shown that polymer solids in a rubbery state at the icing test temperature demonstrate lower ice adhesion values compared to glassy polymers. However, they have reported the difficulty of distinguishing between the contribution of viscoelastic properties (related to T_g) and surface properties of polymer solids because low surface energy polymers typically have low glass transition temperatures [120]. More information on other factors related to the solid material affecting ice adhesion (e.g. molecular flexibility of the solid surface, hardness and water adhesion force) can be found in the following sources [41, 83, 96, 122].

2.2.2 Factors related to ice formation and meteorological conditions

In laboratory-scale tests, ice is generally formed from water. The properties of water, particularly its composition and the presence of contaminants, have been shown to affect ice adhesion [84, 95, 123, 124]. For example, impurities in water, such as salts, lower the ice adhesion compared to pure water [84, 124]. Moreover, air-saturated water can result in more reproducible and realistic results of ice adhesion than de-aired water, considering that water in natural environments is invariably air-saturated [123].

Ice can be formed using different methods, such as accretion from supercooled water droplets and freezing from water, thus resulting in different ice types [43]. Ice can be accreted from supercooled water droplets and is known as impact ice or in-cloud ice [43]. Impact ice is generally accreted on the solid surface using an icing

wind tunnel containing a spray nozzle system, which atomises water to microdroplets. The microdroplets can be supercooled by a cold wind and accelerated at different velocities towards the solid surface, where they accumulate, forming an ice block [125–129]. Different types of impact ice can be formed using an icing wind tunnel, such as glaze ice, rime ice and mixed types, by varying the ice accretion parameters (temperature, airspeed, liquid water content (LWC) and medium volume diameter (MVD) of the droplets in the cloud). A schematisation of glaze ice and rime ice is presented in Figure 5. However, another type of impact ice, known as precipitation ice, can also be formed without a wind tunnel by spraying water droplets from the ceiling of a cold room [43]. Additional information on impact ice, its characteristics and ice accretion parameters can be found in the following studies [2, 33, 130–132]. Another type of ice used for ice adhesion tests is known as moulded ice or bulk water ice [33]. Moulded ice is formed in a mould filled with water, frozen in a refrigerator or on a Peltier plate at freezing temperatures. The solid surface to which ice adheres can already be in contact with the water column before water solidification [22, 84, 133] or placed in contact after moulded ice is formed, following a second refrigeration cycle to allow the formation of the ice-solid bond [134].

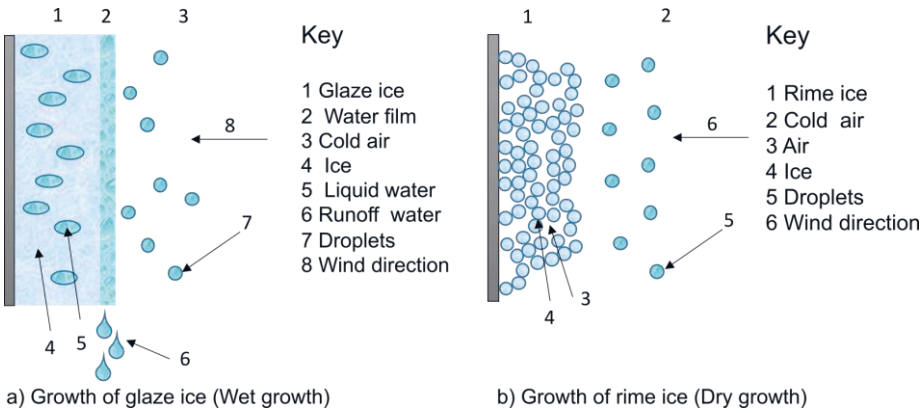

Figure 5. Schematic illustration of a) glaze ice and b) rime ice. Adapted from [131].

The ice formation method affects the properties of the ice and determines its contact with the surface, which influences the ice adhesion results [35, 132, 135–139]. For example, if impact ice is formed from a cloud with high water content, the accreted glaze ice has a significant amount of liquid water in its dense structure. As a result, this ice type can create better contact with the solid surface upon which it is accreted. Conversely, if drier icing conditions are employed, rime ice with a porous structure is accreted on the solid surface. As a result, compared to glaze ice, rime ice has a

reduced contact area with the solid surface, and this can influence ice adhesion strength [2, 135, 140]. Rønneberg et al. [43] have investigated the effect of three different ice types, such as precipitation ice, in-cloud ice and bulk water ice, on ice adhesion for the same aluminium surface under similar environmental conditions. They have found that the ice adhesion strengths measured with the centrifugal ice adhesion test vary with the ice type, and a correlation can be established between ice adhesion strength and the apparent density of ice. The ice adhesion strength has increased, changing from bulk water ice (highly dense ice structure) to in-cloud ice accreted using a wind tunnel (medium dense ice structure) up to precipitation ice (porous ice structure)[43].

Considering moulded ice, the ice adhesion strength can be affected by the freezing rate and time to form the ice block [69, 84, 141, 142]. Kasaai and Farzaneh [69] have reported that higher freezing rates and shorter freezing times can result in decreased ice adhesion values. This effect may be caused by thermally induced stresses (compressive or tensile, depending on the thermal expansion coefficient of the ice and solid material) at the ice-solid interface [84]. The faster the freezing rate, the greater may be the stresses induced at the ice-solid interface. Therefore, slower freezing rates have been recommended to decrease this effect when moulded ice is used in ice adhesion tests [84]. Moreover, several studies have shown that additional freezing time is beneficial before testing to relax the stresses at the ice-solid interface [141] and ensure stable ice adhesion behaviour of the solid surface [142].

Another factor affecting ice adhesion strength is the test temperature [35, 42, 62, 69, 84, 138]. Jellinek [62] has measured the shear ice adhesion strength of moulded ice on steel surfaces at different temperatures. The ice adhesion strength has linearly increased with decreasing temperature up to -13 °C, showing adhesive fracture. For colder temperatures, ice adhesion strength has been independent of temperature, showing the cohesive fracture of ice. Another study has found similar results for aluminium surfaces using impact ice and a centrifugal adhesion test [35]. However, the effect of temperature on ice adhesion may also depend on the mechanical and thermal properties of the solid material at the test temperature and the employed ice adhesion test [42, 84]. Therefore, this dependence has been not always verified [42, 84]. Additional information on other factors related to ice formation and meteorological conditions affecting ice adhesion (e.g. humidity and ice thickness) can be found in the following studies [69, 143–145].

2.2.3 Factors related to the test apparatus and experimental conditions

Ice adhesion tests are performed by applying a load to the ice-solid system or directly to the ice. Different loading modes can be used to detach the ice from the solid surface, and the loading mode determines the type of ice adhesion test. For example, in the tensile ice adhesion test, a tensile load is applied to detach the ice. Moreover, a transverse shear force is applied to detach the ice in the transverse shear ice adhesion test, and a centrifugal force is generated to detach the ice in the centrifugal ice adhesion test. A schematic illustration of the above-mentioned ice adhesion tests is presented in Figure 6. Each loading mode generates a specific stress distribution at the ice-solid interface. For example, in the centrifugal ice adhesion test (CAT, Figure 6c), the ice-solid system rotates with increasing angular velocity and a centrifugal force is generated to detach the ice [146, 147]. Finite element simulations have demonstrated that both in-plane shear and out-of-plane normal stresses are generated at the ice-solid interface by the centrifugal force [147]. However, ice adhesion strength is measured qualitatively taking only the shear stress component into consideration, thus neglecting the effect of minor normal stresses [66, 147].

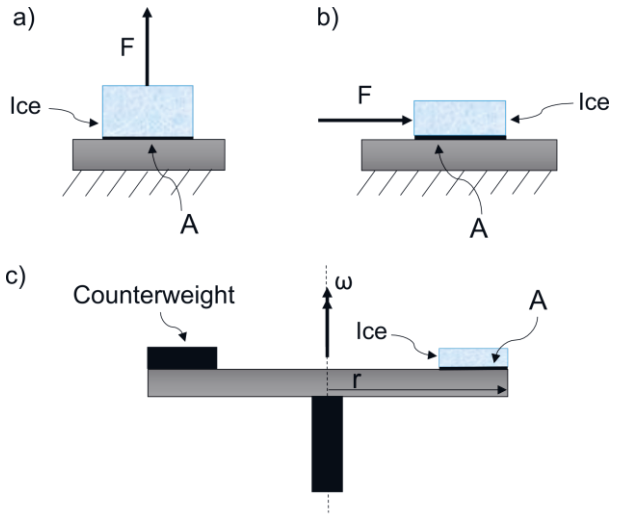

Figure 6. Schematic illustrations of some test methods used for ice adhesion strength measurements: (a) tensile test, (b) transverse shear test and (c) centrifugal test. Adapted from [33, 66].

For each ice adhesion test, the maximum load measured at ice detachment is used to calculate the ice adhesion strength for that test. For example, for the centrifugal test, the maximum centrifugal force $F_{centrif}$ can be expressed using Equation 11:

$$F_{centrif} = mr\omega^2 = wLh\rho r\omega^2 \quad (11)$$

where m [kg] is the mass, w [m] is the width, L [m] is the length, h [m] is the height and ρ [kg/m^3] is the density of ice, r [m] is the radius of rotation and ω [rad/s] is the angular velocity at the instant of ice detachment [147]. The shear ice adhesion strength τ_{ice} [Pa] is estimated as the ratio between the centrifugal force calculated at the time of ice detachment and the ice-solid interfacial area A [m^2] using Equation 12 [147]:

$$\tau_{ice} = \frac{F_{centrif}}{A} \quad (12)$$

Each ice adhesion test has a specific equation to evaluate the ice adhesion strength based on the stress distribution generated by the applied load at the ice-solid interface. More details on ice adhesion test methods can be found in the following literature reviews [33, 34, 36, 66, 69, 84, 123, 148].

The loading mode used to detach the ice from the solid surface influences the ice adhesion strength [34, 42, 149]. In a recent inter-laboratory study presented by Rønneberg et al. [42], moulded ice has been removed from the same solid surface using two different ice adhesion tests, namely the vertical shear and centrifugal tests. The results have shown the ice adhesion of bare aluminium surfaces to be equal to 509 kPa ± 185 kPa using the vertical shear test and 326 kPa ± 30 kPa using the centrifugal test at a test temperature of -10 °C [42]. The results indicate a significant variability in the ice adhesion strength values between different tests for the same surface material and ice type [42]. Moreover, that study has highlighted the challenge in comparing ice adhesion results obtained from different test apparatus. Therefore, more inter-laboratory studies and round-robin testing are necessary and recommended between different research groups in the icing research community. Such collaboration will help to further understand ice adhesion and its comparability between similar and different icing test setups in various laboratories [33, 135].

Another factor influencing ice adhesion is the loading rate, representing how fast the load is applied to the ice-solid system to detach the ice. In a technical report, Jellinek [150] has shown that an increased rate of shear load results in increased ice adhesion strength for mirror polished stainless steel surfaces using moulded ice at a test temperature of -4.5 °C. Kasaai and Farzaneh [69] have suggested that the strain

rate should be constant in the test to obtain reproducible results. In addition, the strain rate should be set carefully, as ice exhibits elastic behaviour at low strain rates and brittle behaviour at high strain rates [69]. However, the mechanical behaviour of ice also depends on the temperature at which the ice is detached. This factor should be considered when determining the effect of strain rate on ice adhesion [95, 151].

3 SURFACE DESIGN TOWARDS LOW ICE ADHESION

Icephobic coatings, such as passive anti-icing methods, are designed to lower the ice adhesion properties of the surfaces where they are applied. Different designs allow different mechanisms to reduce ice adhesion strength. This chapter presents the state of the art of icephobic surfaces presented in the literature. In addition, durability requirements for icephobic surfaces are introduced and discussed briefly.

3.1 Passive surface designs to lower ice adhesion

Lowering the ice adhesion of surfaces represents one of the strategies for designing icephobic surfaces (ice adhesion < 100 kPa [21, 37]). Menini and Farzaneh [41] have stated that "to decrease ice adhesion on a given solid, its surface has to be modified or coated with a material capable, at the molecular or crystal level, of disrupting the structure of the ice immediately adjacent to the solid". According to their study, several strategies can be used to disrupt the ice structure, such as coatings:

- composed of methyl groups ($-CH_3$) or trifluoromethyl groups ($-CF_3$) with low surface free energy properties, which are densely packed at the coating surface;
- having a heterogeneous chemical composition on the surface, containing at least two very hydrophobic components to disrupt the structure of the liquid-like layer at the ice-coating interface;
- able to maintain stable air pockets at the ice-solid interface to reduce the real ice-coating contact area and disrupt bonding by creating stress concentrations (superhydrophobic or porous coatings) [41].

In addition to these strategies, other designs of novel icephobic surfaces have been inspired by nature, such as the superhydrophobic surfaces (SHSs) of lotus leaves and the slippery liquid-infused porous surfaces (SLIPSs) of pitcher plants [20, 87]. The literature presents a vibrant spectrum of anti-icing surfaces, demonstrating great potential with low ice adhesion strengths varying from 0.2 to 10 kPa and large-scale deicing capacity [37, 70, 86, 113, 152, 153]. However, when it comes to the general

question of what defines a real icephobic surface from an engineering perspective, the typical answer is that it depends, because the environment and operating circumstances have a significant impact on ice formation and hence the design of icephobic surfaces [154].

A recent literature review has classified four surface designs, namely smooth surfaces, textured surfaces, slippery surfaces and sub-surface textured surfaces, as the main strategies to lower ice adhesion [112]. These strategies are summarised in Figure 7. The following sections will briefly describe the before-mentioned surface designs, focusing on smooth surfaces, which are more closely related to the coating design fabricated in this work.

Figure 7. Strategies towards designing icephobic surfaces by lowering ice adhesion strength can be roughly divided into four types via surface properties: smooth surfaces, textured surfaces (i.e., hierarchical hydrophobic surfaces or SHSs), slippery surfaces, and sub-surface textured surfaces [112].

3.1.1 Smooth surfaces

Smooth icephobic surfaces are generally made of materials with low surface free energy [79, 87, 155]. Fabrication of smooth surfaces is often facile and cost-effective and can be performed using machining, depositing, moulding, spraying, thermal

spraying, spin-coating, dip-coating and other methods [112]. In addition, smooth surfaces are considered potential icephobic surfaces since their production methods generally cover large areas, which is beneficial for various engineering applications facing icing problems [87]. Concerning the processing of polymeric materials, some processes require several fabrication steps when thermosets and elastomeric polymer coatings are processed, such as post-curing or thermal treatment after spraying, spin-coating and dip coatings. Other processes, such as moulding and thermal spraying, can be completed in one step when thermoplastic polymers are processed. One-step fabrication reduces the processing time of coatings, increasing their appeal in several industrial applications.

To achieve low ice adhesion behaviour, researchers have designed smooth surfaces with tuned mechanical properties, surface chemistry and coating thickness [37, 86, 108, 109, 116, 117, 156]. Table 1 summarises the main strategies reported in the literature with a description of the mechanism responsible for lowering ice adhesion. Moreover, novel smooth surface designs can be derived by combining the strategies listed in Table 1. For instance, He et al. [112] have suggested in their review on the design of icephobic surfaces that several materials, such as polyelectrolytes, ions, salts and lubricants, can be incorporated into smooth coatings. Incorporating different materials into the coating structure can enhance interfacial slippage and create chemical heterogeneity at the ice-solid interface [112]. Both interfacial slippage and chemical heterogeneity at the surface can contribute to further lowering the ice adhesion strength due to the synergic effects of different strategies. Therefore, there is a potential for further development and design of smooth surfaces for applications facing icing problems.

Table 1. Most common strategies to lower ice adhesion of smooth surfaces.

Strategy	Description
Varying the mechanical properties of coatings	The elastic modulus of elastomeric coatings is decreased by reducing their cross-link density. The cross-link density is reduced by tuning the weight ratio of the prepolymer to the curing agent. The lower the cross-link density, the lower the obtained elastic modulus. This results in lowered ice adhesion strength. For polydimethylsiloxane (PDMS) coatings, the weight ratio has been varied from 10:1 to 10:10, leading to a reduction of the ice adhesion strength of about 92.3% from 36.5 kPa to 2.8 kPa [156].
	The shear modulus of elastomeric coatings/gels is decreased by reducing their cross-link density. This reduction results in lowered ice adhesion strength [37, 108, 109].
Varying the coating thickness	An increase in coating thickness causes a decrease in ice adhesion [109, 117].
Varying the surface free energy of coating surfaces	The surface free energy of elastomeric coatings is decreased via a silanisation reaction of perfluorodecyltrichlorosilane. After surface silanisation, ice adhesion strength decreases by approximately 25% [86].
Inducing interfacial slippage (no friction condition) at the ice-coating interface	If the polymeric chains are sufficiently mobile within the elastomer, slippage can occur at the ice-solid interface. Interfacial slippage is achieved by adding a miscible oil (liquid lubricant) to the elastomer network with no formation of an oil liquid layer on top of the coating surface [37, 108].
Inducing crack propagation at the ice-coating interface	The coating is made alternating high shear modulus areas (phase 1) and low shear modulus (phase 2) areas, forming a material known as a stress-localised viscoelastic material. When shear load is applied to the ice-coating system, ice detaches at first from the low shear modulus areas. A cavity (i.e. crack) forms locally between phase 2 and the ice, and a crack propagates at the interface. As a result, stress-localised coatings show reduced ice adhesion compared to coatings made of solely high shear modulus materials [116].
Creating heterogeneity of intermolecular forces and water molecule orientation at the ice-coating interface (molecular level effect)	Heterogeneity of intermolecular forces (hydrogen bond, electrostatic forces) is induced at the ice-coating interface by the presence of chemical heterogeneities. For example, composite coatings were produced by mixing polymeric materials, such as polysiloxane and fluorocarbon polymers. This chemical heterogeneity resulted in reduced ice adhesion compared to plain polysiloxane and fluorocarbon-based homogeneous coatings [41, 157]. In addition, different molecular groups at the coating surface form various disparities in terms of energy bonding and water molecule orientation, thus weakening the ice–material interface and reducing ice adhesion [41, 119, 158].

3.1.2 Other surface designs

Apart from smooth surfaces, other surface designs have been developed to tackle icing problems, such as textured surfaces, slippery surfaces and sub-surface textured surfaces [112]. Textured surface designs have been inspired by the micro-nano structure of lotus leaves, which repel incoming water droplets thanks to the presence

of a hierarchical structure covered by a hydrophobic natural wax [159]. Textured surfaces can be hydrophobic or superhydrophobic surfaces (SHSs), depending on their hierarchical structure and chemical properties [86]. SHSs have been fabricated to lower ice adhesion using different methods on a laboratory scale [26, 152, 160–163], and these methods generally involve several processing steps. For example, SHS surfaces are produced by mixing a polymer matrix with micro- and nano-particles of different dimensions using spraying, spin coating or brushing to deposit the coating and a post-curing process [26, 152, 160, 161]. Then, the particles are added to create a surface texture that induces high water repellence. Moreover, superhydrophobicity can be achieved using a chemical vapour deposition method by growing coatings based on silicone nanofilaments [77, 164]. Furthermore, textured surfaces can be manufactured using the chemical etching of metal substrates prior to surface modification with low free energy materials [162]. More expensive and sophisticated methods, such as laser texturing [136, 165], air plasma treatment [166], lithography [70] and radio frequency sputtering [163], can be used to obtain the desired surface texture. Finally, different processes and surface treatments can be potentially combined to fabricate superhydrophobic coatings.

Some studies have shown lower ice adhesion for SHSs due to a reduced contact area between the ice and the surface [17, 97, 160]. Ideally, this condition is verified if air pockets remain trapped between the ice and the hierarchical structure of the solid surface (Cassie ice regime [74]). However, other studies have reported that SHSs are not always icephobic [56, 75, 87, 167]. SHSs may lose their water repellence in a highly humid environment and sub-zero conditions due to water condensation, which thoroughly wet the hierarchical structure [162, 168]. This case scenario can also be influenced by the icing conditions, type of accreted ice and hierarchical structure of the SHS [61]. Moreover, the water penetrating the surface structure can solidify and form mechanical interlocking with the surface, thus increasing ice adhesion (increased contact area between the ice and the surface compared to a smooth surface) [56, 85]. Finally, the hierarchical structure can be mechanically damaged during icing/deicing cycles, thus causing a loss in superhydrophobic properties [167].

Slippery liquid-infused porous surfaces (SLIPSs) represent another surface design used to reduce ice adhesion strength. Inspired by Nepenthes pitcher plants [147], SLIPSs consist of a nano-microtextured solid, which locks a lubricating fluid in place [169]. The hierarchical nano-microstructure of the solid is fabricated using methods similar to those previously reported for textured surfaces. After the texture is fabricated, it is infused with the lubricating fluid. Several slippery surfaces have been

fabricated for anti-icing applications using various lubricating fluids, such as organic lubricating fluids (e.g. silicone, liquid paraffin, oils, fluorinated fluids) [76, 77, 153, 170–173] and aqueous lubricating fluids [94, 174–176]. The lubricant forms a smooth, slippery surface, which can reduce ice adhesion [20, 153]. Once the ice is formed on a slippery surface, the lubricant layer protects the surface structure by preventing mechanical interlocking between the ice and the surface [177, 178]. However, if the liquid lubricant is depleted from the surface, the icephobicity of slippery surfaces can decrease [76, 179, 180]. Moreover, lubricant depletion can cause environmental pollution [87]. Many solutions for improving the stability of liquid lubricants on slippery surfaces have been proposed [112]. The most common strategies are entrapping the liquid lubricant within a network of cross-linked elastomers [37, 181] or using solid lubricants instead of liquid ones [182, 183] to increase lubricant stability and hence achieve long-term icephobicity. Although this appears to be a promising anti-icing method, currently, there are no commercially available slippery surfaces for industrial applications [87].

Sub-surface textured surfaces have been recently proposed as a novel strategy to reduce ice adhesion. They consist of coatings with a hydrophobic surface and a sub-surface textured structure [112]. This surface design is based on the macro-crack initiator (MACI) concept to reduce ice adhesion [86]. Macro-cracks are initiated at the ice-coating interface due to stiffness inhomogeneity (sub-surface texture in the coating matrix) generated in the structure of coatings [86]. For example, different sub-structures of internal holes have been introduced into the coating structure to create this stiffness inhomogeneity [86]. The fabrication method of these surfaces consists of several steps (spin-coating, curing, bonding) and comprises the use of moulds to create the sub-surface texture. Although this class of surfaces has been demonstrated to weaken the ice–solid interface dramatically [86], further theoretical and experimental investigation is required on their stability and durability [112].

3.2 Alternative surface designs to lower ice adhesion

Recent studies on the design of icephobic surfaces have considered incorporating active anti-icing and deicing methods (e.g. electro-thermal, photo-thermal and magnetic responsive stimuli) in passive icephobic surfaces to improve their deicing reliability and efficiency [112]. Several novel surface designs have been fabricated with a combination of active and passive methods, including magnetic-responsive icephobic surfaces [184–186], photo-thermal promoted icephobic surfaces [177, 187,

188] and electro-thermal icephobic surfaces [189–191]. For example, icephobic surfaces combined with photo-thermal traps can actively melt the interfacial ice using the energy from the sun, thus being more effective in lowering ice adhesion [192]. These emerging anti-icing surfaces have been referred to as dynamic anti-icing surfaces (DAISs), and more information can be found in a recent literature review [193]. Although DAISs have demonstrated increased durability, wider temperature tolerance and greater environmental adaptability [173], further theoretical and experimental investigations are needed to establish their feasibility in real applications [193].

Another recent work has presented a novel approach to designing durable and scalable icephobic surfaces, named buckling elastomer-like anti-icing metallic surfaces or BEAMS [194]. This anti-icing strategy is based on the principle that the deflection of a thin metallic plate during buckling can induce crack-opening displacements, thus facilitating ice de-bonding. Additional information can be found in the following study [194].

3.3 Durability requirements of icephobic surfaces

Durability, defined as the resistance of coatings to external agents affecting the coating performance, is one of the most critical characteristics of icephobic coatings required for practical and long-term use [195]. Although several surface designs have been developed and used to demonstrate their ability to reduce ice adhesion strength, further research is still required to assess their long-term performance. Ideal solutions to icing problems would be passive coatings, which maintain their characteristics and anti-icing properties for a decade or longer and can be easily repaired after damage [196, 197]. However, the design and fabrication of passive anti-icing surfaces are still challenging for long-term use [112]. In addition, each surface design has some advantages and limitations in specific applications that face icing problems. For example, SHSs have shown lower mechanical stability and decreased icephobic performance in comparison with smooth surfaces under repeated icing/deicing cycles due to the fragility of their hierarchical structure [136, 162, 197]. Therefore, the use of certain superhydrophobic surfaces may be not suitable in applications where the long-term mechanical stability of the coating is a requirement. Moreover, durability tests should be planned considering the possible application for the icephobic coating and related environmental stresses. Field tests and exposure to realistic environmental conditions can benefit the development of

icephobic coatings to better understand their behaviour in use for the specific application.

In recent years, passive icephobic surfaces have been developed, focusing on the durability assessment of such materials to improve understanding of their degradation mechanism and, consequently, their potential use in real applications [195, 198]. Several studies have performed cyclic icing/deicing cycles on coatings to test the durability of their icephobic properties [37, 166, 173, 195]. The variations in ice adhesion strength have been monitored over the cycles, indicating changes in the icephobic properties of the coatings. However, no common standard for assessing the durability of icephobic properties has been established yet (icing/deicing processes, number of icing/deicing cycles, water grade, freezing procedure, ice type and other test variables are currently undefined) [197]. Different methods are used for the icing and deicing procedures of icephobic coatings. For example, icing involves pouring water into a mould positioned on the surface and freezing it at specified temperatures in a freezer [22, 37]. In another method, ice is formed from supercooled water microdroplets in an icing wind tunnel under controlled icing conditions [136, 146, 147, 199]. Deicing can be accomplished by heating [153, 165, 200], substrate deformation [73] or, more aggressively, mechanical loading of the ice [22, 166, 201]. Moreover, some researchers have carried out a few icing/deicing cycles [77, 166, 173, 202], while others have used 100 cycles [37, 165, 203] or even 170 cycles [200]. It is evident that each research group has established specific icing/deicing test procedures, and discussions on the icing performance and durability of coatings should be approached with caution when comparing results from different studies [197].

In addition to ice, other external factors, classified as environmental, chemical and mechanical factors, can compromise the durability of icephobic coatings [195]. All these factors can alter the original properties of coatings, thus consequently influencing their icephobic behaviour [195, 198]. For example, oxidation induced by ultraviolet irradiation (UV) and heat degradation represent two environmental factors that can compromise coating durability. Moreover, chemical factors, such as corrosion and hydrolysis, and mechanical stimuli, such as erosion, abrasion and impact, can compromise the durability of icephobic coatings. For instance, typical tests to assess durability against mechanical stimuli have consisted of dry particle erosion [204], wet particle erosion [205], rain erosion [200] and wear tests using an abrasive medium [183, 206]. However, no common standard for assessing the durability of icephobic coatings under environmental stresses has been established yet [197]. Therefore, some studies have proposed testing the durability of icephobic

coatings by following the standard methods employed to assess the durability of coatings in general [195, 197, 207].

The durability of the icephobic coating designed in this work was investigated focusing on the effect of chemical and environmental factors. Coatings were immersed under different corrosive media and exposed to ultraviolet (UV) radiation. The reasons for selecting these conditions are the following. Icephobic coatings may encounter several environments in outdoor applications, such as marine environments, acid rain, solutions containing cleaning agents and detergents, and others [197]. Previous studies have investigated the durability of icephobic coatings immersed in acidic, saline and basic solutions [195, 202, 206, 208]. In those studies, variations in surface morphology, chemical composition and wetting properties of coatings have been found after immersion. Variations in surface properties generally influence the icephobicity of coatings [83, 84, 209, 210]. Moreover, icephobic coatings are used outdoors and exposed to UV radiation from sunlight. UV irradiation causes materials, especially polymers, to degrade, thus decreasing their performance and shortening their lifetime [211]. A recent study has demonstrated that UV ageing of polyurethane-based coatings has a negative influence on the icephobic behaviour of surfaces [198]. Therefore, it is essential to understand the deterioration of coatings under these conditions so as to further improve their durability.

4 THERMAL SPRAYING OF POLYMERS

Thermal spray technology includes a wide selection of coating deposition techniques. For these techniques, an energy source is used to melt the feedstock material and propel it towards a substrate to form a coating. Different materials can be deposited, such as metals, ceramics, polymers and composites. In this research, the flame spray technique was selected to fabricate icephobic polymer coatings as it enables the deposition of thermoplastic polymers in one step on large areas. In this chapter, different thermal spraying methods are described briefly and the effect of the process parameters on coating properties is discussed, focusing on the processing of polymeric materials.

4.1 Processing of polymers via thermal spray technologies

Thermal spraying of polymers can be traced back to the 1940s when the chemical company E.I. du Pont designed and produced the first thermally sprayable polyethylene (PE) powder [212]. The conventional flame spray (FS) process has represented the first thermal spray technique employed to deposit polymer coatings. Moreover, this technique has been frequently used for industrial applications of polymer coatings due to its simplicity and the low economic investment required [213]. The FS process mainly consists of the following fabrication steps, which are illustrated in Figure 8:

1. The polymeric feedstock material, generally in the form of powder, is fed to the spray gun.

2. In the spray gun, the chemical reaction between a fuel (generally acetylene or propane) and an oxidizing gas (generally oxygen or air) produces a combustion flame (heat source) at the nozzle of the spray gun. The combustion flame represents the heat source of the flame spray process. The feedstock material is then transported by carrier gases in the gun and injected into the combustion flame.

3. The feedstock material is accelerated towards the substrate and impacts the substrate in the form of molten or partially molten particles.

4. The particles spread, coalesce with each other and solidify to form a coating [213, 214].

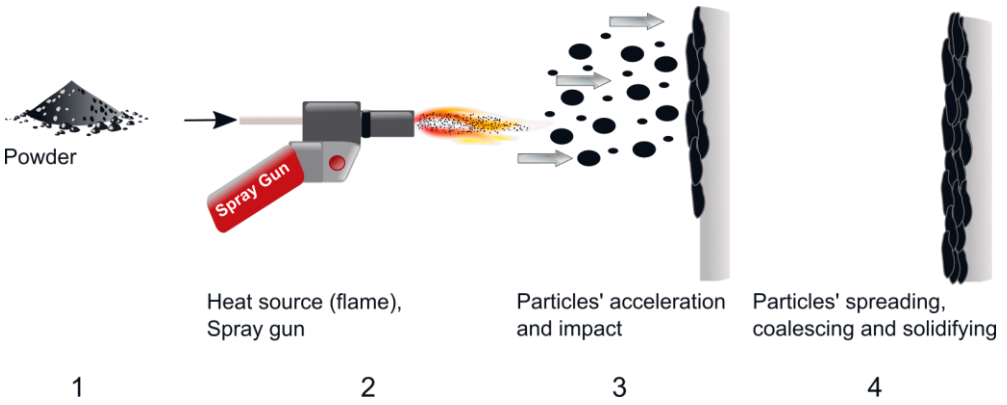

Figure 8. Schematic illustration of the fabrication steps of the flame spray process.

Traditional flame spray guns have been initially designed to deposit metals [212]. However, earlier attempts to spray polymer powders with that equipment have been unsuccessful due to the unavoidable thermal degradation caused to the polymeric material [212]. Therefore, technical adjustments have been applied to the spray gun setups to spray polymers successfully [212]. For example, specific nozzles have been designed to prevent or limit the thermal degradation of polymer powders [215]. In these nozzles, a ring of shroud gas (generally air or nitrogen) is generated between the outer flame ring and the inner stream of polymer powder during spraying [216, 217]. The ring of shroud gas acts as thermal insulation, keeping the polymer powder separated from the hot flame to some extent [215, 217]. A schematic illustration of the flame spray gun used to spray polymer is presented in Figure 9. Several flame spray combustion guns are commercially available (e.g. Metco 6P-II ThermoSpray® Gun model (Oerlikon Metco, Switzerland) and TeroDyn® System 2000, TeroDyn® System 3000, TeroDyn 3500 and Castodyn 8000 models (Castolin Eutectic, Switzerland)) [212]. These flame spray guns have been used to spray different polymer powders using gas combinations of oxygen-propane, air-propane or oxygen-acetylene [212, 218–228].

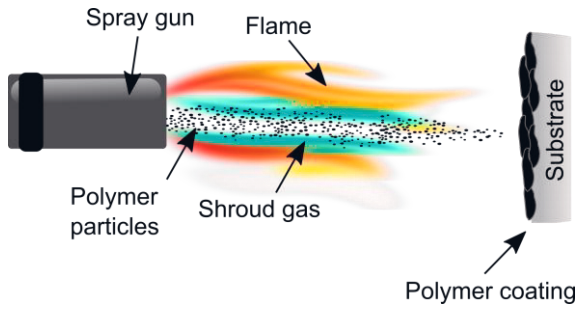

Figure 9. Principle of the flame spray gun used for polymer spraying.

In addition to the flame spray method, the literature reports the use of other thermal spray techniques to produce polymer coatings and polymer composite coatings [213]. Commonly employed thermal spray techniques are air plasma spraying (APS) [229–231], high-velocity oxygen fuel (HVOF) [232–234] and high-velocity air fuel (HVAF) processes [213]. Although the fabrication steps presented above for the FS method are common to all thermal spray techniques, the latter differ in the used heat source, process temperature, particle velocity, gun geometry and other technical details [214, 235]. Figure 10 presents the process temperature and particle velocity for various thermal spray processes.

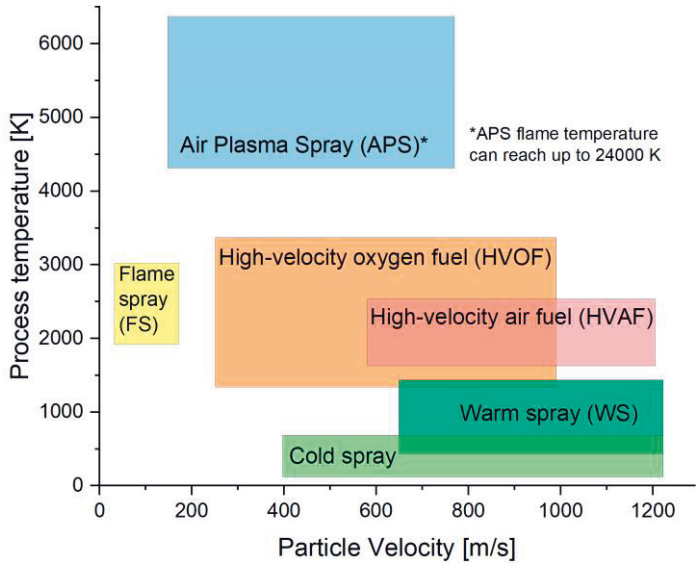

Figure 10. Process temperature and particle velocity for different thermal spray processes. Modified from [214, 217, 236].

Considering the elevated process temperatures reached during various thermal spray processes (Figure 10), the processing of polymeric materials using these methods generally involves a significant risk of thermal degradation [213]. Therefore, alternative thermal spray processes have been developed to overcome the limitations of such high-temperature processes [237–240]. One example is the warm spray (WS) process, also known as two-stage HVOF since this process is based on the high-velocity impact of powder particles [238–240]. The warm spray gun is modified from a commercial HVOF spraying gun, introducing a mixing chamber immediately after the combustion section. The mixing chamber reduces the gas temperature in the nozzle, thus decreasing the heat transferred to the feedstock material [238]. A study has reported that polymer coatings (i.e. ultrahigh-molecular-weight polyethylene) fabricated using the WS process demonstrate reduced thermal degradation compared to same coatings produced by the FS method [239, 241]. Another thermal spray method designed to spray polymeric powders is polymer thermal spraying (PTS) [237]. In this method, the heat source consists of an electro-resistive heater that warms up a compressed process gas, not involved in the combustion reactions. The electric heating element can be set to any temperature depending on the thermal properties of the polymer. The process parameters can be adjusted to not exceed the degradation temperature of the polymer during the whole spray process [237]. Moreover, because no flame is produced at the nozzle of the spray gun, the process is safer, and the deposition can be easily monitored by direct visual inspection. Another study has demonstrated the potential of PTS to fabricate polymer coatings with different coating structures (from porous to dense structures) using various polymeric materials [237]. Unfortunately, the above-mentioned thermal spray processes with reduced process temperature were not available to the author when conducting this study. However, previous studies have shown the potential of the FS method to produce polymer coatings with icephobic properties [222]. Therefore, the flame spray method was utilised in this research.

A more recent process employed to fabricate polymer coatings is the cold spray process [242–246]. In the cold spray process, particles are accelerated to velocities between 500 and 1500 m/s using a stream of pre-heated inert gas with a converging-diverging nozzle [245]. The particles are not melted in flight and maintain their solid state throughout the entire deposition process. As a result, the risk of material overheating is minimised during cold spraying [246], which is especially beneficial for polymeric materials. Additional information on thermal spraying techniques can be found in the following sources [217, 235, 247].

The considerable advancement in thermal spraying of thermoplastic polymers has been due to the advantages of thermal spraying in comparison with traditional fabrication methods of polymer coatings (e.g. painting, dipping and hot melt coating processes) [212, 213]. Firstly, thermal spraying is a one-step process, and no adhesive base layer prior to coating deposition or post-treatment is generally required. Moreover, the process does not involve the use of solvents or the evaporation of volatile organic compounds (VOCs) since polymeric feedstocks are provided in the form of dry powder, and no post-curing is necessary after coating deposition. Another benefit of the technique consists in the possibility of processing polymers with high melt viscosity and composites with high reinforcement content [213]. Other methods of processing such materials require temperatures far higher than the polymer melting temperature (e.g. during the application of hot melt from a roll) or the use of solvents to lower the polymer viscosity. Furthermore, thermal spraying has movable and flexible equipment. The coating preparation can be carried out on-site and on large surfaces under almost any environmental conditions (e.g. high humidity level and low temperature, unsuitable for painting processing) [212, 213]. Last but not least, coatings with superior mechanical properties can be produced with the desired thickness and locally repaired [212, 213]. However, there are also some limitations compared to traditional coating techniques. For example, the coating quality depends on the operator's skills if the deposition is performed manually. Moreover, the surface finish of thermally sprayed polymer coatings can be coarser than that obtained with other coating processes, such as painting, dipping and fluidised deposition. Finally, some difficulties may be encountered in spraying around sharp corners and coating hole surfaces and narrow sections due to the technical limitations and dimensions of the spray gun [212, 213, 247].

4.2 Influence of process parameters on polymer coating properties

Flame spraying involves various process parameters, principally related to the combustion flame, powder injection system, feedstock material and spray process [235]. Figure 11 summarises the principal process parameters that can be varied in the flame spray process.

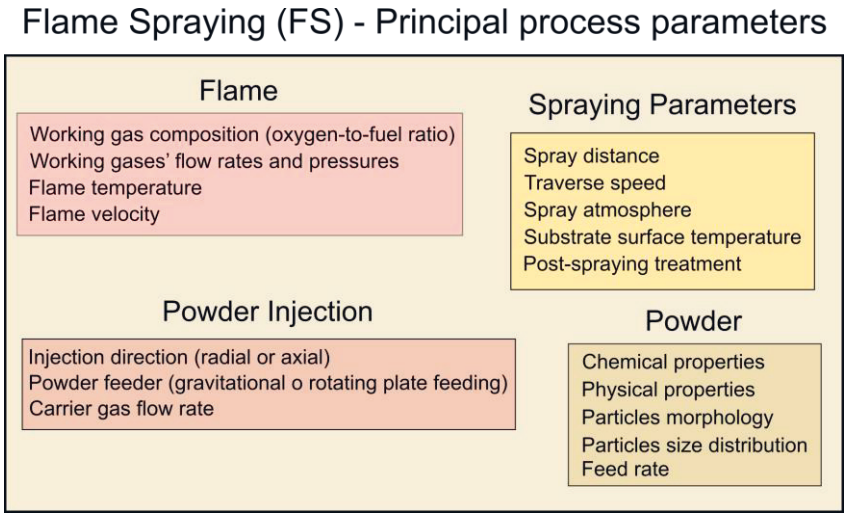

Figure 11. Summary of principal process parameters of the flame spray (FS) process using a feedstock material in the form of powder. This classification is presented in [235].

Several process parameters can influence the same or different process variables and, consequently, various properties of the obtained coating. The process variables relevant to this work are as follows:

1. the thermal energy in the form of heat transferred to the polymer during the process;
2. the spraying time employed to deposit the polymer coating;
3. the environment during spraying, resulting from powder carrier gases, combustion flame and environmental conditions of the spray booth.

Figure 12 presents some correlations between the principal process parameters, process variables and resulting properties of polymer coatings. The influence of the process parameters on the process variables and obtained coating properties, which are relevant to this work, will be discussed in the following paragraph.

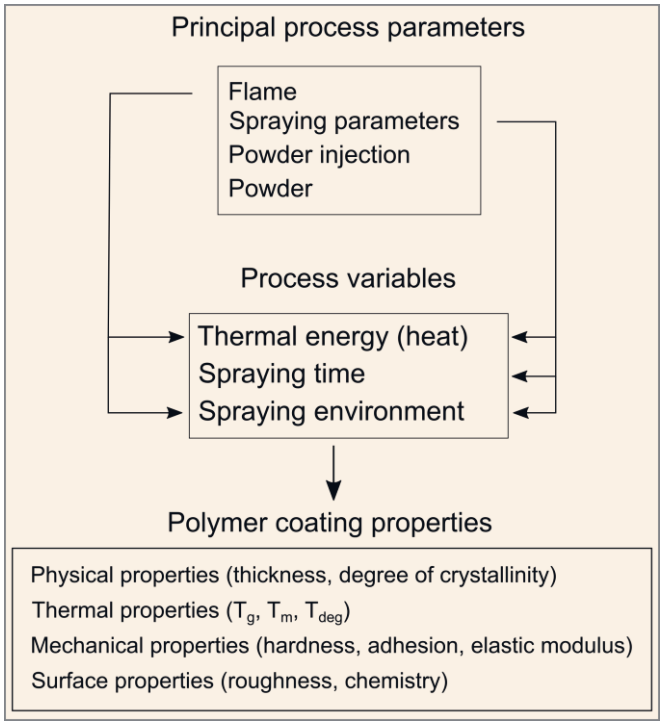

Figure 12. Principal process parameters influencing process variables and polymer coating properties.

Processing thermoplastic polymers by means of flame spraying mainly involves the transfer of thermal energy from the combustion flame to the polymeric material. The heat transfer occurs at different stages of the spray process. Before coating deposition, the substrate is generally pre-heated using the flame to vaporise any trapped water vapour and organic residue. Moreover, pre-heating allows the molten particles to flow into the topography of the grit-blasted substrate to ensure good adhesion of the coating via mechanical interlocking [212]. During deposition, heat is first transferred to the polymer particles in flight. Once these are deposited onto the substrate, the formed polymer layers are continuously heated during the deposition of subsequent coating layers. The amount of heat transferred from the combustion flame to the polymer mainly depends on:

1. The flame temperature, which is determined by the ratio between the fuel and combustion gases, the type of employed gases to form the flame [248], and the presence of additional process gases, such as powder carrier gases and gases used to reduce the flame temperature.

2. The time the particles are exposed to the flame during flight. The longer the time of exposure in flight, the greater is the heat transferred to the particles. This time can be reduced by using shorter nozzles [249] and higher particle velocities [213].
3. The spraying time, mainly defined by the chosen traverse speed of the gun and the number of passes (determined by the distance between the passes) defined to deposit a specific coating area. The slower the traverse speed, the greater is the heat transferred to the deposited layers of coating [235].
4. The spraying distance, which is defined by the distance between the nozzle of the spray gun and the substrate. The closer the nozzle, the closer is the combustion flame to the substrate, and the greater is the heat transferred to the material [235, 249].
5. The conditions of the spray environment, such as the temperature, humidity level and airflow of the spray booth, can influence the heat transferred to the material during spraying.

After coating deposition is completed, post-heating can be performed with the flame (additional heat transferred to the deposited polymer) to remelt the coating surface and obtain the desired surface topography [213]. Finally, the cooling rate of the deposited polymer coating, e.g. the solidification rate of the polymer from a molten state, determines the physical, thermal and morphological properties of the coating and the degree of stress generation in its structure [213].

The amount of heat required to process the polymeric material mainly depends on the thermal and physical properties of the polymer powder (e.g. melting temperature, thermal degradation temperature, degree of crystallinity) [212, 213]. Specifically, the melting temperature and thermal degradation temperature of the polymer powder have been used to define indicatively the lower and upper-temperature limit of the thermal process window, respectively [212]. The thermal process window is, therefore, specific for each polymer. If not enough heat is transferred to the polymer particles (i.e. the achieved temperature is below the melting temperature range of the polymer powder), particles will not coalesce with each other, resulting in porous coating structures [212]. On the other hand, if the material reaches a temperature higher than its melting temperature range, the thermoplastic polymer powders will be in a fully molten state. Complete melting allows the coalescence of the polymer particles by viscous flow to obtain a dense coating. However, if the process temperature exceeds the thermal degradation temperature of the material, gaseous products will be formed due to the vaporisation of the polymer, and thermal degradation and oxidation will occur [212]. At excessive

processing temperatures, the polymer starts to degrade, leading to possible cross-linking of the polymer chain (formation of covalent bonds between the polymer chains), chain scission (breakage of covalent bonds in the polymer chains) and consequent oxidation [212]. Therefore, the material temperature should be maintained within this specific thermal process window throughout the spraying process to obtain a dense coating structure and minimise thermal degradation [224]. In addition to the process temperature, thermal degradation is also affected by the presence of oxygen in the spraying environment, which can contribute to polymer oxidation [212, 235].

Understanding the interrelationships between selected process parameters, process variables and the affected coating properties is crucial in order to deposit coatings with desired properties. The properties of flame-sprayed polymer coatings are mainly affected by the selected process parameters and process variables, which determine the thermal history that the material experienced during spraying [213]. The following discussion will focus on the influence of selected process parameters and process variables on the coating properties. The coating properties relevant to this work, such as surface and physical properties, will be discussed.

Concerning surface properties, the surface topography of flame-sprayed polymer coatings is affected by several parameters. In general, the higher the temperature reached by the polymer during processing, the lower is the roughness obtained on the surface [213, 223]. The lower the spraying distance and the traverse speed of the gun, the greater is the heat transferred to the material and the longer the processing time, thus resulting in smoother coating surfaces. Surface roughness is reduced if post-heating is performed, which causes re-melting and re-solidification of polymers [223]. Furthermore, the surface roughness decreases when the powder feeding rate increases [223]. Another property affected by the employed process parameters (and the feedstock material) is the chemical composition of the obtained coating surface. Changes in the chemical composition of sprayed coatings are generally caused by polymer oxidation during the process [212, 213]. The oxidation increases with increasing processing temperature, indicating the occurrence of thermal degradation for the polymer [212, 250]. The chemical composition of coating surfaces is compared to that of the pristine feedstock powder to investigate the presence of chemical changes in the deposited material [251].

Concerning physical properties, the coating thickness increases with the increasing number of coating layers deposited on the substrate and increasing powder feeding rate [223]. Moreover, for constant powder feeding rates, the coating thickness increases with the decreasing traverse speed of the gun. Another physical

property affected by the process parameters is the degree of crystallinity of the polymer coating. The degree of crystallinity is defined as the fractional amount of polymer chains, which are densely organized and packed in ordered regions of the polymer. The degree of crystallinity represents one of the most important physical parameters, determining various mechanical and physical properties in semi-crystalline polymers. It has been demonstrated that the faster the cooling rate of the polymer after deposition, the lower is the degree of crystallinity obtained for the coatings [252, 253]. Moreover, the amount of heat transferred to the material influences the degree of crystallinity. A study has found that the degree of crystallinity decreases when thermal degradation occurs in the polymeric material during processing [254]. In that study, the decrease in the degree of crystallinity has been mainly related to the reduced molecular weight caused by thermal degradation, which decreases the ability of the polymer to re-crystallise [254]. The reduced degree of crystallinity usually results in decreased mechanical properties for the material, such as tensile strength and Young's modulus [212, 255, 256].

4.3 Coating materials and applications

Several polymeric materials have been used to fabricate thermally sprayed coatings, depending on the polymer properties and specific application [213]. Moreover, one or more additives or reinforcing materials (ceramic, polymer, metallic materials or composite fillers) have been added to the structure of polymer coatings to tailor the properties required for the desired application [213]. Therefore, coatings can be potentially produced for different applications by combining different materials in the coating structure. For instance, anti-corrosion [227, 257, 258], low friction and wear resistance [230, 259, 260], chemical and weathering resistance [261, 262], anti-fouling [263] and anti-icing [222] represent some of the possible applications of thermally sprayed polymer coatings. Table 2 summarises the polymeric material employed to fabricate thermally sprayed coatings and composite coatings and the corresponding applications presented in the literature.

Table 2. Materials of thermally sprayed polymer coatings and polymer composite coatings and their application.

Polymer	Application	References
Polyethylene (PE)	Corrosion resistance	[263]
	Anti-fouling	[263]
	Wear resistance	[241]
	Anti-icing	[222, 264]
Polypropylene (PP)	Corrosion resistance	[224, 237]
	Anti-icing	[264]
PE copolymer (EMAA)	Corrosion resistance	[227, 237, 258, 261, 262]
	Erosion, friction and wear resistance	[241, 257, 262]
	Weathering resistance	[261, 262]
	Impact resistance	[256]
Polyesters (PET)	Friction and wear resistance	[259, 265]
Fluoropolymers	Friction and wear resistance	[260, 266]
	Corrosion resistance	[221, 227]
Polyamides	Ignition resistance	[237]
	Friction and wear resistance	[225][219, 220, 230]
	Corrosion resistance	[220]
	Erosion and oxidation resistance	[267]
Polyetherketone (PEEK)	Friction and wear resistance	[220, 226, 268–271]
	Corrosion resistance	[220, 253]
	Biomedical application	[272]
	Anti-icing	[264]
Polyetherimides (PEI)	Corrosion resistance	[220]
	Friction and wear resistance	[220]
Polyhydroxyalkanoate (PHBV)	Biomedical application	[273]
Polymethylmethacrylate (PMMA)	Wear resistance	[274]
	Biomedical application	[273]

5 AIM OF THE RESEARCH

This thesis aims at designing and fabricating polymer coatings intended for anti-icing applications using flame spray technology. Increased understanding of the icephobic behaviour of polymeric coatings produced using flame spraying is needed. This knowledge is of fundamental importance for fabricating icephobic coatings using this technology. Moreover, such an industrial coating technique can be potentially extended to various applications facing icing problems. Therefore, many industrial sectors may benefit from the advantages of flame spraying as an alternative to the coating technologies currently employed. However, studying the effect of the process parameters on the coating properties and, consequently, on the coating icephobicity is complex. This complexity derives from the synergic effect of various properties of the coatings affecting icephobicity. Moreover, all the factors related to ice formation and ice adhesion testing were kept fixed throughout the work, and their effect on icephobicity will be therefore not discussed in this thesis.

The first objective of the thesis was to understand the effect of the employed process parameters on the icephobic behaviour of flame-sprayed polyethylene coatings (Publication I).

The employed process parameters in flame spraying determine the final structural and surface properties of deposited polymer coatings. Therefore, it is fundamental to understand how the process parameters affect the properties of coatings and how these properties consequently influence the icephobicity. To investigate this, two process parameters were varied, such as spraying distance and transverse speed of the flame spray gun. Both these parameters affect the heat transferred to the polymeric material during spraying, therefore their effect on the properties and icephobicity of low-density polyethylene (LDPE) coatings was studied.

The second objective of the thesis was to understand the effect of additive addition on the properties and icephobic behaviour of flame-sprayed composite coatings (Publication II and Publication III).

Once the effect of the process parameters on coating properties and icephobicity has been studied, the next step of the research aimed at further improving the

icephobic behaviour of coatings. To achieve this, solid lubricants (waxes) with low surface free energy were added to the coating structure. Composite coatings were fabricated, made of two polymeric components, namely matrix material (LDPE) and lubricating additive. These coatings are hereinafter termed lubricated icephobic coatings (LICs). For the fabrication of LICs, technical adjustments were applied to the flame spray process to feed the lubricant and avoid direct contact with the combustion flame during spraying. Specifically, an injector was mounted externally to the flame spray gun to feed the lubricant and the modified spray process was named the flame spray process with hybrid feedstock injection. Moreover, different process parameters were varied to fabricate LICs, and the effect of lubricant addition was studied on the icephobicity, surface roughness, chemical composition and wettability of coatings.

The third objective of the thesis was to understand the durability of lubricated icephobic coatings under repeated icing/deicing cycles (Publication III and Publication IV).

Icephobic coatings should maintain stable icephobic behaviour under icing conditions in real applications. Therefore, it was essential at this stage of the research to understand how durable LICs are under icing conditions. To assess coating durability in icing conditions, repeated icing/deicing cycles were performed, and changes in icephobic behaviour were studied over the cycles. In addition, variations in coating properties, such as morphology, surface roughness and chemical composition, were investigated after the cycles and correlated with icephobicity.

The fourth objective of the thesis was to study the durability of lubricated icephobic coatings under various environmental stresses (Publication III).

In addition to icing conditions, icephobic coatings may come into contact with different environments in real applications and be exposed to various environmental stresses. For this research, the durability of LICs was investigated under immersion in corrosive media and exposure to ultraviolet radiation. Specifically, the coatings were in contact with acidic, saline and basic solutions for 60 days. Moreover, the coatings were artificially aged using UV lamps for 1000 hours. Finally, variations in coating properties, such as morphology, roughness, chemical composition, wettability and colour changes, were monitored to assess coating durability in these conditions.

5.1 Research questions

This thesis aims to answer the following research questions (RQ):

1. How do the flame spray process parameters influence the properties and the icephobicity of plain low-density polyethylene coatings?

2. How does the addition of lubricating additives to the coating structure affect the properties and the icephobicity of flame-sprayed polyethylene coatings?

3. How durable are the lubricated icephobic coatings under repeated icing/deicing cycles?

4. How durable are the lubricated icephobic coatings under various environmental stresses, such as immersion in corrosive media and exposure to ultraviolet radiation?

Table 3 lists the four research questions with corresponding publications and chapters of this dissertation where the above research questions are discussed. Figure 13 summarises the main objectives defined in this thesis, with reference to the corresponding publications and research questions.

Table 3. Summary of research questions with corresponding related publications and dissertation chapters.

Research questions	RQ1	RQ2	RQ3	RQ4
Content	Influence of process parameters on coating properties and icephobicity	Effect of lubricant addition on coating properties and icephobicity	Durability under repeated icing/deicing cycles	Durability under various environmental stresses
Publications	I	II and III	III and IV	III
Chapters	7.1	7.2	7.3	7.4

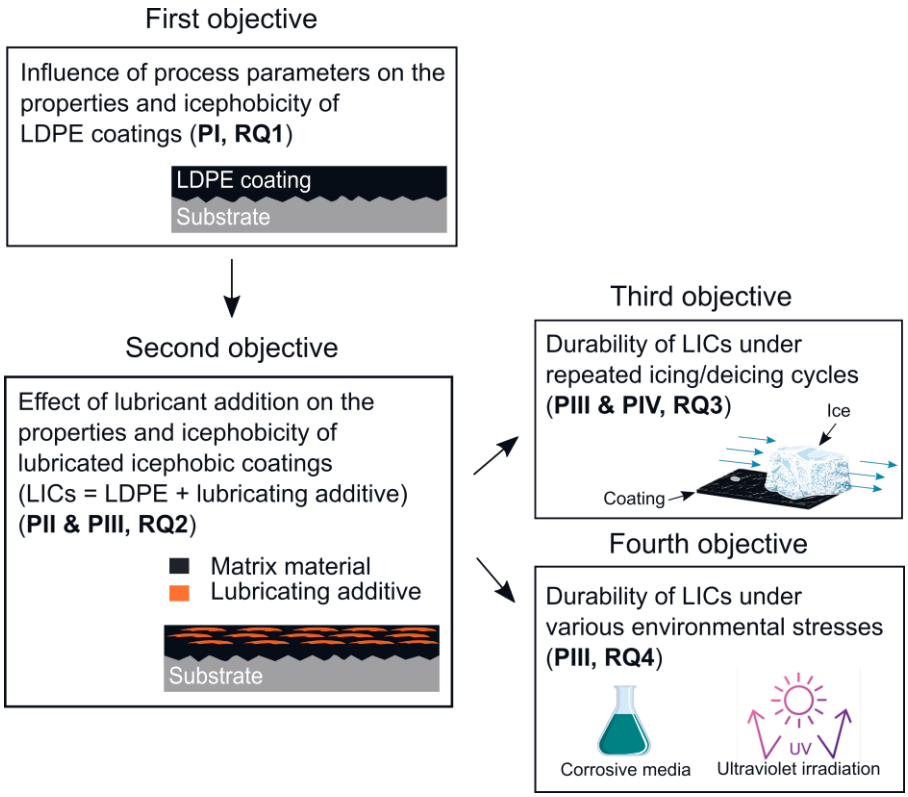

Figure 13. Summary of the objectives defined in this thesis with corresponding publications (PI-IV) and research questions (RQ1-4).

6 EXPERIMENTAL PROCEDURES

This chapter introduces the materials, coating deposition technique and characterisation methods utilised in this research. The first part of the chapter describes the feedstock materials and the coating fabrication method, with a brief explanation of the hybrid feedstock injection system in the flame spray process. The second part of the chapter reports on the characterisation methods employed for the feedstock materials and coatings.

6.1 Materials and coating deposition technique

In this work, coatings were manufactured using commercially available polymeric materials in the form of powders. Table 4 lists the feedstock powders used to produce coatings in this study. The as-received powders were mechanically sieved before flame spraying in cases of powder agglomeration. Mechanical sieving was carried out to improve the powder flowability and ensure uniform powder feeding during the spray process. In the first stage of the research (Publication I), coatings were made of low-density polyethylene (LDPE) powder and fabricated using an oxygen-acetylene flame spray gun (CastoDyn DS 8000, Castolin Eutectic, Switzerland). Coatings were deposited on stainless steel substrates (EN 1.4301/2K (4N)), which were grit-blasted using aluminium oxide grits (grit size of 54 mesh) before flame spraying. A powder feeder (Sulzer Metco 4MP, Oerlikon Metco, Switzerland) was used to axially feed the LDPE powder in the gun. The gun was mounted on a single-arm robot (ABB IRB 4400/60, ABB Robotics, Sweden) that controlled the movement of the gun during coating deposition.

Table 4. Commercially available feedstock powders employed for coating fabrication in this study.

Powder Material	Trade Name	Manufacturer	Publication
Low-density polyethylene (LDPE)	Plascoat LDPE	Plascoat Europe BV	I, II, III, IV
Fully hydrogenated cottonseed oil	Lubritab® capsules	JRS PHARMA GmbH & Co. KG	II, III, IV
Non-functionalised Fischer-Tropsch hard paraffin	VESTOWAX® H 2050 MG	Evonik Industries AG	III

After fabricating plain LDPE coatings, a second solid component, named the lubricating additive, was added to the coating structure to produce lubricated icephobic coatings (LICs). In Publications II-IV, fully hydrogenated cottonseed oil was employed as the lubricating additive. This additive is a naturally derived wax with hydrophobic properties [275]. In Publication III, paraffinic wax was used as a possible alternative to the cottonseed oil additive in the last stage of the research. Both additives were chosen for their chemical compatibility with the matrix material [276, 277]. The additive was sprayed simultaneously with the LDPE powder from an external injector. A similar approach has been used to fabricate polymer composite coatings with low-friction properties in other studies [219, 225]. The external injector was mounted on the left side of the flame spray gun, oriented towards the gun with its axis intersecting the flame spray gun axis at about 280 mm from the flame spray nozzle. The additives were fed using a second powder feeder (PT-10 Twin powder feeder, Oerlikon Metco, Switzerland) and sprayed externally to the flame to prevent their degradation and vaporisation. The modified flame spray process is termed the flame spray process with hybrid feedstock injection in this work. Figure 14 presents a schematisation of the process configuration.

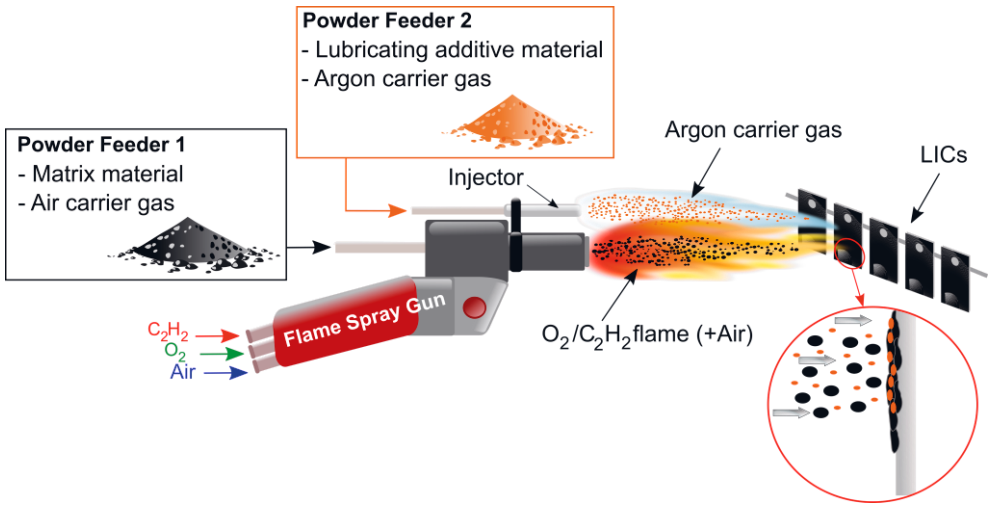

Figure 14. Schematisation of the flame spray process with hybrid feedstock injection to produce lubricated icephobic coatings (LICs). The matrix material is sprayed directly from the flame spray gun, whereas the lubricating additive is externally fed from an injector with argon as a carrier gas [Publication II].

6.2 Characterisation methods

Optical microscopy and scanning electron microscopy

The surface morphology and the cross-sections of the coatings were analysed using a stereomicroscope (MZ7.5, Leica, Germany) and a scanning electron microscope (SEM, Jeol, IT-500, Japan). The coating samples were cut using an automatic cut-off machine (Discotom-10, Struers ApS, Denmark). Cross-sections were prepared by mounting the samples to the epoxy resin at room temperature. The mounted samples were then mechanical ground and polished up to a surface finish of 0.25 μm. Then, all samples were dried in a desiccator and coated with a thin conductive layer to enhance surface conductivity. A secondary electron detector was used to image the topographical characteristics of the samples.

Surface topography and surface roughness measurements

The surface topography of coatings was imaged using an optical profilometer (contactless measuring instrument, Alicona Infinite Focus G5, Alicona Imaging GmbH, Austria). The roughness parameters (Ra, Sa, Sq, Sz, Sdr) were measured from the optical profilometry images, which were acquired using 20× objective magnification at different locations of the coating surface, following standards ISO 4288 [278] and ISO 25178-3[279]. The results were reported as the average and standard deviation of three measurements from different surface locations.

Chemical characterisation

The chemical characterisation of the polymeric materials was performed using Fourier-transform infrared spectrometers (FTIR, Bruker Tensor 27 FT-IR spectrometer, Bruker, Sweden and Spectrum One FT-IR Spectrometer, Perkin Elmer Instruments, United States). Attenuated total reflectance (ATR) sample holders with a diamond crystal were employed (GladiATR, PIKE Technologies, United States and Universal ATR Sampling accessory, Perkin Elmer Instruments, United States). The analyses were carried out in the wavenumber range 4000 cm^{-1} to 600 cm^{-1} by recording 32 scans with a 4 cm^{-1} resolution. For the analysis, feedstock powders and coating surfaces were directly placed in contact with the crystal. For the coatings, measurements were performed at different locations on the surfaces. FTIR spectra were used to determine possible changes in the chemical structure or composition of the coatings after the flame spray process (Publication I).

Wettability measurements

A droplet shape analyser (DSA100, Krüss, Germany) was used to determine the wetting behaviour of the coating surfaces. The instrument was located in a climate-controlled environment (temperature of 22 °C ± 1 °C and relative humidity of 60 % ± 3 %). The samples were placed in these conditions for 24 hours before the measurements to equilibrate with the test environment. The static contact angles were determined by depositing droplets of ultra-pure water (MilliQ, Millipore Corporation, United States) on the coating surfaces. The contact angle between the water droplet and the surface was determined using the tangent method (polynomial fit of droplet shape). Tilting experiments were used to analyse the water mobility behaviour of the surfaces. Water droplets were deposited on the surfaces, and the stage was tilted until the droplets rolled off. When droplet pinning occurred during the tilting experiments, a roll-off angle > 90° was measured. Both the static contact angle and roll-off angle were reported as the average and standard deviations of five measurements taken in different sample locations.

Surface free energy measurements

The surface free energy (SFE) of polymeric materials used in this work was calculated according to the Owens-Wendt-Rabel-Kaelble (WORK) model [88–91]. In this model, the surface free energy of solids is the sum of a dispersive component and a polar component. The dispersive component considered Van der Waals and other non-site-specific interactions. The polar component accounted for dipole-dipole, dipole-induced dipole, hydrogen bonding and other site-specific interactions between the surface and applied liquids [280]. The static contact angle of 3 μL droplets of water, diiodomethane and ethylene glycol was measured on the sample surfaces. The SFE values were calculated using Krüss software. However, measuring the surface free energies of feedstock materials in powders was challenging. Therefore, bulk samples of feedstock materials were produced using an oven (drying oven with natural convection, DL 53, DRY-Line®, VWR, Germany). The feedstock powders were melted and moulded into cylindrical silicon stamps. The surfaces of the bulk samples used for the SFE measurements had values of Ra roughness ranging from 0.2 to 1.7 μm.

Icing tests

The icephobic behaviour of coatings was investigated using the icing test facilities in the Ice Laboratory at Tampere University [147]. An icing wind tunnel (IWiT) and a centrifugal ice adhesion tester (CAT) are located in a cold climate room with

controlled temperature and relative humidity (-10°C ± 1°C and 80% ± 5%). Before the test, the samples were placed in the cold climate room. Once the samples reached the desired test conditions, ice was accreted from supercooled water microdroplets on 30 mm x 30 mm coating areas using the IWiT. A mixed glaze type of ice was accreted from atomised droplets using laboratory-grade II+ water (Purelab Option-R 7/15, Elga, United Kingdom). For mixed glaze ice, the mean volumetric diameter (MVD) of the water droplets was measured to be 22 μm, and the mean droplet velocity was around 23 m/s. Both the MVD and mean droplet velocity were measured using a diagnostic camera (HiWatch HR2 camera, Oseir Oy, Finland) during ice accretion [281]. After ice accretion, the iced samples were kept in the cold climate room for several hours to guarantee complete solidification of the ice. The ice was then detached from the sample surface using CAT, and the ice adhesion was determined. The iced samples were weighed with and without ice to record the mass of accreted ice.

The shear ice adhesion strength, τ_{ice} [kPa], was calculated as the ratio of the centrifugal force $F_{centrif}$ [N] at the instant of ice detachment to the area of the iced surface A [m²], according to Equation 13:

$$\tau_{ice} = \frac{F_{centrif}}{A} = \frac{m_{ice} r \omega^2}{A} = \frac{m_{ice} r (\alpha t)^2}{A} \quad (13)$$

where m_{ice} [kg] is the known mass of the accreted ice on the specimen and r [m] is the radial spinning length at which the iced samples were spun. ω [rad/s] represents the rotational speed of the sample measured at the time t [s] of ice detachment, using a constant angular acceleration α of 300 rpm/s. The ice adhesion strength was reported as the average and standard deviation of four parallel samples. A test reference surface (3M™ PTFE Film Tape 5490, 3M, United States) was used to monitor the ice adhesion at each accretion event, considering possible variations in icing conditions. Moreover, cyclic icing/deicing tests were performed to assess the durability of coatings. Ice accretion and ice removal were repeated four times for each sample. The ice adhesion strength was recorded at each of the four cycles, and variations in ice adhesion enabled the durability assessment of the icephobic properties. Surface properties, such as morphology, roughness, wettability and chemical composition, were analysed before and after the cyclic tests to better understand the variations in icephobicity and durability of coatings.

Thermal characterisation

The thermal characterisation of the as-received powders and coatings was performed using a differential scanning calorimeter (DSC, Netzsch DSC214 Polyma, Netzsch, Germany). Approximately 10 mg of the specimens was weighed and heated at 20 °C/min from −30 °C to 150 °C in a nitrogen atmosphere (40 mL/min nitrogen flow). The degree of crystallinity χ [%] of the feedstock powders and coatings was evaluated using Equation 14:

$$\chi = \frac{\Delta H}{\Delta H_{100\%}} \tag{14}$$

where ΔH [J/g] represents the enthalpy of fusion of the sample (corresponding to the area under the melting transition) and $\Delta H_{100\%}$ [J/g] represents the enthalpy of fusion of the corresponding fully crystalline material. According to the literature, this value equals 293 J/g for fully crystalline polyethylene material [282]. Moreover, the thermal characterisation of as-received powders and coatings was carried out using a thermogravimetric analyser (TGA, Netzsch TGA209F Tarsus, Netzsch, Germany). The 10 mg samples were placed in an alumina pan and heated from 25 to 600 °C at 20 °C/min in a nitrogen atmosphere (20 mL/min nitrogen flow). Both DSC and TGA were used to estimate the content of lubricating additive in the composite coating after deposition. The coefficients of linear thermal expansion (CTEs) of the coatings and substrate material were determined using a dilatometer equipped with a silica probe (DIL 402 Expedis® Select, Supreme, Netzsch, Germany) (Publication III). The samples were cooled to a temperature of -15 °C and then heated to 35 °C at 1 °C/min rate in an inert environment (helium flow rate 50 ml/min). This temperature range was selected and the CTE values were measured in the range of interest from -10 °C to 25 °C. The CTE values were calculated as the average and standard deviation of three measurements.

Exposure to various environmental stresses

The icephobic coating designed in this work was not fabricated for a specific application. Therefore, the author chose to study some aspects of the effect of environmental and chemical agents on the durability of icephobic coatings, such as the immersion in corrosive media and the exposure to ultraviolet (UV) radiation (Publication III). For the immersion experiments, acidic, saline and basic solutions were prepared, and the coating samples were then immersed for 60 days. Using acetic acid (acetic acid 99-100% GPR RECTAPUR®, VWR Chemicals, France), an acidic

solution was prepared to mimic the exposure of the coating to an acid rain event (pH = 4 [283]). Sodium chloride (sodium chloride, BAKER ANALYZED® ACS, J.T. Baker®, VWR Chemicals, France) was used for the saline solution. The saline solutions had an average sea salt concentration of 35 g/L, simulating a saline environment. Sodium hydroxide (Sodium Hydroxide, Tamro Oy, Finland) was employed for the basic solution, which mimicked the environment of cleaning agents, detergents and ammonia solutions (pH = 11). The pH of the solutions was measured using a pH metre (MU 6100 H, multiparameter instrument, VWR, Darmstadt, Germany). The pH meter was calibrated before each measurement using three buffer solutions with pH values of 4, 7 and 10. Coating samples were immersed in acidic, saline and basic solutions for 60 days. The pH of the acidic and basic solutions was monitored during the 60 days and remained stable during the time of the experiments (the pH value was measured to be 4 ± 0.11 and 11 ± 0.03 for the acidic and the basic solutions, respectively, throughout the 60 days). Coating properties, such as chemical composition and surface morphology, were measured after 60 days of immersion. In addition, TGA was performed to detect possible absorbed water in the immersed coating samples.

Concerning UV exposure experiments, coatings were artificially aged using UVA-340 fluorescent lamps to simulate solar ultraviolet (UV) light. Further technical details on the UV chamber can be found in [284]. The samples were exposed for 200, 500 and 1000 h. Colour changes were investigated using visual inspection and a chromameter (CR-200, Konica Minolta Sensing Europe B.V., The Netherlands). The chromaticity experiments employed a measuring mode based on L*a*b* coordinates (CIE 1976). In the L*a*b* colour space, L* indicates the colour lightness, a* the red/green coordinate and b* the yellow/blue coordinate, respectively [285]. According to standard ASTM D2244-02, the colour difference, ΔE^*_{ab}, was calculated using Equation 15:

$$\Delta E^*_{ab} = \sqrt{(L^*_2 - L^*_1)^2 + (a^*_2 - a^*_1)^2 + (b^*_2 - b^*_1)^2} \quad (15)$$

where L^*_1, a^*_1 and b^*_1 indicate the lightness, the red/green coordinate and the yellow/blue coordinate of the as-received samples, corresponding to 0 h exposure time. L^*_2, a^*_2 and b^*_2 represent the values measured for the samples after 200 h, 500 h and 1000 h of exposure time. Moreover, the chemical composition of the coating surfaces was measured using FTIR to determine any possible changes in the chemical structure of coatings after exposure times of 200 h, 500 h and 1000 h.

7 RESULTS AND DISCUSSION

This chapter presents and discusses the main results from Publications I-IV and is divided into four sections. Section 7.1 presents the effect of process parameters on the icephobicity of plain low-density polyethylene coatings and related coating properties. Section 7.2 introduces the fabrication of lubricated icephobic coatings and discusses the effect of lubricant addition on coating icephobicity and related properties. Section 7.3 discusses the durability of lubricated coatings under repeated icing/deicing tests. Finally, section 7.4 presents the results on coating durability under various environmental stresses.

7.1 The effect of flame spraying parameters on the icephobicity of polymer coatings

Plain low-density polyethylene coatings were fabricated using flame spray technology by varying two process parameters, such as the transverse speed and spraying distance of the flame spray gun. Figure 15 summarises the process parameters and the samples analysed in Publication I. For flame spraying of polymers, the higher the transverse speed of the gun, the faster is the deposition process per unit length, and the lower is the time that the material is exposed to the combustion flame. In other words, the higher the traverse speed, the lower is the heat input transferred to the polymeric material [274]. Moreover, the greater the spraying distance, the farther is the flame from the substrate or the already deposited material, resulting in lower heat input transferred to the material [223]. The heat input transferred to the polymeric material determines the topography of the coating surface. The higher the heat input transferred to the polymeric material, the lower the obtained surface roughness of deposited coatings and vice versa [213, 223]. However, too high heat input could cause thermal degradation of the material with a detrimental effect on the properties of the produced coatings [213, 250]. Therefore, a trial-and-error approach was employed in this study to determine the optimal combination of process parameters in order to obtain a coating with preserved properties and enhanced icephobicity.

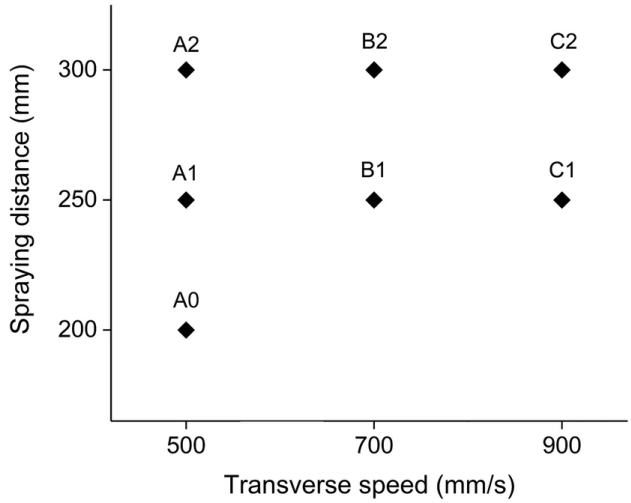

Figure 15. Process window of the chosen parameters for flame spraying of LDPE coatings. Samples were identified with letters (from A to C for increasing transverse speed) and with numbers (from 0 to 2 for increasing spraying distance) [Publication I].

The ice adhesion results are presented in Figure 16 with the corresponding areal roughness of as-sprayed coatings. For this centrifugal ice adhesion test and mixed glaze ice type [173, 264], the ice adhesion values of 50 kPa and 100 kPa represent the low and medium-low ice adhesion limits, respectively. The results indicated that the process parameters had a significant effect on the icephobicity of the coating surfaces. In particular, the ice adhesion was higher for the coatings fabricated with the slowest transverse speed (from A0 to A2). For samples A0-A2, ice adhesion increased with increasing areal roughness, and these results are in accord with previous studies [137, 286]. Samples A0-A2 had the highest ice adhesion here, although they had the smoothest surfaces compared to the other coatings. This result implies that other factors might influence ice adhesion in addition to areal roughness. Moreover, no significant relationship between ice adhesion and areal roughness was found for the medium transverse speeds (samples B1 and B2). Finally, the coatings showed comparable areal roughness for the highest transverse speed (samples C1 and C2), and sample C1 exhibited the lowest ice adhesion value of 32 ± 3 kPa. This combination of process parameters (900 mm/s and 250 mm) resulted in plain LDPE coatings with the lowest ice adhesion strength within the selected process window in Publication I.

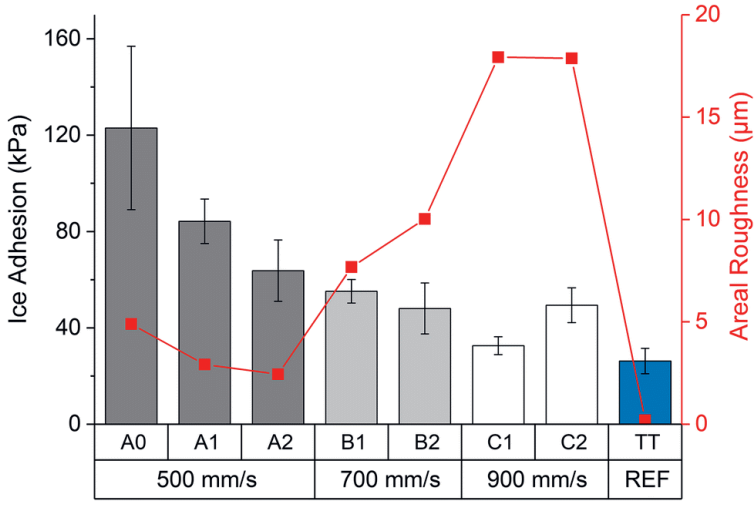

Figure 16. Ice adhesion (left axis) and areal roughness Sa (right axis) of the coatings. Teflon tape (TT) represents the reference material for ice adhesion used in this centrifugal test [Publication I].

The chemical analysis of the coating surfaces was conducted by comparing the FTIR spectra of the coatings and the FTIR spectra of the as-received feedstock powder. The main difference between the coatings and the powder spectra was the formation of absorbance bands in the regions of 1700-1750 cm^{-1} and 800-1300 cm^{-1}. In particular, a new absorbance peak at 1713 cm^{-1} was evident for some coatings. The absorbance peak at 1713 cm^{-1} corresponds to the presence of oxidation products (carbonyl and carboxyl compounds) in the polyethylene material [287]. The higher the absorbance intensity, the higher is the qualitative content of carbonyl and carboxyl compounds in the polyolefin sample. Therefore, the coating material was oxidised during spraying and deposition processes, and the oxidation degree depended on the selected process parameters.

Figure 17 presents the intensity of the absorbance peak at 1713 cm^{-1} and corresponding ice adhesion values measured for the coatings. The absorbance peak intensity at 1713 cm^{-1} was equal to 0.04 for the as-received feedstock powder. According to the results, the absorbance rose from 0.15 for sample A2 to 0.30 for sample A0 when coatings were sprayed using a transverse speed of 500 mm/s. This rise in peak intensity suggests that the chemical structure of the polyethylene coatings was more oxidised with decreasing spraying distance. However, when the combustion flame was moved further away from the coating during deposition, the presence of oxidation compounds at the coating surfaces gradually decreased. Moreover, the absorbance intensity decreased with increasing transverse speed for

the coatings, from A0-A2 to B1-B2 until C1-C2 samples. Finally, specimen C2 had an absorbance intensity at 1713 cm^{-1} of 0.07, similar to that of the feedstock powders, representing the less oxidised coating surface.

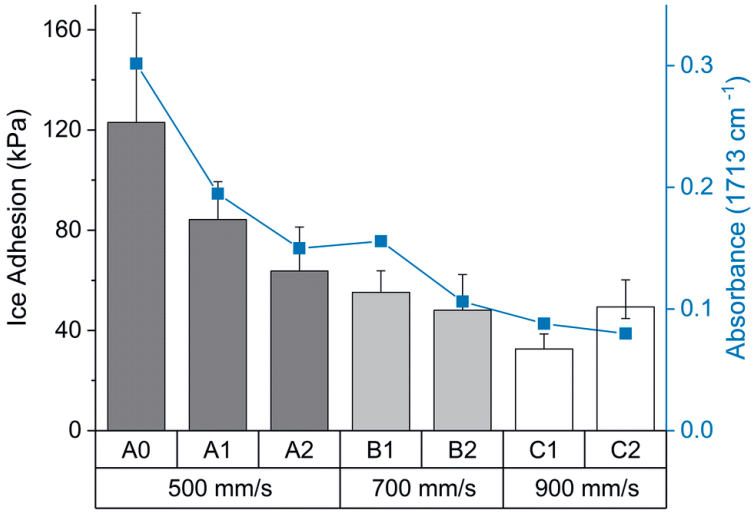

Figure 17. Ice adhesion strength and absorbance intensity at 1713 cm^{-1} for the flame-sprayed LDPE coatings [Publication I].

The results presented in Figure 17 demonstrate that the process parameters had a significant effect on the chemical composition of the coating surfaces and hence on their icephobicity. The oxidation of flame-sprayed polymer coatings is a temperature and time-dependent phenomenon [213, 235, 250]. The oxidation degree strongly depends on the employed process parameters and consequently on the amount of heat input transferred to the material during the process. The slowest transverse speed lengthens the processing time, increasing the heat input transferred to the material and its temperature [274]. The longer the polymeric material is exposed to the flame, the greater the thermal oxidation will be on the deposited material. The mechanism of thermal oxidation of polyethylene is described in detail in Publication I. Moreover, the ice adhesion strength increased with the oxidation of the material, thus supporting the fact that thermal degradation had a negative effect on the icephobic behaviour of such flame-sprayed coatings.

Thermal degradation of polymeric materials causes scission of polymer chains, cross-linking and the oxidation of the polymer, resulting in changes in molecular weight [212, 213, 250]. A loss in molecular weight generally results in a decrease in the degree of crystallinity [254] and a consequent decrease in the mechanical

properties of the polymer [212, 255, 256]. Therefore, the influence of the process parameters on the degree of crystallinity was investigated for the as-received coatings. Figure 18 presents the degree of crystallinity of as-sprayed LDPE coatings and the ice adhesion strength values.

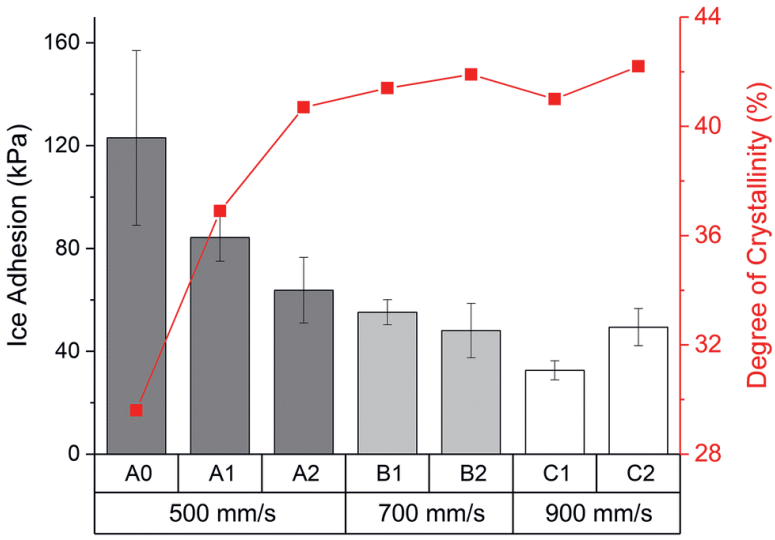

Figure 18. Relationship between the ice adhesion strength (left axis) and the degree of crystallinity (right axis) of flame-sprayed LDPE coatings [Publication I].

The degree of crystallinity increased as the heat input transferred to the material decreased. For samples A0, A1 and A2, the degree of crystallinity increased with increasing spraying distance from 29 % at 200 mm to 40 % at 300 mm. For samples B1-B2, a slight rise in the degree of crystallinity was again noticed with increasing spraying distance, from 41 % to 42 %. After that, the degree of crystallinity remained stable at around 41-42 % for samples C1 and C2. For samples C1 and C2, thermal degradation was limited, according to previous results from the chemical analysis. Considering that the cooling conditions (rate of cooling in the air) after spraying were similar for all coatings, the variation in the degree of crystallinity was related to the effect of the heat input transferred to the polymeric material. Increased heat caused the thermal degradation of flame-sprayed LDPE coatings with a consequent reduction in the degree of crystallinity, as found in a previous study [288]. Therefore, it was concluded that thermal degradation produced by overheating the polymeric material had a detrimental effect on the crystallinity of coatings within the examined processing window.

The wetting properties, such as the water contact angle and water roll-off angle, were measured for the coating surface to establish possible correlations between surface oxidation, water wettability and icephobicity. The water contact angle for the fabricated coatings varied between 89° and 94°, thus indicating the hydrophobic character of all surfaces. Moreover, no roll-off angle was detected for any of the coating surfaces (roll-off angle > 90°). No clear correlation was found between wetting properties and the oxidation of surfaces. As a result, the process parameters seemed to have no effect on the wetting properties of flame-sprayed surfaces, despite the different chemical composition of the surfaces. Moreover, no clear correlation was found between wettability and the icephobic behaviour of these coatings.

In summary, flame-sprayed LDPE coatings were fabricated by varying two process parameters, namely the transverse speed and spraying distance of the flame spray gun. It was found that the process parameters significantly affected the final chemical composition of the coating surfaces and their icephobic behaviour. The higher the heat input transferred to the material (and consequently, the higher the temperature reached by the polymer during processing), the higher was the thermal degradation and material oxidation. Moreover, the icephobic behaviour of surfaces was correlated to the thermal degradation of the material. The ice adhesion strength of surfaces rose with increased surface oxidation. The most icephobic coatings (C1) exhibited an ice adhesion strength of 32 ± 3 kPa. These coatings were fabricated using a transverse speed and spraying distance of 900 mm/s and 250 mm, respectively, and showed limited thermal degradation. Although the surface roughness most probably affected ice adhesion, no clear correlation was found for the samples in this study. The wetting properties seemed not to be significantly affected by the thermal oxidation of the surfaces, and no correlation was found with the icephobic behaviour of coatings. In conclusion, thermal degradation negatively affected the icephobicity of flame-sprayed LDPE coatings. However, further research is required to determine which aspect of thermal degradation, such as chain scission, cross-linking, oxidation, reduction in mechanical properties or surface embrittlement, directly affects the icephobicity of such flame-sprayed surfaces.

7.2 The effect of lubricating additive on the icephobicity of polymer coatings

Solid lubricating additives were added to the structure of plain flame-sprayed LDPE coatings. Therefore, the flame spray method was modified to feed the lubricating

additive externally to the combustion flame, as previously described in Section 6.1. Composite coatings were fabricated using two polymeric components, namely the matrix material and the lubricating additive. These composite coatings are referred to as lubricated icephobic coatings (LICs). For this work, two solid lubricating additives were selected, namely fully hydrogenated cottonseed oil (C) and paraffinic wax (P). Hydrogenated cottonseed oil consists of a hydrophobic waxy solid [275], commonly used in pharmaceutical applications as a coating release agent [289] or taste masking tool [290]. Moreover, waxes, such as paraffinic waxes, are widely used as additives in various coating applications to impart certain surface qualities, such as a glossy or matte appearance and slipperiness [291]. They also act as anti-blocking, anti-settling and anti-sagging agents in coatings [291]. More significantly, waxes are characterised by low surface free energy (SFE) properties [292, 293], which have been shown to promote the icephobic behaviour of smooth polymeric surfaces [87, 92, 94]. Therefore, low surface free energy additives were added to the coating structure of plain flame-sprayed LDPE surfaces to potentially improve their icephobicity. The SFE values determined for the bulk samples of feedstock material are summarised in Table 5. The SFE values measured for LDPE and P were comparable to those reported in the literature [88, 92]. To the best of the author's knowledge, no SFE has been reported for fully hydrogenated cottonseed oil in prior investigations. The results indicated that the lubricating additives had lower SFE values than the matrix material.

Table 5. Surface free energy (SFE) values with dispersive and polar components of low-density polyethylene (LDPE), fully hydrogenated cottonseed oil (C), and paraffinic wax (P), in the form of bulk [Publication III].

Feedstock Material	SFE [mN/m]	Dispersive Component [mN/m]	Polar Component [mN/m]
Low-density polyethylene	30.41 ± 1.25	29.14 ± 0.64	1.27 ± 0.61
Cottonseed oil	19.77 ± 1.48	19.15 ± 1.19	0.62 ± 0.28
Paraffinic wax	22.84 ± 0.04	22.19 ± 0.03	0.64 ± 0.01

This study developed three different classes of LIC surfaces, namely LIC1-4, LIC-C and LIC-P coatings. LIC1-4 coatings were characterised by a 30 % theoretical content of C additive in the coating. The theoretical percentage of the additive content in the coating structure was calculated from the feeding rates imposed for the additive and matrix powders during spraying. LIC-C and LIC-P coatings were characterised by a 20 % content of C additive and P additive, respectively. An asterisk is indicated in the sample name if post-heating by flame was performed after spraying. The naming of the samples in the discussion will follow the one used in

the original publications. The discussion will firstly focus on the results of coatings based on the C additive (LIC1-4 samples with 30 % C content and LIC-C samples with 20 % C content), which were the most thoroughly investigated coatings in this work. After that, the results of coatings based on P additive (LIC-P samples with 20 % P additive content) will be briefly presented.

Figure 19 summarises the process parameters employed to produce coatings with 30 % of cottonseed oil additive (indicated in the graph as LIC1, LIC2, LIC3, LIC3* and LIC4), flame-sprayed polyethylene coatings (FS-PE1) and plain cottonseed oil coatings without matrix material (L4). The L4 samples were fabricated to better understand the icephobic behaviour of the additive material. The FS-PE1 samples were produced using the same process parameters of the best polyethylene icephobic surface (C1 samples) described in Section 7.1 without post-heating by flame after coating deposition. The spraying distance was 250 mm for all coatings. According to the technical datasheets of the feedstock materials, the C additive has a lower melting point (57–70 °C) than the polyethylene matrix material (107 °C). This difference in thermal properties required a further adjustment of the process parameters. Additional compressed air was added to the flame spray gun. This addition allowed the further decrease of heat input during deposition and the reduction of material vaporisation during spraying, especially that of the low melting temperature additive. Moreover, the greater the compressed air pressure added to the gun, the lower is the heat input transferred to the polymeric material.

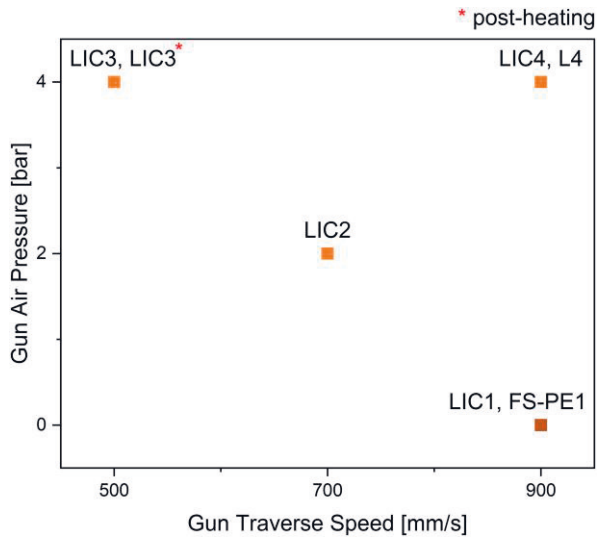

Figure 19. Process window of the chosen parameters for the coatings produced in this work [Publication II].

The visual inspection of coatings revealed that the addition of C additive rendered the surface appearance of LICs more matt compared to the glossy black polyethylene surfaces. However, the employed microscopic techniques could not help to distinguish the two components on the surface and cross-section of the LICs. This difficulty was mainly due to the additive colour after coating deposition and the similarities in chemical structures between the additive and matrix materials. Therefore, a white additive powder with the same particle size distribution as the C additive was used to fabricate one LIC sample (LIC2) to estimate the structure of LICs produced using this technique. The images of the surface and cross-section of the sample acquired using an optical stereomicroscope are presented in Figure 20. The images clearly showed the presence of two components (black matrix and white additive), which seemed well intermixed on both the surface and cross-section of the coating. Moreover, this coating structure was specific for the employed process parameters, and some differences could be produced if the parameters settings were changed.

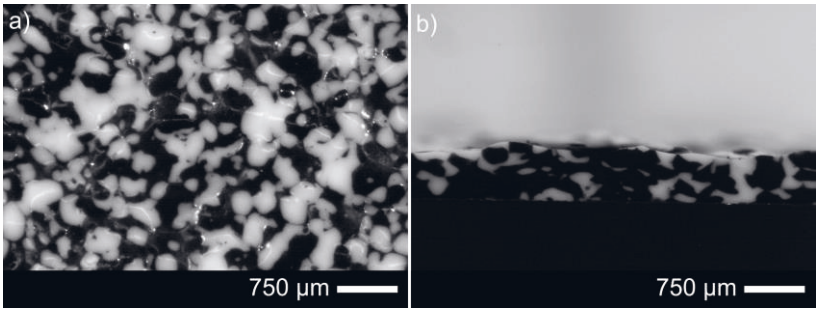

Figure 20. Stereomicroscope optical images of the a) surface and b) cross-section of LIC2 coating sample fabricated with a white coloured additive powder to demonstrate the structure of the lubricated icephobic coatings [unpublished results].

The surface topography of the coatings is presented in Figure 21 with the process parameters of traverse speed and compressed air pressure. The results indicated that the process parameters significantly affected the obtained surface topography. The higher the heat input transferred to the polymer during processing (obtained for lower traverse speeds and air pressures), the smoother is the obtained surface [213, 223]. The lubricant addition decreased the coating roughness when similar process parameters were utilised (LIC1 compared to FS-PE1). This effect was caused by the fully melted lubricant, which filled the surface topography of flame-sprayed polyethylene. Additionally, post-heating smoothed the coating surface due to the re-melting and re-solidification of the polymeric materials (LIC3 compared to LIC3*).

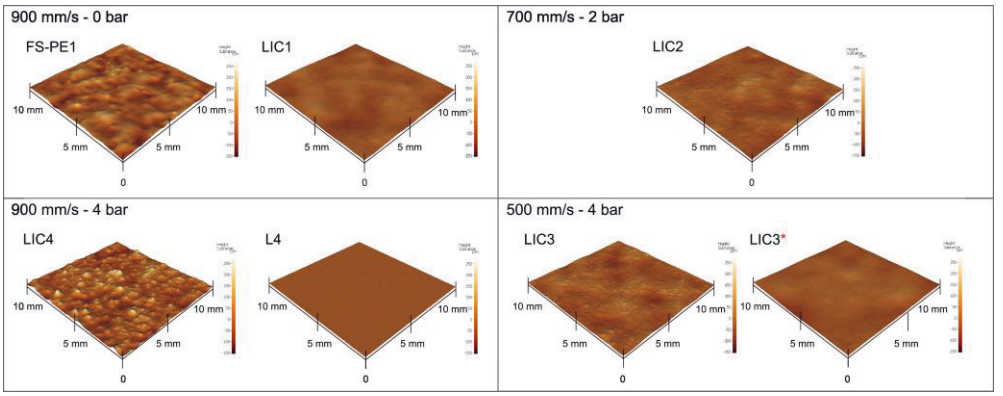

Figure 21. Surface topography of the coatings measured by optical profilometer analysis [Publication II].

The chemical analysis of the LIC surfaces revealed the presence of both matrix and additive materials at each measurement point, indicating that both materials (and indeed the C additive) were uniformly dispersed over the surfaces. However, LIC1 and LIC3* presented additional signals referring to the presence of alkene bonds. Alkene compounds constitute one of the initial products of the thermal degradation of polyethylene [294]. Therefore, this signal indicated that minor thermal degradation was produced for the lubricated coatings when no compressed air was added to the gun and post-heating was performed. In addition, the wetting experiments demonstrated that the addition of lubricant improved the hydrophobic character of LICs compared to plain LDPE coatings. However, water droplets remained pinned onto the surface features of all LICs, resulting in roll-off angles higher than 90°.

Figure 22 presents the ice adhesion strength results and corresponding surface roughness of the coatings. All lubricated surfaces demonstrated low ice adhesion behaviour, with ice adhesion strength lower than 50 kPa. The addition of lubricant was beneficial in reducing the ice adhesion strength of polyethylene coatings (FS-PE1 compared to LIC1 fabricated with the same process parameters). Moreover, the ice adhesion was further reduced by increasing the air pressure cooling the flame (from LIC1 to LIC3). The most icephobic surface of this study demonstrated an ice adhesion strength of 23 kPa ± 6 kPa. The average value of ice adhesion increased by roughly 61 % when post-heating was performed (LIC3* compared to LIC3). Finally, the average value of ice adhesion increased by nearly 35 % when a rougher surface was fabricated (LIC4 compared to LIC3).

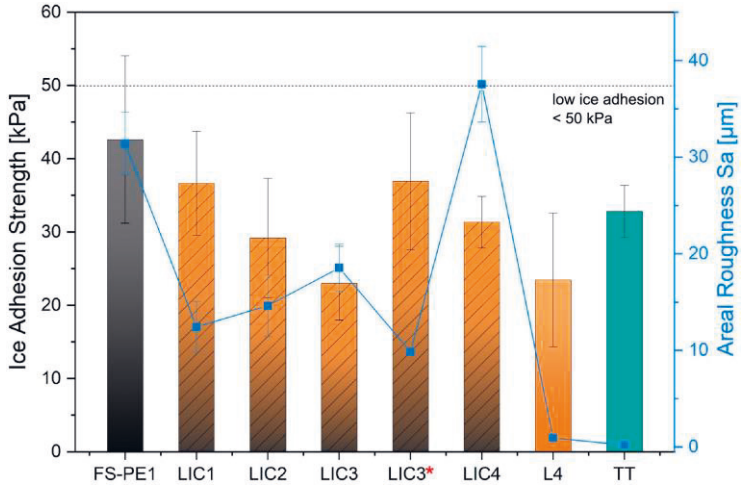

Figure 22. Ice adhesion strength and areal roughness Sa of the coatings. Teflon tape (TT) represents the reference material for the ice adhesion test [Publication II].

Concerning surface roughness, no clear correlation was found with ice adhesion strength. From LIC1 to LIC3 samples, ice adhesion decreased as areal roughness increased. Ice adhesion strength increased from LIC3 to LIC3* when the surface was smoothened by post-heating treatment. Finally, the roughest surface of this study, LIC4, demonstrated slightly better icephobicity than the post-heated surface LIC3*. Moreover, the chemical composition of coatings could have influenced their icephobic behaviour. A greater ice adhesion strength was measured for LIC1 and LIC3*. These coatings presented minor thermal degradation in their surfaces, probably due to the lack of additional air in the flame spray gun and post-heating treatment. The negative effect of thermal degradation on coating icephobicity was already observed for flame-sprayed coatings in the previous Section 7.1. However, further investigations are needed to establish a clear correlation between thermal degradation and icephobicity for lubricated coatings.

Figure 23 presents the ice adhesion results as a function of the areal roughness Sa for lubricated coatings (in orange) and some LDPE coatings, which were previously presented in Section 7.1. The spraying distance for all compared samples was 250 mm. From the comparison shown in Figure 23, some conclusions can be drawn. The addition of C additive to the coating structure improved the icephobicity of flame-sprayed polyethylene coatings (orange squares versus black squares). Even the roughest lubricated coatings of this study (LIC4) exhibited low ice adhesion behaviour. This result indicated that the icephobic behaviour of these coatings was mainly affected by the surface chemistry, rather than the surface roughness.

Moreover, the thermal degradation of the polymers negatively affected the icephobicity of coatings. Material degradation was minimised by cooling the flame using additional air and eliminating post-heating. When the lubricant was included in the coating structure, post-heating by flame was not beneficial for the icephobicity (ice adhesion of LIC3 compared to LIC3*). In contrast, when only LDPE was sprayed, post-heating helped to improve the icephobicity of coatings (ice adhesion of FS-PE1 compared to C1*).

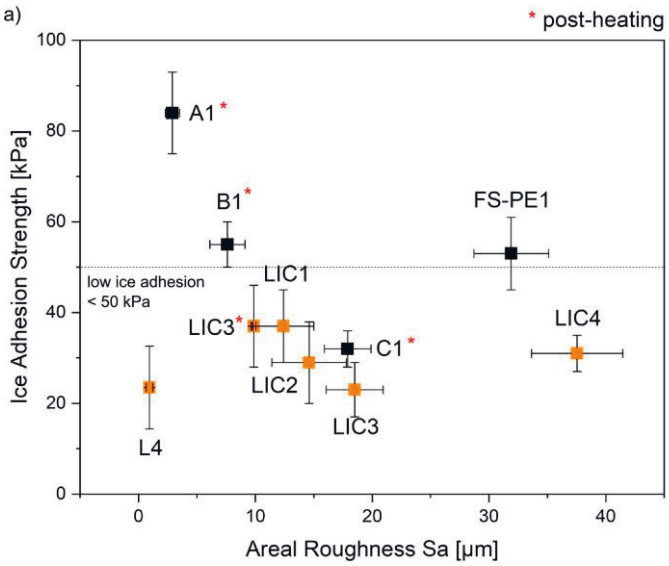

Figure 23. Icephobic performances of lubricated icephobic coatings (in orange) of Publication II compared to flame-sprayed polyethylene coatings (in black) of Publication I. Ice adhesion strength versus areal roughness Sa. Modified from [Publication II].

Lubricated coatings based on the C additive were further developed to investigate the effect of the additive content on the icephobic behaviour of the surfaces. The feeding rate of the C powder was reduced to obtain a theoretical percentage of additive content in the coating structure of approximately 20 m%. Figure 24 compares the ice adhesion strength values of coatings with 20 % (LIC-C and LIC-C*) and 30 % (LIC1-4) of the C additive. Areal roughness values, Sa, are indicated for each surface. According to the results, coatings with 20 % additive content exhibited values of ice adhesion strength above 50 kPa, while coatings with 30 % additive content showed an ice adhesion strength below 50 kPa. Moreover, no clear trend was found between ice adhesion strength and areal roughness for these coatings. Therefore, the lower additive content probably contributed to the increased

ice adhesion strength in LIC-C and LIC-C* coatings. Regarding the effect of post-heating on coating icephobicity, the average value of ice adhesion strength of post-heated LIC-C* coatings increased by roughly 13 % compared to the LIC-C samples. However, these results varied within the standard deviation and the influence of post-heating on the ice adhesion strength was not clear for these coatings.

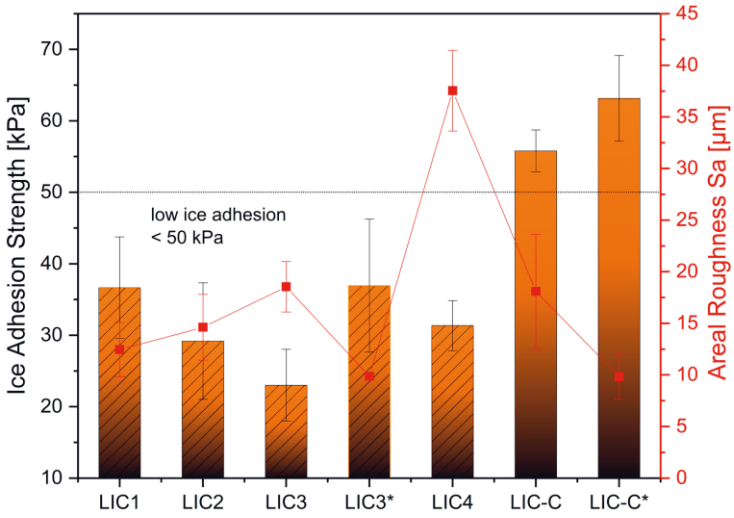

Figure 24. Icephobic behaviour of lubricated icephobic coatings (LICs) with 30 % content (LIC1, LIC2, LIC3, LIC3* and LIC4) and 20 % content (LIC-C and LIC-C*) of cottonseed oil additive. Ice adhesion strength is reported on the left axis and corresponding areal roughness Sa on the right axis.

Figure 25 presents the ice adhesion strength of coatings with 20 % content of C additive, 20 % content of P additive, and plain feedstock material coatings with corresponding areal roughness values. Regarding the P-based coatings, the addition of paraffinic wax seemed to be not beneficial for improving the icephobic behaviour of plain LDPE coatings. This result was confirmed by the icephobic behaviour of the plain paraffinic coatings (FS-P sample in Figure 25), which tended to behave more like plain LDPE coatings than plain C coatings. Therefore, this attempt was not successful as expected, considering the measured low surface free energy of paraffinic wax (Table 5). However, P-based coatings showed ice adhesion values below the medium-low ice adhesion limit, demonstrating the potential for further development of such icephobic surfaces. Therefore, further studies are suggested for coatings based on the P additive.

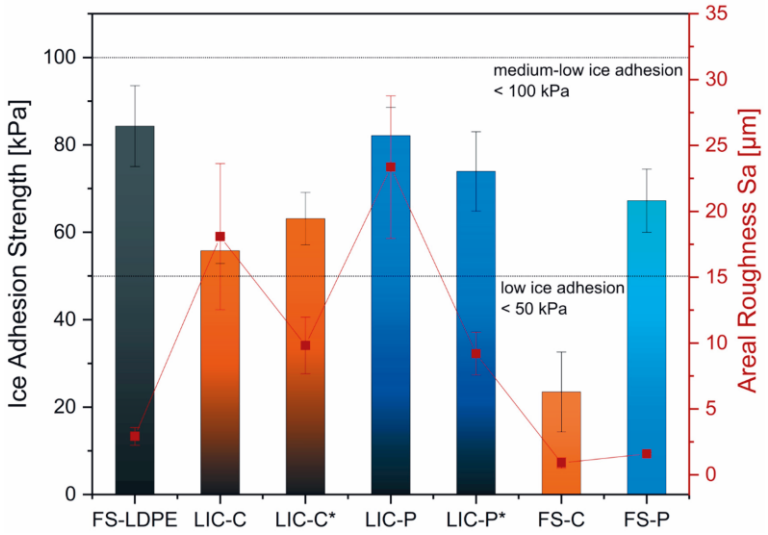

Figure 25. Icephobic behaviour of lubricated icephobic coatings (LICs) and flame-sprayed (FS) feedstock material coatings, measured at −10 °C with mixed glaze ice. Ice adhesion strength is reported on the left axis and corresponding areal roughness Sa on the right axis [Publication III].

In summary, LICs were fabricated in a single step using the flame spray method with hybrid feedstock injection. LICs were two-component coatings formed by the matrix material (LDPE) and the lubricating additive. Two lubricating additives were used, namely fully hydrogenated cottonseed oil (C) and paraffinic wax (P). The additive content in the coating structure was set to be around 30 m%. The addition of C additive improved the hydrophobicity of plain LDPE coatings. All LICs with 30 % C additive demonstrated low ice adhesion behaviour below 50 kPa. Minor thermal degradation, which was detected for some coatings, seemed to have a negative influence on their icephobic behaviour. When the C additive content was reduced to 20 % in the coating structure, an increase in ice adhesion strength was evidenced. Finally, the P additive seemed to not improve the icephobicity of the plain LDPE coatings.

7.3 The durability of lubricated coatings under cyclic icing/deicing

All the lubricated coatings fabricated in this work underwent repeated icing/deicing cycles, and variations in ice adhesion strength were recorded to assess the durability of their icephobic properties. Figure 26 presents the stages of the icing/deicing cycles

performed in this work to assess the durability of lubricated coatings. At first, the samples were cooled to the icing conditions (stage 1). Next, icing was performed by accreting mixed glaze ice from supercooled microdroplets accelerated towards the coating surface (stage 2). After ice solidification, deicing was carried out by applying a centrifugal force to the iced samples (stage 3). Finally, after ice detachment, the samples were placed at room temperature (stage 4) and the cycles were repeated four times in total. The discussion will firstly focus on the durability of coatings with the 30 % of C additive (LIC1-4 samples). After that, the results of coatings based on C and P additives with 20 % content (LIC-C and LIC-P samples) will be presented.

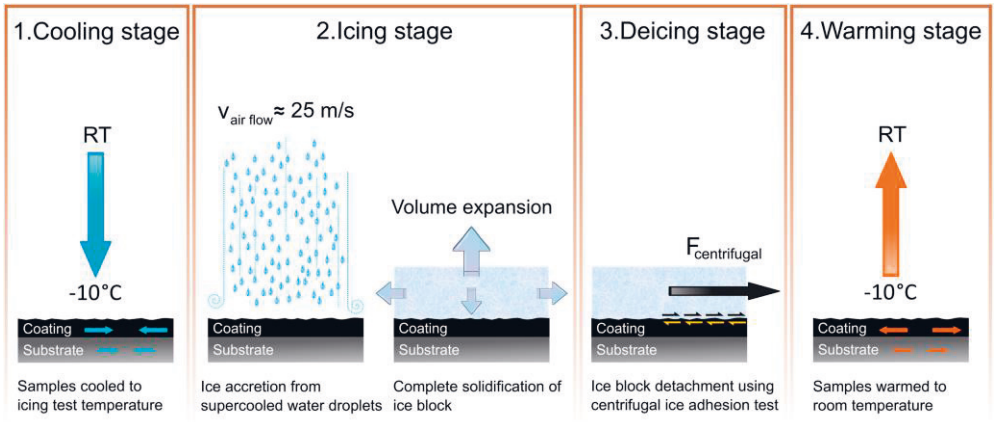

Figure 26. Stages of the cyclic icing/deicing tests. 1) Cooling stage of the samples from room temperature to the icing test temperature. 2) Icing stage with the accretion of mixed glaze ice from supercooled water droplets in the icing wind tunnel and solidification of the ice block. 3) Deicing stage with the removal of the ice block using the centrifugal ice adhesion tester. 4) Warming stage with samples stored at room temperature [Publication IV].

The ice adhesion values measured at each cycle for LICs with 30 % of C additive in the coating structure are presented in Figure 27. All the lubricated coatings exhibited ice adhesion values below 50 kPa in the first cycle. Moreover, all the coatings demonstrated a general increase in ice adhesion strength from the first to the second cycle. This increase in ice adhesion strength corresponded to a reduction in the icephobicity of surfaces. After the second cycle, all the coatings showed increased ice adhesion, except for LIC1, which seemed to exhibit a more stable icephobic behaviour. Similarly, coatings LIC2 and LIC3* seemed to stabilise their icephobic behaviour after the third cycle. In contrast, coatings LIC3 and LIC4 degraded gradually until the fourth cycle. Due to the significant variations in icephobic behaviour from the low to the medium-low ice adhesion limit, this study considered

four cycles to be sufficient to evaluate the icing performance of such coatings. Despite their decreased icephobicity across the cycles, all the LICs maintained an ice adhesion strength of below 100 kPa, thus retaining their icephobicity within the medium-low ice adhesion level.

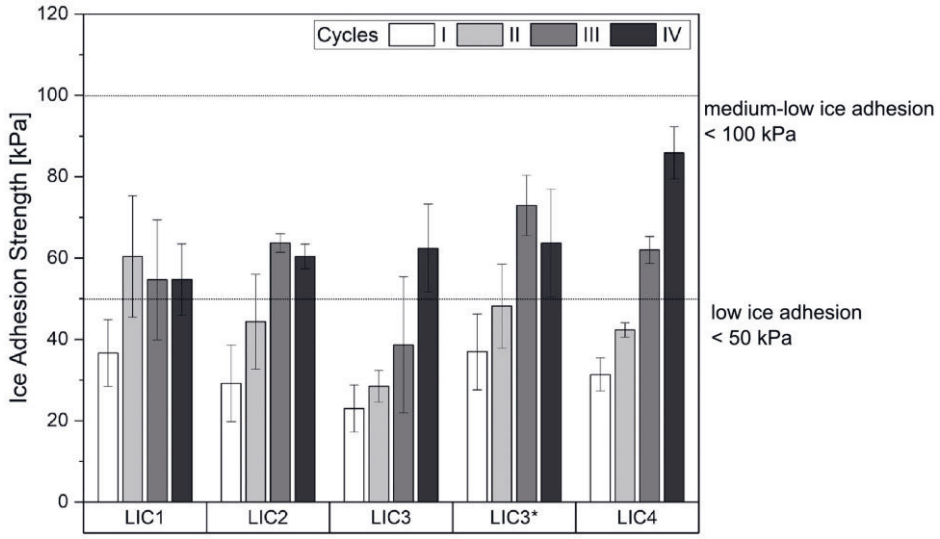

Figure 27. Ice adhesion results for all LICs over four icing/deicing cycles [Publication IV].

Increased ice adhesion over the cycles was probably due to changes in surface properties produced during consecutive icing/deicing actions [98], [156]. Previous studies have shown that mechanical damage and variations in surface chemistry constitute the main causes of decreased icephobic performance for icephobic coatings [82], [155], [156], [159], [195], [199]. Figure 28 shows the surface topography and micrographs of all the coating surfaces before and after four icing/deicing cycles. All the coatings were mechanically damaged after the cyclic tests, as seen from the micrographic analyses. The micrographs revealed different defects, such as surface erosion, scratches and cracks. Surface defects, most commonly scratches, were produced for all the coatings, which were also visible from optical analyses, as reported in the supporting information of Publication IV. However, a few scratches were already evident before icing from the micrographs of the LIC1 and LIC2 samples. Moreover, cracking of the surfaces was revealed between the unmelted particles, indicated in Figure 28, for samples LIC3 and LIC4.

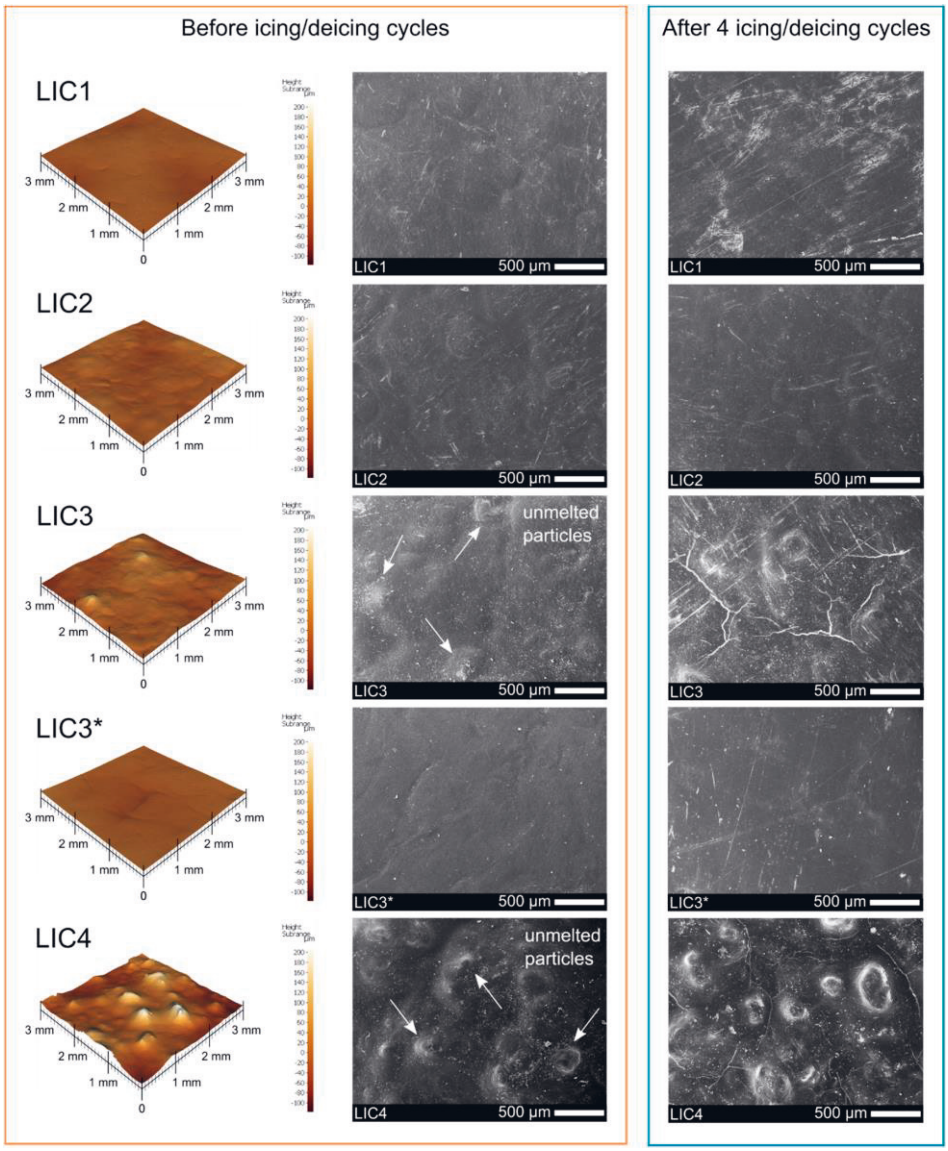

Figure 28. Surface topographies and morphologies of the coatings before and after four icing/deicing cycles. Optical profilometer images of the surface areas before icing/deicing cycles (left). The colour scale in the images indicates the height of the surface: a lighter colour for peaks and a darker colour for valleys. Electron microscope images of the coating surface before (middle) and after four icing/deicing cycles (right) [Publication IV].

The areas between unmelted particles were assumed to be the lubricant-rich regions of the coating surfaces. The experiments showed that cracking occurred after the cooling stage (stage 1) of the icing/deicing tests. However, crack formation was not

revealed after the cooling stage if these coatings were deposited on an LDPE substrate (matrix material). Therefore, the effect of the substrate material on the cracking behaviour was further investigated. A significant mismatch was found between the coefficient of thermal expansions (CTE) of the free coating ($182.4 \pm 1.7 \times 10^{-6}\ °C^{-1}$) and the stainless steel substrate ($15.1 \pm 0.1 \times 10^{-6}\ °C^{-1}$). Considering that the coating had a higher CTE than the substrate material, the latter may constrain the coating from shrinking during the cooling stage, thus inducing tensile stresses in the coating [195, 295]. If induced tensile stresses exceed the cohesive strength of the coating, cracking can occur [296, 297]. For these reasons, crack formation was assumed to be caused by the tensile stresses induced in the coating during cooling, which exceeded the low cohesive strength of the lubricant-rich regions between the unmelted particles of the coating surface. However, the latter issue was not verified for coatings fabricated using different combinations of process parameters (the coatings LIC1, LIC2, LIC3 and LIC3*), previously presented in Figure 19. The results regarding crack formation are discussed in more detail in Publication IV.

Mechanical damage of surfaces definitively represented one cause of the gradual increase in ice adhesion strength for LICs over the cycles, as found in other studies [136, 166, 205, 209]. The presence of surface scratches after the cycles produced a slight increase in average height, Sa, and maximum height, Sz, for all the coatings. However, the Sa and Sz values varied within the standard deviation for most of the coatings. A more significant difference was measured before and after the cycles for the developed interfacial area value, Sdr. The increased area due to mechanical damage may increase mechanical interlocking between the ice and surface features, thus probably explaining the increased ice adhesion strength over the cycles [56]. However, a relationship between the degree of increased interfacial area and the increased ice adhesion could not be systematically established in this study for LICs. Possibly, additional factors could have influenced the icephobicity of such surfaces.

Wetting properties were measured before and after the cycles to better understand the durability of the surfaces when subjected to multiple icing/deicing cycles. According to the wetting results, all the coatings showed a slight reduction in apparent WCA after the cycles, while their hydrophobic character was retained (apparent water contact angle > 90° for all the coatings). However, the values varied within the standard deviation of the measurements for most of the samples. Similar results were observed in other studies, where the decrease in wetting properties was correlated to a decrease in coating icephobicity after the cycles [103, 136, 162, 166, 298]. The changes in surface morphology probably caused the reduction in surface

hydrophobicity, roughness and surface chemistry during the cycles [78]. Mechanical damage of the surfaces during the cycles resulted in changes in surface roughness. Moreover, mechanical damage might alter the local surface chemistry of the coatings as a result of material removal. However, chemical analysis of the surfaces indicated no changes in the surface chemistry before and after the cycles. As a result, the primary cause for the decreased hydrophobicity of surfaces was related to mechanical damage and the presence of scratches might have reduced the hydrophobic character of the surfaces. Moreover, the soft additive, which is more hydrophobic than the matrix material, could have been removed from the surface locally during deicing. This local elimination might account for the modest decrease in hydrophobicity at the surface.

One of the most interesting results of the cyclic tests was the stable icephobic behaviour of the LIC1 sample, although this surface was not the most icephobic one compared to all the other coatings in the first cycle (Figure 22). Several factors could have determined the stability in the icephobic behaviour of this coating. At first, LIC1 was one of the smoothest surface morphologies of this study, together with LIC3*, as revealed by the optical profilometry analysis described in Section 7.2. It was demonstrated that smoother surfaces reduced the formation of mechanical interlocking between the ice and the surface features compared to rougher surfaces [56]. This characteristic could be beneficial during repeated icing/deicing tests since it reduces mechanical interlocking and decreases the possibility of surface damage by ice removal [209]. Additionally, the compositional study of LICs using thermal analyses revealed that LIC1 contained a C additive content of approximately 20-25 m% after deposition, which was lower (approximately half) than the other coatings. This finding was justified by the higher heat input employed to process this coating (no additional compressed air) compared to the other coatings. The warmer combustion flame with no additional air could have vaporised part of the C additive during spraying, thus reducing its amount in the coating structure. Moreover, the reduced quantity of lubricant in the coating structure might have increased the mechanical resistance of the coating surface to ice removal during deicing. Therefore, the more stable icephobicity of the LIC1 sample could derive from a combination of topographical characteristics of the coating surface and lubricating additive content.

To verify the hypotheses on the stable icephobic behaviour of the LIC1 sample, two coatings with relatively smooth surfaces, namely LIC-C and LIC-C*, were fabricated with a reduced amount of cottonseed oil additive (imposed theoretical percentage of C additive of 20 %). From the thermal analyses, the C content in both

coatings after deposition was calculated to be around 18 m%. The durability of these coatings was again evaluated under repeated icing/deicing cycles, and the ice adhesion values obtained at each cycle are presented in Figure 29. The ice adhesion values of LIC-C and LIC-C* coatings were maintained over the cycles within the low and medium-low ice adhesion limits. The coatings showed relatively stable ice adhesion strength values, which varied within the standard deviations over the cycles. Therefore, a more stable icephobic behaviour was obtained for coatings with a reduced amount of C additive. This finding suggested that reducing the C additive in the coating structure could be beneficial in improving the durability of the icephobic properties of lubricated coatings.

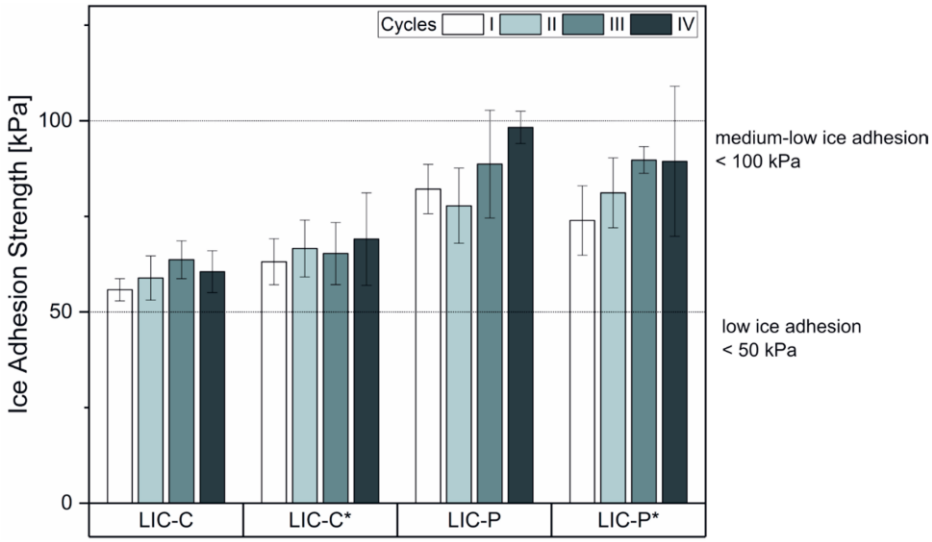

Figure 29. Ice adhesion results for lubricated icephobic coatings (LICs) under four icing/deicing cycles. C and P refer to fully hydrogenated cottonseed oil and paraffinic wax additives, respectively. The asterisk indicates the post-heating treatment by flame [Publication III].

After the cycles, the surfaces were analysed to detect any defect produced during the cyclic tests. The micrographs revealed the presence of scratches on the surfaces of LIC-C and LIC-C* coatings. However, the mechanical damage was visibly lower compared to coatings with a higher C additive content. The revealed surface scratches seemed to not have a significant effect on the icephobic behaviour of LIC-C and LIC-C* coatings, which remained stable over the cycles. Moreover, no substantial changes in surface roughness and surface chemistry were revealed after the cycles. The results on wetting properties indicated that the coatings had a slight

reduction in apparent WCA after the cycles. This slight decrease in hydrophobicity might be related to the presence of a few scratches. In contrast to the apparent WCA results, the cycles affected the water mobility behaviour of the surfaces. After the cycles, no roll-off angles were observed for the LIC-C and LIC-C* coatings, which initially had roll-off angles of around 73° and 49°, respectively. This result was due to water droplets that became trapped in surface defects, such as scratches, formed during the cyclic testing.

The LIC-P and LIC-P* coatings showed higher ice adhesion values compared to the C-based coatings and a slight increase in ice adhesion over the cycles (Figure 29). However, no scratches were revealed on the surfaces of P-based coatings after the cycles, thus demonstrating higher mechanical durability to wear against ice shedding in comparison to the C-based coatings. Therefore, this additive could be considered an alternative to the C additive for further developments of such lubricated coatings.

In summary, this work examined the durability of flame-sprayed lubricated icephobic coatings (LICs) under repeated icing/deicing cycles. Different lubricated coatings underwent repeated icing/deicing cycles, such as coatings with 30 % C additive (LIC1-4), coatings with 20 % C additive (LIC-C and LIC-C*) and coatings with 20 % P additive. Concerning the coatings with 30 % C additive, all the LICs showed low ice adhesion behaviour below 50 kPa at the first icing/deicing cycle. Over the cycles, some coatings (LIC1, LIC2 and LIC3*) tended to maintain a stable icephobic behaviour, while other coatings (LIC3 and LIC4) showed a progressive loss of icephobicity. Surface defects, mainly scratches, were revealed on the surfaces, with a minor reduction in surface hydrophobicity and increased surface roughness. The LIC1 sample demonstrated the most stable icephobic behaviour of all the coatings. This coating was characterised by a relatively smooth surface and a reduced content of the lubricating additive after deposition. Therefore, relatively smooth coatings with reduced C additive content were fabricated (LIC-C and LIC-C*). The results showed that the reduction in C content was beneficial for obtaining more stable icephobic behaviour over the cycles. Furthermore, no significant changes in surface roughness, water contact angle and surface chemistry were revealed after the cycles with the characterisation methods, although minor surface scratches were detected after the cycles. Finally, the P-based coatings showed higher ice adhesion values compared to the C-based coatings. However, no scratches were revealed on the surfaces of P-based coatings after the cycles, demonstrating better mechanical durability than the C-based coatings.

7.4 The durability of lubricated coatings under various environmental stresses

Icephobic coatings may come into contact with various outdoor environments during their use in different applications. Therefore, lubricated coatings were immersed in corrosive media, such as acidic, saline and basic solutions to mimic their exposure to acidic rain, saline environments and solutions of cleaning agents and detergents. Two LIC coatings were selected for this investigation, which contained 20 % of lubricating additive in their structure, namely LIC-C* with cottonseed oil additive and LIC-P* with paraffinic wax additive. In addition, variations in chemical composition and surface morphology were investigated after 60 days of immersion to assess their durability in these environments.

Surface chemical characterisations were performed for LIC-C* and LIC-P* using FTIR. The spectra of the as-received coatings were compared to those obtained after 60 days of immersion in different solutions, and the results are presented in Figure 30. The FTIR spectra of LIC-C* coatings (Figure 30a) revealed no significant changes in the chemical composition of surfaces when exposed to acidic and saline environments. However, slight alterations in the chemical structure were observed for the basic environment. Weak signals were detected in the range from 1650 to 1500 cm^{-1}. These signals probably corresponded to the presence of alkene bonds [299, 300], which constitute one of the initial products of degradation in polyolefins [294]. Moreover, a higher peak intensity was detected at 1740 cm^{-1} and 1173 cm^{-1}, corresponding to the increased presence of ester bonds. Finally, a weak signal was detected between 3700 and 3200 cm^{-1}, probably indicating the presence of hydroxyl bonds [299, 300]. Hydroxyl bonds and the increased intensity of ester bonds might account for the formation of the hydrolysis products of esters, which are primarily carboxylic acids [300]. The FTIR spectra of LIC-P* coatings (Figure 30b) demonstrated no significant chemical changes for surfaces in contact with all the studied corrosive media. Therefore, the paraffinic wax additive better preserved its chemical composition after immersion compared to the fully hydrogenated cottonseed oil additive. Additionally, thermogravimetric studies revealed no absorbed water after 60 days of immersion in the coating structures, suggesting that both lubricated coatings had good barrier properties to water absorption in the studied conditions.

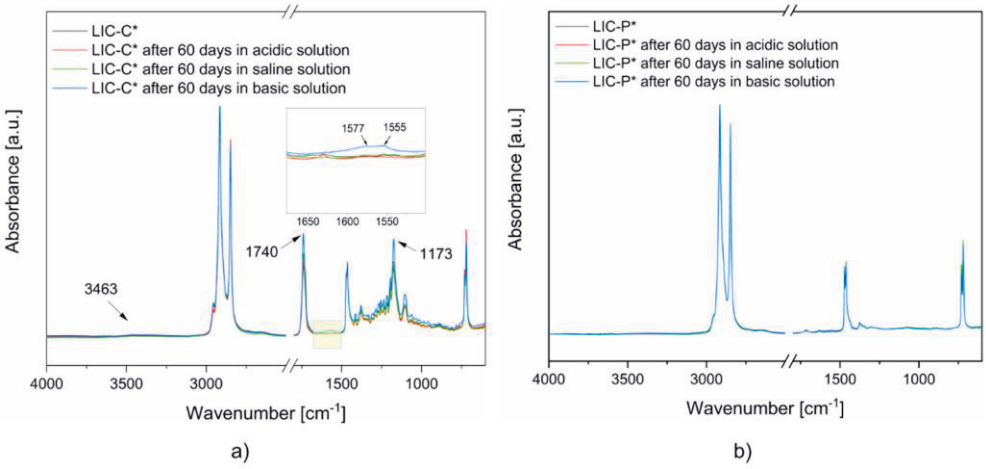

Figure 30. FTIR spectra of LICs surfaces after ageing in different environments: (a) LIC-C*, and (b) LIC-P*. The regions of the spectra are highlighted by yellow boxes when chemical modifications are detected [Publication III].

After immersion, the coating morphologies were analysed to determine their durability in the studied corrosive environments. Figure 31 shows the surface morphologies of the coatings after 60 days of immersion in acidic, saline and basic solutions. The results showed that the surface morphologies of the as-received coatings altered after immersion. The surfaces of as-received coatings were characterised by small protuberances, which were not detected after immersion. Therefore, structural modifications of the coating surfaces were produced in all the solutions. Regarding LIC-C* samples, the surfaces were characterised by flake-like structures after immersion. Moreover, patches of flake-like structures were observed for samples submerged in basic solutions. These flakes could originate from the hydrolytic degradation of the C additive, which could be the most susceptible coating component to hydrolysis. Moreover, structural changes were also observed for the LIC-P* samples after immersion. The immersion in acidic solutions produced finer structures in comparison to saline and basic environments. The revealed structural changes caused variations in surface morphology and surface chemistry for the lubricated coatings, both of which could affect the icephobic behaviour of the coatings after immersion [83, 209, 210]. However, further research is required to establish these correlations.

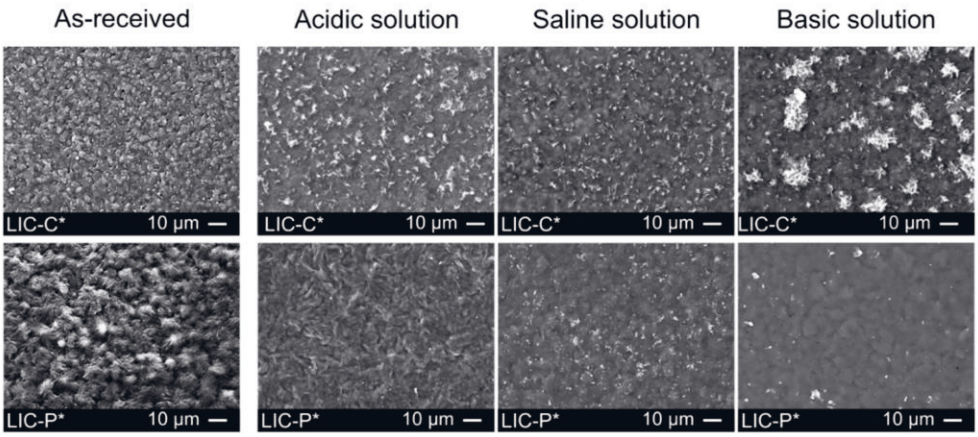

Figure 31. Micrographs of the surface morphologies of LICs after 60 days of immersion in acidic, saline, and basic solutions [Publication III].

Water-induced degradation of polymers, i.e. hydrolysis, can cause cross-linking and the formation of porous structures on the exposed polymer surfaces, thus causing surface structural changes [195]. Moreover, polymers with water-sensitive functional groups are more likely to be affected by hydrolysis [195, 300]. For example, the ester groups found in the C additive are more prone to hydrolysis than the primary and secondary alkyl groups found in polyolefins [195, 299]. This fact could explain the weak hydroxyl signal revealed for all the aged LIC-C* surfaces, which was absent for the LIC-P* surfaces (Figure 30). Moreover, additional factors could influence the effect of hydrolysis, such as surface hydrophobicity, surface porosity and mechanical stresses [195]. For example, the tendency to hydrolysis of the surface decreases with increased hydrophobicity [195]. Therefore, despite the existence of ester bonds, the increased water-repellent characteristics of the LIC-C* samples might have contributed to retarding the hydrolysis reaction in the coatings, thus resulting in minor chemical changes in the surfaces.

Another environmental stress considered in this work for lubricated coatings was the exposure to ultraviolet radiation (UV). Icephobic coatings are typically utilised in outdoor environments, where they are exposed to UV radiation. Degradation of polymers due to UV irradiation generally reduces their performance and shortens their lifetime [211]. Therefore, understanding the degradation process of the polymers used in this work in the presence of UV light is critical to further improve the durability of LICs under these conditions. Figure 32 presents the FTIR spectra of LIC-P* coatings after specific exposure times to UV radiation. According to the results, the aged surfaces exhibited an increased signal intensity in the region between

1850 cm^{-1} and 1650 cm^{-1}. The signal gradually rose in intensity with increasing exposure time up to 1000 h. This signal corresponded to the formation of carbonyl groups in the polymer structure. The broad peak with the strongest signal at 1713 cm^{-1} indicated the formation of numerous oxidation products, such as carboxylic acid, carboxylic ester and carboxylic anhydride, as reported in previous studies on the photodegradation of polyolefins [287, 301, 302].

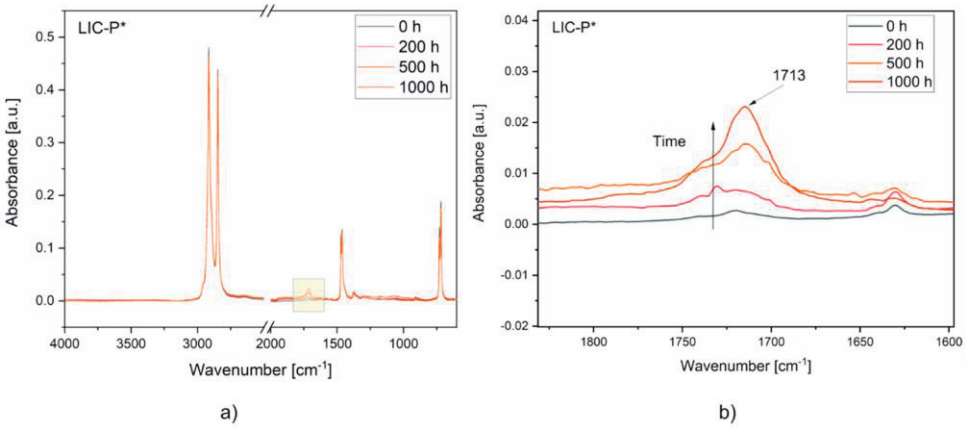

Figure 32. FTIR spectra of the coatings at different exposure times to UV radiation: (a) LIC-P* spectra, (b) LIC-P* spectra enlarged in the region of interest. The spectra region is highlighted by a yellow box when chemical modifications are detected [Publication III].

Figure 33 presents the FTIR spectra of LIC-C* coatings at different exposure times. According to the spectra, the signal intensity progressively increased with exposure time in the region between 2000 and 1000 cm^{-1}. After 200 hours, a slight rise in intensity was observed for the peaks at 1737 and 1173 cm^{-1}. This rise qualitatively indicated the increased stretching signal of the carbonyl bond (C=O) and carbon-oxygen bond (C–O) of the ester group. After 500 hours, the signal intensities of these bonds further increased, and the peak at 1737 cm^{-1} split into two peaks at 1740 cm^{-1} and 1727 cm^{-1}. The first signal at 1740 cm^{-1} indicated a qualitative increase in carbonyl bonds in the polymer structure, and the second signal at 1727 cm^{-1} indicated the formation of carboxylic acids, according to previous work [303]. These findings showed that chemical modifications were produced in the LIC-C* samples after UV exposure, forming oxidation products due to photo-oxidation. Based on the comparison between the LIC-P* and LIC-C* spectra after exposure, the photo-oxidation of LIC-C* coatings was mainly caused by the oxidation of the C additive. No additional peaks were found in the spectra after 1000 h compared to 500 h of

exposure. In general, both coatings demonstrated surface photo-oxidation after exposure to UV radiation. As described in Section 7.1, the ice adhesion values rose with increased surface oxidation for the plain LDPE coatings. The higher the oxidation of the surfaces, the higher was the measured ice adhesion strength. Moreover, a recent study has indicated that the ultraviolet ageing of polyurethane-based coatings has a detrimental effect on their icephobic properties [198]. However, further research is required to ascertain the effect of UV ageing on the icephobicity of lubricated icephobic coatings.

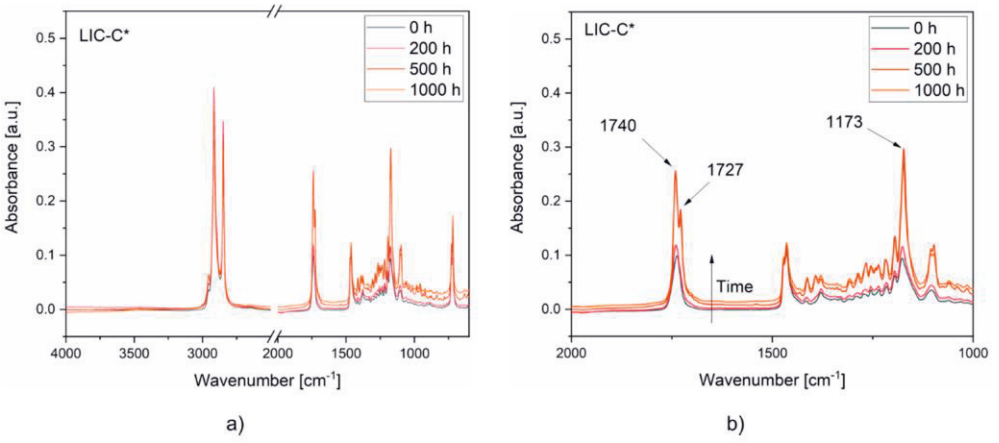

Figure 33. FTIR spectra of the coatings at different exposure times to UV radiation: (a) LIC-C* spectra, (b) LIC-C* spectra enlarged in the region of interest [Publication III].

Photo-oxidation under UV irradiation resulted in colour alterations of the coating surfaces. Figure 34 compares the variation in colour, ΔE^*_{ab}, revealed for the coating surfaces at different exposure times. The colour change value increased with exposure time for LIC-C* coatings but remained stable for LIC-P* coatings. Similar results on colour variations have been found in previous studies for aged polyethylene samples [304]. Moreover, colour observations on aged coatings well correlated with the FTIR results. A more evident variation in colour was found when considerable changes in signal intensities were detected in the FTIR spectra of LIC-C* samples and vice versa for LIC-P* samples. These findings are in accordance with recent research on photodegraded polymers and waxes [305].

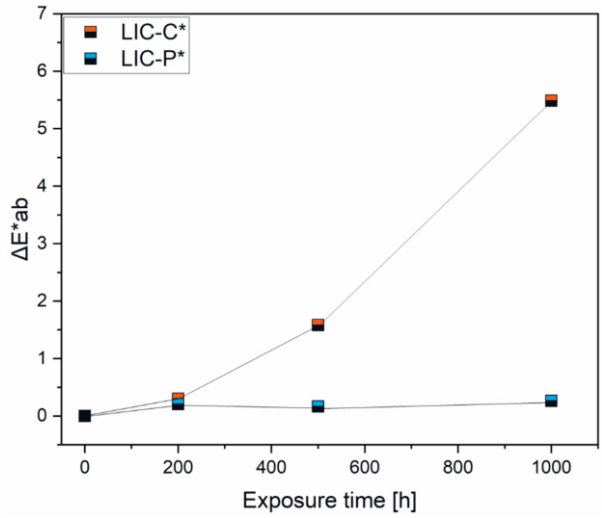

Figure 34. Comparison of colour changes for LIC-C* and LIC-P*coatings at different exposure times to UV irradiation. [Publication III].

Concerning the susceptibility of chemical bonds to UV radiation, the carbonyl groups of ester bonds behave as UV light-absorbing groups [299]. Moreover, ester bonds are more photosensitive than the primary and secondary alkyl groups found in polyolefins [306]. Therefore, the presence of ester bonds in the C additive could explain the reason for the LIC-C* coatings being more susceptible to photodegradation than the LIC-P* coatings. Moreover, non-degraded, pure polyolefins should be resistant to photo-oxidation, considering that they ideally do not absorb UV irradiation. Conversely, the results revealed minor oxidation for the LIC-P* coatings. UV irradiation can be absorbed if unsaturation or carbonyl groups are generated during the production process or if additives sensitive to UV are added [299]. Weak signals were revealed at 1731 cm^{-1} for the LDPE powder feedstock and at 1630 cm^{-1} for the as-received LIC-P* coatings. These signals corresponded to the carbonyl products present in the feedstock material and alkenes produced during the coating fabrication of LIC-P*, respectively. Therefore, their presence in the LIC-P* coatings might have increased their tendency to photodegradation. However, LIC-P* samples better withstood exposure to UV radiation than the LIC-C* samples.

In summary, the durability of lubricated coatings was tested under immersion in various corrosive media, namely acidic, saline and basic solutions, and exposure to UV radiation. Lubricated coatings based on both cottonseed oil additive (LIC-C*) and paraffinic wax additive (LIC-P*) were studied. The LIC-C* and LIC-P* coatings showed good chemical durability in all the studied corrosive media. C-based coatings

demonstrated minor changes in chemical compositions after immersion in basic environments, probably due to hydrolysis of the C additive. After 60 days of immersion, structural changes were observed on the surfaces of both coatings. Moreover, both coatings demonstrated surface photo-oxidation after 1000 hours of exposure to UV radiation, with LIC-C* coatings more oxidised than the LIC-P* coatings.

8 CONCLUSIONS AND SUGGESTIONS FOR FUTURE WORK

For decades, the design and fabrication of novel icephobic coatings with permanent icephobicity and practical durability in various environments have been the primary goal of the scientific community working on mitigating icing problems. In future decades, research on icephobic coating will further develop to meet the requirements of applications facing icing problems. In this work, icephobic polymer coatings were fabricated in one step using flame spray technology. The initial investigation focused on understanding the effect of the process parameters on the icephobic behaviour of plain polyethylene coatings. In the second stage, polymer composite coatings were fabricated by adding a lubricating additive to the polyethylene matrix, to further enhance the icephobicity of such coatings. The final stage of the research focused on a durability assessment of the lubricated coatings. Their durability was tested under various environmental stresses, such as icing/deicing cycles, immersion in corrosive media and exposure to UV radiation, which icephobic coatings might experience in real applications. These tests were performed to increase the understanding on the degradation behaviour of lubricated coatings. The results will support further research in the development of such coatings in future work.

8.1 Scientific contribution

The following discussion addresses the research questions presented in Chapter 5 and describes the scientific contribution of this thesis.

1. How do the flame spray process parameters influence the properties and the icephobicity of plain low-density polyethylene coatings?

The process parameters of spraying distance and transverse speed were varied in the flame spray process to fabricate plain low-density polyethylene coatings. The shorter the spraying distance, the closer is the flame to the substrate or the already deposited material. This condition implies a higher heat transferred to the polymeric material

compared to longer spraying distances. Moreover, the slower the transverse speed of the flame gun, the longer is the deposition time. As a result, the material is heated for a longer time compared to faster transverse speeds. Therefore, the heat input transferred to the polymeric material increases with decreased spraying distance and transverse speed. The higher the heat input transferred to the polymer during spraying, the smoother is the obtained coating surface. It was found that the process parameters had a significant effect on the surface roughness of polyethylene coatings. For a constant spraying distance of 250 mm, the areal roughness Sa varied from 3 μm to 18 μm when transverse speeds of 500 mm/s and 900 mm/s were used, respectively. However, the higher the heat input, the greater the risk of thermal degradation for flame-sprayed polymers. The chemical composition of polyethylene coatings showed the presence of oxidation products due to thermal degradation during flame spraying. The thermal degradation was gradually reduced using a faster transverse speed (900 mm/s) and longer spraying distance (300 mm/s) during the process (signal intensity of oxidation products decreased from 0.30 to 0.07 within the process window analysed in this work). Most importantly, the icephobic behaviour of polyethylene coatings was significantly influenced by thermal degradation and surface oxidation. Ice adhesion strength varied from 123 kPa ± 33 kPa for the most oxidised surface of this work to 32 kPa ± 3 kPa when minor oxidation was detected on the coating surface. Moreover, thermal degradation negatively affected the degree of crystallinity of the polyethylene coatings, which decreased from 41 % to 29 % with increased thermal oxidation within the process window analysed in this work.

2. How does the addition of lubricating additives to the coating structure affect the properties and the icephobicity of flame-sprayed polyethylene coatings?

Two solid lubricating additives were added to low-density polyethylene coatings, namely fully hydrogenated cottonseed oil and paraffinic wax. Compared to the low-density polyethylene material, these additives are characterised by lower surface free energy, which is believed to enhance the icephobicity of surfaces. Three different lubricated coatings were produced by varying the type of additive and its content in the coating structure. Coatings were fabricated with a 30 % cottonseed oil additive, 20 % cottonseed oil additive and 20 % paraffinic wax additive. The addition of both kinds of additives improved the hydrophobicity of the plain low-density polyethylene coatings. Moreover, the results showed that all the lubricated coatings with 30 % cottonseed oil content exhibited low ice adhesion behaviour below

50 kPa, regardless of the surface roughness. The most icephobic coating of this study had an ice adhesion strength of 23 kPa ± 6 kPa. Low ice adhesion behaviour was demonstrated even for the rougher coating of this work (coating with an ice adhesion strength of 31 kPa ± 3 kPa and areal roughness Sa of 37 μm ± 4 μm). These results indicated that adding a 30 % cottonseed oil additive was beneficial in enhancing the icephobicity of plain low-density polyethylene coatings. However, ice adhesion strength increased above 50 kPa when the content of the cottonseed oil additive was reduced from 30 % to 20 %. Therefore, the decrease in additive content negatively affected the icephobic behaviour of lubricated coatings. Finally, the addition of the paraffinic additive seemed to be not beneficial in improving the icephobicity of the plain low-density polyethylene coatings, maintaining their ice adhesion strengths above 50 kPa.

3. How durable are the lubricated icephobic coatings under repeated icing/deicing cycles?

The durability of lubricated icephobic coatings was studied under repeated icing/deicing cycles. Regarding the lubricated coatings with 30 % cottonseed oil content, some coatings demonstrated stable icephobic behaviour, while others showed a gradual increase in adhesion strength over the cycles. The ice adhesion strength increased from values below 50 kPa to 100 kPa over the four cycles for all coatings with a 30 % cottonseed oil content. This increase in ice adhesion strength was related to the formation of defects, mainly surface scratches, formed on the surfaces during ice removal. The formation of surface scratches increased the surface roughness and slightly reduced the surface hydrophobicity of the coatings after the cycles. Regarding the lubricated coatings with a 20 % cottonseed oil content, the ice adhesion strength was stable over the four cycles, varying within the standard deviation of the results. This result indicated that reducing the additive content from 30 % to 20 % was beneficial in achieving stable icephobic behaviour in the lubricated coatings over the cycles. Moreover, surface defects were reduced after the cycles, and no significant variations in surface roughness and hydrophobicity were observed with the employed characterisation methods. Therefore, the durability of the lubricated coatings was improved with a reduction in cottonseed oil content. Finally, coatings with a 20 % paraffinic additive showed higher ice adhesion values and less stable icephobic behaviour over the cycles than those with a 20 % cottonseed oil additive. However, no surface scratches were revealed on the surfaces of coatings

based on paraffinic wax after the cycles, demonstrating better mechanical durability compared to coatings based on cottonseed oil.

4. How durable are the lubricated icephobic coatings under various environmental stresses, such as immersion in corrosive media and exposure to ultraviolet radiation?

The durability of coatings with a 20 % cottonseed oil additive and paraffinic additive was tested under various environmental stresses, such as immersion in acidic, saline and basic solutions and exposure to ultraviolet radiation. According to the results of the immersion experiments, coatings based on cottonseed oil demonstrated good chemical stability in acidic and saline environments. In contrast, changes in chemical composition were revealed after immersion in a basic environment. However, no variations were observed in the chemical composition of coatings based on paraffinic wax after immersion in all the studied corrosive media. As a result, the paraffinic additive showed better chemical stability than the cottonseed oil additive in these conditions. Although no chemical alterations were revealed for coatings based on paraffinic wax, structural changes were observed after immersion for all the studied surfaces. Structural changes generally produce variations in surface morphology and surface chemistry, which may affect the icephobic behaviour of these coatings. However, further research is required to establish these correlations. According to the results on exposure to UV radiation, both coatings showed the presence of photo-oxidation products after exposure. However, the coatings based on paraffinic wax showed less oxidation than those based on cottonseed oil additive. This result was due to the chemical composition of the cottonseed oil additive, which was demonstrated to be more sensitive to photodegradation. Moreover, colour changes after UV exposure were significant in coatings based on cottonseed oil. The colour difference ΔE^*_{ab} was equal to 5.48 between the pristine and aged samples for coatings based on cottonseed oil compared to a value of 0.26 measured for the coatings based on paraffinic wax. These results supported the findings of the chemical analysis. However, further research is required to study the effect of UV ageing on the icephobicity of such lubricated coatings.

8.2 Suggestions for future work

In this thesis, low-density polyethylene coatings were fabricated using flame spray technology. Moreover, lubricating additives with low surface free energy were added to the coatings to further improve their icephobic behaviour. This study demonstrated the feasibility of using flame spraying to produce icephobic coatings with low ice adhesion properties. In the first stage of the research, thermal degradation of the coating surfaces negatively affected the icephobic behaviour of coatings. However, it was not investigated which phenomenon caused by thermal degradation, such as chain scission, cross-linking, oxidation, reduction in mechanical properties or surface embrittlement, had the major effect on the coating icephobicity. Therefore, further research is recommended on these topics. Moreover, previous studies on icephobic surfaces have demonstrated correlations between the bulk properties (Young's modulus and the shear modulus) of the coating material and ice adhesion strength. Therefore, bulk properties could be measured from commercially available materials or bulk samples obtained from the feedstock powder materials (e.g. powder placed in a mould and melted in an oven). Even better, flame spray methods could be used as an additive manufacturing technique to fabricate bulk samples suitable for mechanical testing. However, the latter would require additional experimental work. Furthermore, the relationships between icephobic behaviour and the properties of flame-sprayed coatings, such as surface morphology, surface roughness and wettability, could not be fully explained in this study. This was due to the fact that several coating properties affect icephobicity simultaneously, and it was complex to distinguish the effect of each single property. Moreover, the relationships between the properties could be unclear due to the sensitivity of the employed characterisation techniques. Therefore, more surface-sensitive characterisation techniques are recommended for future studies, which could analyse surface properties in more detail to better understand the factors affecting the icephobicity of such flame-sprayed surfaces.

Regarding the durability assessment of lubricated icephobic coatings under repeated icing/deicing cycles, coatings could be tested using more cycles to establish their long-term performance on a laboratory scale, and different types of ice could be used for these cyclic tests. Moreover, field tests could help to better understand the durability of coatings in use. For example, finding correlations between the ageing of icephobic properties both on laboratory scale and in field use would benefit the development of icephobic coatings. Therefore, collaboration with industrial

partners from sectors that face icing problems would help to further develop this research.

Regarding materials development, an alternative thermoplastic polymer matrix and lubricating additive materials (or even more than two components) could be combined and processed using flame spraying. However, material selection for coating fabrication should be mainly driven by the durability requirement and application of the coating. In this thesis, no specific application was selected for the lubricated coatings. Another suggestion for future work would be to select one or a few applications facing icing problems to understand the possible advantages and limitations of both the fabrication technique and the materials used in this study. This selection would allow the design of lubricating coatings with properties tailored for a specific application. Therefore, this avenue of research is recommended for the future development of lubricated icephobic coatings.

REFERENCES

[1] M.J. Wood, A. Kietzig, "Factors Influencing the Formation, Adhesion, and Friction of Ice", in "Ice Adhesion: Mechanism, Measurement and Mitigation", *Wiley*, pp. 1–54, (2020).

[2] M. Farzaneh, "Atmospheric Icing of Power Networks", *Springer Netherlands*, Dordrecht, (2008).

[3] V.F. Petrenko, "The effect of static electric fields on ice friction", *Journal of Applied Physics*, vol. 76, n. 2, pp. 1216–1219, (1994).

[4] M. Farzaneh, K. Savadjiev, "Statistical Analysis of Field Data for Precipitation Icing Accretion on Overhead Power Lines", *IEEE Transactions on Power Delivery*, vol. 20, n. 2, pp. 1080–1087, (2005).

[5] N. Dalili, A. Edrisy, R. Carriveau, "A review of surface engineering issues critical to wind turbine performance", *Renewable and Sustainable Energy Reviews*, vol. 13, n. 2, pp. 428–438, (2009).

[6] R. Carriveau, A. Edrisy, P. Cadieux, R. Mailloux, "Ice Adhesion Issues in Renewable Energy Infrastructure", *Journal of Adhesion Science and Technology*, vol. 26, n. 4–5, pp. 447–461, (2012).

[7] H.R. Vignisdottir, B. Ebrahimi, G.K. Booto, R. O'Born, H. Brattebø, H. Wallbaum, R.A. Bohne, "A review of environmental impacts of winter road maintenance", *Cold Regions Science and Technology*, vol. 158, pp. 143–153, (2019).

[8] T. Rashid, H.A. Khawaja, K. Edvardsen, "Review of marine icing and anti-/de-icing systems", *Journal of Marine Engineering & Technology*, vol. 15, n. 2, pp. 79–87, (2016).

[9] R.W. Gent, N.P. Dart, J.T. Cansdale, "Aircraft icing", *Philosophical Transactions of the Royal Society A: Mathematical, Physical and Engineering Sciences*, vol. 358, n. 1776, pp. 2873–2911, (2000).

[10] F.T. Lynch, A. Khodadoust, "Effects of ice accretions on aircraft aerodynamics", *Progress in Aerospace Sciences*, vol. 37, n. 8, pp. 669–767, (2001).

[11] B.E.K. Nygaard, J.E. Kristjánsson, L. Makkonen, "Prediction of in-cloud icing

conditions at ground level using the WRF model", *Journal of Applied Meteorology and Climatology*, vol. 50, n. 12, pp. 2445–2459, (2011).

[12] J.-D. Brassard, C. Laforte, F. Guerin, C. Blackburn, "Icephobicity: Definition and Measurement Regarding Atmospheric Icing", in "Advances in Polymer Science", *Springer*, pp. 123–143, (2018).

[13] X. Huang, N. Tepylo, V. Pommier-Budinger, M. Budinger, E. Bonaccurso, P. Villedieu, L. Bennani, "A survey of icephobic coatings and their potential use in a hybrid coating/active ice protection system for aerospace applications", *Progress in Aerospace Sciences*, vol. 105, pp. 74–97, (2019).

[14] L. Vertuccio, F. De Santis, R. Pantani, K. Lafdi, L. Guadagno, "Effective de-icing skin using graphene-based flexible heater", *Composites Part B: Engineering*, vol. 162, pp. 600–610, (2019).

[15] O. Parent, A. Ilinca, "Anti-icing and de-icing techniques for wind turbines: Critical review", *Cold Regions Science and Technology*, vol. 65, n. 1, pp. 88–96, (2011).

[16] R.M. Fillion, A.R. Riahi, A. Edrisy, "A review of icing prevention in photovoltaic devices by surface engineering", *Renewable and Sustainable Energy Reviews*, vol. 32, pp. 797–809, (2014).

[17] J. Lv, Y. Song, L. Jiang, J. Wang, "Bio-Inspired Strategies for Anti-Icing", *ACS Nano*, vol. 8, n. 4, pp. 3152–3169, (2014).

[18] C.C. Ryerson, "Assessment of Superstructure Ice Protection as Applied to Offshore Oil Operations Safety", (2009).

[19] D.M. Ramakrishna, T. Viraraghavan, "Environmental Impact of Chemical Deicers – A Review", *Water, Air, and Soil Pollution*, vol. 166, n. 1, pp. 49–63, (2005).

[20] M.J. Kreder, J. Alvarenga, P. Kim, J. Aizenberg, "Design of anti-icing surfaces: smooth, textured or slippery?", *Nature Reviews Materials*, vol. 1, n. 1, pp. 1–15, (2016).

[21] V. Hejazi, K. Sobolev, M. Nosonovsky, "From superhydrophobicity to icephobicity: Forces and interaction analysis", *Scientific Reports*, vol. 3, (2013).

[22] A.J. Meuler, J.D. Smith, K.K. Varanasi, J.M. Mabry, G.H. McKinley, R.E. Cohen, "Relationships between Water Wettability and Ice Adhesion", *ACS Applied Materials & Interfaces*, vol. 2, n. 11, pp. 3100–3110, (2010).

[23] Y. Shen, X. Wu, J. Tao, C. Zhu, Y. Lai, Z. Chen, "Icephobic materials: Fundamentals, performance evaluation, and applications", *Progress in Materials Science*, vol. 103, pp. 509–557, (2019).

[24] Y. Zhuo, S. Xiao, A. Amirfazli, J. He, Z. Zhang, "Polysiloxane as icephobic materials – The past, present and the future", *Chemical Engineering Journal*, vol. 405, pp. 127088, (2021).

[25] L. Zheng, Z. Li, S. Bourdo, K.R. Khedir, M.P. Asar, C.C. Ryerson, A.S. Biris, "Exceptional superhydrophobicity and low velocity impact icephobicity of acetone-functionalized carbon nanotube films", *Langmuir*, vol. 27, n. 16, pp. 9936–9943, (2011).

[26] S. Jung, M. Dorrestijn, D. Raps, A. Das, C.M. Megaridis, D. Poulikakos, "Are superhydrophobic surfaces best for icephobicity?", *Langmuir*, vol. 27, n. 6, pp. 3059–3066, (2011).

[27] P. Eberle, M.K. Tiwari, T. Maitra, D. Poulikakos, "Rational nanostructuring of surfaces for extraordinary icephobicity", *Nanoscale*, vol. 6, n. 9, pp. 4874–4881, (2014).

[28] C. Antonini, M. Innocenti, T. Horn, M. Marengo, A. Amirfazli, "Understanding the effect of superhydrophobic coatings on energy reduction in anti-icing systems", *Cold Regions Science and Technology*, vol. 67, n. 1–2, pp. 58–67, (2011).

[29] Z. He, W.J. Xie, Z. Liu, G. Liu, Z. Wang, Y.Q. Gao, J. Wang, "Tuning ice nucleation with counterions on polyelectrolyte brush surfaces", *Science Advances*, vol. 2, n. 6, (2016).

[30] G. Bai, D. Gao, Z. Liu, X. Zhou, J. Wang, "Probing the critical nucleus size for ice formation with graphene oxide nanosheets", *Nature*, vol. 576, n. 7787, pp. 437–441, (2019).

[31] S.F. Ahmadi, S. Nath, G.J. Iliff, B.R. Srijanto, C.P. Collier, P. Yue, J.B. Boreyko, "Passive Antifrosting Surfaces Using Microscopic Ice Patterns", *ACS Applied Materials and Interfaces*, vol. 10, n. 38, pp. 32874–32884, (2018).

[32] G. Fang, A. Amirfazli, "Understanding the anti-icing behavior of superhydrophobic surfaces", *Surface Innovations*, vol. 2, n. 2, pp. 94–102, (2014).

[33] S. Rønneberg, J. He, Z. Zhang, "The need for standards in low ice adhesion surface research: a critical review", *Journal of Adhesion Science and Technology*, vol. 34, n. 3, pp. 319–347, (2020).

[34] A. Work, Y. Lian, "A critical review of the measurement of ice adhesion to solid substrates", *Progress in Aerospace Sciences*, vol. 98, pp. 1–26, (2018).

[35] F. Guerin, C. Laforte, M.I. Farinas, J. Perron, "Analytical model based on experimental data of centrifuge ice adhesion tests with different substrates", *Cold Regions Science and Technology*, vol. 121, pp. 93–99, (2016).

[36] A. Laroche, M.J. Grasso, A. Dolatabadi, E. Bonaccurso, "Tensile and Shear Test Methods for Quantifying the Ice Adhesion Strength to a Surface", in "Ice Adhesion:

Mechanism, Measurement and Mitigation", *Wiley*, pp. 237–284, (2020).

[37] K. Golovin, S.P.R. Kobaku, D.H. Lee, E.T. DiLoreto, J.M. Mabry, A. Tuteja, "Designing durable icephobic surfaces", *Science Advances*, vol. 2, n. 3, pp. e1501496, (2016).

[38] L.A. Wilen, J.S. Wettlaufer, M. Elbaum, M. Schick, "Dispersion-force effects in interfacial premelting of ice", *Physical Review B*, vol. 52, n. 16, pp. 12426–12433, (1995).

[39] I.A. Ryzhkin, V.F. Petrenko, "Physical Mechanisms Responsible for Ice Adhesion", *The Journal of Physical Chemistry B*, vol. 101, n. 32, pp. 6267–6270, (1997).

[40] Z. Ghalmi, R. Menini, M. Farzaneh, "Theoretical Studies and Quantification of Ice Adhesion Mechanisms", in "The 13th International Workshop on Atmospheric Icing of Structures", Andermatt, Switzerland, pp. 8–11, (2009).

[41] R. Menini, M. Farzaneh, "Advanced Icephobic Coatings", *Journal of Adhesion Science and Technology*, vol. 25, n. 9, pp. 971–992, (2011).

[42] S. Rønneberg, Y. Zhuo, C. Laforte, J. He, Z. Zhang, "Interlaboratory Study of Ice Adhesion Using Different Techniques", *Coatings*, vol. 9, n. 10, pp. 678, (2019).

[43] S. Rønneberg, C. Laforte, C. Volat, J. He, Z. Zhang, "The effect of ice type on ice adhesion", *AIP Advances*, vol. 9, n. 5, pp. 055304, (2019).

[44] D.E. Packham, "Handbook of Adhesion", Second, *John Wiley & Sons Ltd,* (2005).

[45] J.C. Berg, "Semi-empirical strategies for predicting adhesion", in "Adhesion Science and Engineering", *Elsevier*, pp. 1–73, (2002).

[46] J. Israelachvili, "Intermolecular and Surface Forces", 3rd ed., *Academic press*, (2011).

[47] G.A. Agoston, C. V. Cagle, "Handbook of Adhesive Bonding", *Leonardo*, vol. 8, n. 1, pp. 86, (1975).

[48] A.J. Kinloch, A.J. Kinloch, "Adhesion and adhesives: science and technology", *Springer Science \& Business Media*, (1987).

[49] V. Simpson, "Fundamental studies of adhesion", University of Wollongong, (1997).

[50] V.F. Petrenko, I.A. Ryzhkin, "Surface States of Charge Carriers and Electrical Properties of the Surface Layer of Ice", *Journal of Physical Chemistry B*, vol. 101, n. 32, pp. 6285–6289, (1997).

[51] M. Zou, S. Beckford, R. Wei, C. Ellis, G. Hatton, M.A. Miller, "Effects of surface

roughness and energy on ice adhesion strength", *Applied Surface Science*, vol. 257, n. 8, pp. 3786–3792, (2011).

[52] L.-H. Lee, "Fundamentals of adhesion", *Springer Science \& Business Media*, (2013).

[53] V.F. Petrenko, R.W. Whitworth, "Physics of Ice", *Oxford University Press*, (2002).

[54] S. Thomas, "The Hydrogen Bond in the Solid State", *Angewandte Chemie International Edition*, vol. 41, n. 1, pp. 48–76, (2002).

[55] V.F. Petrenko, S. Peng, "Reduction of ice adhesion to metal by using self-assembling monolayers (SAMs)", *Canadian Journal of Physics*, vol. 81, n. 1–2, pp. 387–393, (2003).

[56] J. Chen, J. Liu, M. He, K. Li, D. Cui, Q. Zhang, X. Zeng, Y. Zhang, J. Wang, Y. Song, "Superhydrophobic surfaces cannot reduce ice adhesion", *Applied Physics Letters*, vol. 101, n. 11, pp. 111603, (2012).

[57] M.R. Kasaai, M. Farzaneh, "Evaluation of Mechanisms of Ice Adhesion on Power Network Equipment", in "23rd International Conference on Offshore Mechanics and Arctic Engineering, Volume 3", vol. 3, *ASMEDC*, pp. 927–932, (2004).

[58] C.J. Van Oss, R.F. Giese, R. Wentzek, J. Norris, E.M. Chuvilin, "Surface Tension Parameters of Ice Obtained From Contact Angle Data and From Positive and Negative Particle Adhesion to Advancing Freezing Fronts", *Journal of Adhesion Science and Technology*, vol. 6, n. 4, pp. 503–516, (1992).

[59] E.J.Y. Ling, V. Uong, J.S. Renault-Crispo, A.M. Kietzig, P. Servio, "Reducing Ice Adhesion on Nonsmooth Metallic Surfaces: Wettability and Topography Effects", *ACS Applied Materials and Interfaces*, vol. 8, n. 13, pp. 8789–8800, (2016).

[60] M.F. Hassan, H.P. Lee, S.P. Lim, "The variation of ice adhesion strength with substrate surface roughness", *Measurement Science and Technology*, vol. 21, n. 7, pp. 75701–9, (2010).

[61] V. Vercillo, S. Tonnicchia, J.M. Romano, A. García-Girón, A.I. Aguilar-Morales, S. Alamri, S.S. Dimov, T. Kunze, A.F. Lasagni, E. Bonaccurso, "Design Rules for Laser-Treated Icephobic Metallic Surfaces for Aeronautic Applications", *Advanced Functional Materials*, vol. 30, n. 16, pp. 1910268, (2020).

[62] H.H.G. Jellinek, "Liquid-like (transition) layer on ice", *Journal of Colloid And Interface Science*, vol. 25, n. 2, pp. 192–205, (1967).

[63] A. Döppenschmidt, H.J. Butt, "Measuring the thickness of the liquid-like layer on ice surfaces with atomic force microscopy", *Langmuir*, vol. 16, n. 16, pp. 6709–6714, (2000).

[64] R. Rosenberg, "Why is ice slippery?", *Physics Today*, vol. 58, n. 12, pp. 50, (2005).

[65] L. Makkonen, "Surface melting of ice", *Journal of Physical Chemistry B*, vol. 101, n. 32, pp. 6196–6200, (1997).

[66] M. Schulz, M. Sinapius, "Evaluation of Different Ice Adhesion Tests for Mechanical Deicing Systems", in "SAE Technical Paper 2015-01-2135", (2015).

[67] K. Golovin, M. Boban, J.M. Mabry, A. Tuteja, "Designing Self-Healing Superhydrophobic Surfaces with Exceptional Mechanical Durability", *ACS Applied Materials and Interfaces*, vol. 9, n. 12, pp. 11212–11223, (2017).

[68] S. Rønneberg, S. Xiao, J. He, Z. Zhang, "Nanoscale correlations of ice adhesion strength and water contact angle", *Coatings*, vol. 10, n. 4, pp. 379, (2020).

[69] M.R. Kasaai, M. Farzaneh, "A Critical Review of Evaluation Methods of Ice Adhesion Strength on the Surface of Materials", in "23rd International Conference on Offshore Mechanics and Arctic Engineering, Volume 3", *ASMEDC*, pp. 919–926, (2004).

[70] A.J. Meuler, G.H. McKinley, R.E. Cohen, "Exploiting topographical texture to impart icephobicity", *ACS Nano*, vol. 4, n. 12, pp. 7048–7052, (2010).

[71] Z. Ghalmi, R. Menini, M. Farzaneh, "Experimental study of the influence of the type of material, roughness and temperature on ice adhesion", in "Proceeding of 14th International Workshop on Atmospheric Icing of Structures", Chongquing, China, pp. 13–18, (2011).

[72] R.M. Fillion, A.R. Riahi, A. Edrisy, "Design factors for reducing ice adhesion", *Journal of Adhesion Science and Technology*, vol. 31, n. 21, pp. 2271–2284, (2017).

[73] S. Yang, Q. Xia, L. Zhu, J. Xue, Q. Wang, Q.M. Chen, "Research on the icephobic properties of fluoropolymer-based materials", *Applied Surface Science*, vol. 257, n. 11, pp. 4956–4962, (2011).

[74] S. Bengaluru Subramanyam, V. Kondrashov, J. Rühe, K.K. Varanasi, S.B. Subramanyam, V. Kondrashov, J. Rgen Rü, K.K. Varanasi, "Low Ice Adhesion on Nano-Textured Superhydrophobic Surfaces under Supersaturated Conditions", *ACS Applied Materials and Interfaces*, vol. 8, n. 20, pp. 12583–12587, (2016).

[75] M. Nosonovsky, V. Hejazi, "Why superhydrophobic surfaces are not always icephobic", *ACS Nano*, vol. 6, n. 10, pp. 8488–8491, (2012).

[76] S.B. Subramanyam, K. Rykaczewski, K.K. Varanasi, "Ice adhesion on lubricant-impregnated textured surfaces", *Langmuir*, vol. 29, n. 44, pp. 13414–13418, (2013).

[77] D. Bottone, V. Donadei, H. Niemelä, H. Koivuluoto, S. Seeger, "Coral-like silicone nanofilament coatings with extremely low ice adhesion", *Scientific Reports*, vol. 11, n. 1, pp.

1–12, (2021).

[78] D. Quéré, "Rough ideas on wetting", *Physica A: Statistical Mechanics and Its Applications*, vol. 313, n. 1–2, pp. 32–46, (2002).

[79] H. Saito, K. Takai, G. Yamauchi, "Water- and ice-repellent coatings", *Surface Coatings International 1997 80:4*, vol. 80, n. 4, pp. 168–171, (1997).

[80] R.N. Wenzel, "Resistance of solid surfaces to wetting by water", *Industrial and Engineering Chemistry*, vol. 28, n. 8, pp. 988–994, (1936).

[81] G. Momen, R. Jafari, M. Farzaneh, "Ice repellency behaviour of superhydrophobic surfaces: Effects of atmospheric icing conditions and surface roughness", *Applied Surface Science*, vol. 349, pp. 211–218, (2015).

[82] S. Rønneberg, "Fundamental Mechanisms of Ice Adhesion", (2020).

[83] H. Memon, J. Liu, D.S.A. De Focatiis, K.S. Choi, X. Hou, "Intrinsic dependence of ice adhesion strength on surface roughness", *Surface and Coatings Technology*, vol. 385, n. October 2019, pp. 125382, (2020).

[84] L. Makkonen, "Ice adhesion - Theory, measurements and countermeasures", *Journal of Adhesion Science and Technology*, vol. 26, n. 4–5, pp. 413–445, (2012).

[85] Q. Fu, X. Wu, D. Kumar, J.W.C. Ho, P.D. Kanhere, N. Srikanth, E. Liu, P. Wilson, Z. Chen, "Development of sol-gel icephobic coatings: Effect of surface roughness and surface energy", *ACS Applied Materials and Interfaces*, vol. 6, n. 23, pp. 20685–20692, (2014).

[86] Z. He, S. Xiao, H. Gao, J. He, Z. Zhang, "Multiscale crack initiator promoted super-low ice adhesion surfaces", *Soft Matter*, vol. 13, n. 37, pp. 6562–6568, (2017).

[87] S. Ozbay, H.Y. Erbil, "On the Relationship between Surface Free Energy and Ice Adhesion of Flat Anti-Icing Surfaces", in "Ice Adhesion: Mechanism, Measurement and Mitigation", *Wiley*, pp. 187–215, (2020).

[88] D.K. Owens, R.C. Wendt, "Estimation of the surface free energy of polymers", *Journal of Applied Polymer Science*, vol. 13, n. 8, pp. 1741–1747, (1969).

[89] W. Rabel, "Einige Aspekte der Benetzungstheorie und ihre Anwendung auf die Untersuchung und Veränderung der Oberflächeneigenschaften von Polymeren", *Farbe Und Lack*, vol. 77, n. 10, pp. 997–1005, (1971).

[90] F.M. Fowkes, "Attractive forces at interfaces", *Industrial & Engineering Chemistry*, vol. 56, n. 12, pp. 40–52, (1964).

[91] D.H. Kaelble, "Dispersion-Polar Surface Tension Properties of Organic Solids", *The Journal of Adhesion*, vol. 2, n. 2, pp. 66–81, (1970).

[92] W. Cui, Y. Jiang, K. Mielonen, T.A. Pakkanen, "The verification of icephobic performance on biomimetic superhydrophobic surfaces and the effect of wettability and surface energy", *Applied Surface Science*, vol. 466, n. October 2018, pp. 503–514, (2019).

[93] S. Ozbay, H.Y. Erbil, "Ice accretion by spraying supercooled droplets is not dependent on wettability and surface free energy of substrates", *Colloids and Surfaces A: Physicochemical and Engineering Aspects*, vol. 504, pp. 210–218, (2016).

[94] D. Chen, M.D. Gelenter, M. Hong, R.E. Cohen, G.H. McKinley, "Icephobic Surfaces Induced by Interfacial Nonfrozen Water", *ACS Applied Materials & Interfaces*, vol. 9, n. 4, pp. 4202–4214, (2017).

[95] L.E. Raraty, D. Tabor, "The Adhesion and Strength Properties of Ice", *Proceedings of the Royal Society A: Mathematical, Physical and Engineering Sciences*, vol. 245, n. 1241, pp. 184–201, (1958).

[96] Z. He, E.T. Vågenes, C. Delabahan, J. He, Z. Zhang, "Room Temperature Characteristics of Polymer-Based Low Ice Adhesion Surfaces", *Scientific Reports*, vol. 7, n. 1, pp. 1–7, (2017).

[97] A. Dotan, H. Dodiuk, C. Laforte, S. Kenig, "The relationship between water wetting and ice adhesion", *Journal of Adhesion Science and Technology*, vol. 23, n. 15, pp. 1907–1915, (2009).

[98] T. Bharathidasan, S.V. Kumar, M.S. Bobji, R.P.S. Chakradhar, B.J. Basu, "Effect of wettability and surface roughness on ice-adhesion strength of hydrophilic, hydrophobic and superhydrophobic surfaces", *Applied Surface Science*, vol. 314, pp. 241–250, (2014).

[99] T. Young, "III. An essay on the cohesion of fluids", *Philosophical Transactions of the Royal Society of London*, vol. 95, pp. 65–87, (1805).

[100] H.J. Butt, J. Liu, K. Koynov, B. Straub, C. Hinduja, I. Roismann, R. Berger, X. Li, D. Vollmer, W. Steffen, M. Kappl, "Contact angle hysteresis", *Current Opinion in Colloid and Interface Science*, vol. 59, pp. 101574, (2022).

[101] T. Huhtamäki, X. Tian, J.T. Korhonen, R.H.A. Ras, "Surface-wetting characterization using contact-angle measurements", *Nature Protocols*, vol. 13, n. 7, pp. 1521–1538, (2018).

[102] A. Dupré, P. Dupré, "Théorie mécanique de la chaleur", (1869).

[103] Z.A. Janjua, B. Turnbull, K.L. Choy, C. Pandis, J. Liu, X. Hou, K.S. Choi, "Performance and durability tests of smart icephobic coatings to reduce ice adhesion", *Applied Surface*

Science, vol. 407, pp. 555–564, (2017).

[104] S.A. Kulinich, M. Farzaneh, "How wetting hysteresis influences ice adhesion strength on superhydrophobic surfaces", *Langmuir*, vol. 25, n. 16, pp. 8854–8856, (2009).

[105] R. Karmouch, G.G. Ross, "Experimental study on the evolution of contact angles with temperature near the freezing point", *Journal of Physical Chemistry C*, vol. 114, n. 9, pp. 4063–4066, (2010).

[106] L. Mazzola, G. Bruno, "Characterization of ice-phobic surfaces: Improvements on contact angle measurements", *Measurement*, vol. 110, pp. 202–210, (2017).

[107] D. Quéré, "Wetting and Roughness", *Annual Review of Materials Research*, vol. 38, n. 1, pp. 71–99, (2008).

[108] K. Golovin, A. Tuteja, "A predictive framework for the design and fabrication of icephobic polymers", *Science Advances*, vol. 3, n. 9, (2017).

[109] D.L. Beemer, W. Wang, A.K. Kota, "Durable gels with ultra-low adhesion to ice", *J. Mater. Chem. A*, vol. 4, n. 47, pp. 18253–18258, (2016).

[110] H. Yao, H. Gao, "Gibson-soil-like materials achieve flaw-tolerant adhesion", *Journal of Computational and Theoretical Nanoscience*, vol. 7, n. 7, pp. 1299–1305, (2010).

[111] Y. Wang, M. Li, T. Lv, Q. Wang, Q. Chen, J. Ding, "Influence of different chemical modifications on the icephobic properties of superhydrophobic surfaces in a condensate environment", *Journal of Materials Chemistry A*, vol. 3, n. 9, pp. 4967–4975, (2015).

[112] Z. He, Y. Zhuo, Z. Zhang, J. He, "Design of Icephobic Surfaces by Lowering Ice Adhesion Strength: A Mini Review", *Coatings*, vol. 11, n. 11, pp. 1343, (2021).

[113] K. Golovin, A. Dhyani, M.D. Thouless, A. Tuteja, "Low-interfacial toughness materials for effective large-scale deicing", *Science (New York, N.Y.)*, vol. 364, n. 6438, pp. 371–375, (2019).

[114] M.K. Chaudhury, K.H. Kim, "Shear-induced adhesive failure of a rigid slab in contact with a thin confined film", *European Physical Journal E*, vol. 23, n. 2, pp. 175–183, (2007).

[115] K. Kendall, "The adhesion and surface energy of elastic solids", *Journal of Physics D: Applied Physics*, vol. 4, n. 8, pp. 1186–1195, (1971).

[116] P. Irajizad, A. Al-Bayati, B. Eslami, T. Shafquat, M. Nazari, P. Jafari, V. Kashyap, A. Masoudi, D. Araya, H. Ghasemi, "Stress-localized durable icephobic surfaces", *Materials Horizons*, vol. 6, n. 4, pp. 758–766, (2019).

[117] C. Wang, T. Fuller, W. Zhang, K.J. Wynne, "Thickness dependence of ice removal stress for a polydimethylsiloxane nanocomposite: Sylgard 184", *Langmuir*, vol. 30, n. 43, pp. 12819–12826, (2014).

[118] E.M. Yorkgitis, K.C. Melancon, A.M. Hine, S.M. Giaquinto, "Glaciphobic polymeric materials", *Journal of Adhesion Science and Technology*, vol. 26, n. 4–5, pp. 681–699, (2012).

[119] H. Murase, K. Nanishi, H. Kogure, T. Fujibayashi, K. Tamura, N. Haruta, "Interactions between heterogeneous surfaces of polymers and water", *Journal of Applied Polymer Science*, vol. 54, n. 13, pp. 2051–2062, (1994).

[120] H. Murase, K. Nanishi, "On the Relationship of Thermodynamic and Physical Properties of Polymers With Ice Adhesion", *Annals of Glaciology*, vol. 6, pp. 146–149, (1985).

[121] H. Becker, "Polymer microfluidic devices", *Talanta*, vol. 56, n. 2, pp. 267–287, (2002).

[122] J.G. Smith, C.J. Wohl, R.E. Kreeger, J. Palacios, T. Knuth, K. Hadley, "Effect of molecular flexibility upon ice adhesion shear strength", in "39th Annual Meeting of the Adhesion Society; 21-24 Feb. 2016; San Antonio, TX; United States", pp. 5–7, (2016).

[123] J.M. Sayward, "Seeking low ice adhesion", (1979).

[124] N.D. Mulherin, J.A. Richter-menge, T.J. Tantillo, L.D. Gould, G.D. Durell, B.C. Elder, "Laboratory test for measurement of adhesion strength of spray ice to coated flat plates", (1990).

[125] G. Fortin, Maryelle Adomou, J. Perron, "Experimental study of hybrid anti-icing systems combining thermoelectric and hydrophobic coatings", *SAE International Journal of Aerospace*, (2011).

[126] O. Gohardani, D.W. Hammond, "Ice adhesion to pristine and eroded polymer matrix composites reinforced with carbon nanotubes for potential usage on future aircraft", *Cold Regions Science and Technology*, vol. 96, pp. 8–16, (2013).

[127] A.G. Kraj, E.L. Bibeau, "Measurement method and results of ice adhesion force on the curved surface of a wind turbine blade", *Renewable Energy*, vol. 35, n. 4, pp. 741–746, (2010).

[128] C. Laforte, C. Blackburn, J. Perron, R. Aubert, "Icephobic Coating Evaluation for Aerospace Application", *55th AIAA/ASME/ASCE/AHS/ASC Structures, Structural Dynamics, and Materials Conference*, pp. 1372, (2014).

[129] T. Strobl, D. Raps, M. Hornung, "Comparative Evaluation of Ice Adhesion Behavior", *World Academy of Science, Engineering and Technology*, vol. 68, pp. 1673–1679, (2012).

[130] C. Antonini, "Superhydrophobicity as a strategy against icing: Analysis of the water/surface dynamic interaction for icing mitigation", Tesi di Dottorato, Universitá degli Studi di Bergamo, Italia, (2011).

[131] M.H. Foder, others, "ISO 12494 "Atmospheric Icing of Structures" and How to Use It", in "The Eleventh International Offshore and Polar Engineering Conference", vol. 4, *International Society of Offshore and Polar Engineers*, Stavanger, Norway, pp. 8, (2001).

[132] C. Stenroos, P. Vuoristo, H. Koivuluoto, "Properties of Icephobic Surfaces in Different Icing Conditions", Master Thesis, Tampere University of Technology, Tampere, Finland, (2015).

[133] C. Wang, W. Zhang, A. Siva, D. Tiea, K.J. Wynne, "Laboratory test for ice adhesion strength using commercial instrumentation", *Langmuir*, vol. 30, n. 2, pp. 540–547, (2014).

[134] K. Matsumoto, T. Kobayashi, "Fundamental study on adhesion of ice to cooling solid surface", *International Journal of Refrigeration*, vol. 30, n. 5, pp. 851–860, (2007).

[135] H. Niemelä-Anttonen, J. Kiilakoski, P. Vuoristo, H. Koivuluoto, "Icephobic Performance of Different Surface Designs and Materials", in "International Workshop on Atmospheric Icing of Structures (IWAIS)", pp. 1–5, (2019).

[136] V. Vercillo, J.T. Cardoso, D. Huerta-Murillo, S. Tonnicchia, A. Laroche, J.A. Mayén Guillén, J.L. Ocaña, A.F. Lasagni, E. Bonaccurso, "Durability of superhydrophobic laser-treated metal surfaces under icing conditions", *Materials Letters: X*, vol. 3, pp. 100021, (2019).

[137] S. Tarquini, C. Antonini, A. Amirfazli, M. Marengo, J. Palacios, "Investigation of ice shedding properties of superhydrophobic coatings on helicopter blades", *Cold Regions Science and Technology*, vol. 100, pp. 50–58, (2014).

[138] Z.A. Janjua, "The influence of freezing and ambient temperature on the adhesion strength of ice", *Cold Regions Science and Technology*, vol. 140, pp. 14–19, (2017).

[139] J.R. Stallabrass, R.D. Price, "On the adhesion of ice to various materials", *National Research Council Canada*, (1962).

[140] L. Makkonen, "Models for the growth of rime, glaze, icicles and wet snow on structures", *Philosophical Transactions of the Royal Society of London. Series A: Mathematical, Physical and Engineering Sciences*, vol. 358, n. 1776, pp. 2913–2939, (2000).

[141] V.F. Petrenko, S. Qi, "Reduction of ice adhesion to stainless steel by ice electrolysis", *Journal of Applied Physics*, vol. 86, n. 10, pp. 5450–5454, (1999).

[142] J. Palacios, E. Smith, J. Rose, R. Royer, "Instantaneous De-Icing of Freezer Ice via

Ultrasonic Actuation", *AIAA Journal*, vol. 49, n. 6, pp. 1158–1167, (2011).

[143] H. Lacks, M. Quatinetz, A. Freiberger, "Ice adhesion apparatus and test method", *ASTM Bulletin*, vol. 224, pp. 48–50, (1957).

[144] C. Laforte, J.L. Laforte, "Deicing strains and stresses of iced substrates", *Journal of Adhesion Science and Technology*, vol. 26, n. 4–5, pp. 603–620, (2012).

[145] R.J. Scavuzzo, M.L. Chu, C.J. Kellackey, "Impact ice stresses in rotating airfoils", *28th Aerospace Sciences Meeting*, vol. 28, n. 7, pp. 450–455, (1991).

[146] C. Laforte, A. Beisswenger, "Icephobic Material Centrifuge Adhesion Test", in "Proceedings of the International Workshop on Atmospheric Icing of Structures (IWAIS XI)", pp. 1–5, (2005).

[147] H. Koivuluoto, C. Stenroos, R. Ruohomaa, G. Bolelli, L. Lusvarghi, P. Vuoristo, "Research on icing behavior and ice adhesion testing of icephobic surfaces", in "International Workshop on Atmospheric Icing of Structures (IWAIS)", Uppsala, pp. 183–188, (2015).

[148] M. Bleszynski, E. Clark, "Current Ice Adhesion Testing Methods and the Need for a Standard: A Concise Review", *Standards*, vol. 1, n. 2, pp. 117–133, (2021).

[149] H. Memon, K. Mirshahidi, K.A. Zarasvand, K. Golovin, D.S.A. De Focatiis, K.S. Choi, X. Hou, "Comparative study on the influence of surface characteristics on de-icing evaluation", *Journal of Materials Science*, vol. 56, n. 30, pp. 17337–17352, (2021).

[150] H.H.G. Jellinek, "Adhesive properties of ice. Part II", pp. 1–10, (1960).

[151] K.F. Voitkovskii, "Mechanical properties of ice", (1960).

[152] S. Kulinich, M. Farzaneh, "Ice adhesion on super-hydrophobic surfaces", *Applied Surface Science*, vol. 255, n. 18, pp. 8153–8157, (2009).

[153] P. Kim, T.S. Wong, J. Alvarenga, M.J. Kreder, W.E. Adorno-Martinez, J. Aizenberg, "Liquid-infused nanostructured surfaces with extreme anti-ice and anti-frost performance", *ACS Nano*, vol. 6, n. 8, pp. 6569–6577, (2012).

[154] T.M. Schutzius, S. Jung, T. Maitra, P. Eberle, C. Antonini, C. Stamatopoulos, D. Poulikakos, "Physics of Icing and Rational Design of Surfaces with Extraordinary Icephobicity", *Langmuir*, vol. 31, n. 17, pp. 4807–4821, (2015).

[155] H.H.G. Jellinek, H. Kachi, S. Kittaka, M. Lee, R. Yokota, "Ice releasing block-copolymer coatings", *Colloid and Polymer Science*, vol. 256, n. 6, pp. 544–551, (1978).

[156] Z. He, Y. Zhuo, J. He, Z. Zhang, "Design and preparation of sandwich-like polydimethylsiloxane (PDMS) sponges with super-low ice adhesion", *Soft Matter*, vol. 14, n. 23, pp. 4846–4851, (2018).

[157] V.K. Croutch, R.A. Hartley, "Adhesion of Ice to Coatings and the Perfomance of Ice Release Coatings", *Journal of Coatings Technology*, vol. 64, pp. 41–53, (1992).

[158] H. Murase, T. Fujibayashi, "Characterization of molecular interfaces in hydrophobic systems", *Progress in Organic Coatings*, vol. 31, n. 1–2, pp. 97–104, (1997).

[159] C. Neinhuis, W. Barthlott, "Characterization and distribution of water-repellent, self-cleaning plant surfaces", *Annals of Botany*, vol. 79, n. 6, pp. 667–677, (1997).

[160] F. Arianpour, M. Farzaneh, S. Kulinich, "Hydrophobic and ice-retarding properties of doped silicone rubber coatings", *Applied Surface Science*, vol. 265, pp. 546–552, (2013).

[161] L. Cao, A.K. Jones, V.K. Sikka, J. Wu, D. Gao, "Anti-Icing superhydrophobic coatings", *Langmuir*, vol. 25, n. 21, pp. 12444–12448, (2009).

[162] S. Farhadi, M. Farzaneh, S.A. Kulinich, "Anti-icing performance of superhydrophobic surfaces", *Applied Surface Science*, vol. 257, n. 14, pp. 6264–6269, (2011).

[163] R. Jafari, R. Menini, M. Farzaneh, "Superhydrophobic and icephobic surfaces prepared by RF-sputtered polytetrafluoroethylene coatings", *Applied Surface Science*, vol. 257, n. 5, pp. 1540–1543, (2010).

[164] G.R.J. Artus, S. Jung, J. Zimmermann, H.P. Gautschi, K. Marquardt, S. Seeger, "Silicone nanofilaments and their application as superhydrophobic coatings", *Advanced Materials*, vol. 18, n. 20, pp. 2758–2762, (2006).

[165] L.B. Boinovich, E.B. Modin, A.R. Sayfutdinova, K.A. Emelyanenko, A.L. Vasiliev, A.M. Emelyanenko, "Combination of Functional Nanoengineering and Nanosecond Laser Texturing for Design of Superhydrophobic Aluminum Alloy with Exceptional Mechanical and Chemical Properties", *ACS Nano*, vol. 11, n. 10, pp. 10113–10123, (2017).

[166] S. Asadollahi, M. Farzaneh, L. Stafford, "On the Icephobic Behavior of Organosilicon-Based Surface Structures Developed Through Atmospheric Pressure Plasma Deposition in Nitrogen Plasma", *Coatings*, vol. 9, n. 10, pp. 679, (2019).

[167] S.A. Kulinich, S. Farhadi, K. Nose, X.W. Du, "Superhydrophobic surfaces: Are they really ice-repellent?", *Langmuir*, vol. 27, n. 1, pp. 25–29, (2011).

[168] K.K. Varanasi, T. Deng, J.D. Smith, M. Hsu, N. Bhate, "Frost formation and ice adhesion on superhydrophobic surfaces", *Applied Physics Letters*, vol. 97, n. 23, pp. 234102,

(2010).

[169] T.S. Wong, S.H. Kang, S.K.Y. Tang, E.J. Smythe, B.D. Hatton, A. Grinthal, J. Aizenberg, "Bioinspired self-repairing slippery surfaces with pressure-stable omniphobicity", *Nature*, vol. 477, n. 7365, pp. 443–447, (2011).

[170] Y. Liu, Y. Tian, J. Chen, H. Gu, J. Liu, R. Wang, B. Zhang, H. Zhang, Q. Zhang, "Design and preparation of bioinspired slippery liquid-infused porous surfaces with anti-icing performance via delayed phase inversion process", *Colloids and Surfaces A: Physicochemical and Engineering Aspects*, vol. 588, pp. 124384, (2020).

[171] W.S.Y. Wong, K.I. Hegner, V. Donadei, L. Hauer, A. Naga, D. Vollmer, "Capillary Balancing: Designing Frost-Resistant Lubricant-Infused Surfaces", *Nano Letters*, vol. 20, n. 12, pp. 8508–8515, (2020).

[172] P.W. Wilson, W. Lu, H. Xu, P. Kim, M.J. Kreder, J. Alvarenga, J. Aizenberg, "Inhibition of ice nucleation by slippery liquid-infused porous surfaces (SLIPS)", *Physical Chemistry Chemical Physics*, vol. 15, n. 2, pp. 581–585, (2013).

[173] H. Niemelä-Anttonen, H. Koivuluoto, M. Tuominen, H. Teisala, P. Juuti, J. Haapanen, J. Harra, C. Stenroos, J. Lahti, J. Kuusipalo, J.M. Mäkelä, P. Vuoristo, "Icephobicity of Slippery Liquid Infused Porous Surfaces under Multiple Freeze-Thaw and Ice Accretion-Detachment Cycles", *Advanced Materials Interfaces*, vol. 5, n. 20, pp. 1800828, (2018).

[174] S. Ozbay, C. Yuceel, H.Y. Erbil, "Improved Icephobic Properties on Surfaces with a Hydrophilic Lubricating Liquid", *ACS Applied Materials and Interfaces*, vol. 7, n. 39, pp. 22067–22077, (2015).

[175] R. Dou, J. Chen, Y. Zhang, X. Wang, D. Cui, Y. Song, L. Jiang, J. Wang, "Anti-icing coating with an aqueous lubricating layer", *ACS Applied Materials and Interfaces*, vol. 6, n. 10, pp. 6998–7003, (2014).

[176] J. Chen, R. Dou, D. Cui, Q. Zhang, Y. Zhang, F. Xu, X. Zhou, J. Wang, Y. Song, L. Jiang, "Robust prototypical anti-icing coatings with a self-lubricating liquid water layer between ice and substrate", *ACS Applied Materials and Interfaces*, vol. 5, n. 10, pp. 4026–4030, (2013).

[177] X. Yin, Y. Zhang, D. Wang, Z. Liu, Y. Liu, X. Pei, B. Yu, F. Zhou, "Integration of Self-Lubrication and Near-Infrared Photothermogenesis for Excellent Anti-Icing/Deicing Performance", *Advanced Functional Materials*, vol. 25, n. 27, pp. 4237–4245, (2015).

[178] M.J. Coady, M. Wood, G.Q. Wallace, K.E. Nielsen, A.-M. Kietzig, F.O. Lagugnelabarthet, P.J. Ragogna, "Icephobic Behavior of UV-Cured Polymer Networks Incorporated into Slippery Lubricant-Infused Porous Surfaces: Improving SLIPS Durability", *ACS Applied Materials and Interfaces*, vol. 10, n. 3, pp. 2890–2896, (2018).

[179] H.Y. Erbil, "Improvement of lubricant-infused surfaces for anti-icing applications", *Surface Innovations*, vol. 4, n. 4, pp. 214–217, (2016).

[180] K. Rykaczewski, S. Anand, S.B. Subramanyam, K.K. Varanasi, "Mechanism of frost formation on lubricant-impregnated surfaces", *Langmuir*, vol. 29, n. 17, pp. 5230–5238, (2013).

[181] Y. Zhuo, F. Wang, S. Xiao, J. He, Z. Zhang, "One-Step Fabrication of Bioinspired Lubricant-Regenerable Icephobic Slippery Liquid-Infused Porous Surfaces", *ACS Omega*, vol. 3, n. 8, pp. 10139–10144, (2018).

[182] A. Sandhu, O.J. Walker, A. Nistal, K.L. Choy, A.J. Clancy, "Perfluoroalkane wax infused gels for effective, regenerating, anti-icing surfaces", *Chemical Communications*, vol. 55, n. 22, pp. 3215–3218, (2019).

[183] D. Wu, L. Ma, F. Zhang, H. Qian, B. Minhas, Y. Yang, X. Han, D. Zhang, "Durable deicing lubricant-infused surface with photothermally switchable hydrophobic/slippery property", *Materials and Design*, vol. 185, pp. 108236, (2020).

[184] G. Zhang, Q. Zhang, T. Cheng, X. Zhan, F. Chen, "Polyols-Infused Slippery Surfaces Based on Magnetic Fe3O4-Functionalized Polymer Hybrids for Enhanced Multifunctional Anti-Icing and Deicing Properties", *Langmuir*, vol. 34, n. 13, pp. 4052–4058, (2018).

[185] P. Irajizad, M. Hasnain, N. Farokhnia, S.M. Sajadi, H. Ghasemi, "Magnetic slippery extreme icephobic surfaces", *Nature Communications*, vol. 7, n. 1, pp. 1–7, (2016).

[186] S.H. Lee, M. Seong, M.K. Kwak, H. Ko, M. Kang, H.W. Park, S.M. Kang, H.E. Jeong, "Tunable Multimodal Drop Bouncing Dynamics and Anti-Icing Performance of a Magnetically Responsive Hair Array", *ACS Nano*, vol. 12, n. 11, pp. 10693–10702, (2018).

[187] S. Wu, Y. Du, Y. Alsaid, D. Wu, M. Hua, Y. Yan, B. Yao, Y. Ma, X. Zhu, X. He, "Superhydrophobic photothermal icephobic surfaces based on candle soot", *Proceedings of the National Academy of Sciences*, vol. 117, n. 21, pp. 11240–11246, (2020).

[188] G. Jiang, L. Chen, S. Zhang, H. Huang, "Superhydrophobic SiC/CNTs Coatings with Photothermal Deicing and Passive Anti-Icing Properties", *ACS Applied Materials and Interfaces*, vol. 10, n. 42, pp. 36505–36511, (2018).

[189] C. Urata, R. Hönes, T. Sato, H. Kakiuchida, Y. Matsuo, A. Hozumi, "Textured Organogel Films Showing Unusual Thermoresponsive Dewetting, Icephobic, and Optical Properties", *Advanced Materials Interfaces*, vol. 6, n. 2, pp. 1801358, (2019).

[190] A. Kim, S. Kim, M. Huh, H. Kim, C. Lee, "Superior anti-icing strategy by combined sustainable liquid repellence and electro/photo-responsive thermogenesis of oil/MWNT

composite", *Journal of Materials Science & Technology*, vol. 49, pp. 106–116, (2020).

[191] P. Wang, T. Yao, Z. Li, W. Wei, Q. Xie, W. Duan, H. Han, "A superhydrophobic/electrothermal synergistically anti-icing strategy based on graphene composite", *Composites Science and Technology*, vol. 198, pp. 108307, (2020).

[192] S. Dash, J. de Ruiter, K.K. Varanasi, "Photothermal trap utilizing solar illumination for ice mitigation", *Science Advances*, vol. 4, n. 8, pp. eaat0127, (2018).

[193] F. Wang, Y. Zhuo, Z. He, S. Xiao, J. He, Z. Zhang, "Dynamic Anti-Icing Surfaces (DAIS)", *Advanced Science*, vol. 8, n. 21, pp. 2101163, (2021).

[194] K. Alasvand Zarasvand, C. Pope, M. Mohseni, D. Orchard, C. Clark, K. Golovin, "Metallic Plate Buckling As a Low Adhesion Mechanism for Durable and Scalable Icephobic Surface Design", *Advanced Materials Interfaces*, vol. 9, n. 1, pp. 2101402, (2022).

[195] A. Hakimian, S. Nazifi, H. Ghasemi, "Durability Assessment of Icephobic Coatings", in "Ice Adhesion: Mechanism, Measurement and Mitigation", *Wiley*, pp. 521–545, (2020).

[196] J.L. Laforte, M.A. Allaire, J. Laflamme, "State-of-the-art on power line de-icing", *Atmospheric Research*, vol. 46, n. 1–2, pp. 143–158, (1998).

[197] S.A. Kulinich, D. Masson, X. Du, A.M. Emelyanenko, "Testing the Durability of Anti-Icing Coatings", in "Ice Adhesion: Mechanism, Measurement and Mitigation", *Wiley*, pp. 495–520, (2020).

[198] N. Rehfeld, B. Speckmann, C. Schreiner, V. Stenzel, "Assessment of Icephobic Coatings—How Can We Monitor Performance Durability?", *Coatings*, vol. 11, n. 6, pp. 614, (2021).

[199] E. Tetteh, E. Loth, "Reducing Static and Impact Ice Adhesion with a Self-Lubricating Icephobic Coating (SLIC)", *Coatings*, vol. 10, n. 3, pp. 262, (2020).

[200] S. Brown, J. Lengaigne, N. Sharifi, M. Pugh, C. Moreau, A. Dolatabadi, L. Martinu, J.E. Klemberg-Sapieha, "Durability of superhydrophobic duplex coating systems for aerospace applications", *Surface and Coatings Technology*, vol. 401, pp. 126249, (2020).

[201] C. Laforte, J.-L. Laforte, "Tensile, Torsional and Bending Strain at the Adhesive Rupture of an Iced Substrate", in "International Conference on Offshore Mechanics and Arctic Engineering", vol. 43451, pp. 79–86, (2009).

[202] M. Balordi, G. Santucci de Magistris, C. Chemelli, "A Novel Simple Anti-Ice Aluminum Coating: Synthesis and In-Lab Comparison with a Superhydrophobic Hierarchical Surface", *Coatings*, vol. 10, n. 2, pp. 111, (2020).

[203] L.B. Boinovich, A.M. Emelyanenko, V.K. Ivanov, A.S. Pashinin, "Durable icephobic coating for stainless steel", *ACS Applied Materials and Interfaces*, vol. 5, n. 7, pp. 2549–2554, (2013).

[204] N. Sharifi, A. Dolatabadi, M. Pugh, C. Moreau, "Anti-icing performance and durability of suspension plasma sprayed TiO2 coatings", *Cold Regions Science and Technology*, vol. 159, pp. 1–12, (2019).

[205] H. Memon, D.S.A. De Focatiis, K.S. Choi, X. Hou, "Durability enhancement of low ice adhesion polymeric coatings", *Progress in Organic Coatings*, vol. 151, pp. 106033, (2021).

[206] F. Veronesi, G. Boveri, M. Raimondo, "Amphiphobic nanostructured coatings for industrial applications", *Materials*, vol. 12, n. 5, pp. 787, (2019).

[207] P. Irajizad, S. Nazifi, H. Ghasemi, "Icephobic surfaces: Definition and figures of merit", *Advances in Colloid and Interface Science*, vol. 269, pp. 203–218, (2019).

[208] F. Veronesi, G. Guarini, A. Corozzi, M. Raimondo, "Evaluation of the Durability of Slippery, Liquid-Infused Porous Surfaces in Different Aggressive Environments: Influence of the Chemical-Physical Properties of Lubricants", *Coatings*, vol. 11, n. 10, pp. 1170, (2021).

[209] S.A. Kulinich, M. Farzaneh, "On ice-releasing properties of rough hydrophobic coatings", *Cold Regions Science and Technology*, vol. 65, n. 1, pp. 60–64, (2011).

[210] M. Psarski, D. Pawlak, J. Grobelny, G. Celichowski, "Relationships between surface chemistry, nanotopography, wettability and ice adhesion in epoxy and SU-8 modified with fluoroalkylsilanes from the vapor phase", *Applied Surface Science*, vol. 479, pp. 489–498, (2019).

[211] J.R. White, A. Turnbull, "Weathering of polymers: mechanisms of degradation and stabilization, testing strategies and modelling", *Journal of Materials Science*, vol. 29, n. 3, pp. 584–613, (1994).

[212] J.A. Brogan, "Thermal-Spraying of Polymers and Polymer Blends", *MRS Bulletin*, vol. 25, n. 7, pp. 48–53, (2000).

[213] E. Petrovicova, L.S. Schadler, "Thermal spraying of polymers", *International Materials Reviews*, vol. 47, n. 4, pp. 169–190, (2002).

[214] P. Vuoristo, "Thermal Spray Coating Processes", in "Comprehensive Materials Processing", *Elsevier*, pp. 229–276, (2014).

[215] Working Group V7 "Thermal coating Processes" of the Technical Comittee of the German Welding Society (DVS), "Guidelines for thermal spraying of plastics - Technical

Bulletin DVS 2312", Düsseldorf, (2011).

[216] T. Yasui, "The plastic flame-spraying process without preheating", in "Surface engineering international Conference", Tokyo, pp. 163–172, (1988).

[217] P.L. Fauchais, J.V.R. Heberlein, M.I. Boulos, "Thermal Spray Fundamentals", (2014).

[218] J. Brogan, "Processing and Property Relationships of Thermally Sprayed Polymer Systems", (1996).

[219] N. Espallargas, L. Vitoux, S. Armada, "The wear and lubrication performance of liquid-solid self-lubricated coatings", *Surface and Coatings Technology*, vol. 235, pp. 342–353, (2013).

[220] C.R.C. Lima, N.F.C. de Souza, F. Camargo, "Study of wear and corrosion performance of thermal sprayed engineering polymers", *Surface and Coatings Technology*, vol. 220, pp. 140–143, (2013).

[221] E. Leivo, T. Wilenius, T. Kinos, P. Vuoristo, T. Mäntylä, "Properties of thermally sprayed fluoropolymer PVDF, ECTFE, PFA and FEP coatings", *Progress in Organic Coatings*, vol. 49, n. 1, pp. 69–73, (2004).

[222] H. Koivuluoto, C. Stenroos, M. Kylmälahti, M. Apostol, J. Kiilakoski, P. Vuoristo, "Anti-icing Behavior of Thermally Sprayed Polymer Coatings", *Journal of Thermal Spray Technology*, vol. 26, n. 1–2, pp. 150–160, (2017).

[223] J.A. Brogan, C.C. Berndt, "The coalescence of combustion-sprayed ethylene-methacrylic acid copolymer", *Journal of Materials Science*, vol. 32, n. 8, pp. 2099–2106, (1997).

[224] K. Alamara, S. Saber-Samandari, C.C. Berndt, "Splat formation of polypropylene flame sprayed onto a flat surface", *Surface and Coatings Technology*, vol. 205, n. 7, pp. 2518–2524, (2010).

[225] S. Armada, R. Schmid, S. Equey, I. Fagoaga, N. Espallargas, "Liquid-solid self-lubricated coatings", *Journal of Thermal Spray Technology*, vol. 22, n. 1, pp. 10–17, (2013).

[226] J. Li, H. Liao, C. Coddet, "Friction and wear behavior of flame-sprayed PEEK coatings", *Wear*, vol. 252, n. 9–10, pp. 824–831, (2002).

[227] C.C. Berndt, D. Otterson, M.L. Allan, C.C. Berndt, D. Otterson, "Polymer Coatings for Corrosion Protection in Biochemical Treatment of Geothermal Residues", *Geothermal Resources Council Transactions*, vol. 22, pp. 425–429, (1998).

[228] C.R.C. Lima, M.A.R. Mojena, C.A. Della Rovere, N.F.C. de Souza, H.D.C. Fals, "Slurry Erosion and Corrosion Behavior of Some Engineering Polymers Applied by Low-

Pressure Flame Spray", *Journal of Materials Engineering and Performance*, vol. 25, n. 11, pp. 4911–4918, (2016).

[229] Y. Bao, D.T. Gawne, "Process modelling of thermal spray deposition of thermosets", *Surface Engineering*, vol. 11, n. 3, pp. 215–222, (1995).

[230] Y. Bao, D.T. Gawne, T. Zhang, "The Effect of Feedstock Particle Size on the Heat Transfer Rates and Properties of Thermally Sprayed Polymer Coatings", *Transactions of the IMF*, vol. 73, n. 4, pp. 119–124, (1995).

[231] Y. Bao, D.T. Gawne, D. Vesely, M.J. Bevis, "Formation and microstructure of plasma sprayed polyamide coatings", *Surface Engineering*, vol. 10, n. 4, pp. 307–313, (1994).

[232] T. Twardowski, V. Bhargava, R. Knight, "Properties of HVOF sprayed multi-scale polymer/silica nanocomposite coatings", in "ITSC 2004: International Thermal Spray Conference 2004: Advances in Technology and Application", pp. 1072–1075, (2004).

[233] E. Petrovicova, R. Knight, R.W. Smith, L.S. Schadler, "Structure and properties of HVOF sprayed ceramic/polymer nanocomposite coatings", in "Thermal spray: A united forum for scientific and technological advances", pp. 877–883, (1998).

[234] E. Petrovicova, R.W. Smith, R. Knight, L.S. Schadler, "Particulate Nanoreinforced Polymer Composites Processing and Properties", *J. Therm. Spray Technol*, vol. 7, n. 3, pp. 426–427, (1998).

[235] L. Pawlowski, "The Science and Engineering of Thermal Spray Coatings", second Edi, *John Wiley & Sons, Ltd*, Chichester, UK, (2008).

[236] A.S.M. Ang, N. Sanpo, M.L. Sesso, S.Y. Kim, C.C. Berndt, "Thermal spray maps: Material genomics of processing technologies", *Journal of Thermal Spray Technology*, vol. 22, n. 7, pp. 1170–1183, (2013).

[237] M. Ivosevic, S.L. Coguill, S.L. Galbraith, "Polymer thermal spraying: A novel coating process", in "Proceedings of the International Thermal Spray Conference", pp. 1078–1083, (2009).

[238] H.L. Yao, G.C. Ji, Q.Y. Chen, X.B. Bai, Y.L. Zou, H.T. Wang, "Microstructures and Properties of Warm-Sprayed Carbonated Hydroxyapatite Coatings", *Journal of Thermal Spray Technology*, pp. 1–14, (2018).

[239] S. Kuroda, J. Kawakita, M. Watanabe, H. Katanoda, "Warm spraying—a novel coating process based on high-velocity impact of solid particles", *Science and Technology of Advanced Materials*, vol. 9, n. 3, pp. 033002, (2008).

[240] M. Watanabe, K.H. Kim, M. Komatsu, S. Kuroda, "Understandings of Solid Particle

Impact and Bonding Behaviors in Warm Spray Deposition", in "Materials Challenges and Testing for Supply of Energy and Resources", *Springer Berlin Heidelberg*, Berlin, Heidelberg, pp. 203–212, (2012).

[241] Y. Bao, T. Zhang, D.T. Gawne, "Influence of composition and process parameters on the thermal spray deposition of UHMWPE coatings", *Journal of Materials Science*, vol. 40, n. 1, pp. 77–85, (2005).

[242] W. Lock Sulen, K. Ravi, C. Bernard, Y. Ichikawa, K. Ogawa, "Deposition Mechanism Analysis of Cold-Sprayed Fluoropolymer Coatings and Its Wettability Evaluation", *Journal of Thermal Spray Technology*, vol. 29, n. 7, pp. 1643–1659, (2020).

[243] K. Ravi, W.L. Sulen, C. Bernard, Y. Ichikawa, K. Ogawa, "Fabrication of micro-/nano-structured super-hydrophobic fluorinated polymer coatings by cold-spray", *Surface and Coatings Technology*, vol. 373, n. April, pp. 17–24, (2019).

[244] Y. Maly, "Cold Sprayed SLIPS Coatings: A pathway towards process optimization and icephobicity", (2020).

[245] Y. Xu, I.M. Hutchings, "Cold spray deposition of thermoplastic powder", *Surface and Coatings Technology*, vol. 201, n. 6, pp. 3044–3050, (2006).

[246] Z. Khalkhali, J.P. Rothstein, "Characterization of the cold spray deposition of a wide variety of polymeric powders", *Surface and Coatings Technology*, vol. 383, pp. 125251, (2020).

[247] N. Espallargas, "Future Development of Thermal Spray Coatings: Types, Designs, Manufacture and Applications", *Elsevier Science & Technology*, (2015).

[248] IBEDA Sicherheitsgeräte und Gastechnik GmbH & Co. KG, "Fuel gas properties", n.d.

[249] L.S. Schadler, K.O. Laul, R.W. Smith, E. Petrovicova, "Microstructure and mechanical properties of thermally sprayed silica/nylon nanocomposites", *Journal of Thermal Spray Technology*, vol. 6, n. 4, pp. 475–485, (1997).

[250] J.A. Brogan, C.C. Berndt, G.P. Simon, D. Hewitt, "Physical and Relaxation Properties of Flame-Sprayed Ethylene-Methacrylic Acid Copolymer", *Polymer Engineering and Science*, vol. 38, n. 11, pp. 1873–1881, (1998).

[251] S. Turri, T. Trombetta, M. Levi, L. Simonin, H. Liao, "Characterization of flame-sprayed PEEK coatings by FTIR-ATR, DSC and acoustic microscopy", *Macromolecular Materials and Engineering*, vol. 283, pp. 153–162, (2000).

[252] X. Shoudong, P. Huiru, Q. Guoling, "Tensile properties and bond strength of polyamide coatings produced by thermal spraying", *Transactions of the Institute of Metal Finishing*, vol. 75, n. 2, pp. 70–72, (1997).

[253] B. Normand, H. Takenouti, M. Keddam, H. Liao, G. Monteil, C. Coddet, "Electrochemical impedance spectroscopy and dielectric properties of polymer: Application to PEEK thermally sprayed coating", *Electrochimica Acta*, vol. 49, n. 17–18, pp. 2981–2986, (2004).

[254] T. Palathai, J. Tharajak, N. Sombatsompop, "Hardness, adhesion index and microstructure of PEEK coating on Al or Fe substrate by LVOF flame spray", *Materials Science and Engineering A*, vol. 485, n. 1–2, pp. 66–73, (2008).

[255] F. Mai, W. Tu, E. Bilotti, T. Peijs, "The influence of solid-state drawing on mechanical properties and hydrolytic degradation of melt-spun poly(lactic acid) (PLA) tapes", *Fibers*, vol. 3, n. 4, pp. 523–538, (2015).

[256] E.R. George, J. Reimer, "Flamesprayed thermoplastic powder coatings", *Polymer Engineering and Science*, vol. 31, n. 11, pp. 789–792, (1991).

[257] F.Y. Yan, K.A. Gross, G.P. Simon, C.C. Berndt, "Mechanical and erosion properties of CaCO3-EMAA thermal sprayed coatings", *Polymer Engineering and Science*, vol. 44, n. 8, pp. 1448–1459, (2004).

[258] T. Sugama, R. Kawase, C.C. Berndt, H. Herman, "An evaluation of methacrylic acid-modified poly(ethylene) coatings applied by flame spray technology", *Progress in Organic Coatings*, vol. 25, n. 2, pp. 205–216, (1995).

[259] R.A.X. Nunes, S. Wagner, J.R.T. Branco, "Atrito e Desgaste de Recobrimentos de PET, Politeraftalato de Etileno, Pós-consumo Processados por Aspersão Térmica", *Polímeros: Ciência e Tecnologia*, vol. 17, n. 3, pp. 244–249, (2007).

[260] C. Mateus, S. Costil, R. Bolot, C. Coddet, "Ceramic/fluoropolymer composite coatings by thermal spraying—a modification of surface properties", *Surface and Coatings Technology*, vol. 191, n. 1, pp. 108–118, (2005).

[261] L.D. Stephenson, A.D. Beitelman, R.G. Lampo, A. Kumar, D. Neale, L. Clark, K. Palutke, M. Surratt, D. Butler, "Demonstration of Thermally Sprayed Metal and Polymer Coatings for Steel Structures at Fort Bragg, NC", (2017).

[262] P.J. Loustannau, D. Horton, "EMAA thermoplastic powder coatings in shop and field applications", *Materials Performance*, vol. 33, n. 7, pp. 32–36, (1994).

[263] Z. Jia, Y. Liu, Y. Wang, Y. Gong, P. Jin, X. Suo, H. Li, "Flame spray fabrication of polyethylene-Cu composite coatings with enwrapped structures: A new route for constructing antifouling layers", *Surface and Coatings Technology*, vol. 309, pp. 872–879, (2017).

[264] H. Koivuluoto, E. Hartikainen, H. Niemelä-Anttonen, "Thermally sprayed coatings:

Novel surface engineering strategy towards icephobic solutions", *Materials*, vol. 13, n. 6, pp. 1434, (2020).

[265] J.R.T. Branco, S. V Campos, "Wear behavior of thermally sprayed PET", *Surface and Coatings Technology*, vol. 120–121, pp. 476–481, (1999).

[266] R. Gadow, D. Scherer, "Composite coatings with dry lubrication ability on light metal substrates", *Surface and Coatings Technology*, vol. 151, n. 152, pp. 471–477, (2002).

[267] M. Ivosevic, R. Knight, S.R. Kalidindi, G.R. Palmese, J.K. Sutter, "Adhesive/cohesive properties of thermally sprayed functionally graded coatings for polymer matrix composites", *Journal of Thermal Spray Technology*, vol. 14, n. 1, pp. 45–51, (2005).

[268] J. Tharajak, T. Palathai, N. Sombatsompop, "The effects of magnetic field-enhanced thermal spraying on the friction and wear characteristics of poly(ether-ether-ketone) coatings", *Wear*, vol. 372–373, pp. 68–75, (2017).

[269] J. Tharajak, T. Palathai, N. Sombatsompop, "Recommendations for h-BN loading and service temperature to achieve low friction coefficient and wear rate for thermal-sprayed PEEK coatings", *Surface and Coatings Technology*, vol. 321, pp. 477–483, (2017).

[270] J. Tharajak, T. Palathai, N. Sombatsompop, "Morphological and physical properties and friction/wear behavior of h-BN filled PEEK composite coatings", *Surface and Coatings Technology*, vol. 273, n. 1, pp. 20–29, (2015).

[271] G. Zhang, W.Y. Li, M. Cherigui, C. Zhang, H. Liao, J.M. Bordes, C. Coddet, "Structures and tribological performances of PEEK (poly-ether-ether-ketone)-based coatings designed for tribological application", *Progress in Organic Coatings*, vol. 60, n. 1, pp. 39–44, (2007).

[272] S. Tailor, N. Vashishtha, A. Modi, "Thermally Sprayed Porous PEEK Coating for Biomedical Implants Thermally Sprayed Porous PEEK Coating for Biomedical Implants", *Journal of Thermal Spray and Engineering*, vol. 1, n. 1, pp. 32–36, (2019).

[273] A. Chebbi, J. Stokes, "Thermal spraying of bioactive polymer coatings for orthopaedic applications", *Journal of Thermal Spray Technology*, vol. 21, n. 3–4, pp. 719–730, (2012).

[274] T. Zhang, D.T. Gawne, Y. Bao, "The influence of process parameters on the degradation of thermally sprayed polymer coatings", *Surface and Coatings Technology*, vol. 96, pp. 337–344, (1997).

[275] V. Jannin, Y. Cuppok, "Hot-melt coating with lipid excipients", *International Journal of Pharmaceutics*, vol. 457, n. 2, pp. 480–487, (2013).

[276] R. Mukherjee, M. Habibi, Z.T. Rashed, O. Berbert, X. Shi, J.B. Boreyko, "Oil-

Impregnated Hydrocarbon-Based Polymer Films", *Scientific Reports*, vol. 8, n. 1, pp. 1–13, (2018).

[277] L.A. Utracki, C.A. Wilkie, "Polymer Blends Handbook", *Springer Netherlands*, Dordrecht, (2014).

[278] "ISO 4288:1996 Geometrical Product Specifications (GPS) . Surface texture: Profile method for the assessment of surface texture", *Geometrical Product Specifications (GPS)*, (1996).

[279] "ISO 25178-3:2012 - Geometrical product specifications (GPS) — Surface texture: Areal — Part 3: Specification operators", (2012).

[280] A. Rudawska, E. Jacniacka, "Analysis for determining surface free energy uncertainty by the Owen-Wendt method", *International Journal of Adhesion and Adhesives*, vol. 29, n. 4, pp. 451–457, (2009).

[281] N. Kandelin, "Icing Factors Affecting Railway Traffic", Tampere University, (2021).

[282] B. Wunderlich, "Thermal analysis of polymeric materials", *Springer-Verlag*, Berlin/Heidelberg, (2005).

[283] G.E. Likens, F.H. Bormann, "Acid Rain: A Serious Regional Environmental Problem", *Science (New York, N.Y.)*, vol. 184, n. 5, pp. 1176–1179, (1974).

[284] V. Mylläri, T.P. Ruoko, P. Järvelä, "The effects of UV irradiation to polyetheretherketone fibres - Characterization by different techniques", *Polymer Degradation and Stability*, vol. 109, pp. 278–284, (2014).

[285] "Identifying Color Differences Using L*a*b* or L*C*H* Coordinates", *Sensing.Konicaminolta.Us*, (2020).

[286] R.J. Scavuzzo, M.L. Chu, "Structural Properties of Impact Ices Accreted on Aircraft Structures", (1987).

[287] M. Sugimoto, A. Shimada, H. Kudoh, K. Tamura, T. Seguchi, "Product analysis for polyethylene degradation by radiation and thermal ageing", *Radiation Physics and Chemistry*, vol. 82, n. 1, pp. 69–73, (2013).

[288] A.G. Pedroso, D.S. Rosa, "Mechanical, thermal and morphological characterization of recycled LDPE/corn starch blends", *Carbohydrate Polymers*, vol. 59, n. 1, pp. 1–9, (2005).

[289] E.N. Griffin, P.J. Niebergall, "Release Kinetics of a Controlled-Release Multiparticulate Dosage Form Prepared Using a Hot-Melt Fluid Bed Coating Method", *Pharmaceutical Development and Technology*, vol. 4, n. 1, pp. 117–124, (1999).

[290] J.P. Reo, W.M. Johnson, "Tastemasked pharmaceutical system", *U.S. Patent No. 5,891,476*, (1999).

[291] A.. Tracton, "Coatings Technology Handbook", 3rd Editio, *CRC Press*, Boca Raton, (2005).

[292] K. Mittal, K. Lee, "Polymer surfaces and interfaces: characterization, modification and application", (1997).

[293] I. Novák, I. Krupa, A.S. Luyt, "Modification of a fischer-tropsch wax by grafting with maleic anhydride", *Journal of Applied Polymer Science*, vol. 93, n. 2, pp. 662–668, (2004).

[294] H. Bockhorn, A. Hornung, U. Hornung, D. Schawaller, "Kinetic study on the thermal degradation of polypropylene and polyethylene", *Journal of Analytical and Applied Pyrolysis*, vol. 48, n. 2, pp. 93–109, (1999).

[295] A.A. Abubakar, A.F.M. Arif, K.S. Al-Athel, S.S. Akhtar, J. Mostaghimi, "Modeling Residual Stress Development in Thermal Spray Coatings: Current Status and Way Forward", *Journal of Thermal Spray Technology*, vol. 26, n. 6, pp. 1115–1145, (2017).

[296] G. Montay, A. Cherouat, A. Nussair, J. Lu, "Residual stresses in coating technology", *Journal of Materials Science and Technology*, vol. 20, pp. 81–84, (2004).

[297] M.E. Nichols, C.A. Darr, C.A. Smith, M.D. Thouless, E.R. Fischer, "Fracture energy of automotive clearcoats - I. Experimental methods and mechanics", *Polymer Degradation and Stability*, vol. 60, n. 2–3, pp. 291–299, (1998).

[298] A. Laroche, D. Bottone, S. Seeger, E. Bonaccurso, "Silicone nanofilaments grown on aircraft alloys for low ice adhesion", *Surface and Coatings Technology*, vol. 410, pp. 126971, (2021).

[299] G.W. Ehrenstein, S. Pongratz, "Resistance and Stability of Polymers", in "Resistance and Stability of Polymers", *Carl Hanser Verlag GmbH & Co. KG*, München, (2013).

[300] W.H. Brown, T. Poon, "Introduction to organic chemistry", 5th ed., *John Wiley & Sons*, Hoboken, NJ, (2014).

[301] M. Iring, F. Tüdős, "Thermal oxidation of polyethylene and polypropylene: Effects of chemical structure and reaction conditions on the oxidation process", *Progress in Polymer Science*, vol. 15, n. 2, pp. 217–262, (1990).

[302] H. Kaczmarek, D. Oldak, A. Podgórski, "Photochemical Properties of Polyethylene Modified by Low-Molecular Organic Compounds", *Polymer Journal*, vol. 35, n. 8, pp. 634–639, (2003).

[303] K.J. Kim, T.J. Eom, "Chemical characteristics of degraded beeswax in the waxed volume of the annals of King Sejong in the Joseon Dynasty", *Journal of Cultural Heritage*, vol. 16, n. 6, pp. 918–921, (2015).

[304] G.R. Fedor, P.J. Brennan, "Comparison between natural weathering and fluorescent UV exposures: UVA-340 lamp test results", *ASTM Special Technical Publication*, vol. 1294, pp. 91–105, (1996).

[305] B. Lesar, M. Pavlič, M. Petrič, A.S. Škapin, M. Humar, "Wax treatment of wood slows photodegradation", *Polymer Degradation and Stability*, vol. 96, n. 7, pp. 1271–1278, (2011).

[306] A. Hakimian, S. Nazifi, H. Ghasemi, "Physics of Ice Nucleation and Growth on a Surface", in "Ice Adhesion: Mechanism, Measurement and Mitigation", *Wiley*, pp. 87–110, (2020).

PUBLICATIONS

PUBLICATION I

Icephobic behaviour and thermal stability of flame-sprayed polyethylene coating: the effect of process parameters

V. Donadei, H. Koivuluoto, E. Sarlin, and P. Vuoristo

Journal of Thermal Spray Technology, 29.1 (2020), 241-254
DOI: 10.1007/s11666-019-00947-0

J Therm Spray Tech (2020) 29:241–254
https://doi.org/10.1007/s11666-019-00947-0

PEER REVIEWED

Icephobic Behaviour and Thermal Stability of Flame-Sprayed Polyethylene Coating: The Effect of Process Parameters

Valentina Donadei[1] · Heli Koivuluoto[1] · Essi Sarlin[1] · Petri Vuoristo[1]

Submitted: 28 June 2019 / in revised form: 21 October 2019 / Published online: 11 November 2019

Abstract The present work investigates the effect of different process parameters on the production of low-density polyethylene (LDPE) coatings by flame spray technology. Previously, flame spraying of polymers has been successfully performed to obtain durable icephobic coatings, providing an interesting solution for applications facing icing problems, e.g. in marine, aviation, energy, and transportation industry. However, the fine tailoring of the process parameters represents a necessary strategy for optimising the coating production due to the unique thermal properties of each polymer. For this purpose, we vary the heat input of the process during flame spraying of the coating, by changing the transverse speed and the spraying distance. The results show that the variation in the process parameters strongly influenced the quality of the polymer coating, including its areal roughness, thickness, chemical composition, thermal stability, and degree of crystallinity. Furthermore, we demonstrate that these properties significantly affect the icephobic behaviour of the surface within the spray window of the chosen parameters. In conclusion, the relationship between the thermal degradation of the polymer and the icephobicity of the surface was defined. This highlights the importance of process parameter optimisation in order to achieve the desired icephobic performance of the LPDE coatings.

Keywords flame spraying · ice adhesion strength · icephobic surface · polymer coating · thermal degradation

Introduction

The accumulation of ice and snow on outdoor structures represents a serious problem in Nordic regions as well as in several countries in both hemispheres (Ref 1). In fact, the atmospheric ice strongly adheres to bare surfaces and its accumulation contributes to compromising the effectiveness and efficiency of different applications, for example, power lines and electrical conductors during winter storms (Ref 2). Moreover, ice accretion on aircraft surfaces produces severe changes in their aerodynamic properties (Ref 3). Since the accumulation of ice represents an adverse impact on both safety and structure performances (Ref 4, 5), different strategies are developed to prevent ice adhesion on outdoor surfaces. Several active and passive methods have been adopted to avoid ice accumulation and reduce safety issues. On one hand, active methods include processes involving the mechanical removal of ice by scraping and vibrating the structure, the use of de-icing chemical fluids, and thermal heating above the freezing point (Ref 6). Unfortunately, these active methods produce environmental pollution, energy consumption, and ineffective manual operations. On the other hand, passive methods represent a smart strategy, which aims to develop efficient and durable anti-ice solutions. These methods consist of using icephobic material to coat the ice-exposed surfaces, preventing ice accumulation and consequent safety issues. Theoretically, the surface is considered as icephobic when it effectively reduces the adhesion strength of ice and prevents ice accumulation (Ref 7). In particular, the adhesion forces should be low in order to practically

This article is an invited paper selected from presentations at the 2019 International Thermal Spray Conference, held May 26-29, 2019 in Yokohama, Japan and has been expanded from the original presentation.

✉ Valentina Donadei
valentina.donadei@tuni.fi

[1] Faculty of Engineering and Natural Sciences, Tampere University, P.O. Box 589, FI-33014 Tampere, Finland

shed the ice off from the surface (Ref 8). However, only a few coatings have been achieved this, withstanding their durability (Ref 9).

The research and development of icephobic surfaces have been achieved a considerable interest in the speciality of coating design, during the last two decades (Ref 10, 11). Different coating technologies have been used for the production of icephobic surfaces, mainly chemical synthesis (Ref 12), sol–gel methods (Ref 13), and other laboratory-scale coating and painting processes. However, these methods generally require extended processing time, a large waste of chemicals, and controlled environmental conditions. Therefore, thermal spray technology represents a valid alternative to the chemical synthesis for the production of smart coatings (Ref 14). This technique aims to improve the performance of a component by adding a functionalised coating to the surface (Ref 15). Anti-corrosion (Ref 16-19), low friction and wear resistance (Ref 20-23), chemical and weathering resistance (Ref 24, 25), and antifouling (Ref 26, 27) represent some of the applications of the thermally sprayed coatings. In particular, flame spraying represents one of the thermal spray techniques used for the production of polymer coatings. In this process, the material in the form of powder is fed into a spray gun. The powder is injected into a combustion flame, which is used to melt the thermoplastic polymers during spraying. The melted particles hit the substrate, spread, and coalesce within each other to form a coating (Ref 28). The main advantage of flame spraying is that the melting and the consolidation of the polymer happen almost simultaneously during a single-step spraying process. Consequently, additional post-treatments are not necessary after the material deposition for the coating consolidation, such as post-curing at room temperature, ultraviolet radiation, or oven treatment, which are needed in some other surface technologies (Ref 9, 12). However, the temperature of the flame in thermal spraying is much higher than the melting temperature of polymers (Ref 29). Although specific equipment is available for flame spraying of polymers, a certain degree of material degradation always takes place during the flame processes (Ref 29). Therefore, fine tailoring of the process parameters is necessary to avoid the thermal degradation of the material, consisting of polymer chain scission, oxidation, surface embrittlement (Ref 30), and decrease in mechanical properties (Ref 29).

Our previous studies (Ref 31, 32) have demonstrated the icephobic property of thermally sprayed polymer coatings. For instance, polyethylene coatings showed potential icephobicity with ice adhesion value of 54 kPa for the polished surface (69 kPa for the as-sprayed surface). In addition, good coating durability was achieved for high-velocity impact test and particle erosion tests (Ref 31). Moreover, lubricant-infused porous coating (slippery liquid impregnated porous surface, SLIPS) showed extremely low ice adhesion (21 kPa for Thermally Sprayed SLIPS) and enhanced water repellency (Ref 32). However, further research is needed to optimise the manufacturing process of thermally sprayed icephobic coatings. Therefore, investigations are necessary on the effect of flame spraying parameters on the icephobicity of the surface. In particular, the process parameters strongly influence the performance of the coating (Ref 33). In addition, we have noticed that the chemical and thermal characterisations of the polymer coatings are essential in order to optimise the spray process for the selected purposes and coating requirements. Therefore, this study aims the optimisation of the process parameters to obtain an icephobic coating with preserved mechanical and structural properties. The influence of the process parameters on the coating properties was investigated by varying transverse speed and spraying distance of the spray gun for the polyethylene material. These parameters affect the heat input on the material during the process and thus the coating properties and its possible thermal degradation. In addition, the relationship between the icephobicity and the degradation of the coating is investigated, referring to the chemical and thermal characteristics of the flame-sprayed polymer coatings.

Materials and Methods

Material and Coating Fabrication

The material used in this work was a low-density polyethylene (LDPE) powder (Plascoat Europe BV, Zuidland, The Netherlands). The morphology of the polymer powder was analysed by a scanning electron microscope (SEM, Philips XL30, The Netherlands). The size distribution of the powder was below 300 μm for 95% of the particles, as given by the powder supplier. In addition, the particle size distribution was investigated by laser diffraction analysis using the dry powder method (LS 13 320 Laser Diffraction Particle Size Analyser, Beckman Coulter, Inc., United States). The coatings were prepared by using an oxygen-acetylene flame spray gun (CastoDyn DS 8000, Castolin Eutectic, Switzerland) with gas pressure for oxygen and acetylene of 4.2 bar and 0.7 bar, respectively. A powder feeder (Sulzer Metco 4MP, Oerlikon Metco, Switzerland) was used with compressed air as the carrier gas for feeding the powder in the gun. A powder feed rate of 26 g/min was defined for coating production. The coatings were automatically sprayed by a single-arm robot (ABB IRB 4400/60, ABB Robotics, Sweden), controlling the transverse speed and the spraying distance of the spray gun during the coating production. These two parameters were varied for the production of the polyethylene coatings,

keeping as constant all the others. In particular, the heat input of the combustion flame on the sprayed surface changed based on the combination of the chosen process parameters. In fact, the closer the spraying distance and the slower the transverse speed, the higher the heat transferred to the polymeric material. Consequently, a systematic study was designed to investigate the effect of the heat input of the process on the coating performances. The values of transverse speed and spraying distance and the number of specimens analysed in this work are summarised in Fig. 1. These values were chosen based on the parameters suggested by the spray gun manufacturer for spraying polymers. In particular, it was recommended to use a minimum spraying distance of 250 mm during the process production. However, we decided to spray only one sample by using 200-mm distance to investigate the effect of the heat input for an extreme condition of the chosen process window (sample A0). The coatings were sprayed on grit-blasted (alumina grits, 54 Mesh) stainless steel substrate (UNS S31603) with dimensions of 200 mm × 50 mm × 1.5 mm. Each coating was sprayed following fixed production steps, such as pre-heating of the substrate, spraying, and post-heating by flame. In particular, prior to the spraying, the substrates were pre-heated with the flame, to ensure good coating adhesion. After pre-heating, three layers of powder were sprayed with 5-mm step on the whole substrate to obtain a thick coating. A thermal imaging camera (Ti300 Infrared Camera IR Fusion Technology, Fluke Corporation, United States) was used to monitor the temperature of the metal substrate before spraying. The thermal camera was calibrated by experimentally measuring the emissivity of the substrate material. Then, the spraying of the coating started when the substrate reached the melting transition temperature of the polymer powder (around 120 °C). This monitoring avoided the over-melting of the substrate, which might cause the vaporisation of the polymer powder hitting the substrate. Moreover, this prevents the formation of defects in the polymer coating, such as voids, contaminants, and degradation (Ref 34). However, the monitored temperature was representative of the substrate until the spraying of the coating started. This is due to the different emissivities between the stainless steel substrate and polymer coating.

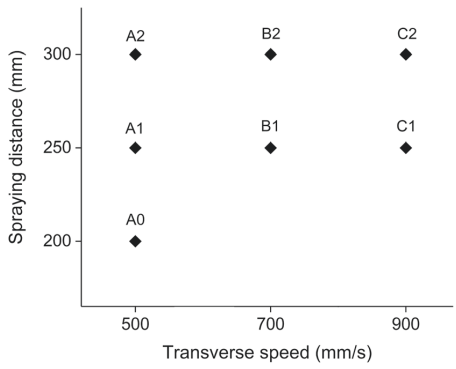

Fig. 1 Process window of the chosen parameters for flame spraying of LDPE coatings. Samples were identified with letters (from A to C for increasing transverse speed) and with numbers (from 0 to 2 for increasing spraying distance)

Microstructural and Surface Characterisation

The microstructure of the coating was analysed by a scanning electron microscope (SEM, Jeol, IT-500, Japan), investigating the presence of defects within the coating structure, such as voids and contaminations. In addition, energy dispersive x-ray spectroscopy (SEM/EDS) was used to obtain a semi-quantitative elemental composition (oxygen and carbon mass percentage, in the case of our material) in very specific locations of the cross section for coatings sprayed with different process parameters. For this test, the cross sections of the sample were coated by both carbon and gold sputtering to enhance the surface conductivity. The analysis was carried out by using an acceleration voltage of 10 kV in high vacuum by using a back-scattered electrons detector. This permitted the analysis of the coating chemical composition for different process parameters. Moreover, an optical microscope (Leica DM2500 M, Germany) was used to measure the thickness of the coating as an average of nine measurements in different points along the width of the specimen. The areal roughness (*Sa*) was measured with an optical profilometer (Alicona Infinite Focus G5, Alicona Imaging GmbH, Austria) by using 20× objective magnification in the areas of 2 × 2 mm^2, according to ISO 4288 procedure. The texture of the surface was analysed by using 5× objective magnification in areas of approximately 30 × 30 mm^2.

Ice Accretion and Ice Adhesion

Ice adhesion test of the coatings was performed using the icing facilities at Tampere University (Ref 35). Firstly, artificial ice was accreted from supercooled droplets in the icing wind tunnel on a surface area of 30 × 30 mm^2 of the specimen. In the present and previous studies (Ref 31, 32, 35), a mixed-glaze type of ice was accreted onto the specimen surface. The characteristic icing parameters are summarised in Table 1. After the ice was formed, the ice adhesion was measured using the centrifugal ice adhesion test (CAT) in sub-zero ambient condition. In this method, the iced specimen is rotated with increasing speed until the ice detaches from the surface of the specimen. A sensor monitors the moment at which the ice detaches from the surface, and therefore, the ice adhesion can be evaluated. The test setup is described in detail in the previous work (Ref 35).

Table 1 Parameters of the icing wind tunnel

Parameter	
Room temperature	− 10 °C
Relative humidity	83-86%
Water temperature	6-7 °C
Air pressure	3.5-4 bar
Airflow	60-70 l/min
Water pressure	3.5-4 bar
Water flow	0.15-0.2 l/min

The shear ice adhesion strength is evaluated as the ratio between the centrifugal force, F(N), at the moment of ice detachment and the iced area, $A(\mathrm{m}^2)$, of the specimen. Equation 1 evaluates the adhesion strength, τ_{ice}(kPa), as follows:

$$\tau_{ice} = \frac{F}{A} = \frac{m_{ice} r \omega^2}{A} \quad \text{(Eq 1)}$$

where $m_{ice}(\mathrm{kg})$ is the mass of the accreted ice on the surface of the specimen, r(m) is the radial spinning length, and $\omega(\mathrm{rad/s})$ is the rotational speed. The ice adhesion of the coating was evaluated as an average of four parallel samples during the icing accretion event. A test reference surface (TT) (Teflon tape, 3 M, United States) was tested to control the value of the ice adhesion for every accretion event. The reference material is essential to ensure the repeatability of the results, due to the variability of the ice adhesion strength for different icing conditions (Ref 36-38).

Wettability

The wettability of the surfaces was examined using a droplet shape analyser (DSA100, Krüss, Germany) to evaluate the static contact angle and the roll-off angle of the water droplets on the coating surface. The experiments were performed by pouring 6 µl water droplets of ultra-high purity water (MilliQ, Millipore Corporation, United States) onto the surfaces. The tendency of the water droplet to roll off from the surface was investigated by tilting experiment. In particular, the angle of inclination of the sample was measured when the droplet rolled off from the coating surface. The values were evaluated as an average of five measurements in different areas of the same coating surface at 21 °C and 60% relative humidity.

Chemical and Thermal Characterisations

Polymers are well-known heat-sensitive materials, and consequently, their structure is strongly influenced by the temperature reached by the material during flame spraying. This is mainly related to the time that the material spends in contact with the flame. In fact, the heat input of the process increases as the transverse speed and the spraying distance decreases (longer time process), producing possible oxidation and physical degradation of the sprayed polymer (Ref 34). For this reason, a thermal-processing window is recommended for each polymer to prevent excessive thermal degradation and consequently to ensure the quality of the coating. Therefore, chemical and thermal analyses of both the feedstock material and the coating were performed to analyse the possible thermal degradation produced by the process parameters, influencing the performance of the coating.

Fourier-Transform Infrared Spectroscopy (FTIR)

The chemical characterisation of the polymer powder and the variation in the chemical structure of the coatings were investigated by using Fourier-transform infrared spectroscopy (FTIR) (Bruker Tensor 27 FT-IR spectrometer, Bruker, Sweden). The FTIR spectra were measured at room temperature using an attenuated total reflection (ATR) spectrometer whereas the internal reflection element (IRE) was a diamond crystal. The degree of polymer oxidation was determined by monitoring the change in intensity of non-volatile carbonyl oxidation products. The intensity of the absorbance peak at 1713 cm^{-1} was taken as a measure of the concentration of carbonyl compounds derived by the polyethylene degradation (mainly carboxylic acids) (Ref 39, 40). All measurements were performed by using three samples taken from every coating surface.

Thermogravimetric Analysis (TGA)

The variations in the thermal stability of the coating within the spraying-process window were investigated by thermogravimetric analysis (TGA) (Netzsch TGA209F Tarsus, Netzsch, Germany). The specimen weight was approximately 10 mg and a dynamical heating was performed at 20 °C/min from 25 to 600 °C in nitrogen atmosphere. Firstly, the degradation temperature of the polymer powder was measured at the maximum deflection point of the TG curve. Secondly, the thermal stability of the coatings and their degradation degree were evaluated by comparing the temperatures at which the 2% ($T_{98\%}$), the 5% ($T_{95\%}$), and the 10% ($T_{90\%}$) of the mass of the coating were lost during the thermal heating (Ref 41). In particular, the lower these temperatures, the higher the degree of degradation of the polymer coating during flame spraying.

Differential Scanning Calorimetry (DSC)

The thermal characterisation of the powder and the influence of the process parameters on the degree of crystallinity of the coatings were evaluated by using a

differential scanning calorimetry (DSC) (Netzsch DSC214 Polyma, Netzsch, Germany). Test specimens were weighed approximately 10 mg. First dynamical heating was performed at 20 °C/min from − 20 to 150 °C in nitrogen atmosphere in order to evaluate the degree of crystallinity of the produced coating. In addition to this, to evaluate the maximum degree of crystallinity of the powder, a slow cooling at 1 °C/min was performed after the first heating to remove the effect of the thermal history due to the production process of the powder. Then, the second dynamic heating was carried out with parameters identical to the first heating only for the powder. The degree of crystallinity of the powder was compared to one of the coatings to understand the effect of the process parameters on the degree of crystallinity of the material after flame spraying. The degree of crystallinity χ was derived by the ratio of the measured heat of fusion and the heat of fusion for finite crystals for the considered polymer, as shown in Eq 2:

$$\chi = \frac{\Delta H}{\Delta H_{100\%}} \quad \text{(Eq 2)}$$

where ΔH (J/g) represents the melting enthalpy of the specimen (corresponding to the melting-peak area) and $\Delta H_{100\%}$ (J/g) represents the measured enthalpy based upon a perfect crystal heat of fusion of 293 J/g (Ref 42).

Results and Discussion

Thermal spray technology, and especially flame spraying, represents a fast technique for the production of thermoplastic polymer coatings due to the advantage of the melting-consolidation transition of the polymer in one-step process. However, polymers are known to be heat-sensitive materials, and therefore, a thorough study is necessary to evaluate in detail the influence of the process parameters on the coating properties, such as thermal properties, mechanical performance, and durability. Moreover, the spray process parameters can influence the areal roughness of the coating, which has been considered as one of the main factors affecting the icephobicity of the surface (Ref 43, 44). For this reason, a compromise should be reached between the coating performances and the resulting surface properties affecting icephobicity, when selecting the process parameters.

Powder Properties

The morphological analysis of the powder showed the presence of the different dimensions and shapes of the polymer particles. The powder morphology is shown in Fig. 2. In particular, the particle shape varied from small grain to stretched and narrowed flakes due to the method used for the powder production. The analysis of the powder dimensions indicated that 90% of the total particles count has a diameter smaller than 278 µm and that 10% of the total particles count is smaller than 104 µm. Moreover, the thermal characterisation of the powder was carried out to define the processing temperature of the coating. The LDPE powder showed a melting-peak temperature of 109 °C and a thermal degradation temperature of 427 °C (measured at the 2% mass loss of the TG curve of the LDPE powder, as it is indicated in Fig. 9). Table 2 summaries the LDPE powder properties.

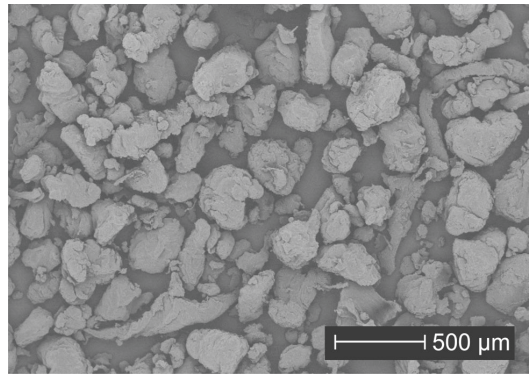

Fig. 2 SEM image of LDPE powder

Table 2 Properties of LDPE powder

Powder properties	
Particle size distribution	− 278 + 104 µm
Peak melting, T	109 °C
Degradation, T	427 °C

Microstructural and Surface Properties of the Coatings

The microscopic analyses of the coatings revealed no defects within the structure, such as voids, even for the specimen that was visibly degraded using the spraying distance of 200 mm and the transverse speed 500 mm/s (sample A0), as shown in Fig. 3. The variation in coating thicknesses can be clearly visible from the cross sections of the coatings sprayed by using different parameters. In fact, the process parameters affected the deposition efficiency of the polymer powder, as we can see from the results of the thickness measurements in Fig. 4. Considering the powder-feeding rate and the spraying distance as constant, the thickness of the coating decreased as the transverse speed increased from 500 to 900 mm/s (A1, B1, C1 and A2, B2, C2 in Fig. 4). This result is reasonable if we assume that

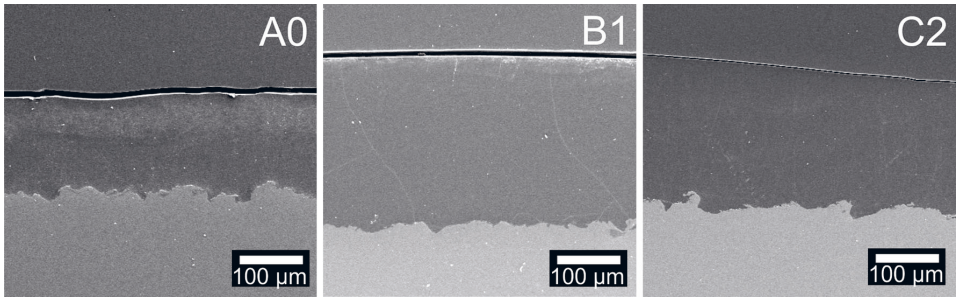

Fig. 3 SEM images of the cross sections of LDPE coatings sprayed with different process parameters. In particular from left to right: A0 with 200 mm and 500 mm/s; B1 with 250 mm and 700 mm/s; C1 with 300 mm and 900 mm/s

the amount of material deposited per unit length decreases as the transverse speed increases during the spraying process (powder-feeding rate and spraying distance as constant). However, for heat-sensitive material, this fact is not obvious, due to the strong dependence of the flow properties of the polymer from the process temperature and the effect of the combustion flame on the polymer powder (Ref 33). In fact, for the specimens sprayed at 500 mm/s, we can see that the coating thickness is influenced by the heat input within the material produced by lower transverse speed (see A0, A1, A2 in Fig. 4).

The standard deviations of the thickness measurements increased as the transverse speed increased from 500 to 900 mm/s. This is due to the variability in the coating texture, being rougher for samples produced with the higher transverse speed. This result was confirmed by the optical profilometer analyses of the coating surface. These analyses showed a gradual increase in the areal roughness with increasing transverse speed. The resulting areal roughness was related to the chosen process parameters and varied from 5 µm for the sample A0 to 18 µm for the sample C2. Figure 5 summarises the surface texture images and the areal roughness values for all of the specimens analysed in this study.

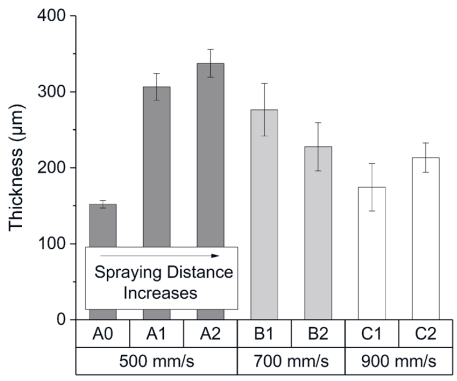

Fig. 4 Thicknesses measurement from the cross-sectional images of the coatings

Icephobicity and Wettability of the Coating Surface

A coating is considered icephobic when the adhesion of the ice formed on its surface is low enough that this can be easily removed by shear. However, different methods are used to evaluate the icephobicity of the surface. In particular, this can be evaluated by measuring the ice adhesion with different tests (Ref 45, 46), by studying the delay of droplet freezing (Ref 47, 48), the frost formation (Ref 49, 50), and the attitude of a cold surface to repel impacting water droplets (Ref 11, 51). In this work, the ice adhesion was measured by using the centrifugal adhesion method (Ref 35) to compare the icephobic characteristic of the produced coatings. For this test method, we defined a surface with low ice adhesion when the adhesion of ice is below 50 kPa (Ref 52). Moreover, the surface shows extremely low ice adhesion when the ice is shed off with a force lower than 10 kPa (Ref 52). Figure 6 represents the ice adhesion value (and standard deviation) and the areal roughness of the as-sprayed coatings.

The results showed a strong influence of the process parameters on the icephobicity of the coating surfaces. Firstly, for the slowest transverse speed (from A0 to A2), ice adhesions represented the highest values obtained in this study. The ice adhesion decreased with decreasing areal roughness according to the previous research (Ref 37, 53, 54). In particular, samples A resulted in the highest ice adhesion here, despite they represented the smoothest surfaces in comparison with the other coatings. This indicates that other factors are affecting the icephobicity of the surface in addition to areal roughness. Secondly, with the medium transverse speed (B1 and B2), no clear relation was found between the ice adhesion and the areal roughness. Thirdly, the lowest ice adhesion is reached with the specimen C1 (32 ± 3 kPa), showing an optimal combination of parameters in the process window of this study.

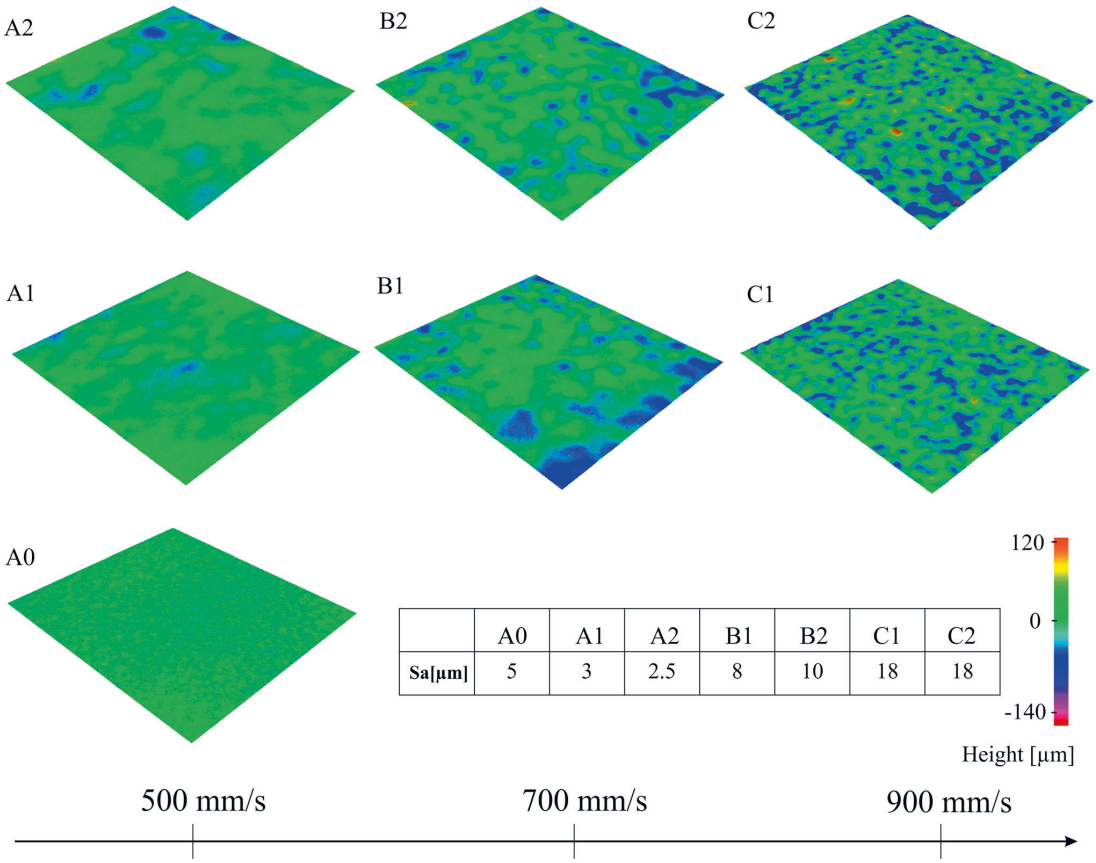

	A0	A1	A2	B1	B2	C1	C2
Sa[µm]	5	3	2.5	8	10	18	18

Fig. 5 Surface texture and areal roughness (Sa) of the coatings measured by optical profilometre analysis. The surface textures correspond to coating areas of approximately 30 × 30 mm^2

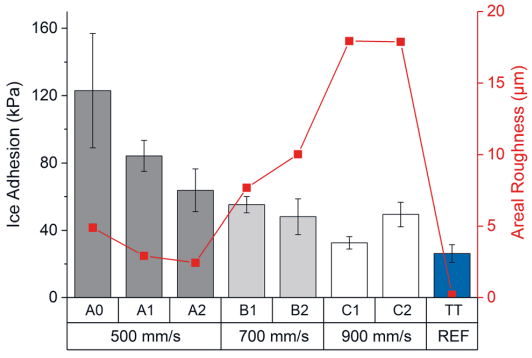

Fig. 6 Ice adhesion (left axis) and areal roughness Sa (right axis) of the coatings. Teflon tape (TT) represents the reference material for ice adhesion used in this centrifugal test

The wettability of the surface represents another important property in the analysis of the icephobicity of the coatings. In previous studies, the wettability of the surface has shown to be beneficial for the icephobicity of surfaces (Ref 46). The hydrophobicity (water contact angle greater than 90°) or the superhydrophobicity (water contact angle greater than 150°) of the surface would prevent water droplets to strongly adhere to the surface before freezing occurs (Ref 55). The increased water contact angle and the decreased roll-off angle have shown a reduced ice adhesion for superhydrophobic coating when ice is frozen onto the surface (Ref 56). However, when the ice is accreted from supercooled droplets, no clear connection has been found between the ice adhesion and the wettability properties of the surface (Ref 52). The wettability properties of the polyethylene coatings analysed in this work are

Table 3 The wettability properties of the polyethylene coatings

Sample	Water contact angle, °	Water roll-off angle, °
A0	93(± 1)	> 90
A1	90(± 1)	> 90
A2	94(± 1)	> 90
B1	93(± 1)	> 90
B2	93(± 3)	> 90
C1	89(± 2)	> 90
C2	92(± 3)	> 90

summarised in Table 3. The water contact angle for the produced coatings varied from 89° to 94°, showing a general hydrophobic character of the surface. Moreover, all the surfaces showed a roll-off angle higher than 90°, with the water droplets pinned onto the surface; hence, no roll off was observed. No relation between the wettability and icephobicity of the surface was found for all the coatings on which impact ice was accreted. Consequently, we can conclude that the process parameters did not strongly affect the wettability of the produced surfaces, although their icephobicity varied. Considering the trend of the ice adhesion results in Fig. 6, one of the factors influencing the icephobicity of the coating can be related to the different heat inputs of the process on the polymer material. In the case of heat-sensitive polymers, thermal degradation plays an important role in the coating process due to the presence of the combustion flame (Ref 33). In fact, thermal degradation might cause crosslinking of the polymer chains, chain scission, oxidation, and loss in the molecular weight (Ref 34). Moreover, degradation produces the embrittlement of the polymer surface that visually shows the presence of surface micro-cracks. These promote the formation of mechanical interlocking between ice and the damaged coating surface, increasing the ice adhesion strength (Ref 57). In addition, the chemical structure of the surface influences on the icephobicity. The possible chemical modification of the coating during the flame spray process might play a role in the variation in the ice adhesion strength with the process parameters. These factors affecting icephobicity will be investigated by using chemical and thermal analyses.

Chemical and Thermal Properties

In flame spraying, the combustion flame melts the polymer powder and the coating is formed by the molten particles hitting into the substrate surface (Ref 28). However, this flame causes the degradation of the polymer powder, especially for the smallest powder particles that do not withstand the flame temperature (they produce “sparks” in the flame). Moreover, the slowest transverse speed increases the time of the process, increasing the coating temperature (Ref 33). Consequently, degradation occurs by the mechanism of chain scission (producing short polymer chains and decreasing the molecular weight) and oxidation (Ref 29, 30, 58). The oxidation of thermally sprayed material is temperature and time-dependent process (Ref 28, 29, 59). The greater the time of exposition of the polymeric material to the flame, the higher the effect of the thermal oxidation in the deposited material. Two types of oxidation processes can be distinguished during the thermal spray process. Firstly, the oxidation process of the polymer powder occurs during the spraying of the powder passing the flame, known as in-flight oxidation. Secondly, the oxidation of the polymer splats, already deposited on the substrate, can happen during the coating formation. However, different researchers underlined the fundamental difficulty of separating the effect of these two stages of oxidation (Ref 28). The substrate temperature increases with increasing process time and decreased spraying distance (Ref 29, 60). For this reason, the chemical and thermal characterisations were needed for the flame-sprayed coatings to avoid the damage of mechanical properties, such as toughness and strength, and embrittlement of the coating surface (Ref 33).

The chemical analysis of the surfaces was carried out by investigating the possible variation in the FTIR spectra obtained for the different coatings in comparison with the virgin powder. Figure 7 represents the FTIR spectra of the powder (black curve) together with selected coating samples (AO, A1, A2, and C2). The FTIR spectrum of the LDPE powder (black curve in Fig. 7) showed the presence of the typical methylene peaks of the polyethylene polymer. In addition, the powder probably incorporates a conventional thermal stabiliser of an undisclosed composition containing polar (-OH) and carbonyl products (peak at 1734 cm^{-1}) (Ref 61). The main difference between the powder and the coatings spectra relied on the development of absorbance bands in the regions 1700-1750 cm^{-1} and 800-1300 cm^{-1}, respectively. In addition, the presence of a new absorbance peak at 1713 cm^{-1} was really evident for some of the sprayed coatings (intensity of absorbance peak at 1713 cm^{-1} of 0.04 for the virgin powder). Specifically, the intensity of the absorbance peak at 1713 cm^{-1} increased from 0.15 for the sample A2 to 0.30 for the sample A0, considering the coatings sprayed with the transverse speed of 500 mm/s. This increase in peak intensity indicated the greater modification of the chemical structure of the polyethylene with decreasing spraying distance during flame spraying. In particular, this new peak was related to the primary oxidation product formed by the thermal oxidation of polyethylene, mainly consisting of carboxylic acids and carbonyl compounds (Ref 40). In this research, oxygen is present both in the spraying

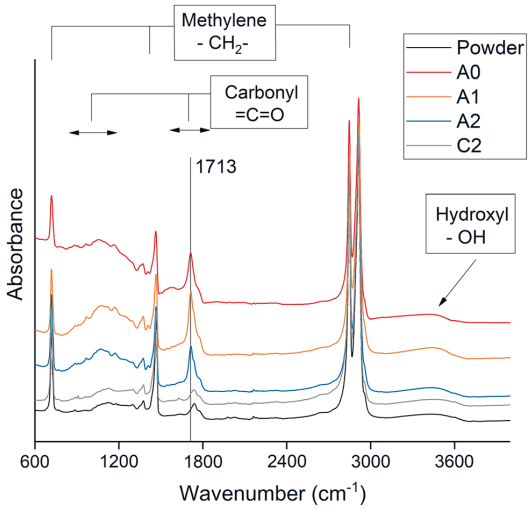

Fig. 7 FTIR spectra of LDPE powder and flame-sprayed LDPE coating sprayed with 500 mm/s (A0, A1, A2) and with 900 mm/s (C2)

environment and in the gas mixture used for the production of LDPE coatings. The principal chemical reactions of the oxidation mechanism of polyethylene can be described by three main stages (Ref 62). Firstly, free carbon radicals are produced from the polyethylene polymer chain via chain scission. The reaction is thermally initiated by the energy available from the combustion flame. Secondly, the oxygen reacts with the free carbon radicals to form peroxyl radicals, carbonyl compounds, and additional free carbon radicals. Finally, the free radicals react between each other to form carbonyl product, shorter polymer chain, and oxygen molecules (Ref 40, 62). The enhanced presence of the carbonyl products in the chemical structure confirmed that the thermal degradation of polyethylene gradually occurred at the coating surface as the heat input of the process increased. However, the production of carbonyl products gradually decreased as the combustion flame was further away from the coating surface and the time of the process was reduced. In particular, the specimen C2 (Fig. 7) revealed an FTIR spectrum similar to the polymer powder spectrum (the absorbance intensity at 1713 cm^{-1} equal to 0.07) with no evidence of the peak at 1713 cm^{-1}. This verified that the process parameters strongly affect the chemical composition of the coating and consequently its icephobicity. Figure 8 shows the relationship between the absorbance intensity of the peak at 1713 cm^{-1} for the produced coatings and the ice adhesion. We can see that the lower the intensity of the absorbance peak at 1713 cm^{-1}, the higher the icephobic behaviour of the coating. However, this trend was not verified for the

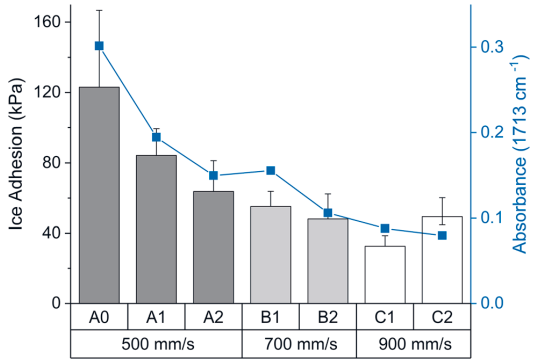

Fig. 8 Ice adhesion strength and absorbance intensity at 1713 cm^{-1} for the flame-sprayed LDPE coatings

sample C2 sprayed with 900 mm/s and 300 mm, where the degree of degradation was strongly decreased due to reduced process heat input for this combination of parameters (intensity equal to 0.07 for C2 and no evident peak at 1713 cm^{-1} in Fig. 7).

To compare the effect of process parameters on polymer degradation, the time the polymer is exposed to elevated temperatures was approximately estimated. The time of exposition of the in-flight particles to the flame can be considered of the same order for every produced coating, as the polymer particles passed through the same combustion flame with the same velocity. Therefore, the main effect of degradation would directly depend on the oxidation of the polymer splats on the substrate during the coating deposition. This oxidation mainly depends on the combination of process parameters chosen for the coating production, such as the transverse speed and the spraying distance. The transverse speed mostly influences the duration of the process and the spraying distance mainly controls the temperature reached by the substrate during the process. For a chosen spraying distance, the lower the transverse speed, the higher the degree of thermal oxidation experienced by the coating (see absorbance value between A1, B1, C1 and A2, B2, C2 in Fig. 8). Moreover, for a chosen transverse speed, the lower the spraying distance, the higher the temperature reached by the substrate, the higher the degree of oxidation of LPDE coatings (see absorbance value between A0, A1, A2 and B1, B2 in Fig. 8). Previously, FTIR analysis verified the increase in carbonyl and carboxyl compounds (containing oxygen element) limited at the coating surface for different spraying parameters. To support this, the energy dispersive x-ray spectroscopy (SEM/EDS) was used to evaluate the possible presence of carbonyl compounds (containing oxygen) in the coating structure. The mass percentage of oxygen was measured to be 14 ± 1 and $8 \pm 0.5\%$ for samples A0 and C2,

respectively. These values corresponded to the average of three measurements analysed from the coating cross section. In particular, sample A0 showed a higher amount of oxygen in the coating structure, confirming the greater level of degradation produced during the process.

The thermogravimetric analysis (TGA) was used as an additional technique to investigate the thermal degradation of the coating. TGA represents a thermal analysis that reveals the temperature where the polymer can be processed without breaking down it into a gas. The FTIR results confirmed the formation of new carbonyl and carboxyl groups for the sprayed coating. This fact implied the chain scission of polyethylene and consequently the formation of short polymer chains (Ref 40, 62). These short chains will evaporate at a lower temperature than the longer polymer chain. Consequently, the higher the amount of short polymer chains within the coating structure, the lower the temperature measured for a certain percentage of mass loss. Based on this, the thermal stability of the coating was evaluated by comparing the temperatures at which the 2% ($T_{98\%}$), 5% ($T_{95\%}$), and 10% ($T_{90\%}$) of coating mass were lost during TGA test. The TGA curves of the virgin powder (black curve) and the sample A0 (red curve) are represented in Fig. 9. In addition, the temperature at 98, 95, and 90% of mass loss are indicated in the magnified part (grey rectangular area) of the TGA curves. The results from the thermogravimetric analysis are summarised in Table 4.

For all the test samples, no relevant mass loss was measured below 150 °C, confirming the absence of moisture within the material and ensuring that the evaluated mass loss was referring only to the polymer chain degradation. Firstly, the results showed a good initial thermal stability of the powder that could withstand the temperature of 427 °C by evaporating only 2% of its total mass. In fact, the higher the value of $T_{98\%}$, the greater the thermal stability of the coating. Secondly, this good thermal stability was generally reduced for all the produced coatings. Therefore, the stability was decreased for the A specimens, confirming the highest degree of degradation for the sample sprayed with the closer distance, A0. For medium transverse speed (B1), the thermal stability of the coating slightly improved in comparison with the coatings sprayed with 500 mm/s. Moreover, even lower degradation was revealed for the sample C2, showing the loss of mass of 2% around 417 °C. This behaviour was reproduced for all the coating, also if we consider the temperatures at 5% mass loss ($T_{95\%}$) and 10% mass loss ($T_{90\%}$) in Table 4. These results strongly confirmed the decrease in thermal stability of the coating with the increased heat input on the polymer during the process. In fact, with decreasing transverse speed and spraying distance, the substrate can heat-up for a longer period of time, producing thermal degradation of the coating.

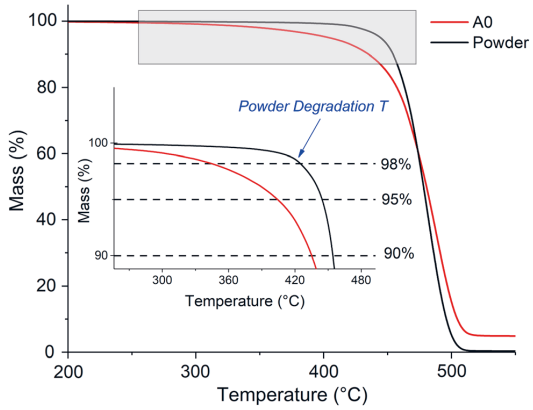

Fig. 9 TGA curve of the virgin powder (black curve) and sample A0 (red curve). The magnified part of the graph represents the evaluation of the temperature corresponding to mass loss of 2, 5, and 10% (Color figure online)

Table 4 Results of the thermogravimetric analysis

Sample	$T_{98\%}$, °C	$T_{95\%}$, °C	$T_{90\%}$, °C
Powder	427	444	454
A0	350	404	435
A1	363	408	434
A2	370	415	434
B1	380	424	443
C2	417	438	451

The effect of the thermal history produced by the flame spray process on the degree of crystallinity of the coating was investigated by differential scanning calorimetry (DSC). The degree of crystallinity represents an important feature for semi-crystalline thermoplastic polymers, such as LDPE. In fact, this property is directly proportional to the mechanical properties of the coating, such as tensile strength and modulus (Ref 63), and to its barrier properties, such as moisture, solvent absorption, and oxygen permeation (Ref 64). For this reason, the degree of crystallinity of the coatings should be as close as possible to the one of the original powder, as an indication of reduced thermal degradation. Figure 10 represents the endothermic melting peaks of the LDPE polymer both for the powder (black curve) and the coatings sprayed with 500 and 900 mm/s.

The curves in Fig. 10 showed the broadening of the melting-peak transition and the decrease in the melting-peak intensity, gradually passing from the virgin powder (black curve) to the sample A0 (red curve). This effect was clearly related to the degradation process (mainly polymer chain scission) of the low-density polyethylene polymer, as

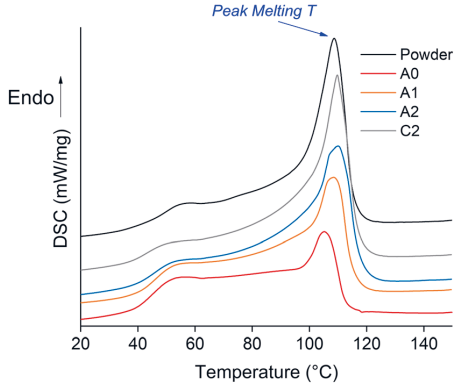

Fig. 10 Melting transition of LDPE powder and flame-sprayed coatings with 500 mm/s (A0, A1, and A2) and 900 mm/s (C2)

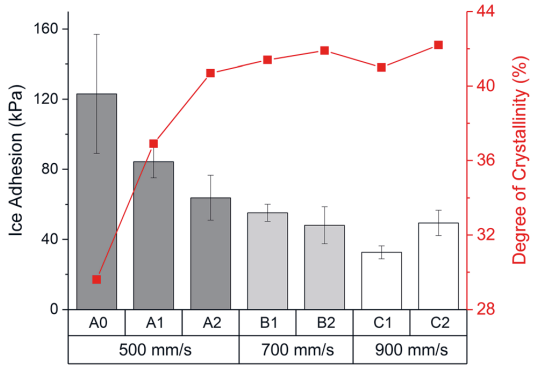

Fig. 11 Relationship between the ice adhesion strength (left axis) and the degree of crystallinity (right axis) of flame-sprayed LDPE coatings

Table 5 Melting temperatures and degree of crystallinity of LDPE powder and flame-sprayed coatings

Sample	ΔH, J/g	T_m, °C	χ, %
Powder	126.3	107.7	43
A0	86.8	105.2	29
A1	108.2	108.5	37
A2	119.4	110.0	40
B1	121.3	107.6	41
B2	123.0	108.7	42
C1	120.3	107.9	41
C2	123.8	109.8	42

observed in the previous studies (Ref 65). No evident differences were found between the curve of the powder and sample C2, confirming the reduced thermal degradation. The melting temperature (T_m), the melting enthalpy (ΔH), and the degree of crystallinity (χ) were evaluated for the flame-sprayed coatings by analysing the first dynamical heating. These values are summarised in Table 5. The values of the powder referred to the second heating after a slow cooling in the test. In fact, the melting transition of the first heating of the powder is related to the thermal history that the polymer undergoes during its production process. Consequently, this is not representative of the degree of crystallinity of the virgin material. For this reason, a second heating after the slow cooling was performed to obtain the maximum degree of crystallinity of the virgin powder.

The degree of crystallinity for the LDPE powder after a slow cooling was evaluated as 43%. This value was in the typical range of crystallinity for LDPE polymer, evaluated by DSC (Ref 66). Moreover, the degree of crystallinity of the polymer gradually increased as the heat input of the process decreased (increased spraying distance from A0 to A2 in Table 5). This effect was reduced for samples C, showing decreased thermal degradation (FTIR graph in Fig. 7). In addition, as shown by the FTIR spectrum (Fig. 7), the gradual degradation of the coating probably generated radical reactions that caused the crosslinking of the LDPE and, in some cases, reduced its crystallinity (Ref 67). In this study, a clear correlation was found between the ice adhesion strength and the degree of crystallinity of the coating, as shown in Fig. 11.

The degree of crystallinity was strongly influenced by the heat input of the process for the samples A0, A1, and A2, increasing from 29 to 40%. A slightly further increase was revealed for samples B, and then, the degree of crystallinity was independent of the chosen process parameters for the coldest temperatures. We can generally conclude that the thermal degradation of the polymer negatively influenced its degree of crystallinity within the considered process window. Moreover, the variation in the degree of crystallinity due to thermal degradation strongly influenced the mechanical properties of the polyethylene, such as its tensile strength, ductility, stiffness, and toughness (Ref 62). In addition, the barrier properties of the coating, such as permeability to air and moisture, represent an important aspect in relation to the ice adhesion of the coating. The previous studies have shown that the permeability of thermally aged PE film increases for both moisture and air, showing a decrease in the barrier properties of the material (Ref 68). In fact, the higher permeability of water within the coating structure could be easily related to the tendency of supercooled droplets to penetrate the surface. However, these properties were not investigated in this study. Therefore, it cannot be excluded that they could be connected with the reduction in the icephobic behaviour of the surface with increasing thermal degradation. We can conclude that the thermal degradation of the polymer is

correlated with the icephobicity of the surface, showing the higher ice adhesion strength for the most degraded polymer surfaces. However, further investigations are necessary to evaluate which aspect of thermal degradation, such as chain scission, oxidation, or surface embrittlement, directly influences the surface icephobicity.

Conclusions

In this study, icephobic LDPE coatings were produced with flame spraying by varying the heat input during coating processing. This was done by changing the transverse speed and the spraying distance of the spray gun. The optimisation of the parameters for the icephobic application was achieved through the process window designed for the LDPE coatings. In particular, it was found that the process parameters strongly affected the areal roughness of the coatings and the heat input during the production process. This increased the thermal degradation of the polymer coating, compromising its thermal stability, degree of crystallinity, and consequently its icephobic behaviour. For this reason, the heat input should be monitored during flame spraying of polymeric material to avoid the decrease in the coating properties. Here, we found that the most icephobic coating (ice adhesion strength 32 ± 3 kPa) was produced by using 900-mm/s transverse speed and 250-mm spraying distance. The areal roughness affected the ice adhesion, but no clear relationship was established for these samples. However, the thermal effect was shown to represent the main factor influencing the icephobicity of the coating. The heat input of the process influences both on the areal roughness and the thermal degradation of the coating. The higher the processing temperature of the polymer, the smoother the surface produced and the greater the material degradation. Connections were found between the thermal properties of the LDPE coating and the icephobic characteristic of the surface. In particular, an increase in the coating degradation (intensity of the absorbance peak at 1713 cm^{-1}) was strongly correlated with the decrease in the icephobicity for certain heat-input limit. After that, coatings achieve a relatively stable behaviour within the property deviation. Similarly, the degree of crystallinity increased as the degree of thermal degradation decreased and a good relationship was found with the decrease in ice adhesion until the limit. Moreover, this study showed that thermal stability is necessary for higher ice adhesion performance. This can be assumed to be one of the dominant factors in flame spraying of polymers. However, the coating degradation can be caused during both spraying and post-heating steps for these samples. Therefore, to understand better the effect of the process steps on the coating quality, further investigations will focus on their influence on the coating degradation and consequently on the icephobicity of the surface.

Acknowledgments Authors thank the LubISS (Lubricant Impregnated Slippery Surfaces) project that has received funding from the European Union's Horizon 2020 research and innovation programme under the Marie Sklodowska-Curie Grant Agreement No. 722497. Mr. Anssi Metsähonkala of Tampere University is acknowledged for operating the flame spray process, M.Sc. Jarmo Laakso of Tampere University for the SEM/EDS analysis, and M.Sc. Matteo Orlandini of Millidyne Oy for the particle size analysis. M.Sc. Henna Niemelä-Anttonen and B.Sc. Enni Hartikainen of Tampere University are thanked for assisting the ice accretion and the ice adhesion testing.

References

1. M. Farzaneh, *Atmospheric Icing of Power Networks*, M. Farzaneh, Ed., Springer Science + Business Media B.V, New York, 2008, https://doi.org/10.1007/978-1-4020-8531-4
2. J.L. Laforte, M.A. Allaire, and J. Laflamme, State-of-the-Art on Power Line de-Icing, *Atmos. Res.*, 1998, **46**(1–2), p 143-158. https://doi.org/10.1016/s0169-8095(97)00057-4
3. F.T. Lynch and A. Khodadoust, Effects of Ice Accretions on Aircraft Aerodynamics, *Prog. Aerosp. Sci.*, 2001, **37**(8), p 669-767. https://doi.org/10.1016/S0376-0421(01)00018-5
4. X. Huang, N. Tepylo, V. Pommier-Budinger, M. Budinger, E. Bonaccurso, P. Villedieu, and L. Bennani, A Survey of Icephobic Coatings and Their Potential Use in a Hybrid Coating/Active Ice Protection System for Aerospace Applications, *Prog. Aerosp. Sci.*, 2019, **105**, p 74-97. https://doi.org/10.1016/j.paerosci.2019.01.002
5. O. Parent and A. Ilinca, Anti-Icing and de-Icing Techniques for Wind Turbines: Critical Review, *Cold Reg. Sci. Technol.*, 2011, **65**(1), p 88-96. https://doi.org/10.1016/j.coldregions.2010.01.005
6. G.D. Lunn, M.A. Riley, and D.G. McCartney, A Study of Wire Breakup and In-Flight Particle Behavior During Wire Flame Spraying of Aluminum, *J. Therm. Spray Technol.*, 2017, **26**(8), p 1947-1958. https://doi.org/10.1007/s11666-017-0639-1
7. J.-D. Brassard, C. Laforte, F. Guerin, and C. Blackburn, Icephobicity: Definition and Measurement Regarding Atmospheric Icing, *Adv. Polym. Sci.*, 2017, https://doi.org/10.1007/12_2017_36
8. Y. Wang, M. Li, T. Lv, Q. Wang, Q. Chen, and J. Ding, Influence of Different Chemical Modifications on the Icephobic Properties of Superhydrophobic Surfaces in a Condensate Environment, *J. Mater. Chem. A*, 2015, **3**(9), p 4967-4975. https://doi.org/10.1039/C4TA07077A
9. K. Golovin, S.P.R. Kobaku, D.H. Lee, E.T. DiLoreto, J.M. Mabry, and A. Tuteja, Designing Durable Icephobic Surfaces, *Sci. Adv.*, 2016, **2**(3), p e1501496. https://doi.org/10.1126/sciadv.1501496
10. M.J. Kreder, J. Alvarenga, P. Kim, and J. Aizenberg, Design of Anti-Icing Surfaces: Smooth, Textured or Slippery?, *Nat. Rev. Mater.*, 2016, **1**(1), p 15003

11. L. Cao, A.K. Jones, V.K. Sikka, J. Wu, and D. Gao, Anti-Icing Superhydrophobic Coatings, *Langmuir*, 2009, **25**(21), p 12444-12448. https://doi.org/10.1021/la902882b
12. Y.H. Yeong, A. Milionis, E. Loth, and J. Sokhey, Self-Lubricating Icephobic Elastomer Coating (SLIC) for Ultralow Ice Adhesion with Enhanced Durability, *Cold Reg. Sci. Technol.*, 2018, **148**, p 29-37. https://doi.org/10.1016/j.coldregions.2018.01.005
13. Q. Fu, X. Wu, D. Kumar, J.W.C. Ho, P.D. Kanhere, N. Srikanth, E. Liu, P. Wilson, and Z. Chen, Development of Sol–Gel Icephobic Coatings: Effect of Surface Roughness and Surface Energy, *ACS Appl. Mater. Interfaces.*, 2014, **6**(23), p 20685-20692. https://doi.org/10.1021/am504348x
14. D. Tejero-Martin, M. Rezvani Rad, A. McDonald, and T. Hussain, Beyond Traditional Coatings: A Review on Thermal-Sprayed Functional and Smart Coatings, *J. Therm. Spray Technol.*, 2019, **28**(4), p 598-644. https://doi.org/10.1007/s11666-019-00857-1
15. N. Espallargas, *Future Development of Thermal Spray Coatings: Types, Designs, Manufacture and Applications*, Elsevier, Cambridge, 2015, https://doi.org/10.1016/B978-0-85709-769-9.00006-3
16. F.Y. Yan, K.A. Gross, G.P. Simon, and C.C. Berndt, Mechanical and Erosion Properties of CaCO3-EMAA Thermal Sprayed Coatings, *Polym. Eng. Sci.*, 2004, **44**(8), p 1448-1459. https://doi.org/10.1002/pen.20141
17. C.C. Berndt, D. Otterson, M.L. Allan, C.C. Berndt, and D. Otterson, Polymer Coatings for Corrosion Protection in Biochemical Treatment of Geothermal Residues, *Geotherm. Resour. Counc. Trans.*, 1998, **22**, p 425-429
18. T. Sugama, R. Kawase, C.C. Berndt, and H. Herman, An Evaluation of Methacrylic Acid-Modified Poly(Ethylene) Coatings Applied by Flame Spray Technology, *Prog. Org. Coat.*, 1995, **25**(2), p 205-216. https://doi.org/10.1016/0300-9440(94)00507-W
19. X. Chen, J. Yuan, J. Huang, K. Ren, Y. Liu, S. Lu, and H. Li, Large-Scale Fabrication of Superhydrophobic Polyurethane/Nano-Al_2O_3 Coatings by Suspension Flame Spraying for Anti-Corrosion Applications, *Appl. Surf. Sci.*, 2014, **311**, p 864-869. https://doi.org/10.1016/j.apsusc.2014.05.186
20. R.A.X. Nunes, S. Wagner, and J.R.T. Branco, Atrito e Desgaste de Recobrimentos de PET, Politeraftalato de Etileno, Pós-Consumo Processados Por Aspersão Térmica (Friction and Wear of Polyethylene Terephthalate (PET) coating after consumption processed by thermal spraying), *Polímeros Ciência e Tecnol.*, 2007, **17**(3), p 244-249 ((In Portuguese))
21. C. Mateus, S. Costil, R. Bolot, and C. Coddet, Ceramic/Fluoropolymer Composite Coatings by Thermal Spraying—a Modification of Surface Properties, *Surf. Coat. Technol.*, 2005, **191**(1), p 108-118. https://doi.org/10.1016/j.surfcoat.2004.04.084
22. Y. Bao, D.T. Gawne, and T. Zhang, Effect of Feedstock Particle Size on the Heat Transfer Rates and Properties of Thermally Sprayed Polymer Coatings, *Trans. Inst. Met. Finish.*, 1995, **73**(pt 4), p 119-124
23. X. Chen, Y. Gong, X. Suo, J. Huang, Y. Liu, and H. Li, Construction of Mechanically Durable Superhydrophobic Surfaces by Thermal Spray Deposition and Further Surface Modification, *Appl. Surf. Sci.*, 2015, **356**, p 639-644. https://doi.org/10.1016/j.apsusc.2015.08.156
24. L.D. Stephenson, A.D. Beitelman, R.G. Lampo, A. Kumar, D. Neale, L. Clark, K. Palutke, M. Surratt, and D. Butler, Demonstration of Thermally Sprayed Metal and Polymer Coatings for Steel Structures at Fort Bragg, NC, No. ERDC/CERL TR-17-30, ERDC-CERL Champaign United States, 2017
25. P.J. Loustaunau and D. Horton, EMAA Thermoplastic Powder Coatings: Shop and Field Applications of Powder Coatings for Aggressive Environments, No. CONF.-94022-, NACE International, Houston, TX (United States), 1994. https://www.osti.gov/biblio/70079
26. Z. Jia, Y. Liu, Y. Wang, Y. Gong, P. Jin, X. Suo, and H. Li, Flame Spray Fabrication of Polyethylene-Cu Composite Coatings with Enwrapped Structures: A New Route for Constructing Antifouling Layers, *Surf. Coat. Technol.*, 2017, **309**, p 872-879. https://doi.org/10.1016/j.surfcoat.2016.10.071
27. M. Zhai, Y. Gong, X. Chen, T. Xiao, G. Zhang, L. Xu, and H. Li, Mass-Producible Hydrophobic per Fl Uoroalkoxy/Nano-Silver Coatings by Suspension Fl Ame Spraying for Antifouling and Drag Reduction Applications, *Surf. Coat. Technol.*, 2017, **328**, p 115-120. https://doi.org/10.1016/j.surfcoat.2017.08.049
28. L. Pawlowski, *The Science and Engineering of Thermal Spray Coatings*, 2nd ed., Wiley, Chichester, 2008, https://doi.org/10.1002/9780470754085
29. E. Petrovicova and L.S. Schadler, Thermal Spraying of Polymers, *Int. Mater. Rev.*, 2002, **47**(4), p 169-190. https://doi.org/10.1179/095066002225006566
30. J.A. Brogan, C.C. Berndt, G.P. Simon, and D. Hewitt, Physical and Relaxation Properties of Flame-Sprayed Ethylene-Methacrylic Acid Copolymer, *Polym. Eng. Sci.*, 1998, **38**(11), p 1873-1881
31. H. Koivuluoto, C. Stenroos, M. Kylmälahti, M. Apostol, J. Kiilakoski, and P. Vuoristo, Anti-Icing Behavior of Thermally Sprayed Polymer Coatings, *J. Therm. Spray Technol.*, 2017, **26**(1–2), p 150-160. https://doi.org/10.1007/s11666-016-0501-x
32. H. Niemelä-Anttonen, H. Koivuluoto, M. Kylmälahti, J. Laakso, and P. Vuoristo, Thermally Sprayed Slippery and Icephobic Surfaces, *ITSC2018-Proceedings of the International Thermal Spray Conference*, F. Azarmi, K. Balani, T. Eden, T. Hussain, Y.-C. Lau, H. Li, and K. Shinoda, Ed., ASM International, Orlando, 2018, p 380-384
33. T. Zhang, D.T. Gawne, and Y. Bao, The Influence of Process Parameters on the Degradation of Thermally Sprayed Polymer Coatings, *Surf. Coat. Technol.*, 1997, **96**, p 337-344. https://doi.org/10.1016/S0257-8972(97)00269-7
34. J.A. Brogan, Thermal-Spraying of Polymers and Polymer Blends, *MRS Bull.*, 2000, **25**(7), p 48-53. https://doi.org/10.1557/mrs2000.124
35. H. Koivuluoto, C. Stenroos, R. Ruohomaa, G. Bolelli, L. Lusvarghi, and P. Vuoristo, Research on Icing Behavior and Ice Adhesion Testing of Icephobic Surfaces, *Proceedings of* 16*th International Workshop on Atmospheric Icing of Structures-IWAIS XVI*, Jun 28–Jul 3, (Uppsala, Sweden), 2015, p 6
36. F. Guerin, C. Laforte, M.I. Farinas, and J. Perron, Analytical Model Based on Experimental Data of Centrifuge Ice Adhesion Tests with Different Substrates, *Cold Reg. Sci. Technol.*, 2016, **121**, p 93-99. https://doi.org/10.1016/j.coldregions.2015.10.011
37. S. Tarquini, C. Antonini, A. Amirfazli, M. Marengo, and J. Palacios, Investigation of Ice Shedding Properties of Superhydrophobic Coatings on Helicopter Blades, *Cold Reg. Sci. Technol.*, 2014, **100**, p 50-58. https://doi.org/10.1016/j.coldregions.2013.12.009
38. C. Stenroos, P. Vuoristo, and H. Koivuluoto, "Properties of Icephobic Surfaces in Different Icing Conditions," Master thesis, Tampere University Technology, Tampere, Finland, 2015
39. S. Therias, J.-L. Gardette, B. Pukánszky, T. Janecska, A. Perthue, M. Gardette, and E. Földes, Photo- and Thermal-Oxidation of Polyethylene: Comparison of Mechanisms and Influence of Unsaturation Content, *Polym. Degrad. Stab.*, 2013, **98**(11), p 2383-2390. https://doi.org/10.1016/j.polymdegradstab.2013.07.017
40. M. Sugimoto, A. Shimada, H. Kudoh, K. Tamura, and T. Seguchi, Product Analysis for Polyethylene Degradation by Radiation

and Thermal Ageing, *Radiat. Phys. Chem.*, 2013, **82**(1), p 69-73. https://doi.org/10.1016/j.radphyschem.2012.08.009
41. P. Gałka, J. Kowalonek, and H. Kaczmarek, Thermogravimetric Analysis of Thermal Stability of Poly(Methyl Methacrylate) Films Modified with Photoinitiators, *J. Therm. Anal. Calorim.*, 2014, **115**(2), p 1387-1394. https://doi.org/10.1007/s10973-013-3446-z
42. B. Wunderlich, *Thermal Analysis of Polymeric Materials*, Springer, Berlin, 2005, https://doi.org/10.1007/b137476
43. M. Zou, S. Beckford, R. Wei, C. Ellis, G. Hatton, and M.A. Miller, Effects of Surface Roughness and Energy on Ice Adhesion Strength, *Appl. Surf. Sci.*, 2011, **257**(8), p 3786-3792. https://doi.org/10.1016/j.apsusc.2010.11.149
44. M.F. Hassan, H.P. Lee, and S.P. Lim, The Variation of Ice Adhesion Strength with Substrate Surface Roughness, *Meas. Sci. Technol.*, 2010, **21**(7), p 75701-75709. https://doi.org/10.1088/0957-0233/21/7/075701
45. C. Laforte and J.-L.J. Laforte, Tensile, Torsional and Bending Strain at the Adhesive Rupture of an Iced Substrate, *Proceedings of the* 28*th International Conference on Ocean, Offshore and Arctic Engineering - OMAE* 2009, May 31–Jun 5, (Honolulu, Hawaii, USA), ASME, 2009, p 79–86
46. A.J. Meuler, J.D. Smith, K.K. Varanasi, J.M. Mabry, G.H. McKinley, and R.E. Cohen, Relationships between Water Wettability and Ice Adhesion, *ACS Appl. Mater. Interfaces.*, 2010, **2**(11), p 3100-3110. https://doi.org/10.1021/am1006035
47. P. Tourkine, M. Le Merrer, and D. Quéré, Delayed Freezing on Water Repellent Materials, *Langmuir*, 2009, **25**(13), p 7214-7216. https://doi.org/10.1021/la900929u
48. F. Arianpour, M. Farzaneh, and S.A. Kulinich, Hydrophobic and Ice-Retarding Properties of Doped Silicone Rubber Coatings, *Appl. Surf. Sci.*, 2013, **265**, p 546-552. https://doi.org/10.1016/j.apsusc.2012.11.042
49. P. Kim, T.S. Wong, J. Alvarenga, M.J. Kreder, W.E. Adorno-Martinez, and J. Aizenberg, Liquid-Infused Nanostructured Surfaces with Extreme Anti-Ice and Anti-Frost Performance, *ACS Nano*, 2012, **6**(8), p 6569-6577. https://doi.org/10.1021/nn302310q
50. A. Kirillova, L. Ionov, I.V. Roisman, and A. Synytska, Hybrid Hairy Janus Particles for Anti-Icing and De-Icing Surfaces: Synergism of Properties and Effects, *Chem. Mater.*, 2016, **28**(19), p 6995-7005. https://doi.org/10.1021/acs.chemmater.6b02765
51. K.K. Varanasi, T. Deng, J.D. Smith, M. Hsu, and N. Bhate, Frost Formation and Ice Adhesion on Superhydrophobic Surfaces, *Appl. Phys. Lett.*, 2010, **97**(90), p 234102. https://doi.org/10.1063/1.2731434
52. H. Niemelä-Anttonen, H. Koivuluoto, M. Tuominen, H. Teisala, P. Juuti, J. Haapanen, J. Harra, C. Stenroos, J. Lahti, J. Kuusipalo, J.M. Mäkelä, and P. Vuoristo, Icephobicity of Slippery Liquid Infused Porous Surfaces under Multiple Freeze-Thaw and Ice Accretion-Detachment Cycles, *Adv. Mater. Interfaces*, 2018, **5**(20), p 1800828. https://doi.org/10.1002/admi.201800828
53. R.J. Scavuzzo and M.L. Chu, *Structural Properties of Impact Ices Accreted on Aircraft Structures*, NASA Cr-179580, NASA-Lewis Research Centre, Cleveland, 1987
54. D.L. Loughborough and E.G. Hass, Reduction of the Adhesion of Ice to De-Icer Surfaces, *J. Aeronaut. Sci.*, 1946, **13**(3), p 126-134. https://doi.org/10.2514/8.11328
55. J. Chanda, L. Ionov, A. Kirillova, and A. Synytska, New Insight into Icing and De-Icing Properties of Hydrophobic and Hydrophilic Structured Surfaces Based on Core-Shell Particles, *Soft Matter*, 2015, **11**(47), p 9126-9134. https://doi.org/10.1039/c5sm02143j
56. Y. Shen, H. Tao, S. Chen, L. Zhu, T. Wang, and J. Tao, Icephobic/Anti-Icing Potential of Superhydrophobic Ti6Al4 V Surfaces with Hierarchical Textures, *RSC Adv.*, 2015, **5**(3), p 1666-1672. https://doi.org/10.1039/C4RA12150C
57. J. Chen, J. Liu, M. He, K. Li, D. Cui, Q. Zhang, X. Zeng, Y. Zhang, J. Wang, and Y. Song, Superhydrophobic Surfaces Cannot Reduce Ice Adhesion, *Appl. Phys. Lett.*, 2012, **101**(11), p 111603. https://doi.org/10.1063/1.4752436
58. F. Khabbaz, A.C. Albertsson, and S. Karlsson, Chemical and Morphological Changes of Environmentally Degradable Polyethylene Films Exposed to Thermo-Oxidation, *Polym. Degrad. Stab.*, 1999, **63**(1), p 127-138. https://doi.org/10.1016/S0141-3910(98)00082-2
59. R. Perrin and J.P. Scharff, *Chimie Industrielle*, 2nd ed., Industrial Chemistry, Masson, 1997 ((In French))
60. Y. Bao, D.T. Gawne, D. Vesely, and M.J. Bevis, Formation and Microstructure of Plasma Sprayed Polyamide Coatings, *Surf. Eng.*, 1994, **10**(4), p 307-313
61. A.C. Albertsson, C. Barenstedt, and S. Karlsson, Susceptibility of Enhanced Environmentally Degradable Polyethylene to Thermal and Photo-Oxidation, *Polym. Degrad. Stab.*, 1992, **37**(2), p 163-171. https://doi.org/10.1016/0141-3910(92)90080-O
62. B. Zhao, S. Zhang, C. Sun, J. Guo, Y.X. Yu, and T. Xu, Aging Behaviour and Properties Evaluation of High-Density Polyethylene (HDPE) in Heating-Oxygen Environment, *IOP Conf. Ser. Mater. Sci. Eng.*, 2018, **369**, p 012021. https://doi.org/10.1088/1757-899X/369/1/012021
63. R. Ferhoum, Analysis of Thermal Ageing Effect (Hold Time - Crystallinity Rate - Mechanical Property) on High Density Polyethylene (HDPE), *Int. J. Mater. Sci. Appl.*, 2013, **2**(3), p 109-114. https://doi.org/10.11648/j.ijmsa.20130203.17
64. E.R. George and J. Reimer, Flamesprayed Thermoplastic Powder Coatings, *Polym. Eng. Sci.*, 1991, **31**(11), p 789-792. https://doi.org/10.1002/pen.760311105
65. J.V. Gulmine, P.R. Janissek, H.M. Heise, and L. Akcelrud, Degradation Profile of Polyethylene after Artificial Accelerated Weathering, *Polym. Degrad. Stab.*, 2003, **79**(3), p 385-397. https://doi.org/10.1016/S0141-3910(02)00338-5
66. P. Guo, M. Wen, L. Wang, and Y. Zheng, Strong Anti-Ice Ability of Nanohairs over Micro-Ratchet Structures, *Nanoscale*, 2014, **6**(8), p 3917-3920. https://doi.org/10.1039/C3NR04061E
67. A.G. Pedroso and D.S. Rosa, Mechanical, Thermal and Morphological Characterization of Recycled LDPE/Corn Starch Blends, *Carbohydr. Polym.*, 2005, **59**(1), p 1-9. https://doi.org/10.1016/j.carbpol.2004.08.018
68. C. Li and S.L. Xiao, Effects on the Properties of Polyethylene Film Aging by Different Methods, *Adv. Mater. Res.*, 2013, **830**, p 49-52. https://doi.org/10.4028/www.scientific.net/AMR.830.49

PUBLICATION II

Lubricated icephobic coatings prepared by flame spraying with hybrid feedstock injection

V. Donadei, H. Koivuluoto, E. Sarlin, and P. Vuoristo

Surface and Coatings Technology, 403 (2020),126396
DOI: 10.1016/j.surfcoat.2020.126396

Surface & Coatings Technology 403 (2020) 126396

Contents lists available at ScienceDirect

Surface & Coatings Technology

journal homepage: www.elsevier.com/locate/surfcoat

Lubricated icephobic coatings prepared by flame spraying with hybrid feedstock injection

Valentina Donadei*, Heli Koivuluoto, Essi Sarlin, Petri Vuoristo

Materials Science and Environmental Engineering, Faculty of Engineering and Natural Sciences, Tampere University, P.O. Box 589, FI-33014 Tampere, Finland

ARTICLE INFO

Keywords:
Thermal spraying
Icephobic coatings
Ice adhesion
Polymer coatings
Thermal degradation

ABSTRACT

Lubricated icephobic coatings were fabricated by flame spraying with hybrid feedstock injection. In this one-step process, composite coatings were produced by spraying a matrix material from a combustion flame spray gun and a lubricating additive from an injector, externally to the flame. External injection avoided possible thermal degradation of the heat sensitive additive during spraying. Inexpensive and widely available feedstock materials were used, polyethylene as the matrix and solid cottonseed oil as the lubricating additive. The coating properties were investigated by thermal and chemical analyses, surface roughness and wettability measurements at room temperature and in cold conditions. The icephobic behaviour was evaluated by accreting ice from supercooled water droplets in the icing wind tunnel. Ice adhesion was measured by the centrifugal ice adhesion test. The results showed that lubricant addition improved the icephobic performance of the coatings. Moreover, cooling the flame temperature with compressed air addition reduced thermal degradation of polymers. This was beneficial for the icephobic behaviour, thus lowering the shear ice adhesion strength down to 23 kPa ± 6 kPa. In conclusion, lubricated icephobic coatings were successfully produced by combining the hybrid feedstock injection and the thorough optimization of process parameters. This approach provides a potential surface engineering solution for the industrial sectors facing icing problems.

1. Introduction

In recent years, the demand for icephobic surface solutions has increased in industrial applications facing icing problems, such as power lines [1,2], wind turbines [3,4], solar panels [5,6], telecommunication and transportation in outdoor environments [7–9]. The accumulation and accretion of ice on functional surfaces represent a serious risk for several applications. For example, accumulation of ice on infrastructures can compromise their mechanical stability and, eventually, cause their collapse [10]. Moreover, accretion of ice on aircraft structures can modify the aerodynamics, endangering flight operations [7]. For this reason, the development of icephobic surface solutions is fundamental to solve this problem affecting industrial applications. Different strategies have been adopted to face icing problems, namely active and passive methods of ice removal. Active methods involve physical removal of ice by scraping operation and/or mechanical vibration, melting of ice by thermal heating or application of de-icing chemicals on surfaces [11,12]. However, these active methods require repetitive manual operations, waste of resources, environmental pollution and, consequently, additional costs [13–15]. Considering these disadvantages, an alternative strategy is represented by passive methods. These consist of smart paints, coatings and surface modifications [16], which lower the ice adhesion of surfaces and, then, easily promote passive ice removal. Recently, passive icephobic solutions have been developed to address industrial needs [17–20]. These include the availability of coatings or surface treatments, which show permanent icephobicity and withstand severe weather conditions, such as exposure to ultraviolet (UV) light radiation, changes of temperature and humidity, wind, rain, sandstorm, or some combination of these. Furthermore, the industry requires suitable coating techniques, which should preferably be fast, scalable, versatile and cost-efficient.

Different surface designs have been proposed in the literature with potential icephobic properties to reduce ice accumulation and/or ice adhesion on surfaces [21]. For example, superhydrophobic surfaces (SHS) (water contact angle ≥ 150°) effectively reduce the accumulation of ice compared to untreated metal surfaces [22,23]. The hierarchical micro/nanostructure of SHS helps to repel water droplets approaching the surface. Moreover, if water droplets are deposited on SHS, their hierarchical structure delays ice nucleation [24,25]. However, researchers have demonstrated that the icephobic properties of SHS are

* Corresponding author at: Tampere University, Korkeakoulunkatu 6, P.O. Box 589, FI-33014 Tampere, Finland.
E-mail addresses: valentina.donadei@tuni.fi (V. Donadei), heli.koivuluoto@tuni.fi (H. Koivuluoto), essi.sarlin@tuni.fi (E. Sarlin), petri.vuoristo@tuni.fi (P. Vuoristo).

https://doi.org/10.1016/j.surfcoat.2020.126396
Received 18 July 2020; Received in revised form 3 September 2020; Accepted 7 September 2020
Available online 09 September 2020

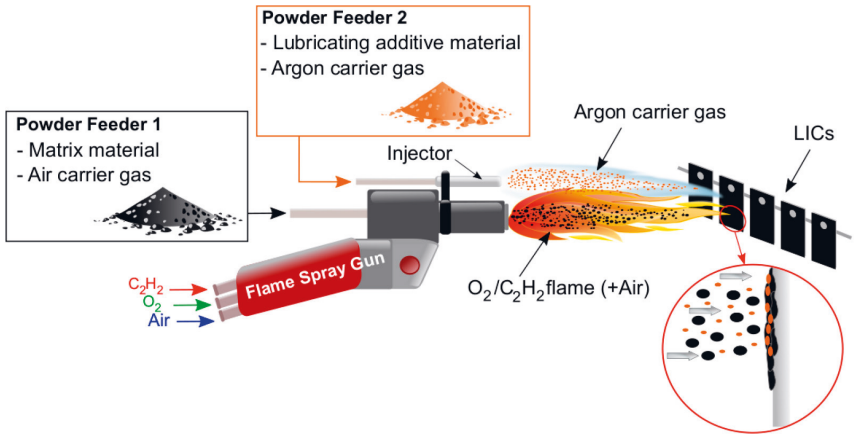

Fig. 1. Schematization of the flame spray process with hybrid feedstock injection to produce lubricated icephobic coatings (LICs). The matrix material is sprayed directly from the flame spray gun whereas the lubricating additive is externally fed from an injector with argon as a carrier gas.

severely damaged in high humidity and sub-zero conditions because of water condensation within surface features [26,27]. Therefore, alternative surface solutions are under consideration. Another surface design, namely slippery liquid-infused porous surface (SLIPS) [28], has been proposed as a solution for facing icing problems. SLIPS commonly consist of a micro/nanostructure infused with a liquid lubricant. These surfaces show potential anti-icing and anti-frost properties due to the presence of the liquid layer, which promotes the inhibition of ice nucleation [29,30]. Furthermore, once the ice forms on SLIPS, the extremely smooth layer of lubricant serves as a protection of the surface structure by preventing mechanical interlocking between the ice and the surface [31,32]. However, if the liquid lubricant is depleted, the surface experiences degradation of its icephobicity [21]. To solve this challenge, different strategies have been developed to improve the stability of liquid lubricant in SLIPS [32,33]. For example, one common strategy consists of entrapping the liquid lubricant within a network of cross-linked elastomers [34,35]. Furthermore, lubricant in the form of solid is infused within the coating structure to improve lubricant stability and thus obtaining long-term icephobicity [36,37].

Inspired by the infusion of solid lubricant, we fabricated a composite coating, composed of a matrix material and a lubricating additive, hereafter termed lubricated icephobic coating (LIC). Lubricating additives, in the form of liquid oil [34,38], grease paste [17] and solid wax [36,39], have shown potential icephobic behaviour [40]. In the present study, the matrix material is made of low-density polyethylene (LDPE), previously used to produce flame sprayed icephobic coatings [41–43]. The lubricant, namely fully hydrogenated cottonseed oil, represents the solid additive of LICs. The hydrogenated cottonseed oil consists of a hydrophobic waxy solid [44], generally employed as a coating release agent [45] or taste masking tool [46] for pharmaceutical purposes. Additionally, this specific combination of materials, namely polyethylene and liquid cottonseed oil, has been successfully used in SLIPS for packaging applications because of their excellent chemical compatibility [47].

In the last decades, icephobic coatings have been fabricated with different techniques, consisting mainly of laboratory-scale coating synthesis [21,34] and paint technology [48,49]. However, these methods require post-curing with evaporation of volatile organic compounds (VOCs), large waste of chemicals, and/or controlled environmental conditions. Therefore, alternative coating technologies are under consideration. Recently, icephobic coatings have been manufactured using different thermal spray techniques, such as suspension plasma spray [50], high-velocity oxygen-fuel (HVOF) spray [51–53], and flame spray processes [41,42,54,55]. However, some of these require a post-treatment to render the surface water repellent [50,53] or to infuse the liquid lubricant [54]. In this study, we propose a one-step flame spray process as a potential method to produce icephobic coatings, thus eliminating VOCs, post-curing and need for controlled environments [56]. We modified flame spraying by adding an injector externally to the flame spray gun. Matrix material was sprayed with the flame spray gun and lubricating additive was fed with an external injector. This protects the heat sensitive lubricant from the flame torch, thus limiting its degradation. We referred to this method as the flame spray process with hybrid feedstock injection. The objectives of the study were to (1) modify flame spray technique to process such heat sensitive materials and to produce lubricated coatings in one-step, (2) optimise the process parameters for these specific materials to produce coatings with enhanced icephobic properties, (3) study the effect of process parameters on coating properties, such as surface chemistry, topography and wettability, and (4) evaluate the icephobic behaviour of lubricated coatings, understanding possible correlations between surface properties and icephobicity.

2. Experimental procedure

2.1. Materials and coating manufacturing

Commercially available low-density polyethylene (LDPE) powder (Plascoat LDPE, Plascoat Europe BV, The Netherlands) was used as a feedstock material to produce the lubricated coatings. This represents the main component of the coatings, considered as the matrix material of the composite structure. A solid lubricant (Lubritab® capsules, JRS PHARMA GmbH & Co. KG, Germany), made of fully hydrogenated cottonseed oil, was used as the lubricating additive. The lubricated icephobic coatings (LICs) were manufactured by the flame spray process with hybrid feedstock injection, which is schematically represented in Fig. 1.

A similar approach has been used to produce low friction coatings by externally feeding additives in the form of suspension [57,58]. In our study, the dry additive was fed externally to the spray gun to avoid direct contact with flame. The solid lubricant, made of hydrocarbons, can serve as a fuel in the flame and, therefore, its interaction with the combustion flame should be avoided. In this hybrid process, the matrix powder was sprayed by an oxygen-acetylene flame spray gun (CastoDyn DS 8000, Castolin Eutectic, Switzerland). This was axially fed using a powder feeder (Sulzer Metco 4MP, Oerlikon Metco, Switzerland) with

Table 1
Process parameters of the flame spray process with hybrid feedstock injection.

Process parameters	Value
CastoDyn DS 8000 – flame spray gun	
Nozzle model	SSM10
Combustion gasses	
Oxygen pressure [bar]	4.2
Acetylene pressure [bar]	0.7
Compressed air pressure [bar]	0, 2, 4
Gun spray distance [mm]	250
Gun traverse speed [mm/s]	500, 700, 900
Step size [mm]	5
Number of coating layers	4
Sulzer Metco 4MP-850D dual powder feeder - matrix powder	
Matrix material feed rate [g/min]	26
Carrier gas (air) flow rate [L/min]	10
Carrier gas (air) input pressure [bar]	5
PT-10 twin powder feeder – additive powder	
Lubricating additive material feed rate [g/min]	11
Carrier gas (argon) flow rate [L/min]	6

compressed air as a carrier gas. Simultaneously, the lubricating additive was sprayed from an injector mounted on the left side of the gun. The external injector was oriented towards the gun with its axis intersecting the flame spray gun axis at the distance of about 280 mm from the flame spray nozzle. The lubricant was fed using a powder feeder (PT-10 Twin powder feeder, Oerlikon Metco, Switzerland) with argon as a carrier gas, to further protect the additive from thermal oxidation. Mechanical sieving prior to spraying was necessary for the additive to increase its flowability and ensure continuity during powder feeding. The spray gun was mounted on a single-arm robot (ABB IRB 4400/60, ABB Robotics, Sweden), controlling traverse speed and spray distance during coating production. The process parameters used for the fabrication of LICs are listed in Table 1.

Coatings were deposited on stainless steel substrates (EN 1.4301/2K (4N)), 30 mm × 60 mm × 1.5 mm in dimensions. The steel substrates were grit-blasted prior to spraying using aluminium oxide powder (grit size of 54 mesh), resulting in surface roughness of Ra ≈ 2.8 μm. The substrates were pre-heated by flame to ensure good adhesion between coating and substrate. The substrate temperature was monitored during pre-heating by a thermal imaging camera (Ti300 Infrared Camera IR Fusion Technology, Fluke Corporation, United States). The thermal camera was calibrated for the substrate material prior to spraying. Coating deposition started when the substrate exceeded the melting range of the matrix powder. This monitoring avoided the overheating of the substrate, which could cause polymer degradation [59].

From technical datasheets of the feedstock materials, the lubricant has a lower melting temperature range (57–70 °C) compared to the polyethylene material (107 °C). This requires the adjustment of the process parameters to reduce the heat load transferred to different polymeric materials. To achieve this, the following process parameters were varied (Table 1). Firstly, compressed air was added to the flame with variable pressure, namely 0, 2 and 4 bar. Addition of air reduces the flame temperature with the increase of pressure used. Secondly, a higher gun traverse speed was employed when no additional compressed air was added to the flame to reduce the heat load on the polymeric materials. The traverse speed was gradually reduced when compressed air was added to the combustion gasses. Finally, the post-heating by flame was performed for one selected coating to study its effect on the surface properties. The gun spray distance was fixed to 250 mm, according to our previous studies [42,43]. Fig. 2 summaries the process parameters used for LICs, flame-sprayed polyethylene coating (FS-PE1) and plain lubricant coating without matrix material (L4). L4 was produced to better understand the effect of lubricant addition on the properties of LICs. The FS-PE1 sample was fabricated with the same process parameters of the best polyethylene icephobic surface reported in our previous study [42], avoiding the post-heating by flame

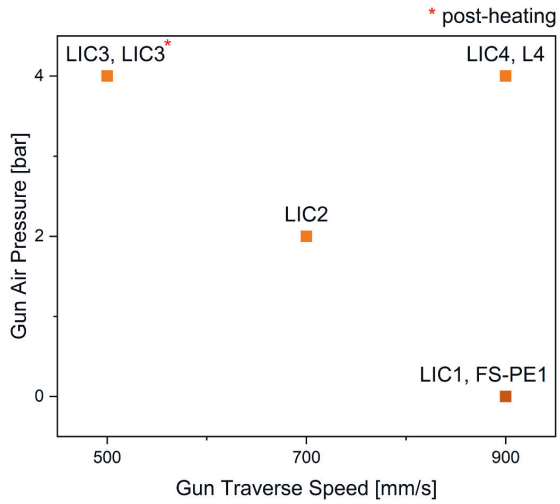

Fig. 2. Process window of the chosen parameters for the coatings produced in this work. The designation LIC indicates the coating made of both LDPE and lubricant powder by the flame spray process with hybrid feedstock injection. L4 corresponds to the coating produced by spraying the sole lubricant from the external injector. FS-PE1 represents the polyethylene coating produced by flame spraying. The number in the sample name corresponds to a specific combination of process parameters.

in this work.

2.2. Structural and thermal characterization of the powders and coatings

The morphology of the powders was analysed by a scanning electron microscope (SEM, Jeol, IT-500, Japan). The particle size distribution was measured by a laser diffraction analysis using dry powder method (LS 13 320 Laser Diffraction Particle Size Analyser, Beckman Coulter, Inc., United States). The coating thickness was estimated by a digital micrometre (293-676 micrometre IP54 SPC, Mitutoyo, United States). The results were obtained by the average and standard deviation of nine measurements. The thermal characterization of as-received powders and coatings was carried out by differential scanning calorimetry (DSC, Netzsch DSC214 Polyma, Netzsch, Germany). The specimens were weighed (approximately 10 mg) and placed in a concavus aluminium pan for the thermal analysis. Dynamic heating was performed at 20 °C/min from −30 °C to 150 °C in a nitrogen atmosphere (40 mL/min nitrogen flow in addition to 60 mL/min protective nitrogen flow) to evaluate melting range and peak melting temperatures of as-received feedstock powders and coatings. The thermal stability of the powders was investigated by thermogravimetric (TG) analysis (Netzsch TGA209F Tarsus, Netzsch, Germany). The specimen weight was approximately 10 mg and dynamic heating was performed at 20 °C/min from 25 to 600 °C in a nitrogen atmosphere (20 mL/min nitrogen flow in addition to 20 mL/min protective nitrogen flow). The onset decomposition temperature, T_{onset}, was evaluated for the powders from the dynamic TG curve according to the standard ISO 11358-1. This temperature is used as an indicator of the thermal stability of materials. Moreover, the maximum degradation rate temperature of the powders was measured at the peak of the first derivative of the TG curve (DTG curve). The DTG curve represents the rate of mass loss of the material versus temperature.

2.3. Characterization of the coating surfaces

The surface topography was analysed using an optical profilometer

(contactless measuring instrument, Alicona Infinite Focus G5, Alicona Imaging GmbH, Austria) with 5× objective magnification on 10 mm × 10 mm areas. The areal roughness parameters (Sa, Sq, Sz) were evaluated with 20× objective magnification on 2 mm × 2 mm areas at different locations of the surface, according to the standard ISO 25178-3. The areal roughness values were obtained by the average and standard deviation of three measurements from corrected and filtered surface datasets. The chemical characterization of the coatings was carried out by Fourier-transform infrared spectroscopy (FTIR, Bruker Tensor 27 FT-IR spectrometer, Bruker, Sweden) and compared to the data obtained from the feedstock powders. For this analysis, an attenuated total reflectance (ATR) sample holder (GladiATR, PIKE Technologies, United States) was used with a diamond crystal. This allows the recording of FTIR spectra directly on the pristine material surface without any sample preparation. The FTIR absorbance spectra were measured in the wavenumber range 4000 cm^{-1} to 600 cm^{-1} in air at room temperature by recording 32 scans with a resolution of 4 cm^{-1}. For the measurements, the coating surface was directly placed in contact with the crystal. The measurements were performed at 15 different locations of the coating surface for each sample.

The wetting behaviour of the coating surfaces was evaluated by a droplet shape analyser (DSA100, Krüss, Germany) in controlled conditions (22 °C ± 1 °C temperature and 60% ± 3% relative humidity). Static contact angles were measured by placing 10 μL droplets of ultra-high purity water (MilliQ, Millipore Corporation, United States) onto the surfaces. The apparent water contact angle was estimated using the tangent method (polynomial fit of droplet shape). The dynamic wetting behaviour was evaluated by tilting experiments. The 10 μL droplet was placed onto the coating surfaces, which were tilted until the droplet rolled off. The roll-off angle was recorded when no droplet pinning was observed during tilting experiments. Both static contact angle and roll-off angle were calculated as the average of at least five measurements on different locations of the sample. Moreover, the wetting behaviour was evaluated at −10 °C, which corresponds to the temperature we used for the ice adhesion test. For this purpose, a temperature control chamber was installed (Krüss TC40, Krüss, Germany) on the stage of the droplet shape analyser. The chamber includes a movable Peltier plate unit, which temperature is adjusted and monitored by a glycol bath circulator (F12-MA, Julabo GmbH, Germany) and a temperature controller (2216e controller, Eurotherm Controls LTD, United Kingdom), respectively. The sample was placed on the Peltier stage, gradually cooling the surface from room temperature to −10 °C ± 1 °C. Coating surface temperature was monitored by a type K thermocouple with a digital thermometer (Fluke 51 II digital thermometer, Fluke Corporation, United States). After the surface reached the desired temperature, static contact angle and roll-off angle were measured by depositing 10 μL water droplet. The results were evaluated as the average of at least three measurements. During this experiment, a dry atmosphere was maintained in the chamber by continuously flushing dry nitrogen to avoid water condensation. The air temperature of the chamber was monitored with a temperature sensor (Pt-100, Krüss TP20, Krüss GmbH, Germany) and measured to be around 11 °C ± 1 °C at 10 mm distance above the sample. The chamber was preventively sealed with paraffinic laboratory film to further insulate it from the surrounding environment.

The icephobic behaviour of the coating was evaluated by using the icing wind tunnel (IWiT) and the centrifugal ice adhesion test (CAT) facilities at Tampere University. The test equipment sits in a climate-controlled cold room with monitored temperature and relative humidity (−10 °C ± 1 °C and 80% ± 5%). The test apparatus is described in detail in previous studies [38,60,61]. Mixed-glaze type of ice was accreted from supercooled water droplets on 30 mm × 30 mm sample areas in the IWiT at −10 °C. After accretion, the ice adhesion strength was measured with the CAT at the same temperature. In the centrifugal method, the specimen with accreted ice, placed on a blade and carefully counterweighted, is spun with a constant acceleration rate until the ice detaches. An acceleration sensor records the value of the rotational speed, which corresponds to the ice detachment. The shear ice adhesion strength is evaluated as the ratio of the centrifugal force, F $[N]$ at the moment of ice detachment, to the area of the iced surface, A $[m^2]$. Eq. (1) estimates the shear ice adhesion strength, τ_{ice} $[kPa]$, as follows:

$$\tau_{ice} = \frac{F}{A} = \frac{m_{ice} r \omega^2}{A} \tag{1}$$

where m_{ice} $[kg]$ is the known mass of the accreted ice on the specimen, r $[m]$ is the radial spinning length and ω $[rad/s]$ is the rotational speed. The ice adhesion of the coating was evaluated as the average and standard deviation of four parallel samples during icing accretion events. A reference surface, namely Teflon tape (TT, 3M, United States), was tested to monitor the ice adhesion variation during ice accretion. The use of the reference material is essential to ensure the repeatability of the test results because of variability in ice adhesion strength for different icing conditions [60,62,63].

3. Results and discussion

3.1. Structural and thermal properties of the feedstock powders

Fig. 3a shows the morphology of LDPE powder. The shape of the particles varied from blocky irregular grains to long stretched flakes, produced by the powder manufacturing process. Conversely, the hydrogenated cottonseed oil powder showed particles with spherical shape (Fig. 3b) and capsule geometry (Fig. 3c). The particle analysis revealed a broader size distribution for the LDPE powder (−482 + 154 μm) compared to the lubricant powder (−152 + 34 μm).

The thermal analysis of the as-received powders represents a powerful tool to understand the thermal behaviour of polymeric materials, especially when their processing involves high-temperature flame and oxidative atmosphere. The main purpose was to drastically reduce or, in the best case, avoid thermal degradation, which has been demonstrated to negatively affect the icephobicity of flame sprayed polyethylene

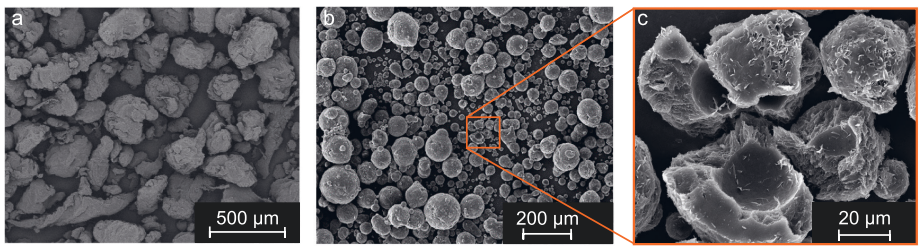

Fig. 3. SEM micrographs of the feedstock powders: a) LDPE powder, b) hydrogenated cottonseed oil powder, and c) capsule geometry of the hydrogenated cottonseed oil powder.

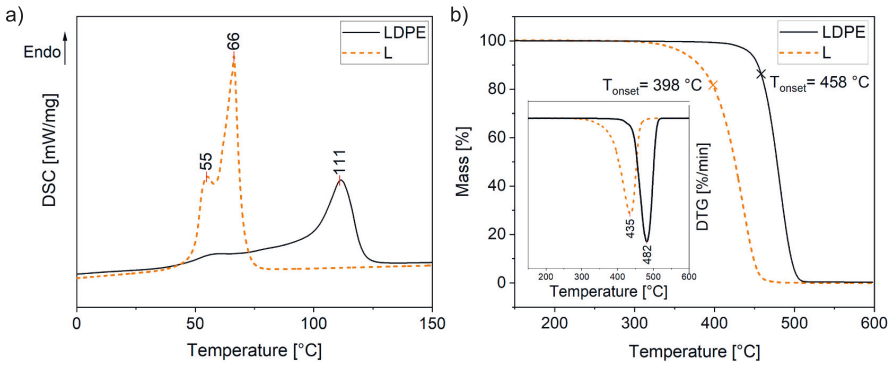

Fig. 4. Thermal properties of the matrix (LDPE) and lubricating additive (L) powders: a) melting range with peak melting temperatures from the DSC analysis, and b) onset decomposition temperatures (T_{onset}) from the TG curves and maximum degradation temperatures from the DTG curves.

coatings [42]. Fig. 4a shows the DSC curves of both as-received powders, highlighting two distinct melting temperature ranges. The lubricant had a lower melting range (two different melting peaks at around 55 °C and 66 °C) compared to LDPE (melting peak at around 111 °C). Moreover, the TG analysis of the powders revealed the onset temperatures (T_{onset}) of 458 °C and 398 °C for the LDPE and lubricant degradation, respectively (Fig. 4b). Above T_{onset} the material decomposes, and this temperature should not be exceeded during processing. Both TG and DTG curves confirmed that the thermal degradation process in inert conditions happened in one stage for both powders. The rate of weight loss was maximum at 482 °C and 435 °C for the LDPE and lubricant, respectively. These two maximum degradation temperatures were used to identify the presence of these components in the coating once the powders were flame sprayed.

These analyses highlight the differences in dimensions and thermal properties of the feedstock powders, resulting in their different thermal behaviour in contact with the flame. In particular, the lubricant has smaller particle size distribution, lower melting range and thermal stability than polyethylene. This implies that the chance of thermal degradation is higher for the additive during spraying, and justifies our decision to use an external injector for it.

3.2. Structural and thermal properties of the coatings

Fig. 5a shows the visual appearance of two coating surfaces and Fig. 5b represents the schematic structure of LICs. The lubricant addition rendered the surface visually opaquer compared to the glossy black polyethylene coating, FS-PE1. Moreover, this addition helped to obtain a visually smoother surface topography (LIC1 compared to FS-PE1, sprayed with identical process parameters). Fig. 5c shows the measured coating thicknesses.

The used process parameters influenced the coating thickness. The lower the gun traverse speed, the greater the deposited amount of material per unit length. This resulted in increased coating thickness. Producing the plain lubricant coating was challenging because the melted additive was continuously dripping down from the substrate. Therefore, an uneven coating layer was produced (L4 thickness around 20 μm ± 6 μm). The deposition of lubricant improved the coating build-up when this was simultaneously sprayed with LDPE, as can be seen from the difference in thickness between FS-PE1 and LIC1. For the coatings sprayed with a gun traverse speed of 900 mm/s, the increased cooling effect of the flame (from 0 to 4 bar air pressure) resulted in gradually higher thicknesses. The cooling effect might reduce the degree of melting of polyethylene splats and the in-flight degradation of powders, especially for the lubricant. Both of these factors led to an

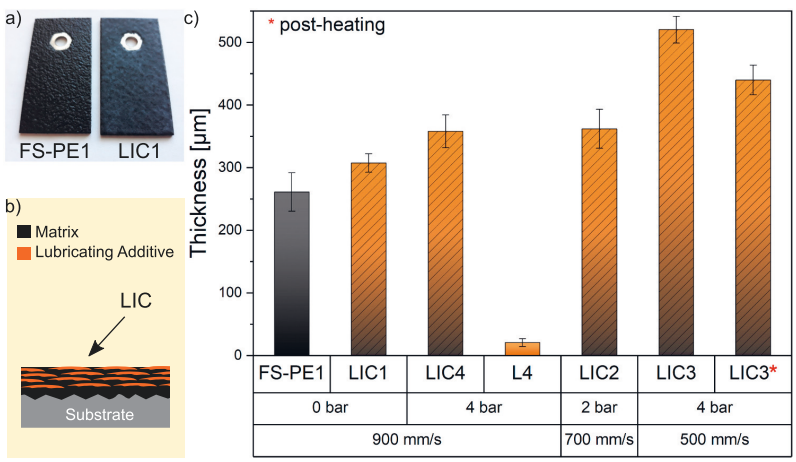

Fig. 5. Coating properties: a) visual inspection image of coatings FS-PE1 and LIC1, b) schematization of the LIC structure, and c) coating thickness measurements. The results are grouped in the histogram based on the used process parameters.

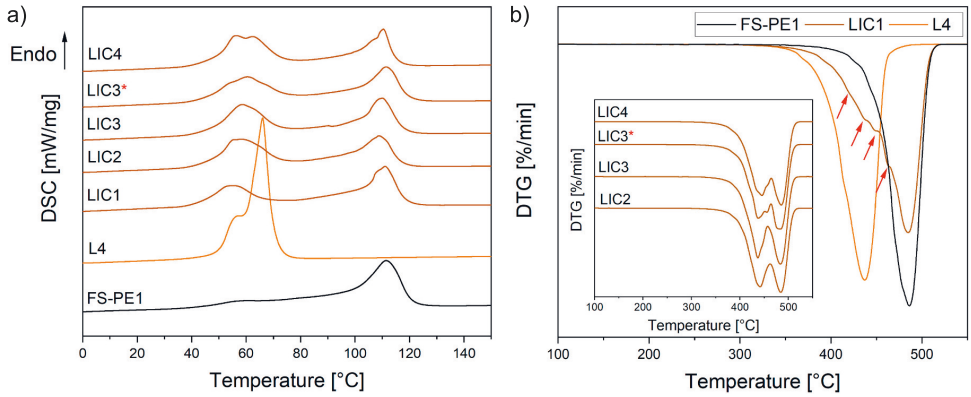

Fig. 6. Thermal properties of the FS-PE1, L4 and LIC coatings: a) melting transition from the DSC analysis, and b) degradation peaks evaluated from the first derivative of the TG curve (DTG). Additional shoulders are indicated by red arrows for the sample LIC1 in the DTG curve. (For interpretation of the references to colour in this figure legend, the reader is referred to the web version of this article.)

increase of the obtained coating thickness. The thickest coating was produced by combining both the cooling effect of flame and the lowering of traverse speed (4 bar and 500 mm/s for LIC3). However, if post-heating was performed by flame, the coating thickness decreased. This decrease was probably caused by re-melting of polymers and possible vaporisation of the most heat sensitive component in contact with flame.

Fig. 6 shows the results of the thermal analyses for the coatings. In Fig. 6a, two distinct melting temperature transitions were noticed for the lubricated coatings, confirming the presence of both components within the structure. However, the melting peak signal for the lubricant in LIC1 was less pronounced. This probably indicated a reduced amount of lubricant in the structure caused by the highest flame temperature, even if this was externally fed. The previous hypothesis was confirmed by thermogravimetric analyses. Fig. 6b shows the DTG curves of the coatings. In these curves, two regions of degradation were revealed for LIC2, LIC3, LIC3* and LIC4. These peaks confirmed the presence of both lubricant and polyethylene in the coating structure. However, LIC1 showed no identifiable peak for the additive, indicating a lower amount of this component in the coating. Moreover, several shoulders (indicated by the red arrows in Fig. 6b) were identified in this region. These confirmed the presence of residual lubricant and/or shorter polyethylene chains, produced by the scission reaction during thermal oxidation by flame [42,64,65].

3.3. Surface topography and surface chemistry of the coatings

Fig. 7 shows the surface topography of the coatings together with the process parameters. The areal roughnesses (Sa, Sq, Sz) are summarised in Table 2. From the results, the process parameters greatly influenced the obtained surface topography. As a rule of thumb for thermal spraying of polymers, the higher the temperature reached by the polymer during processing, the greater the smoothness obtained for the surface [56,66]. For this reason, the higher the gun traverse speed, the lower the time in which the polymers are heated, thus producing a rougher coating surface (LIC4 compared to LIC3). Moreover, the greater the cooling effect of the flame, the lower the degree of melting for the polymer matrix, thus newly resulting in rougher surfaces (LIC1 compared to LIC4). The addition of lubricant reduced the coating roughness when identical process parameters were used (LIC1 compared to FS-PE1), as confirmed by visual inspections in Fig. 5a. This was probably caused by the complete melting of lubricant, which filled the surface topography of flame sprayed polyethylene. Furthermore, if post-heating was performed, this smoothened the coating surface because of re-melting and re-solidification of the polymers (LIC3 compared to LIC3*). Similar behaviour has been reported when using different post-heating treatments to re-melt the surface of thermally sprayed polymer coatings [67]. Finally, L4 resulted in the smoothest surface because of the lubricant dripping down from the substrate during spraying.

The presence of thermal degradation was further investigated by the chemical characterization of the coating surfaces, considering the feedstocks as reference materials. The infrared (IR) spectra of LDPE and lubricant powders are represented in Fig. 8. Compared to LDPE, the lubricant had additional peaks at 2955 cm^{-1} (=C−H cis stretching vibration), at 1737 cm^{-1} (−C=O ester stretching vibration), and in the fingerprint region from 1200 cm^{-1} to 800 cm^{-1}.

From the comparison between the feedstock powders and corresponding coatings, little chemical modifications were detected for FS-PE1. These chemical modifications produced an increase in peak absorbance at 1713 cm^{-1}. This indicated the presence of carbonyl compounds formed by thermal oxidation when no additional air was used in the flame [42]. Moreover, weak peaks appeared around 1600 cm^{-1}. The signals corresponded to the vibrations in C=C bonds, revealing the presence of alkene compounds (unsaturated carbon-carbon covalent bond). Alkenes constitute an initial product of thermal degradation of polyethylene [68]. Fig. 8c shows representative FTIR spectra of the lubricated coatings. The characteristic peaks of both matrix and additive materials were revealed for every coating, confirming that the materials (and surely the lubricant) were evenly distributed on the coating surface. However, LIC1 and LIC3* showed alkene signals, similarly to FS-PE1. This demonstrated that little thermal degradation of the polymers occurred when both post-heating and no additional cooling were used, as confirmed by thermal analyses. Additionally, the presence of the carbonyl peak (signal at 1713 cm^{-1}) was impossible to reveal for the coating surfaces because it overlaps the strong ester signal of the lubricant in the same region.

3.4. Wetting properties of the coatings

The analysis of the wetting properties serves as a preliminary investigation to understand the tendency of the surface to like or dislike water. This tendency is commonly evaluated by measuring the water contact angle (WCA) formed by the water droplet with the surface. If the surface likes water, this angle lies between 0° and 90° (i.e., the hydrophilic case). Conversely, if the surface dislikes water, this angle is higher than 90° (i.e., the hydrophobic case) and even greater than 150° for strong water repellency (i.e., the superhydrophobic case) [69]. Since ice is the solidified form of water, the wetting behaviour has been

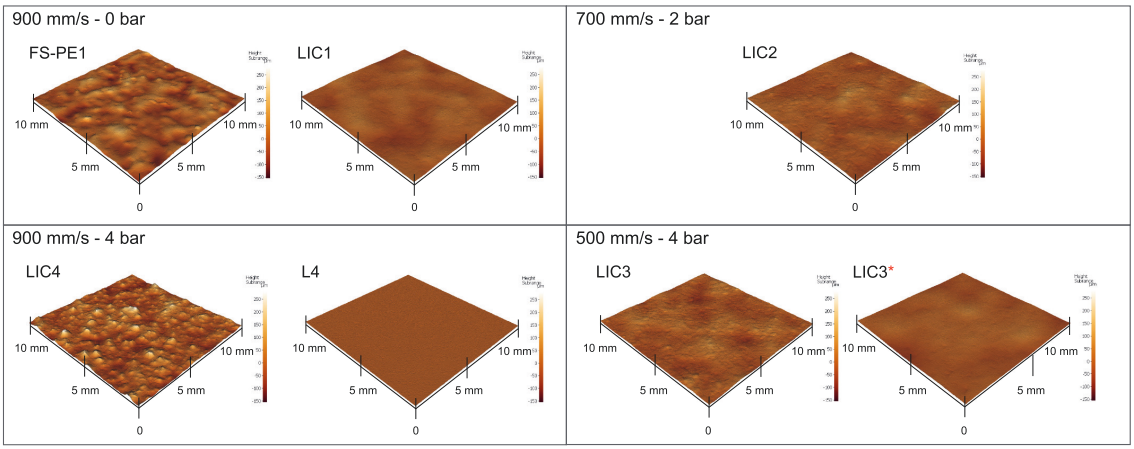

Fig. 7. Surface topography of the coatings measured by optical profilometer analysis.

Table 2
Average and standard deviation of the areal roughness: average height (Sa), root-mean-square height (Sq) and maximum height (Sz) evaluated for the coating surfaces.

Sample	Average height, Sa [μm] ± SD [μm]	Root-mean-square height, Sq [μm] ± SD [μm]	Maximum height, Sz [μm] ± SD [μm]
FS-PE1	31 ± 3	39 ± 5	214 ± 10
LIC1	12 ± 2	15 ± 3	75 ± 9
LIC2	14 ± 3	18 ± 5	115 ± 23
LIC3	18 ± 2	23 ± 4	160 ± 42
LIC3*	10 ± 0.2	12 ± 0.5	76 ± 15
LIC4	37 ± 4	47 ± 6	282 ± 38
L4	0.9 ± 0.3	1 ± 0.3	64 ± 10

widely tested as the first screening of potential low ice adhesion surfaces [12,70]. Fig. 9a shows the apparent WCA at different surface temperatures of the coating surfaces. The apparent WCA, which is schematically defined for a non-ideal surface in Fig. 9b, was measured both at room temperature and in cold conditions of the surface. The sub-zero temperature of −10 °C was chosen, which corresponds to the icing test temperature. A few studies have recommended performing wetting measurements at conditions as similar as possible to icing test environments [71] or real icing conditions [72] to better understand the icephobicity of surfaces.

From the results at room temperature, FS-PE1 showed a hydrophilic character with WCA of 84° ± 3°. Here, the water droplet probably was in intimate contact with the valleys and peaks of the surface topography, remaining in a Wenzel wetting state [73]. Conversely, L4 reached WCA of 146° ± 3°. Being aware that on the most hydrophobic flat solids (fluorinated materials) the contact angle never exceeds approximately 120° in the Wenzel state [69,74], this suggested that the surface was partially wetted. Air pockets were probably trapped beneath the water droplet, which was in a Cassie−Wenzel mixed wetting state [73]. This wetting state was promoted by the microroughness of grit-blasted substate (Ra ≈ 2.8 μm) beneath the uneven lubricant coating. LICs showed intermediate wetting properties, more similar to the lubricant coating (L4). This wetting behaviour was justified by the presence of the additive on the coating surfaces, as confirmed by chemical analyses. At room temperature, L4 showed a roll-off angle of 31° ± 1.5°. Conversely, 10 μL water droplets were pinned onto the surface for the other coatings, resulting in roll-off angles higher than 90°. The wettability of the surfaces generally fell with lowering the substrate temperature. This can be explained by considering the cold experimental conditions. When water, at room temperature, is deposited on a cold surface, a temperature gradient is generated between the droplet and the surface. The higher the gradient, the greater the induced formation of water nuclei (water condensation phenomenon), which grow beneath the drop on the surface [75]. The water condensation phenomenon is schematically shown in Fig. 9c. This effect is reduced when no temperature gradients exist between the water droplet and the surface [75], which is ideally the case of our room temperature experiments. Therefore, the water condenses within the microstructure, eliminating the presence of air pockets and thus resulting in lower apparent contact angles [71,76]. In our study, this explained the more evident drop in WCA for some surfaces (L4, LIC3*, LIC2 and LIC1), in which air pockets were still trapped beneath the water drop at room temperature. No evident drop in WCA was revealed for other surfaces (LIC3 and LIC4) when the droplet might be already in a Wenzel state at room temperature. However, it cannot be excluded that water might also condense onto the surface from the humid air of the chamber during sample cooling, despite the presence of continuous nitrogen flow. The roll-off experiments in cold conditions were also influenced by the condensation phenomenon, showing systematically pinning of the water droplets for every coating surface.

The wetting properties at room temperature demonstrated the presence of air pockets trapped beneath the drop for some coatings. This air volume was filled with water in cold temperature experiments, thus causing a general decrease in WCA. The effect of the areal roughness on the wetting properties was evaluated in this study. The apparent WCA measured at different temperature is plotted as a function of the areal roughness Sa for the lubricated coatings, as shown in Fig. 10.

In the room temperature experiments, the WCA decreased with areal roughness (Fig. 10a). This behaviour can be explained by understanding the wetting regime of water droplets. If a fixed water volume is deposited on the surface, a higher apparent WCA is measured when the surface is partially wetted (Cassie−Wenzel mixed wetting state for L4). Conversely, a lower apparent WCA is revealed when the surface is completely wetted (Wenzel wetting state for LIC4). The transition from a partial non-wetting to a complete wetting state is influenced by the surface geometry (relative size of surface features and drop dimension) and by gravity effects [69]. Until a certain limit of roughness, the hydrophobicity of the surface was enhanced allowing air pockets to be stably trapped beneath the drop. After that limit, the increased roughness produced a larger surface area, which geometrically enhanced the Wenzel state [69]. In the cold temperature

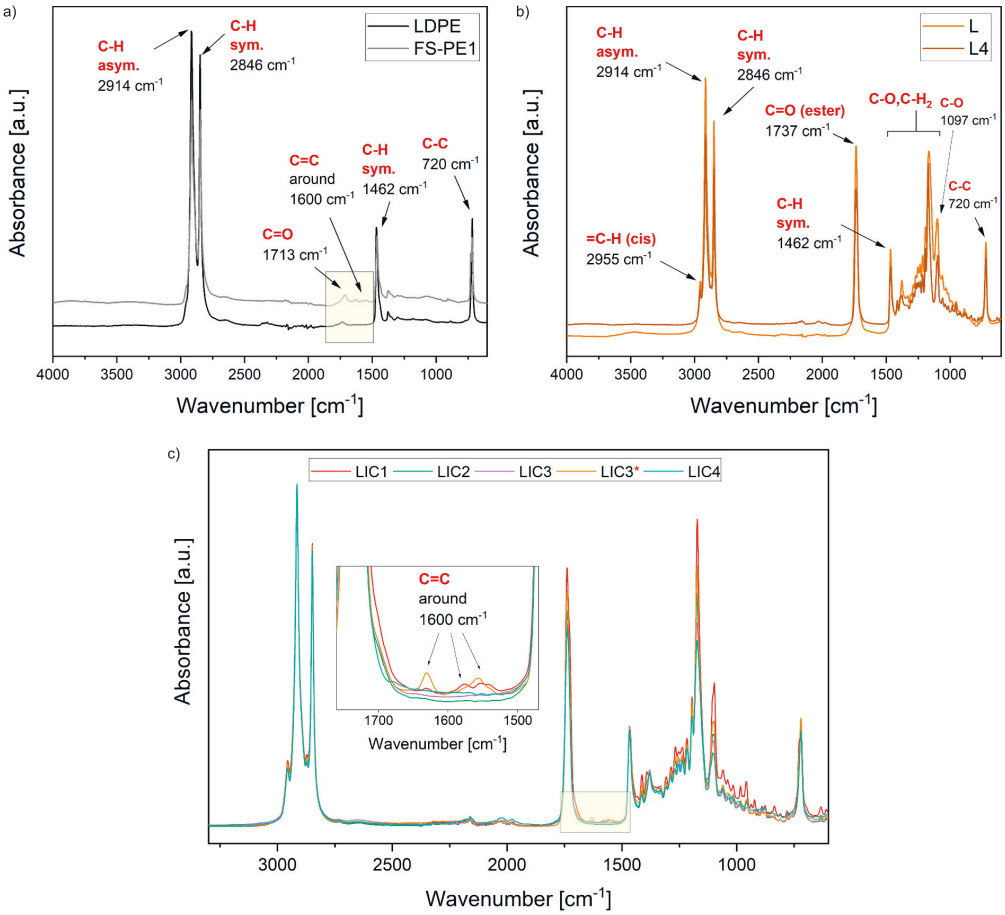

Fig. 8. The FTIR spectra of feedstock materials and coatings: a) LDPE feedstock material and corresponding coating, b) hydrogenated cottonseed oil feedstock material and corresponding coating, and c) LICs. LIC1 and LIC3* showed peaks similarly to FS-PE1. The regions of the spectra, in which chemical modifications are detected, are highlighted by yellow boxes. (For interpretation of the references to colour in this figure legend, the reader is referred to the web version of this article.)

experiments, the decrease of WCA with areal roughness was less pronounced (Fig. 10b). Here, water condensation forced the droplet in a Wenzel state, thus being the variation of WCA less dependent from the roughness in these conditions. Several studies on the influence of surface roughness on wettability have shown an increase of WCA (reaching superhydrophobicity) when passing from a flat and to a rougher surface. This has been verified for the same material in the range of surface roughnesses below 5 μm [77–79]. Increased hydrophobicity was also observed for the same range of roughnesses in this study, as can be seen for L4 in Fig. 10a. Above surface roughnesses of 5 μm, we observed a gradual decrease of WCA with increasing roughness. To the best of the authors' knowledge, no studies correlating wetting properties and surface roughness were presented in the literature for the range of roughnesses considered in this work.

3.5. Icephobic behaviour of the coatings and influence of the surface properties

The icephobic behaviour is defined as the intrinsic ice-repellency of the surface, generally resulting in low ice adhesion strength [21]. In this study, the ice adhesion strength was evaluated at temperature conditions of −10 °C by accreting mixed glaze ice. Fig. 11 summaries the ice adhesion results together with the areal roughness measured for the coatings and test reference material, Teflon tape (TT).

The as-sprayed lubricated surfaces revealed ice adhesion strength below to 50 kPa. The value represents the low ice adhesion limit defined for this ice adhesion test [38]. Firstly, LICs generally showed lower average ice adhesion compared to the polyethylene coating. Secondly, the ice adhesion further decreased with the increased cooling effect of the flame (from LIC1 to LIC3). Thirdly, optimised process parameters allowed the best icephobic surface of this study, lowering the ice adhesion strength down to 23 kPa ± 6 kPa. If post-heating was performed, the ice adhesion increased approximately 61% (LIC3* compared to LIC3). Moreover, if a rougher surface was produced, the ice adhesion rose again approximately 35% (LIC4 compared to LIC3). Finally, L4 showed average ice adhesion in the same range of LIC3 with a broader standard deviation. This was probably caused by the unevenness of the lubricant coating, increasing the standard deviation of the results [63].

Different material properties have been shown to influence ice adhesion strength, such as chemical composition, surface topography, stiffness and thermal expansion, without considering the effect of the test variables as well [80]. Concerning surface topography, several researchers have demonstrated that roughness affects the icephobicity of

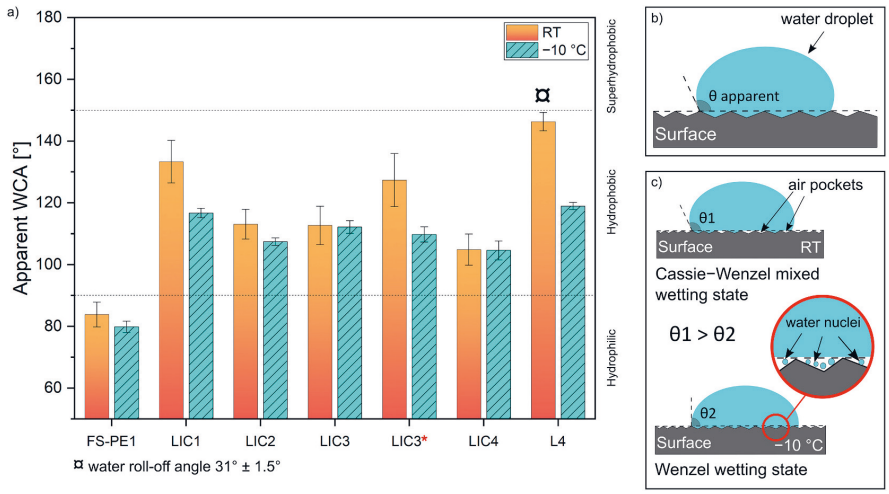

Fig. 9. Results of the wetting experiments: a) apparent WCA at room temperature and cold (−10 °C) surface conditions, b) schematization of a water droplet on a real surface with the definition of apparent water contact angle, and c) transition from Cassie-Wenzel mixed wetting state at room temperature to Wenzel wetting state at cold temperature surface (θ1 > θ2). Description of the water nuclei formation (water condensation) under the drop during wetting experiments in cold surface conditions.

surfaces [77,81,82]. Ice adheres on surface features, forming intimate mechanical interlocking and thus increasing ice adhesion [83]. The ice adhesion strength increases with surface roughness when coatings with identical surface chemistry are considered [81,82,84,85]. However, no similar relationship is found when other factors are influencing the icephobic behaviour of surfaces [81,86]. In this study, no clear correlation was found between areal roughness and ice adhesion strength for the lubricated coatings. Firstly, the ice adhesion decreased from LIC1 to LIC3 while areal roughness increased. Secondly, the ice adhesion surprisingly increased for the smoother surface LIC3*. Finally, the roughest surface of this study (LIC4) showed ice adhesion lower than the post-heated coating. This implied that another dominant factor was influencing icephobicity. In particular, the coating chemistry, which is directly correlated with coating degradation, could determine the icephobic behaviour of the surface. We measured the highest ice adhesion strength for degraded LICs, such as LIC1 and LIC3*. The degradation was caused by the absence of additional air in the flame and performed post-heating. The coatings experienced thermal degradation and

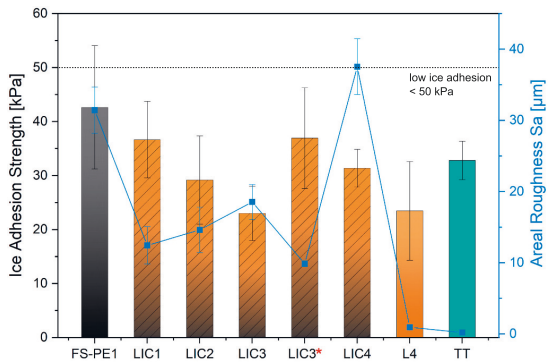

Fig. 11. Ice adhesion strength and areal roughness Sa of the coatings. Teflon tape (TT) represents the reference material for the ice adhesion test.

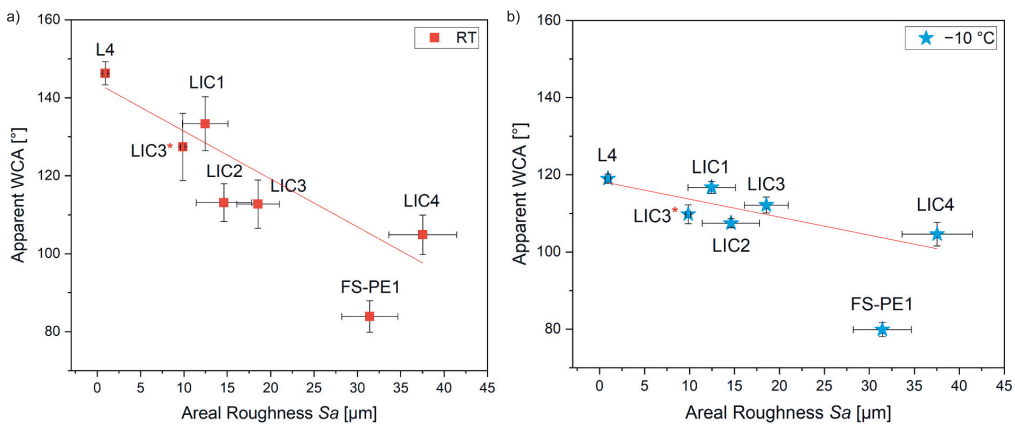

Fig. 10. Correlation between the apparent water contact angle and the areal roughness a) at room temperature, and b) at −10 °C.

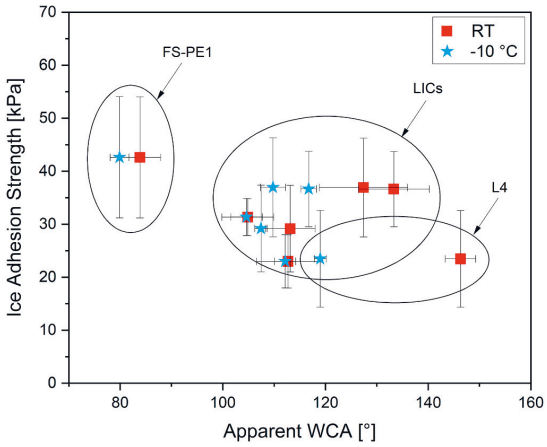

Fig. 12. Ice adhesion strength versus water contact angle at room temperature and −10 °C. FS-PE1 indicates the flame sprayed polyethylene coating, L4 the plain lubricant coating, and LICs the coatings composed by both polyethylene and lubricant.

possible surface embrittlement, which have been shown to negatively affect icephobicity [42]. Conversely, the cooling effect of the flame was beneficial for the icephobic behaviour (gradual decrease of ice adhesion passing from LIC1 to LIC3). Finally, the ice adhesion increased with areal roughness, passing from LIC3 to LIC4 samples. This increase was probably caused by the formation of mechanical interlocking. We can assume that when no degradation was revealed, surface roughness might become the main factor influencing icephobicity. However, further analyses are required to define this specific correlation.

Concerning surface wettability, several studies have found a relationship between apparent WCA and ice adhesion strength [26,70,87]. Conversely, other researches have claimed no clear correlation between these properties [88–91]. Fig. 12 shows the ice adhesion strength plotted as a function of the apparent WCA at room temperature and in cold conditions.

Three different coating groups were distinguished for the wettability at room temperature, namely FS-PE1, LICs and L4. We noticed that the icephobic behaviour was enhanced when passing from a hydrophilic surface (FS-PE1 with WCA below 90°) to a more hydrophobic surface (LICs and L4), confirming the benefits of lubricant addition. This tendency has been reported in previous studies [70,86,87]. No clear relationship could be established between ice adhesion strength and WCA at room temperature and cold conditions. However, the wetting properties in cold conditions showed a narrower distribution of the data compared to the results at room temperature (distribution of star symbols narrower than that of square symbols). The data reported here appear to support the assumption that wetting properties, evaluated in conditions similar to icing test, might provide useful information on the icephobic behaviour of surfaces [71,72]. However, this requires additional research and further development of the actual test equipment. Furthermore, other factors could influence icephobicity. Several recent studies have demonstrated the dependence of the icephobic behaviour from mechanical properties, such as Young modulus [92,93], shear modulus [34,94,95], interfacial toughness [19], and other physical-chemical properties of materials [87,96,97]. In this study, we cannot exclude the influence of these beforementioned factors on the icephobicity of presented coatings. Therefore, further investigations are needed to understand possible correlations with these other influencing factors.

3.6. Icephobic performance of lubricated coatings compared to polyethylene coatings

Fig. 13a summarises the results of the ice adhesion strength plotted as a function of the areal roughness Sa for lubricated coatings (in orange) and LDPE coatings (in black). Fig. 13b shows the corresponding process parameters. The lubricated coatings were manufactured by modifying the traditional flame spray process, previously used to produce the LDPE coatings [42,43]. In this study, the hybrid feedstock injection system was added to the flame spray gun to feed the lubricating additive. The spray distance was constant at 250 mm for the compared samples.

From the comparison of the results, we can draw the following conclusions. Firstly, the addition of selected lubricant further enhanced the icephobic behaviour of flame sprayed polyethylene coatings (orange squares versus black squares). This was achieved by using flame spraying with hybrid feedstock injection when such heat sensitive materials were involved in the process. The roughest lubricated coating

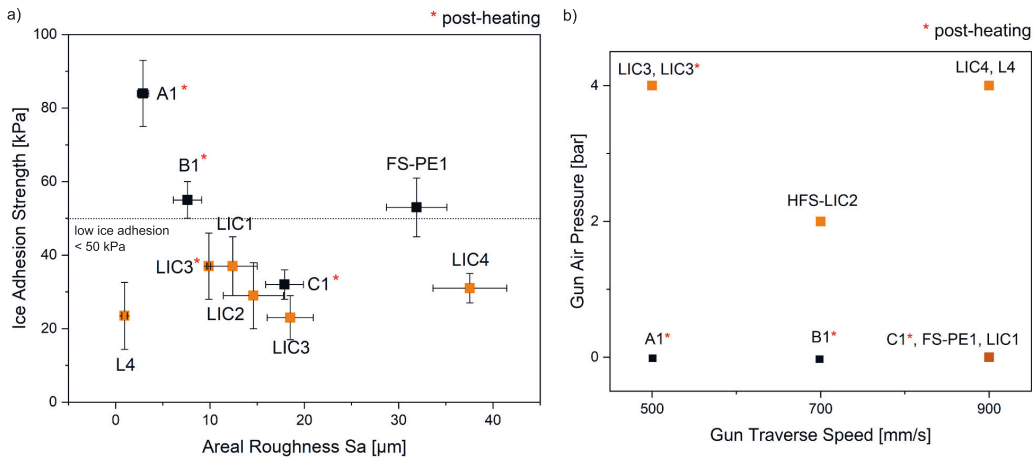

Fig. 13. Icephobic performances of lubricated icephobic coatings (in orange) of this study compared to flame sprayed polyethylene coatings (in black) from the previous work [33]: a) ice adhesion strength versus areal roughness Sa for the lubricated icephobic coatings (LICs) and flame sprayed PE coatings, and b) summary of the process parameters.

showed icephobicity below the limit of low ice adhesion strength. This implied a great influence of the surface chemistry over the roughness on the icephobic behaviour of the coatings. Secondly, the thermal degradation of the polymers was identified as another factor negatively influencing the icephobicity. Material degradation was reduced by cooling the flame and avoiding post-heating. The avoided post-heating was beneficial to the icephobicity, when the lubricant was present in the coating structure (ice adhesion of LIC3 compared to LIC3*). In this case, the post-heating probably produced degradation and partial vaporisation of the surface components, thus compromising the icephobicity. Conversely, the post-heating enhanced the coating icephobicity in the case of flame sprayed polyethylene (ice adhesion of FS-PE1 compared to C1*). Here, a smoother surface was beneficial to reduce the ice adhesion. In conclusion, a full investigation of the chemical and thermal properties of the sprayed coatings is strongly recommended. In our study, this supports the optimization of process parameters to obtain high quality icephobic coatings for the selected materials.

4. Conclusions

This research work presented the one-step fabrication of lubricated icephobic coatings by flame spraying with hybrid feedstock injection. In this process, the matrix material and the lubricating additive with different thermal properties were simultaneously sprayed to form a composite coating. The higher melting temperature polymer, namely matrix material, was sprayed from the oxy-acetylene gun. Differently, the lower melting temperature polymer, namely lubricating additive, was externally fed by an injector. This protected the additive from thermal degradation. The main conclusions of this study can be summarised as follows:

- Processing of heat sensitive materials, such as lubricants in solid form, was achieved by flame spray technology with hybrid feedstock injection. This was done to enhance the icephobicity of flame sprayed polyethylene coatings. The use of this process and further cooling of the flame allowed the protection of sprayed materials from thermal degradation, ensuring the production of good quality coatings.
- The optimization of process parameters was carried out by comparing chemical and thermal properties of materials before and after spraying. The results demonstrated that cooling of the flame was beneficial to reduce the thermal degradation of polymers.
- The surface topography was tailored by the chosen process parameters. The lower the heat load involved in the process, the rougher the obtained surface. The post-heating treatment produced smoothening of the coating surface caused by re-melting effects.
- Lubricated coatings showed enhanced hydrophobic character compared to the plain polyethylene coatings. Additionally, the surface topography influenced the surface wettability. The greater the roughness, the lower the apparent WCA for both room and cold temperature experiments. The hydrophobic character of the surfaces fell in cold temperature because of water condensation within surface features.
- The ice adhesion was mainly influenced by both thermal degradation and surface chemistry of the coatings. The lubricant addition enhanced the icephobic behaviour of the coatings. The thermal degradation compromised the icephobic performance of surfaces. The degradation was avoided by optimising the process parameters, which lowered the ice adhesion down to 23 kPa ± 6 kPa.

Future studies will focus on the fabrication of thermally sprayed coatings made of different combinations of materials to further tailor the surface icephobicity. Moreover, the icing durability of the coatings will be investigated under repeated icing/de-icing cycles in cold conditions.

CRediT authorship contribution statement

Valentina Donadei: Conceptualization, Methodology, Investigation, Visualization, Writing - original draft. **Heli Koivuluoto:** Conceptualization, Supervision, Funding acquisition, Resources, Writing - review & editing. **Essi Sarlin:** Supervision, Writing - review & editing. **Petri Vuoristo:** Supervision, Funding acquisition, Resources, Writing - review & editing.

Declaration of competing interest

The authors declare that they have no known competing financial interests or personal relationships that could have appeared to influence the work reported in this paper.

Acknowledgement

Authors thank the LubISS (Lubricant Impregnated Slippery Surfaces) project that has received funding from the European Union's Horizon 2020 research and innovation programme under the Marie Sklodowska-Curie Grant Agreement No. 722497. Mr. Anssi Metsähonkala and Mr. Jarkko Lehti, of Tampere University, are acknowledged for technical support in the flame spray process. Moreover, the authors acknowledge M.Sc. Matteo Orlandini, of Millidyne Oy, for the particle size analysis. Prof. Shrikant Joshi, of University West, and M.Sc. Saurabh Nath, of ESPCI Paris, are thanked for the stimulating discussions. M.Sc. Henna Niemelä-Anttonen and B.Sc. Enni Hartikainen, of Tampere University, are thanked for assisting the icing testing.

References

[1] M. Farzaneh, K. Savadjiev, Statistical analysis of field data for precipitation icing accretion on overhead power lines, IEEE Trans. Power Deliv. 20 (2005) 1080–1087, https://doi.org/10.1109/TPWRD.2004.838518.
[2] L. Makkonen, Modeling power line icing in freezing precipitation, Atmos. Res. 46 (1998) 131–142, https://doi.org/10.1016/S0169-8095(97)00056-2.
[3] N. Dalili, A. Edrisy, R. Carriveau, A review of surface engineering issues critical to wind turbine performance, Renew. Sust. Energ. Rev. 13 (2009) 428–438, https://doi.org/10.1016/j.rser.2007.11.009.
[4] O. Parent, A. Ilinca, Anti-icing and de-icing techniques for wind turbines: critical review, Cold Reg. Sci. Technol. 65 (2011) 88–96, https://doi.org/10.1016/j.coldregions.2010.01.005.
[5] R. Carriveau, A. Edrisy, P. Cadieux, R. Mailloux, Ice adhesion issues in renewable energy infrastructure, J. Adhes. Sci. Technol. 26 (2012) 447–461, https://doi.org/10.1163/016942411X574592.
[6] F. Cucchiella, I. Dadamo, Estimation of the energetic and environmental impacts of a roof-mounted building-integrated photovoltaic systems, Renew. Sust. Energ. Rev. 16 (2012) 5245–5259, https://doi.org/10.1016/j.rser.2012.04.034.
[7] M.B. Bragg, A.P. Broeren, L.A. Blumenthal, Iced-airfoil aerodynamics, Prog. Aerosp. Sci. 41 (2005) 323–362, https://doi.org/10.1016/j.paerosci.2005.07.001.
[8] T. Rashid, H.A. Khawaja, K. Edvardsen, Review of marine icing and anti-/de-icing systems, J. Mar. Eng. Technol. 15 (2016) 79–87, https://doi.org/10.1080/20464177.2016.1216734.
[9] H.R. Vignisdottir, B. Ebrahimi, G.K. Booto, R. O'Born, H. Brattebø, H. Wallbaum, R.A. Bohne, A review of environmental impacts of winter road maintenance, Cold Reg. Sci. Technol. 158 (2019) 143–153, https://doi.org/10.1016/j.coldregions.2018.10.013.
[10] M. Farzaneh, Atmospheric Icing of Power Networks, (2008), https://doi.org/10.1007/978-1-4020-8531-4.
[11] B. Liu, K. Zhang, C. Tao, Y. Zhao, X. Li, K. Zhu, X. Yuan, Strategies for anti-icing: low surface energy or liquid-infused? RSC Adv. 6 (2016) 70251–70260, https://doi.org/10.1039/c6ra11383d.
[12] A.J. Meuler, J.D. Smith, K.K. Varanasi, J.M. Mabry, G.H. McKinley, R.E. Cohen, Relationships between water wettability and ice adhesion, ACS Appl. Mater. Interfaces 2 (2010) 3100–3110, https://doi.org/10.1021/am1006035.
[13] J. Lv, Y. Song, L. Jiang, J. Wang, Bio-inspired strategies for anti-icing, ACS Nano 8 (2014) 3152–3169, https://doi.org/10.1021/nn406522n.
[14] C.C. Ryerson, Ice protection of offshore platforms, Cold Reg. Sci. Technol. 65 (2011) 97–110, https://doi.org/10.1016/j.coldregions.2010.02.006.
[15] D.M. Ramakrishna, T. Viraraghavan, Environmental impact of chemical deicers – a review, Water Air Soil Pollut. 166 (2005) 49–63, https://doi.org/10.1007/s11270-005-8265-9.
[16] B. Sunden, Z. Wu, On icing and icing mitigation of wind turbine blades in cold climate, J. Energy Resour. Technol. 137 (2015), https://doi.org/10.1115/1.

4030352.
[17] C. Laforte, C. Blackburn, J. Perron, A Review of Icephobic Coating Performances over the Last Decade, SAE 2015 Int. Conf. Icing Aircraft, Engines, Struct, (2015), pp. 8–12, https://doi.org/10.4271/2015-01-2149.
[18] X. Huang, N. Tepylo, V. Pommier-Budinger, M. Budinger, E. Bonaccurso, P. Villedieu, L. Bennani, A survey of icephobic coatings and their potential use in a hybrid coating/active ice protection system for aerospace applications, Prog. Aerosp. Sci. 105 (2019) 74–97, https://doi.org/10.1016/j.paerosci.2019.01.002.
[19] K. Golovin, A. Dhyani, M.D. Thouless, A. Tuteja, Low-interfacial toughness materials for effective large-scale deicing, Science 364 (2019) 371–375, https://doi.org/10.1126/science.aav1266.
[20] R.M.M. Fillion, A.R.R. Riahi, A. Edrisy, A review of icing prevention in photovoltaic devices by surface engineering, Renew. Sust. Energ. Rev. 32 (2014) 797–809, https://doi.org/10.1016/j.rser.2014.01.015.
[21] M.J. Kreder, J. Alvarenga, P. Kim, J. Aizenberg, Design of anti-icing surfaces: smooth, textured or slippery? Nat. Rev. Mater. 1 (2016) 15003, , https://doi.org/10.1038/natrevmats.2015.3.
[22] L.B. Boinovich, A.M. Emelyanenko, V.K. Ivanov, A.S. Pashinin, Durable icephobic coating for stainless steel, ACS Appl. Mater. Interfaces 5 (2013) 2549–2554, https://doi.org/10.1021/am3031272.
[23] L. Cao, A.K. Jones, V.K. Sikka, J. Wu, D. Gao, Anti-icing superhydrophobic coatings, Langmuir 25 (2009) 12444–12448, https://doi.org/10.1021/la902882b.
[24] L. Wang, M. Wen, M. Zhang, L. Jiang, Y. Zheng, Ice-phobic gummed tape with nanocones on microspheres, J. Mater. Chem. A 2 (2014) 3312–3316, https://doi.org/10.1039/c3ta14779g.
[25] A. Alizadeh, M. Yamada, R. Li, W. Shang, S. Otta, S. Zhong, L. Ge, A. Dhinojwala, K.R. Conway, V. Bahadur, A.J. Vinciquerra, B. Stephens, M.L. Blohm, Dynamics of ice nucleation on water repellent surfaces, Langmuir 28 (2012) 3180–3186, https://doi.org/10.1021/la2045256.
[26] K.K. Varanasi, T. Deng, J.D. Smith, M. Hsu, N. Bhate, Frost formation and ice adhesion on superhydrophobic surfaces, Appl. Phys. Lett. 97 (2010), https://doi.org/10.1063/1.2731434 234102–111603.
[27] S. Farhadi, M. Farzaneh, S.A. Kulinich, Anti-icing performance of superhydrophobic surfaces, Appl. Surf. Sci. 257 (2011) 6264–6269, https://doi.org/10.1016/j.apsusc.2011.02.057.
[28] T.S. Wong, S.H. Kang, S.K.Y. Tang, E.J. Smythe, B.D. Hatton, A. Grinthal, J. Aizenberg, Bioinspired self-repairing slippery surfaces with pressure-stable omniphobicity, Nature 477 (2011) 443–447, https://doi.org/10.1038/nature10447.
[29] P. Kim, T.S. Wong, J. Alvarenga, M.J. Kreder, W.E. Adorno-Martinez, J. Aizenberg, Liquid-infused nanostructured surfaces with extreme anti-ice and anti-frost performance, ACS Nano 6 (2012) 6569–6577, https://doi.org/10.1021/nn302310q.
[30] P.W. Wilson, W. Lu, H. Xu, P. Kim, M.J. Kreder, J. Alvarenga, J. Aizenberg, Inhibition of ice nucleation by slippery liquid-infused porous surfaces (SLIPS), Phys. Chem. Chem. Phys. 15 (2013) 581–585, https://doi.org/10.1039/c2cp43586a.
[31] X. Yin, Y. Zhang, D. Wang, Z. Liu, Y. Liu, X. Pei, B. Yu, F. Zhou, Integration of self-lubrication and near-infrared photothermogenesis for excellent anti-icing/deicing performance, Adv. Funct. Mater. 25 (2015) 4237–4245, https://doi.org/10.1002/adfm.201501101.
[32] M.J. Coady, M. Wood, G.Q. Wallace, K.E. Nielsen, A.M. Kietzig, F.O. Lagugnelabarthet, P.J. Ragogna, Icephobic behavior of UV-cured polymer networks incorporated into slippery lubricant-infused porous surfaces: improving SLIPS durability, ACS Appl. Mater. Interfaces 10 (2018) 2890–2896, https://doi.org/10.1021/acsami.7b14433.
[33] J.H. Kim, M.J. Kim, B. Lee, J.M. Chun, V. Patil, Y.S. Kim, Durable ice-lubricating surfaces based on polydimethylsiloxane embedded silicone oil infused silica aerogel, Appl. Surf. Sci. 512 (2020) 145728, , https://doi.org/10.1016/j.apsusc.2020.145728.
[34] K. Golovin, S.P.R. Kobaku, D.H. Lee, E.T. DiLoreto, J.M. Mabry, A. Tuteja, Designing durable icephobic surfaces, Sci. Adv. 2 (2016) e1501496, , https://doi.org/10.1126/sciadv.1501496.
[35] Y. Zhuo, F. Wang, S. Xiao, J. He, Z. Zhang, One-step fabrication of bioinspired lubricant-regenerable Icephobic slippery liquid-infused porous surfaces, ACS Omega 3 (2018) 10139–10144, https://doi.org/10.1021/acsomega.8b01148.
[36] A. Sandhu, O.J. Walker, A. Nistal, K.L. Choy, A.J. Clancy, Perfluoroalkane wax infused gels for effective, regenerating, anti-icing surfaces, Chem. Commun. 55 (2019) 3215–3218, https://doi.org/10.1039/c8cc09818b.
[37] D. Wu, L. Ma, F. Zhang, H. Qian, B. Minhas, Y. Yang, X. Han, D. Zhang, Durable deicing lubricant-infused surface with photothermally switchable hydrophobic/slippery property, Mater. Des. 185 (2020) 108236, , https://doi.org/10.1016/j.matdes.2019.108236.
[38] H. Niemelä-Anttonen, H. Koivuluoto, M. Tuominen, H. Teisala, P. Juuti, J. Haapanen, J. Harra, C. Stenroos, J. Lahti, J. Kuusipalo, J.M. Mäkelä, P. Vuoristo, Icephobicity of slippery liquid infused porous surfaces under multiple freeze-thaw and ice accretion-detachment cycles, Adv. Mater. Interfaces 5 (2018) 1800828, , https://doi.org/10.1002/admi.201800828.
[39] Y.H. Ng, S.W. Tay, L. Hong, Formation of Icephobic surface with micron-scaled hydrophobic heterogeneity on polyurethane aerospace coating, ACS Appl. Mater. Interfaces 10 (2018) 37517–37528, https://doi.org/10.1021/acsami.8b13403.
[40] D.L. Loughborough, E.G. Hass, Reduction of the adhesion of ice to de-icer surfaces, J. Aeronaut. Sci. 13 (1946) 126–134, https://doi.org/10.2514/8.11328.
[41] H. Koivuluoto, C. Stenroos, M. Kylmälahti, M. Apostol, J. Kiilakoski, P. Vuoristo, Anti-icing behavior of thermally sprayed polymer coatings, J. Therm. Spray Technol. 26 (2017) 150–160, https://doi.org/10.1007/s11666-016-0501-x.
[42] V. Donadei, H. Koivuluoto, E. Sarlin, P. Vuoristo, Icephobic behaviour and thermal stability of flame-sprayed polyethylene coating: the effect of process parameters, J. Therm. Spray Technol. 29 (2020) 241–254, https://doi.org/10.1007/s11666-019-00947-0.
[43] V. Donadei, H. Koivuluoto, P. Vuoristo, Effect of process parameters on properties of flame-sprayed icephobic polymer coatings, in: F. Azarmi, Y.C. Lau, J. Veilleux, C. Wiedener, F.L. Toma, H. Koivuluoto, K. Balani, H. Li, K. Shinoda (Eds.), ITSC 2019 - Proc. Int. Therm. Spray Conf, ASM International, Yokohama, 2019, pp. 563–570.
[44] V. Jannin, Y. Cuppok, Hot-melt coating with lipid excipients, Int. J. Pharm. 457 (2013) 480–487, https://doi.org/10.1016/j.ijpharm.2012.10.026.
[45] E.N. Griffin, P.J. Niebergall, Release kinetics of a controlled-release multiparticulate dosage form prepared using a hot-melt fluid bed coating method, Pharm. Dev. Technol. 4 (1999) 117–124, https://doi.org/10.1080/10837459908984231.
[46] J.P. Reo, W.M. Johnson, Tastemasked pharmaceutical system, U.S. Pat. No. 5,891, 476. (1999). https://patents.google.com/patent/US5891476A/en (accessed May 4, 2020).
[47] R. Mukherjee, M. Habibi, Z.T. Rashed, O. Berbert, X. Shi, J.B. Boreyko, Oil-impregnated hydrocarbon-based polymer films, Sci. Rep. 8 (2018) 1–13, https://doi.org/10.1038/s41598-018-29823-7.
[48] S. Kimura, Y. Yamagishi, A. Sakabe, T. Adachi, M. Shimanuki, A new surface coating for prevention of icing on airfoils, SAE Tech. Pap, 2007, https://doi.org/10.4271/2007-01-3315.
[49] H. Pang, S. Zhou, G. Gu, L. Wu, Long-term hydrophobicity and ice adhesion strength of latex paints containing silicone oil microcapsules, J. Adhes. Sci. Technol. 27 (2013) 46–57, https://doi.org/10.1080/01694243.2012.701503.
[50] N. Sharifi, A. Dolatabadi, M. Pugh, C. Moreau, Anti-icing performance and durability of suspension plasma sprayed TiO_2 coatings, Cold Reg. Sci. Technol. 159 (2019) 1–12, https://doi.org/10.1016/j.coldregions.2018.11.018.
[51] N. Xi, Y. Liu, X. Zhang, N. Liu, H. Fu, Z. Hang, G. Yang, H. Chen, W. Gao, Steady anti-icing coatings on weathering steel fabricated by HVOF spraying, Appl. Surf. Sci. 444 (2018) 757–762, https://doi.org/10.1016/j.apsusc.2018.03.075.
[52] J. Mora, P. García, R. Muelas, A. Agüero, Hard quasicrystalline coatings deposited by hvof thermal spray to reduce ice accretion in aero-structures components, Coatings. 10 (2020) 1–22, https://doi.org/10.3390/coatings10030290.
[53] J. Liu, J. Wang, H. Memon, Y. Fu, T. Barman, K.S. Choi, X. Hou, Hydrophobic/icephobic coatings based on thermal sprayed metallic layers with subsequent surface functionalization, Surf. Coatings Technol. 357 (2019) 267–272, https://doi.org/10.1016/j.surfcoat.2018.10.002.
[54] H. Niemelä-Anttonen, H. Koivuluoto, M. Kylmälahti, J. Laakso, P. Vuoristo, Thermally sprayed slippery and icephobic surfaces, in: F. Azarmi, K. Balani, T. Eden, T. Hussain, Y.C. Lau, H. Li, K. Shinoda (Eds.), ITSC2018-Proceedings Int. Therm. Spray Conf. May 7–10, 2018, Orlando, Florida, 2018, pp. 380–384.
[55] H. Koivuluoto, E. Hartikainen, H. Niemelä-Anttonen, Thermally sprayed coatings: novel surface engineering strategy towards icephobic solutions, Materials 13 (2020), https://doi.org/10.3390/ma13061434.
[56] E. Petrovicova, L.S. Schadler, Thermal spraying of polymers, Int. Mater. Rev. 47 (2002) 169–190, https://doi.org/10.1179/095066002225006566.
[57] N. Espallargas, L. Vitoux, S. Armada, The wear and lubrication performance of liquid-solid self-lubricated coatings, Surf. Coatings Technol. 235 (2013) 342–353, https://doi.org/10.1016/j.surfcoat.2013.07.063.
[58] S. Armada, R. Schmid, S. Equey, I. Fagoaga, N. Espallargas, Liquid-solid self-lubricated coatings, J. Therm. Spray Technol. 22 (2013) 10–17, https://doi.org/10.1007/s11666-012-9847-x.
[59] J.A. Brogan, Thermal-spraying of polymers and polymer blends, MRS Bull. 25 (2000) 48–53, https://doi.org/10.1557/mrs2000.124.
[60] C. Stenroos, P. Vuoristo, H. Koivuluoto, Properties of Icephobic Surfaces in Different Icing Conditions, Master Thesis Tampere Univ. Technol, Tampere, Finl, 2015.
[61] H. Koivuluoto, C. Stenroos, R. Ruohomaa, G. Bolelli, L. Lusvarghi, P. Vuoristo, Research on icing behavior and ice adhesion testing of icephobic surfaces, IWAIS XVI, Uppsala, 2015, p. 6.
[62] S. Rønneberg, Y. Zhuo, C. Laforte, J. He, Z. Zhang, Interlaboratory study of ice adhesion using different techniques, Coatings 9 (2019) 678, https://doi.org/10.3390/coatings9100678.
[63] H. Niemelä-Anttonen, J. Kiilakoski, P. Vuoristo, H. Koivuluoto, Icephobic performance of different surface designs and materials, Proc. Int. Work. Atmos. Icing Struct, 2019, pp. 1–5.
[64] M. Sugimoto, A. Shimada, H. Kudoh, K. Tamura, T. Seguchi, Product analysis for polyethylene degradation by radiation and thermal ageing, Radiat. Phys. Chem. 82 (2013) 69–73, https://doi.org/10.1016/j.radphyschem.2012.08.009.
[65] B. Zhao, S. Zhang, C. Sun, J. Guo, Y.X. Yu, T. Xu, Aging behaviour and properties evaluation of high-density polyethylene (HDPE) in heating-oxygen environment, IOP Conf. Ser. Mater. Sci. Eng. 369 (2018) 012021, , https://doi.org/10.1088/1757-899X/369/1/012021.
[66] J.A. Brogan, C.C. Berndt, The coalescence of combustion-sprayed ethylene methacrylic acid copolymer, J. Mater. Sci. 32 (1997) 2099–2106, https://doi.org/10.1023/A:1018526906452.
[67] G. Zhang, H. Liao, H. Yu, S. Costil, S.G. Mhaisalkar, J.M. Bordes, C. Coddet, Deposition of PEEK coatings using a combined flame spraying–laser remelting process, Surf. Coatings Technol. 201 (2006) 243–249, https://doi.org/10.1016/j.surfcoat.2005.11.094.
[68] H. Bockhorn, A. Hornung, U. Hornung, D. Schawaller, Kinetic study on the thermal degradation of polypropylene and polyethylene, J. Anal. Appl. Pyrolysis 48 (1999) 93–109, https://doi.org/10.1016/S0165-2370(98)00131-4.
[69] D. Quéré, Wetting and roughness, Annu. Rev. Mater. Res. 38 (2008) 71–99, https://doi.org/10.1146/annurev.matsci.38.060407.132434.
[70] A. Dotan, H. Dodiuk, C. Laforte, S. Kenig, The relationship between water wetting and ice adhesion, J. Adhes. Sci. Technol. 23 (2009) 1907–1915, https://doi.org/10.1163/016942409X12510925843078.

[71] Q. Fu, X. Wu, D. Kumar, J.W.C. Ho, P.D. Kanhere, N. Srikanth, E. Liu, P. Wilson, Z. Chen, Development of sol-gel icephobic coatings: effect of surface roughness and surface energy, ACS Appl. Mater. Interfaces 6 (2014) 20685–20692, https://doi.org/10.1021/am504348x.
[72] L. Mazzola, G. Bruno, Characterization of ice-phobic surfaces: improvements on contact angle measurements, Measurement 110 (2017) 202–210, https://doi.org/10.1016/j.measurement.2017.06.036.
[73] A. Lafuma, D. Quéré, Superhydrophobic states, Nat. Mater. 2 (2003) 457–460, https://doi.org/10.1038/nmat924.
[74] E. Shafrin, W. Zisman, Upper limits to the contact angles of liquids on solids, in: R.F. Gou (Ed.), Contact Angle, Wettability Adhes. Adv. Chem. Ser, DC: Am. Chem. Soc, Washington, 1964, pp. 478–479, , https://doi.org/10.1007/bf01150624.
[75] T. Mouterde, G. Lehoucq, S. Xavier, A. Checco, C.T. Black, A. Rahman, T. Midavaine, C. Clanet, D. Quéré, Antifogging abilities of model nanotextures, Nat. Mater. 16 (2017) 658–663, https://doi.org/10.1038/nmat4868.
[76] G. Momen, M. Farzaneh, R. Jafari, Wettability behaviour of RTV silicone rubber coated on nanostructured aluminium surface, Appl. Surf. Sci. 257 (2011) 6489–6493, https://doi.org/10.1016/j.apsusc.2011.02.049.
[77] H. Memon, J. Liu, D.S.A. De Focatiis, K.S. Choi, X. Hou, Intrinsic dependence of ice adhesion strength on surface roughness, Surf. Coatings Technol. 385 (2020) 125382, , https://doi.org/10.1016/j.surfcoat.2020.125382.
[78] M. Susoff, K. Siegmann, C. Pfaffenroth, M. Hirayama, Evaluation of icephobic coatings - screening of different coatings and influence of roughness, Appl. Surf. Sci. 282 (2013) 870–879, https://doi.org/10.1016/j.apsusc.2013.06.073.
[79] F. Piscitelli, A. Chiariello, D. Dabkowski, G. Corraro, F. Marra, L. Di Palma, Superhydrophobic coatings as anti-icing systems for small aircraft, Aerospace 7 (2020), https://doi.org/10.3390/aerospace7010002.
[80] L. Makkonen, Ice adhesion - theory, measurements and countermeasures, J. Adhes. Sci. Technol. 26 (2012) 413–445, https://doi.org/10.1163/016942411X574583.
[81] R.M. Fillion, A.R. Riahi, A. Edrisy, Design factors for reducing ice adhesion, J. Adhes. Sci. Technol. 31 (2017) 2271–2284, https://doi.org/10.1080/01694243.2017.1297588.
[82] M. Zou, S. Beckford, R. Wei, C. Ellis, G. Hatton, M.A. Miller, Effects of surface roughness and energy on ice adhesion strength, Appl. Surf. Sci. 257 (2011) 3786–3792, https://doi.org/10.1016/j.apsusc.2010.11.149.
[83] J. Chen, J. Liu, M. He, K. Li, D. Cui, Q. Zhang, X. Zeng, Y. Zhang, J. Wang, Y. Song, Superhydrophobic surfaces cannot reduce ice adhesion, Appl. Phys. Lett. 101 (2012) 111603, , https://doi.org/10.1063/1.4752436.
[84] T. Aoyama, M. Ishikawa, T. Hirata, K. Ukigai, Effect of surface roughness on adhesive shear strength between pure ice and a solid surface, Trans. Japan Soc. Refrig. Air Cond. Eng (2006) 23.
[85] S. Yang, Q. Xia, L. Zhu, J. Xue, Q. Wang, Q.M. Chen, Research on the icephobic properties of fluoropolymer-based materials, Appl. Surf. Sci. 257 (2011) 4956–4962, https://doi.org/10.1016/j.apsusc.2011.01.003.
[86] T. Bharathidasan, S.V. Kumar, M.S. Bobji, R.P.S. Chakradhar, B.J. Basu, Effect of wettability and surface roughness on ice-adhesion strength of hydrophilic, hydrophobic and superhydrophobic surfaces, Appl. Surf. Sci. 314 (2014) 241–250, https://doi.org/10.1016/j.apsusc.2014.06.101.
[87] V.F. Petrenko, S. Peng, Reduction of ice adhesion to metal by using self-assembling monolayers (SAMs), Can. J. Phys. 81 (2003) 387–393, https://doi.org/10.1139/p03-014.
[88] Z. He, E.T. Vågenes, C. Delabahan, J. He, Z. Zhang, Room temperature characteristics of polymer-based low ice adhesion surfaces, Sci. Rep. 7 (2017) 1–7, https://doi.org/10.1038/srep42181.
[89] W.D. Bascom, R.L. Cottington, C.R. Singleterry, Ice adhesion to hydrophilic and hydrophobic surfaces, J. Adhes. 1 (1969) 246–263, https://doi.org/10.1080/00218466908072188.
[90] J. Liu, C. Zhu, K. Liu, Y. Jiang, Y. Song, J.S. Francisco, X.C. Zeng, J. Wang, Distinct ice patterns on solid surfaces with various wettabilities, Proc. Natl. Acad. Sci. U. S. A. 114 (2017) 11285–11290, https://doi.org/10.1073/pnas.1712829114.
[91] M. Landy, A. Freiberger, Studies of ice adhesion. I. Adhesion of ice to plastics, J. Colloid Interface Sci. 25 (1967) 231–244, https://doi.org/10.1016/0021-9797(67)90026-4.
[92] M. Nosonovsky, V. Hejazi, Why superhydrophobic surfaces are not always icephobic, ACS Nano 6 (2012) 8488–8491, https://doi.org/10.1021/nn302138r.
[93] Z. He, S. Xiao, H. Gao, J. He, Z. Zhang, Multiscale crack initiator promoted superlow ice adhesion surfaces, Soft Matter 13 (2017) 6562–6568, https://doi.org/10.1039/c7sm01511a.
[94] P. Irajizad, A. Al-Bayati, B. Eslami, T. Shafquat, M. Nazari, P. Jafari, V. Kashyap, A. Masoudi, D. Araya, H. Ghasemi, Stress-localized durable icephobic surfaces, Mater. Horizons. 6 (2019) 758–766, https://doi.org/10.1039/c8mh01291a.
[95] D.L. Beemer, W. Wang, A.K. Kota, Durable gels with ultra-low adhesion to ice, J. Mater. Chem. A 4 (2016) 18253–18258, https://doi.org/10.1039/C6TA07262C.
[96] J.G. Smith, C.J. Wohl, R.E. Kreeger, J. Palacios, T. Knuth, K. Hadley, Effect of molecular flexibility upon ice adhesion shear strength, 39th Annu. Meet. Adhes. Soc. 21–24 Feb. 2016; San Antonio, TX; United States, 2016, pp. 5–7 https://ntrs.nasa.gov/search.jsp?R=20160007710.
[97] R. Menini, M. Farzaneh, Advanced icephobic coatings, J. Adhes. Sci. Technol. 25 (2011) 971–992, https://doi.org/10.1163/016942410X533372.

PUBLICATION III

Durability of lubricated icephobic coatings under various environmental stresses

V. Donadei, H. Koivuluoto, E. Sarlin, and P. Vuoristo

Polymers, 14.2 (2022), 303
DOI: 10.3390/polym14020303

polymers

MDPI

Article

Durability of Lubricated Icephobic Coatings under Various Environmental Stresses

Valentina Donadei [1,*], Heli Koivuluoto [1,2], Essi Sarlin [1] and Petri Vuoristo [1]

[1] Materials Science and Environmental Engineering, Faculty of Engineering and Natural Sciences, Tampere University, P.O. Box 589, FI-33014 Tampere, Finland; heli.koivuluoto@tuni.fi (H.K.); essi.sarlin@tuni.fi (E.S.); petri.vuoristo@tuni.fi (P.V.)
[2] Tampere Institute for Advanced Study, Tampere University, P.O. Box 1001, FI-33014 Tampere, Finland
* Correspondence: valentina.donadei@tuni.fi

Abstract: Icephobic coatings interest various industries facing icing problems. However, their durability represents a current limitation in real applications. Therefore, understanding the degradation of coatings under various environmental stresses is necessary for further coating development. Here, lubricated icephobic coatings were fabricated using a flame spray method with hybrid feedstock injection. Low-density polyethylene represented the main coating component. Two additives, namely fully hydrogenated cottonseed oil and paraffinic wax, were added to the coating structure to enhance coating icephobicity. Coating properties were characterised, including topography, surface roughness, thermal properties, wettability, and icephobicity. Moreover, their performance was investigated under various environmental stresses, such as repeated icing/deicing cycles, immersion in corrosive media, and exposure to ultraviolet (UV) irradiation. According to the results, all coatings exhibited medium-low ice adhesion, with slightly more stable icephobic behaviour for cottonseed oil-based coatings over the icing/deicing cycles. Surface roughness slightly increased, and wetting performances decreased after the cyclic tests, but chemical changes were not revealed. Moreover, coatings demonstrated good chemical resistance in selected corrosive media, with better performance for paraffin-based coatings. However, a slight decrease in hydrophobicity was detected due to surface structural changes. Finally, paraffin-based coatings showed better resistance under UV irradiation based on carbonyl index and colour change measurements.

Keywords: thermal spraying; flame spraying; polymer coatings; lubricated coatings; icephobicity; durability; polymer degradation

Citation: Donadei, V.; Koivuluoto, H.; Sarlin, E.; Vuoristo, P. Durability of Lubricated Icephobic Coatings under Various Environmental Stresses. *Polymers* **2022**, *14*, 303. https://doi.org/10.3390/polym14020303

Academic Editors: Cătălin Croitoru and Iosif Hulka

Received: 15 December 2021
Accepted: 6 January 2022
Published: 12 January 2022

1. Introduction

In the past decades, passive icephobic solutions, i.e., coatings or surface modifications enabling ice removal, have emerged as potential strategies to face icing problems [1]. Ice accretes and accumulates on surfaces, affecting the operational performances of many engineering applications from aerospace and maritime transportation to renewable energy and power distribution [2,3]. Malfunction, decreased performance, economic losses, and endangerment of human life represent some of the consequences of atmospheric ice accumulating on infrastructure [4]. Current strategies to mitigate icing problems, known as active deicing methods, consist of ice removal from surfaces using external mechanical and thermal loads [5–7]. Moreover, ice accretion is prevented or limited by applying chemicals on surfaces, known as anti-icing or deicing fluids. However, these active methods require costly operations, wasting time, energy, and resources while causing environmental pollution [8,9]. Therefore, the current research is oriented towards more sustainable anti-icing strategies.

Icephobic coatings as passive anti-icing strategies are highly desirable as alternative solutions to solve icing problems. However, current durability challenges preclude their

applicability in various fields [10,11]. Specifically, icephobic coatings should exhibit permanent icephobic properties under application-related icing conditions. Cyclic icing/deicing tests have been performed to investigate the icing durability of coatings in several studies [12–16]. In addition to icing durability, the stability of coatings has been tested under external loads, such as mechanical [17–20], chemical [21,22], and thermal stresses and irradiation [10,23,24], to extend their use to real applications [11]. Moreover, recent studies have proposed combining icephobic coatings with active anti-icing methods to mitigate icing problems in harsher icing conditions [4,25,26]. Therefore, more durable passive anti-icing methods are strongly desired, and further research is needed to improve the durability of current icephobic solutions.

The literature presents extensive work on investigating the durability of passive icephobic surfaces, specifically for designs such as superhydrophobic surfaces (SHSs) and slippery liquid-infused porous surfaces (SLIPSs) [11,14,20,22,27–32]. However, little attention has been given to assessing the durability of icephobic polymer coatings and composite polymer coatings [10,13,18,33,34]. Therefore, the present study investigates the durability of icephobic polymer coatings under various environmental stresses. Firstly, the durability of coatings is tested under repeated icing/deicing cycles. Secondly, the coating performance is investigated under environmental loads, such as chemical stresses and irradiation, which have not been considered in our previous works [35–37]. Coatings are fabricated using a one-step method, previously termed a flame spray process with hybrid feedstock injection [35]. This versatile method was used to produce composite coatings named lubricated icephobic coatings (LICs) [35]. LICs consist of two polymeric components, namely matrix material and lubricating additive. In this study, the matrix material is low-density polyethylene. Two different materials are employed as lubricating additives of the coatings, namely fully hydrogenated cottonseed oil and paraffinic wax. Waxes are generally used in different coating applications to achieve specific surface-related properties, such as glossy or matte appearance and slipperiness [38]. Moreover, they can function as anti-blocking, anti-settling, and anti-sagging agents [38]. More importantly, waxes and polymers, particularly polyolefins, have demonstrated low surface free energy properties [39,40], which can promote reduced ice adhesion strength on smooth polymeric surfaces [41]. Therefore, in this study, waxes are added to the coating structure, aiming at enhancing the icephobic properties of LIC surfaces.

In summary, this study focuses on (1) producing LICs based on low surface free energy additives by one-step fabrication method, (2) characterising the properties of feedstock materials and obtained coatings, (3) testing the icephobic behaviour of coatings, and (4) assessing the durability of coatings under various environmental stresses, such as repeated icing/deicing cycles, immersion in corrosive environments and exposure to ultraviolet (UV) irradiation. Some significant results indicate that cottonseed oil-based coatings show a better icephobic behaviour than paraffinic wax-based coatings. However, the latter better tolerate corrosive conditions and exposure to UV irradiation.

2. Materials and Methods

2.1. Materials and Coating Fabrication

Composite polymer coatings were fabricated from commercially available feedstock powders. The primary component of coatings was low-density polyethylene (LDPE) powder (Plascoat LDPE, Plascoat Europe BV, Zuidland, Netherlands). Two different additive powders were selected as the lubricating component of the coatings. The first additive was made of fully hydrogenated cottonseed oil (Lubritab® capsules, JRS PHARMA GmbH & Co. KG, Rosenberg, Germany) and hereafter indicated with the letter C in the sample codes. The second additive was a non-functionalised Fischer–Tropsch hard paraffinic wax (VESTOWAX® H 2050 MG, Evonik Industries AG, Essen, Germany) and hereafter indicated with the letter P.

LICs were manufactured using a flame spray method with hybrid feedstock injection [35], schematically represented in Figure 1. In this method, LDPE was sprayed by

an oxygen-acetylene flame spray gun (CastoDyn DS 8000, Castolin Eutectic, Dällikon, Switzerland). This powder was fed using a first powder feeder (Sulzer Metco 4MP, Oerlikon Metco, Wohlen, Switzerland) with nitrogen as a carrier gas. The lubricating additive was sprayed from an external injector mounted on the left side of the gun. The additive was fed using a second powder feeder (PT-10 Twin powder feeder, Oerlikon Metco, Wohlen, Switzerland) with argon as a carrier gas. The spray gun was mounted on a single-arm robot (ABB IRB 4400/60, ABB Robotics, Västerås, Sweden), and the spraying process was automated.

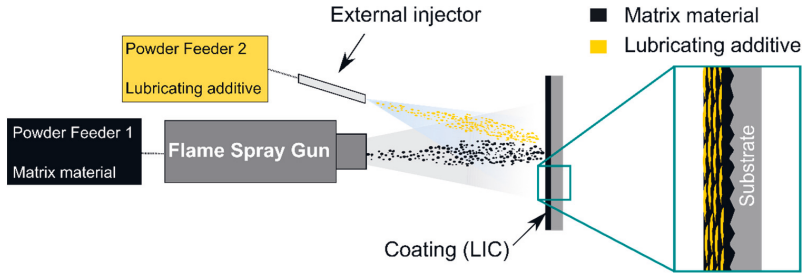

Figure 1. Schematisation of the flame spray process with hybrid feedstock injection to produce lubricated icephobic coatings (LICs).

Coatings were deposited on stainless steel substrates (EN 1.4301/2K (4N)), cut in dimensions of 30 mm × 60 mm × 1.5 mm. Substrates were grit-blasted before spraying using aluminium oxide grits (grit size of 54 Mesh). Grit blasting ensures the adhesion of polymer coatings on metal surfaces via a mechanical interlocking mechanism. Substrates were pre-heated by flame, and spraying started when the substrate temperature exceeded the melting range of the LDPE powder at approximately 120 °C. The substrate temperature was monitored using a thermal imaging camera (Ti300 Infrared Camera IR Fusion Technology, Fluke Corporation, Everett, WA, USA). Firstly, the matrix material was sprayed to produce an LDPE coating layer. After the first layer, matrix and additive materials were sprayed simultaneously to fabricate LICs. Coatings with a thickness of approximately 700 µm were deposited on the substrate. Once the coating deposition was completed, some coatings underwent a post-heating treatment by flame. Table 1 provides the process parameters of the flame spray process with hybrid feedstock injection. Table 2 presents the coatings produced in this study with details on employed materials and process parameters. The asterisk in the sample name indicates the post-heating treatment by flame.

Table 1. Process parameters of the flame spray process with hybrid feedstock injection.

Process Parameters	Value
CastoDyn DS 8000—flame spray gun	
Nozzle model	SSM10
Combustion gasses	
Oxygen pressure [bar]	4.0
Acetylene pressure [bar]	0.7
Gun spray distance [mm]	250
Step size [mm]	5
Sulzer Metco 4MP-850D dual powder feeder—matrix powder	
Matrix material feed rate [g/min]	26
Carrier gas (nitrogen) flow rate [L/min]	10
Carrier gas (nitrogen) input pressure [bar]	5
PT-10 twin powder feeder—additive powder	
Lubricating additive material feed rate [g/min]	8
Carrier gas (argon) flow rate [L/min]	6

Table 2. List of lubricated icephobic coatings (LICs) and flame-sprayed (FS) feedstock material coatings with details on employed materials and process parameters. LDPE, C, and P refer to low-density polyethylene, fully hydrogenated cottonseed oil, and paraffinic wax powders, respectively.

Sample	Materials	Gun Traverse Speed [mm/s]	Gun Air Pressure [bar]	Post-Heating [Y/N]
FS-LDPE	LDPE	500	0	Y
LIC-C	LDPE + C	500	2	N
LIC-C *				Y
LIC-P	LDPE + P			N
LIC-P *				Y
FS-C [1]	C	900	4	N
FS-P [1]	P			N

* Coatings were post-heated using the flame of the spray gun; [1] Additive coatings (FS-C and FS-P) were fabricated using the external injector of the hybrid feedstock injection system.

Plain additive coatings were fabricated using the external injector of the hybrid feedstock injection system. Deposition of additive coatings was challenging because the melted materials dripped down from the metal substrates during spraying. However, these coatings were produced to better understand the icephobic properties of additives and the icephobic behaviour of corresponding composite coatings.

2.2. Characterisation Methods

2.2.1. Feedstock Material Characterization

The morphology of powders was imaged using a scanning electron microscope (SEM, IT-500, JEOL Ltd., Tokyo, Japan). Before the analysis, the powders were sputtered with a thin gold layer to enhance surface conductivity. A secondary electron detector was used to image the powder morphologies.

Particle size distribution was analysed using a laser diffraction analysis with a dry powder method (LS 13 320 Laser Diffraction Particle Size Analyser, Beckman Coulter, Inc., Brea, CA, USA). The particle size distributions were reported using the annotation −d90 + d10, where d90 and d10 represent the particle sizes below which 90% and 10% of total particles, respectively, are counted.

The chemical characterisation of the feedstock materials was performed using a Fourier-transform infrared spectrometer (Spectrum One FT-IR Spectrometer, Perkin Elmer Instruments, Waltham, MA, USA). This analysis was carried out using an attenuated total reflectance (ATR) sample holder (Universal ATR Sampling accessory, Perkin Elmer Instruments, Waltham, MA, USA) with a diamond crystal. The FTIR spectra were acquired in the wavenumber range 4000 cm^{-1} to 600 cm^{-1} by recording 32 scans with a 4 cm^{-1} resolution. The measurements were repeated three times.

The thermal characterisation was performed using differential scanning calorimetry (DSC, Netzsch DSC214 Polyma, Netzsch, Selb, Germany). Specimens (approx. 10 mg) were placed in a concavus aluminium pan. Dynamic heating was carried out at 20 °C/min from −30 °C to 150 °C in nitrogen atmosphere (40 mL/min nitrogen flow), and glass transition, melting transition, and melting peaks were identified. The thermal stability was investigated by thermogravimetric (TG) analysis (Netzsch TGA209F Tarsus, Netzsch, Selb, Germany). Specimens (approx. 10 mg) were placed in open alumina pans, and dynamic heating was performed at 20 °C/min from 25 to 600 °C in nitrogen atmosphere (20 mL/min nitrogen flow). The thermal stability of the material was estimated by measuring the onset decomposition temperature, T_{onset}, of the dynamic TG curve, according to the standard ISO 11358-1. Furthermore, the maximum degradation rate temperature of the powders was estimated at the peak of the first derivative of the TG curve (DTG curve). The results of the thermal analyses were obtained as the average and standard deviation of three measurements.

The thermal oxidation resistance of the feedstock powders was evaluated by measuring the oxidation induction time (OIT) by DSC. This analysis is relevant to predict possible degradation of the feedstock materials in flame spray processes. Specimens (approx. 10 mg) were placed in an open concavus aluminium pan. Firstly, the specimens were heated from room temperature to the oxidation temperature (150 °C or 200 °C) in nitrogen atmosphere at 20 °C/min. After stabilisation of 2 min at the oxidation temperature, the atmosphere of the furnace was changed to oxygen (40 mL/min oxygen flow) for 30 min. The OIT was measured from the gas change until the observed exothermic reaction. The OIT results were obtained as the average and standard deviation of three measurements.

2.2.2. Coating Characterisation

The surface morphology was imaged using a stereomicroscope (MZ7.5, Leica, Wetzlar, Germany) and a scanning electron microscope (SEM, IT-500, JEOL Ltd., Tokyo, Japan). Before the microscopic analysis, the surface samples were sputtered with a thin platinum/palladium layer to enhance surface conductivity. A secondary electron detector was used to image the surface morphologies.

The surface topography was analysed using an optical profilometer (contactless measuring instrument, Alicona Infinite Focus G5, Alicona Imaging GmbH, Raaba, Austria). Roughness parameters (Ra, Sa, Sz) were measured using a 20× objective magnification on 2 mm × 2 mm areas, according to standards ISO 4288 [42] and ISO 25178–3 [43]. Roughness values were obtained by the average and standard deviation of three measurements at different coating locations.

The chemical characterisation of the coating surfaces was conducted using the same methodology employed for the powders. Surfaces were directly placed on the crystal for the analysis. The measurements were performed in three different locations of the sample surfaces.

The thermal characterization of the coatings was carried out using similar methods to those employed for the thermal analysis of feedstock powders to qualitatively investigate the presence of the additives within the coating structure after coating production. The lubricating additive percentage was qualitatively estimated as the ratio between the enthalpy of fusion of the additive and the total enthalpy of fusion obtained from the DSC curve of the coating.

The wetting behaviour was measured by a droplet shape analyser (DSA100, Krüss, Hamburg, Germany) in controlled conditions (22 °C ± 1 °C temperature and 60% ± 3% relative humidity). Static contact angles were investigated using the sessile drop method by placing 10 µL droplets of ultra-high-purity water (MilliQ, Millipore Corporation, Burlington, MA, USA) onto the surfaces. The apparent water contact angle (WCA) was measured using the tangent method (polynomial fit of droplet shape). Tilting experiments were performed to evaluate the dynamic wetting behaviour of coatings. A 10 µL water droplet was placed onto the coating surfaces, which were tilted until the droplet rolled off, and the tilting angle was recorded. Both WCA and roll-off angle were calculated as the average and standard deviation of five measurements on different sample locations.

Surface free energy (SFE) of coatings was calculated according to the Owens–Wendt–Rabel–Kaelble (WORK) model [44–47], measuring the static contact angle of water, diiodomethane, and ethylene glycol. This model obtains the SFE of solids as the sum of a dispersive and a polar component. Table 3 presents the polar and dispersive components of the reference liquids used for calculation. The measurements were carried out by depositing ten drops of 3 µL of each liquid on the sample surface. Additionally, surface free energies were measured for the feedstock materials. Feedstock powders were melted and moulded in cylindrical silicon stamps using an oven (drying oven with natural convection, DL 53, DRY-Line®, VWR, Darmstadt, Germany). This procedure was carried out to obtain polymer samples in the form of bulks suitable for the SFE measurements.

Table 3. Surface tension components of the reference liquids from the substance database of Krüss Advance software.

Reference Liquid	Chemical Formula	Surface Tension at RT [mN/m]	Dispersive Component [mN/m]	Polar Component [mN/m]
water	H_2O	72.8	21.8	51
diiodomethane	CH_2I_2	50.8	50.8	0
ethylene glycol	$C_2H_6O_2$	47.7	26.4	21.3

Icephobic behaviour was measured using the icing facilities in the Ice Laboratory at Tampere University [48]. The test equipment is located in a climate-controlled cold room with monitored temperature and relative humidity ($-10\ ^{\circ}C \pm 1\ ^{\circ}C$ and $80\% \pm 5\%$). Mixed-glaze ice was accreted on 30 mm × 30 mm sample areas from supercooled water droplets in an icing wind tunnel (IWiT). After accretion, the ice adhesion strength was measured using a centrifugal ice adhesion test (CAT). In the centrifugal test, specimens with the accreted block of ice are counterweighted and spun with a constant acceleration rate of 300 rpm/s until ice detachment. An acceleration sensor records the value of the rotational speed corresponding to the ice detachment. The shear ice adhesion strength is evaluated as the ratio of the centrifugal force, F [N] at the moment of ice detachment, to the area of the iced surface, A [m^2]. Equation (1) estimates the shear ice adhesion strength, τ_{ice} [kPa], as follows:

$$\tau_{ice} = \frac{m_{ice} r \omega^2}{A} \quad (1)$$

where m_{ice} [kg] is the known mass of the accreted ice on the specimen, r [m] is the radial spinning length, and ω [rad/s] is the rotational speed. Ice adhesion values were obtained from the average and standard deviation of four parallel samples tested in the icing accretion event. Ice adhesion of a reference surface, namely Teflon tape (TT, 3M™ PTFE Film Tape 5490, 3M, Flemington, NJ, USA), was tested during each ice accretion event to monitor possible ice adhesion variation. The ice adhesion of the reference must necessarily be in the same range of values for a specific ice type to ensure the repeatability and reliability of the icing test and comparison of the results [49].

2.3. Durability Tests

2.3.1. Durability under Repeated Icing/Deicing Cycles

The durability of icephobic properties was tested using cyclic icing/deicing tests. Ice was repetitively accreted, and the centrifugal ice adhesion test was performed on the same surfaces four times in total. Four parallel samples of each coating were tested, and the results were calculated as the average and standard deviation of obtained shear ice adhesion values. Variations in ice adhesion were used to assess the durability of the icephobic properties over the cycles. Moreover, changes in surface properties, such as surface morphology, roughness, chemistry, and wettability, were investigated after the cyclic tests. These analyses were conducted to better understand the durability of the icephobic properties.

2.3.2. Durability in Acidic, Saline and Basic Solutions

The durability of coatings was tested by immersing as-received samples in different chemical solutions. Different aqueous solutions were prepared. An acidic solution was prepared using acetic acid (Acetic acid 99–100% GPR RECTAPUR®, VWR Chemicals, Fontenay-sous-Bois, France), and this simulated the interaction of coatings with an acidic rain (pH = 4, considering the average value of the annual rain acidity [50]). A saline solution was prepared using sodium chloride (Sodium chloride, BAKER ANALYZED® ACS, J.T. Baker®, VWR Chemicals, Fontenay-sous-Bois, France). The saline solutions mimicked a saline environment with the average sea salt concentration (sodium chloride 35 g/L). A basic solution (pH = 11) was prepared using sodium hydroxide (Sodium Hydroxide,

Tamro Oy, Vantaa, Finland), thus recreating the environment of solutions containing cleaning agents, detergents, and ammonia. The pH of the solutions was measured using a pH metre (MU 6100 H, multiparameter instrument, VWR, Darmstadt, Germany). The pH meter was calibrated before each measurement using three buffer solutions with pH of 4, 7, and 10.

Variations in wetting properties were monitored for all coatings after 7, 15, 30, and 60 days of immersion. The samples were rinsed with de-ionised water, dried with compressed air, and left in controlled conditions (22 °C ± 1 °C temperature and 60% ± 3% relative humidity) for 24 h before the wetting experiments. Possible changes in surface chemistry were investigated by FTIR analysis. TGA analyses were carried out to detect absorbed water in immersed polymers. Surface morphologies were analysed after 60 days of immersion.

2.3.3. Durability under Exposure to Ultraviolet (UV) Irradiation

As-received coatings were artificially aged using simulated solar UV light. The UV irradiation chamber was equipped with four UVA-340 fluorescent lamps. This lamp provides an excellent simulation of natural sunlight in the short-wavelength UV region (ranging from approximately 365 nm to 295 nm). Because the UVA-340 lamp simulates sunlight in the spectrum area that causes the most polymer degradation, this could theoretically ensure better correlation with outdoor test results than other used light sources [38,51]. The dose rate of the chamber was measured as 0.7 W/ m^2 at the UVB range (290–315 nm), 12.1 W/m^2 at the UVA range (315–400 nm), and 3.1 W/m^2 at the visible range (400–600 nm) [52]. The temperature of the UV chamber reached 31 °C when all lamps were functioning. Further technical details on the UV chamber are reported in a previous study [52]. For the UV irradiation tests, samples were exposed for 0, 200, 500, and 1000 h. Changes in chemical composition were investigated using FTIR analysis. The carbonyl index (CI) was used to assess the degree of photodegradation of the coatings. This index was calculated as the ratio between the integrated band absorbances of the carbonyl (C=O) peak from 1850 to 1650 cm^{-1} and the methylene (CH_2) scissoring peak from 1500 to 1420 cm^{-1}, following the specified area under band (SAUB) methodology [53]. Colour changes of the surfaces were observed using visual inspection and a chromameter (CR-200, Konica Minolta Sensing Europe B.V., Nieuwegein, The Netherlands). The chromaticity experiments employed a measuring mode based on $L^*a^*b^*$ coordinates (CIE 1976). In the $L^*a^*b^*$ colour space, L^* indicates the colour lightness, a^* refers to the red/green coordinate, and b^* refers to the yellow/blue coordinate [54]. According to the standard ISO/CIE 11664-4 [55], the colour difference, ΔE^*_{ab}, is calculated at 200, 500, and 1000 h with the following Equation (2):

$$\Delta E^*_{ab} = \sqrt{\left(L^*_2 - L^*_1\right)^2 + \left(a^*_2 - a^*_1\right)^2 + \left(b^*_2 - b^*_1\right)^2} \quad (2)$$

where L^*_1, a^*_1, and b^*_1 represent the lightness, the red/green coordinate, and the yellow/blue coordinate of the as-received samples, corresponding to 0 h exposure time. L^*_2, a^*_2, and b^*_2 represent the values for the samples after 200 h, 500 h, and 1000 h of exposure time.

3. Results and Discussion

3.1. Properties of the Feedstock Powders

Figure 2 shows the morphology of the feedstock powders used to fabricate lubricated icephobic coatings in this study. The LDPE powder (Figure 2a), which constitutes the main component of the coating, was characterised by particle shapes varying from blocky irregular grains to long stretched flakes. The particle analysis revealed a size distribution of −482 + 154 µm. The fully hydrogenated cottonseed oil additive powder (C) showed particles with a spherical shape (Figure 2b) and narrower size distribution of −152 + 34 µm. The hard paraffinic wax (P) presented particles with various irregular shapes (Figure 2c) and a broader size distribution of −450 + 29 µm, as compared to the other additive powder.

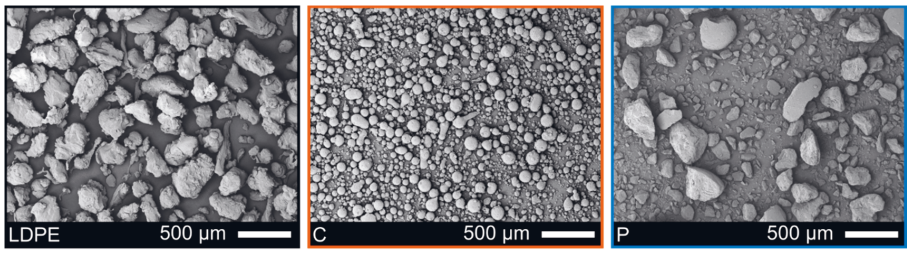

Figure 2. SEM micrographs of the as-received feedstock powders: (**a**) LDPE powder (LDPE), (**b**) fully hy-drogenated cottonseed oil powder (C), and (**c**) hard paraffinic wax powder (P).

Figure 3 presents the FTIR spectra of the feedstock powders. The chemical analysis of feedstock materials aimed at monitoring possible chemical changes occurring in the polymers interacting with the combustion flame during coating fabrication. All the spectra presented typical peaks, characteristics of polymers made of long aliphatic hydrocarbon chains, such as polyethylene [56]. The signals at 2915 and 2848 cm^{-1} corresponded to the asymmetric and symmetric stretching of aliphatic hydrocarbons, respectively. The signals at 1472, 1470, 1467, 1462, and 1376 cm^{-1} represented the in-plane vibrations of aliphatic hydrocarbons [56,57]. The signals at 730 and 719 cm^{-1} indicated the rocking of the same vibrational group [56,57]. As expected, the spectra of LDPE and P were remarkably similar due to their identical chemical composition. However, P powder showed double peaks in the range of the in-plane vibrations and rocking of aliphatic hydrocarbons compared to LDPE powder. Similar spectra for paraffinic waxes have been found in previous studies [57–60]. Additionally, LDPE presented a weak signal at 1731 cm^{-1}. This signal probably indicates the presence of conventional stabilisers of undisclosed composition (probably carbonyl products), which are generally incorporated into commercial products [61]. In addition to the aliphatic chain signals, C powder presented two intense absorption peaks at 1737 cm^{-1} and 1173 cm^{-1}. These signals are related to the stretching of the carbonyl group (C=O) and the carbon–oxygen bond (C-O) of the ester group, generally present in natural waxes [57,62]. Moreover, the weak signal at 2955 cm^{-1} was present in both additives. This peak arose from the asymmetric stretching of the methyl (CH_3) in the aliphatic chain [63,64]. However, this small peak could also be associated with =C-H cis stretching in cottonseed oil in case of residual unsaturation (double carbon–carbon bond) after hydrogenation [65].

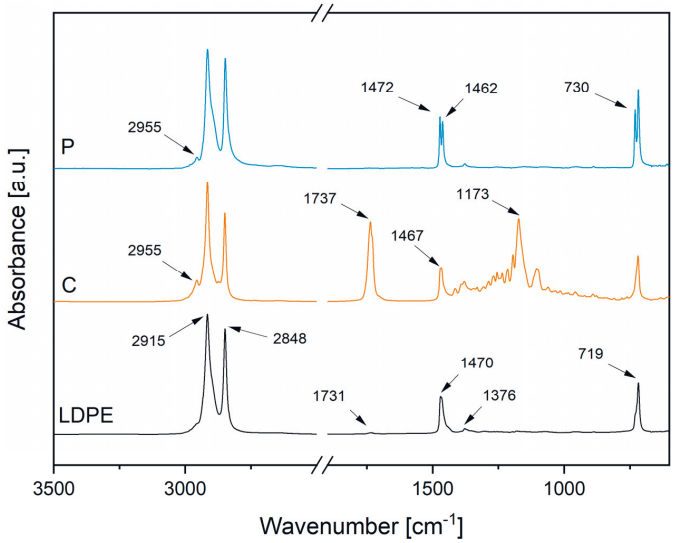

Figure 3. FTIR spectra of feedstock powders with characteristic absorbance peaks. LDPE, C, and P refer to low-density polyethylene, fully hydrogenated cottonseed oil, and paraffinic wax powders, respectively.

Table 4 presents the thermal properties of feedstock powders obtained from differential scanning calorimetry and thermogravimetric analyses. The curves are presented in Supplementary Figure S1.

Table 4. Thermal properties of low-density polyethylene (LDPE), fully hydrogenated cottonseed oil (C), and paraffinic wax (P): temperature at the melting peaks ($T_{melting\ peak}$) from the DSC analyses, onset decomposition temperatures (T_{onset}) from the TG curves, and maximum degradation temperatures ($T_{max\ degradation}$) from the DTG curves.

Sample	$T_{melting\ peak}$ [°C]	T_{onset} [°C]	$T_{max\ degradation}$ [°C]
LDPE	111.9 ± 0.6	458.2 ± 1.3	481.1 ± 1.9
C	55.6 ± 0.5 68.9 ± 2.3	402.5 ± 4.6	437.1 ± 1.7
P	100.3 ± 0.2 118.8 ± 0.6	435.0 ± 7.0	480.2 ± 1.7

No glass transitions were revealed for the as-received feedstock powders in the temperature range of the analysis. LDPE and P powders had melting peaks at higher temperatures than C powder. Both additive powders showed two distinct melting peaks. Moreover, in the TG analyses, the higher the T_{onset}, the greater the thermal stability of polymers in the considered atmosphere. Therefore, the results indicated improved thermal stability passing from C to P until the LDPE powder. This temperature is essential when considering flame spray processing of polymers, and T_{onset} should not be exceeded to avoid thermal degradation. The maximum degradation temperatures were later utilized to detect the presence of these components in flame-sprayed coatings.

The feedstock materials are fed using inert carrier gasses, such as nitrogen for the matrix materials and argon for the additives. However, the materials are molten by the heat produced from the combustion flame, which generates an oxidative environment. Moreover, when post-heating by flame is performed, the deposited materials are re-melted in contact with the oxidative atmosphere. Considering the complexity of the spraying

environment, the resistance of the feedstock powders was further evaluated in oxidative conditions. The OIT results showed no degradation for the feedstock powders exposed to an oxidative atmosphere at 150 °C. However, oxidative degradation was detected at 200 °C almost immediately for LDPE and P, after 1.5 ± 0.2 min and 0.8 ± 0.1 min, respectively. Surprisingly, the degradation of C powder initiated after 27.9 ± 0.3 min. These results indicate a far greater resistance for C than the other feedstock materials. It is well known that the thermal–oxidative resistance of cottonseed oil increases with reduced unsaturation in the chemical structure [66]. Therefore, the fact that our cottonseed oil powder was fully saturated (the commercial product was fully hydrogenated, i.e., all unsaturations were removed) could justify its remarkable oxidative resistance. Oxidation resistance is beneficial for polymers processed using flame spraying, considering the negative influence of thermal degradation on icephobic properties [67]. Moreover, oxidative degradation could be avoided by maintaining the material temperatures below 150 °C during the whole spraying process.

Table 5 reports the surface free energy values measured for the feedstock samples in the form of bulk. Bulk surfaces were relatively smooth, with Ra values ranging from 0.2 to 1.7 μm. Measured SFE values for LDPE and P were similar to the values found in the literature [44,68]. To the best of our knowledge, no SFE has been reported in other studies for fully hydrogenated cottonseed oil. The results showed lower SFE values for the lubricating additives than for the matrix material. In laboratory-scale studies, it has been shown that surfaces with lower SFE demonstrated enhanced icephobic character [41,68,69]. Moreover, similar results were reported in our previous study, where adding the C additive to the LDPE matrix improved the icephobic behaviour of plain LDPE coatings [35].

Table 5. Surface free energy (SFE) values with dispersive and polar components of low-density polyeth-ylene (LDPE), fully hydrogenated cottonseed oil (C), and paraffinic wax (P), in the form of bulk.

Feedstock Material	SFE [mN/m]	Dispersive Component [mN/m]	Polar Component [mN/m]
LDPE	30.41 ± 1.25	29.14 ± 0.64	1.27 ± 0.61
C	19.77 ± 1.48	19.15 ± 1.19	0.62 ± 0.28
P	22.84 ± 0.04	22.19 ± 0.03	0.64 ± 0.01

3.2. Composition and Surface Properties of the Coatings

Figure 4 presents the surface topography of the coatings together with the employed process parameters. Table 6 provides the areal roughness values (Sa, Sz) for all coating surfaces. From the results, both selected process parameters and thermal properties of feedstock materials influenced the obtained surface topography. If the same process parameters were employed, smoother surfaces were achieved when the lower-melting-temperature additive was sprayed with LDPE (LIC-C compared to LIC-P). Moreover, post-heating by flame smoothened the surfaces by re-melting and re-solidification of polymers, thus producing coatings with a comparable level of roughness (LIC-C* and LIC-P*). Finally, even smoother surfaces were obtained when plain additive coatings were produced, with P-based coatings slightly rougher than C-based coatings (FS-P and FS-C).

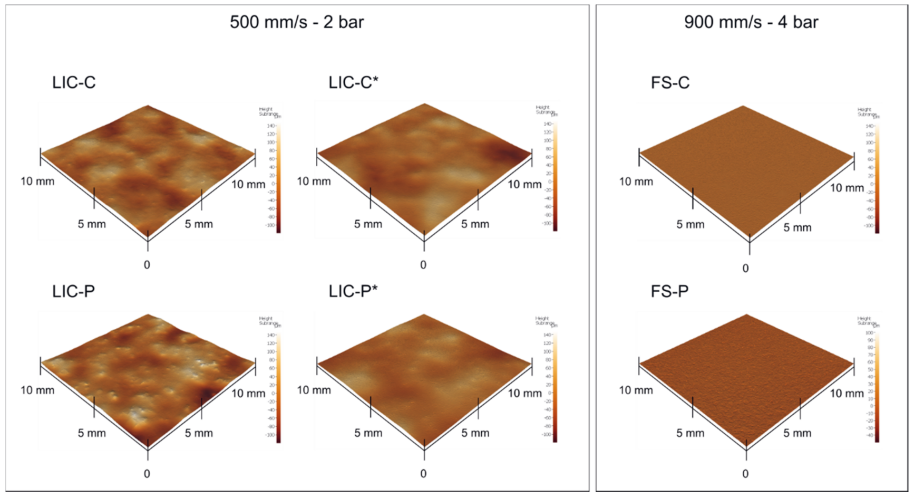

Figure 4. Surface topography of lubricated icephobic coatings (LICs) and flame-sprayed (FS) additive coatings measured using optical profilometry.

Table 6. Average and standard deviation (SD) of the areal roughness parameters evaluated for lubricated icephobic coatings (LICs) and flame-sprayed (FS) additive coatings: average height (Sa) and maximum height (Sz).

Sample	Sa [μm] ± SD [μm]	Sz [μm] ± SD [μm]
LIC-C	18.1 ± 5.5	122.8 ± 13.8
LIC-C*	9.8 ± 2.1	98.1 ± 10.8
LIC-P	23.4 ± 5.4	168.3 ± 13.5
LIC-P*	9.2 ± 1.6	101.5 ± 19.8
FS-C	0.9 ± 0.4	64.2 ± 10.6
FS-P	1.6 ± 0.1	74.1 ± 6.3

After coating deposition, chemical characterization of the surfaces was carried out to investigate the presence of the components on surfaces and possible chemical modifications. Figure 5 represents the FTIR spectra of lubricated coatings. The chemical analyses confirmed the presence of matrix material and corresponding additives for all coating surfaces. No significant changes in surface chemistry were revealed for C-based coatings as an effect of the post-heating treatment. Conversely, a small signal at 1630 cm^{-1} was detected for sample LIC-P* compared to LIC-P. This signal might indicate the presence of alkene compounds, which constitutes the initial product of thermal degradation of polyolefins [70]. This behaviour could derive from the lower resistance to thermal oxidation of P compared to C, as demonstrated by previous OIT experiments.

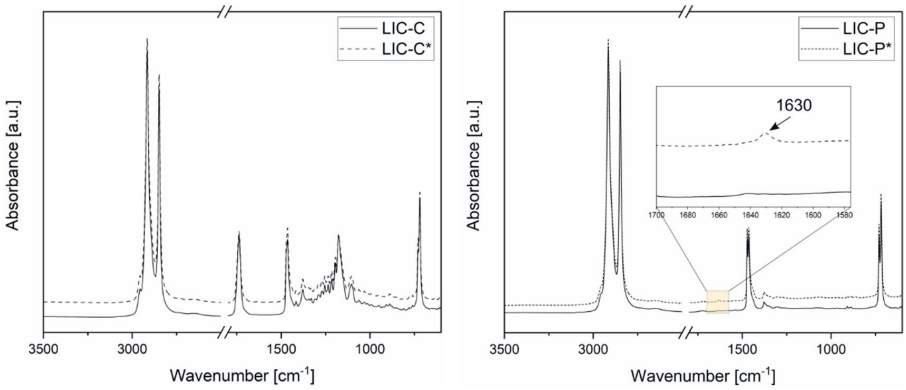

Figure 5. FTIR spectra of lubricated icephobic coatings: (**a**) LIC-C and LIC-C*, and (**b**) LIC-P and LIC-P*. The spectra region is highlighted by a yellow box when chemical modifications are detected.

The presence of the additives was further investigated using thermal analyses. Differential scanning calorimetric curves of LIC-C and LIC-C* revealed two distinct melting transitions corresponding to LDPE and C additive. From the ratio between the enthalpies of fusion of additives and coating samples, C content was estimated to be approximately 18 m% ± 1 m% for both coatings. This value approached the theoretical percentage of additive content (20%) determined by the settled feed rates of feedstock powders during spraying. However, the enthalpies of fusion refer solely to the crystalline content of the polymers, and therefore some uncertainty could affect these evaluations. Conversely, LIC-P and LIC-P* coatings showed one melting transition, with melting peaks at intermediate temperatures between the feedstock materials. Identifying P additive was more challenging with this technique, considering the overlapping of melting ranges of P and LDPE. The results obtained from the DSC analyses are provided in Supplementary Figure S2. Similar to DSC results, thermogravimetric curves of LIC-C and LIC-C* evidenced the presence of C additive in the coating structure. The first derivative of the TG curves showed two regions of degradations. The first region was characterized by several shoulders in the degradation range of C. This result evidenced the presence of the minor component C in the coating structure, in accordance with our previous study [35]. The second region referred to the degradation of the main component, LDPE. Conversely, the presence of P additive was hardly identifiable with this technique. One degradation peak was evidenced for LIC-P and LIC-P*. This was due to the overlapping of degradation phenomena of related feedstock materials. The TG and DTG curves of coatings and corresponding feedstock materials are reported in Supplementary Figure S3.

The analysis of wetting properties evaluates the tendency of surfaces to repel water. Wettability has been extensively investigated and used as a screening tool for potential icephobic surfaces [41,71–74]. Table 7 presents the results of the wetting experiments. For plain flame-sprayed LDPE coatings, water contact angles vary approximately from 84° to 93° for different ranges of roughness [35,67]. From the wetting results of this study, the surface hydrophobicity of plain LDPE coatings was enhanced by the addition of additives. LICs showed intermediate wetting properties, more similar to the additives, with C-based coatings more hydrophobic than P-based coatings. Water contact angles reached approximately 112° and 146° for FS-P and FS-C, respectively, and post-processing by flame had a minor influence on water contact angles. Conversely, the smoothening of LIC-C surfaces lowered the measured roll-off angles, thus improving the water mobility behaviour of post-treated coatings. No roll-off angle was recorded for P-based coatings.

Table 7. Results of the wetting experiments for lubricated icephobic coatings (LICs) and flame-sprayed (FS) additive coatings.

Sample	Water Contact Angle [°]	Water Roll-Off Angle [°]
LIC-C	112.1 ± 1.0	73.2 ± 3.9
LIC-C*	112.3 ± 1.9	48.6 ± 5.2
LIC-P	99.9 ± 1.7	>90
LIC-P*	101.2 ± 1.5	>90
FS-C	146.3 ± 3.0	31.4 ± 1.4
FS-P	112.6 ± 1.7	>90

The surface free energy was investigated for LIC-C* and LIC-P* post-heated coatings. SFE values of 22.5 ± 1.9 mN/m and 29.8 ± 0.03 mN/m were measured for LIC-C* and LIC-P* coatings, respectively. SFEs of coatings were intermediate to the corresponding SFEs of feedstock materials (Table 5), with lower values for C-based coatings than P-based coatings. Particularly, SFE of LIC-C* tended towards the SFE value of C additive material, while SFE of LIC-P* was more similar to LDPE matrix material. These results could indicate that the amount of C additive was higher on the surface of post-heated coatings than the P additive. Moreover, the SFE of LIC-P* could tend to LDPE due to possible partial removal of the paraffinic wax from the coating surfaces after post-heating, considering the poorer thermal–oxidative resistance of P compared to C additive, as previously demonstrated by OIT results.

3.3. Icephobic Behaviour of Coatings

Icephobicity of surfaces is commonly assumed to be the property of repelling ice, delaying ice formation, and/or reducing ice adhesion strength [75]. Moreover, the lower the recorded ice adhesion strength, the higher the icephobicity. In this work, the ice adhesion strength was measured to assess the icephobic behaviour of coatings. For this specific ice adhesion test and these specific icing conditions [14,76], ice adhesion values of 50 kPa and 100 kPa indicate the low and the medium-low ice adhesion limit, respectively. Figure 6 presents the ice adhesion strength of LICs and plain feedstock material coatings with corresponding areal roughness values.

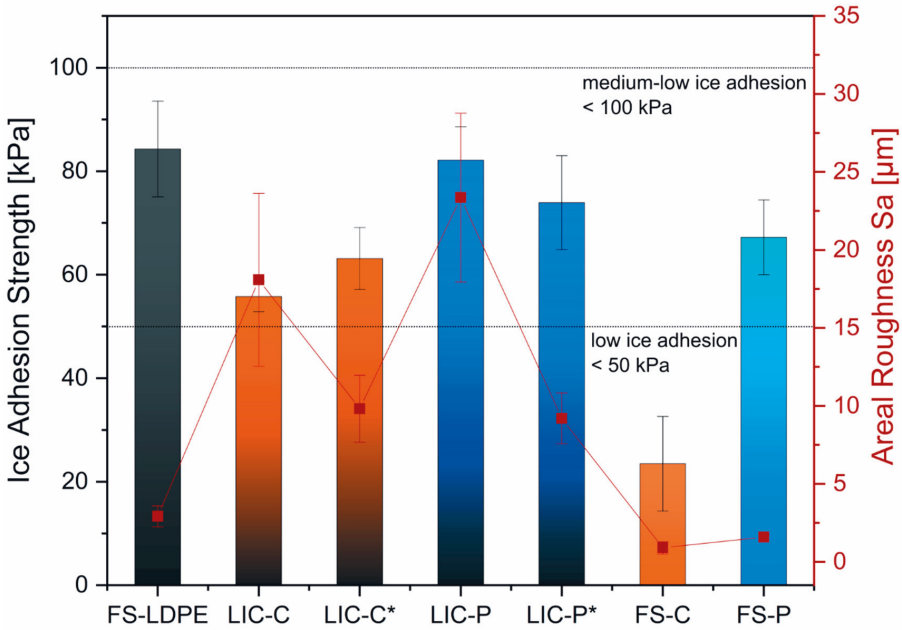

Figure 6. Icephobic behaviour of lubricated icephobic coatings (LICs) and flame-sprayed (FS) feedstock material coatings, measured at −10 °C with mixed glaze ice. Ice adhesion strength is reported on the left axis and corresponding areal roughness Sa on the right axis.

Feedstock material coatings demonstrated medium-low ice adhesion behaviour. Plain LDPE coatings, namely FS-LDPE, showed ice adhesion strength of 84 ± 9 kPa. Plain additive coatings, namely FS-C and FS-P, resulted in ice adhesion values of 23 ± 9 kPa and 67 ± 7 kPa, respectively. Although they showed comparable coating roughness, the ice adhesion values of feedstock material coatings significantly varied, increasing from C to P until LDPE plain coatings. SFE values of corresponding bulk materials similarly rose, passing from C to P until LDPE (Table 5). These results might support the findings of some studies, which evidenced a correlation between low SFE and reduced ice adhesion for smooth polymer coatings [41,68,69]. However, further investigations are needed to establish correlations between ice adhesion strength and SFE values for these materials.

LICs exhibited ice adhesion values between the corresponding plain feedstock material coatings, with C-based coatings slightly more icephobic than P-based coatings. Particularly for C-based coatings, LIC-C and LIC-C* showed medium-low ice adhesion behaviour with a 20% theoretical additive percentage in the coating structure. However, C-based coatings have demonstrated even lower ice adhesion values when a higher additive percentage (30%) has been present in the coating structure [35]. Therefore, the lower additive content could have determined the increased ice adhesion of C-based coatings in this study. Moreover, employed process parameters influence the icephobicity of flame-sprayed polymer coatings [35,67], and this factor needs to be considered when discussing the icephobic behaviour of C-based coatings in this study. For further details on the effect of process parameters on the coating icephobicity, the authors refer to their previous studies [35,67].

Considering the effect of the post-heating treatment by flame, the ice adhesion strength rose approximately 13% for LIC-C* compared to LIC-C. Conversely, the ice adhesion decreased about 10% for LIC-P* compared to LIC-P. However, these results varied within the standard deviation, and the effect of post-heating on the ice adhesion strength was not significant for these materials. This was also confirmed by a *t*-test.

Other factors have been considered to influence the ice adhesion strength, such as surface chemistry, surface roughness, Young's modulus, shear modulus, and hardness [74,77–79], as well as the icing conditions and testing methods [80,81]. Considering surface roughness, various studies have shown that ice adhesion strength rises with surface roughness when surfaces with similar chemistry are considered [82,83]. In this study, post-heating decreased the surface roughness for both coatings with similar surface chemistry, as shown in Figure 6. However, the decrease in roughness seemed to have no significant influence on ice adhesion strength. Specifically, the adhesion values varied within the standard deviation of the test, and a relationship could not be established.

Considering surface wettability, previous studies have demonstrated relationships between apparent water contact angle and ice adhesion strength [74,84]. In contrast, others have claimed no clear correlations between these properties [72,85]. The results showed that C-based coatings were more hydrophobic than P-based coatings, and water droplet mobility was evidenced only for C-based coatings. The latter demonstrated slightly improved icephobicity, thus indicating a possible correlation between wetting properties and icephobic performance [15,74,84]. Additionally, C-based coatings showed lower surface free energy values than P-based coatings, which could justify their enhanced icephobic character [41,68,69]. However, other factors could affect the ice adhesion of these surfaces [35,67,81]. Therefore, further investigations are needed to establish possible correlations between wetting properties, SFE, and ice adhesion strength for these coatings.

3.4. Coating Performance under Cyclic Icing/Deicing

In order to test icing performance and durability, researchers have carried out tests based on consecutive icing/deicing actions [12–16,30]. Icing of surfaces is performed using different methods. For example, in one method, water is poured in a mould placed on the surface and then frozen in a freezer at specific temperatures [13,73]. In another method, ice is accreted from supercooled microdroplets hitting the coating surface in the icing wind tunnel under specific icing conditions [16,48,86], representing the icing method employed in this study. Deicing can be pursued through heating [87,88], deformation of the substrate [89], or, more aggressively, applying mechanical loads to the ice itself [14,15,90]. Here, deicing was performed by applying a centrifugal force to the iced samples. Shear ice adhesion strength was recorded at each cycle, and its variations qualitatively indicated the durability of the icephobic properties of coatings. It is essential to underline that the icing durability depends on the methods employed for icing and deicing, the adhesive properties of ice type, and other variables [11]. Moreover, no universal standard has been established yet to test icing durability (icing/deicing procedures, number of icing/deicing cycles, water grade, freezing procedure, ice type, and other test conditions are not defined) [11]. Therefore, discussions on coatings' icing performance and durability need to be cautiously addressed when comparing results from different studies.

Figure 7 presents the shear ice adhesion strength measured at each cycle for LICs. C-based coatings demonstrated slightly lower ice adhesion values and smaller standard deviations than P-based coatings. After four icing/deicing cycles, all coatings retained their icephobicity within the medium-low limit. Particularly for C-based coatings, the four repeated icing/deicing cycles indicated no increasing nor decreasing trends in ice adhesion strength, and the values remained within the standard deviation. This result indicated enhanced icing durability for these coatings compared to our previous studies, where ice adhesion significantly increased over four cycles for C-based coatings [36,37]. This increase over the cycles was evidenced for rougher surfaces containing a higher amount of additive in their coating structure. In the current study, the reduced amount of C additive improved the durability of icephobic properties, maintaining the ice adhesion values within the standard deviation over the cycles.

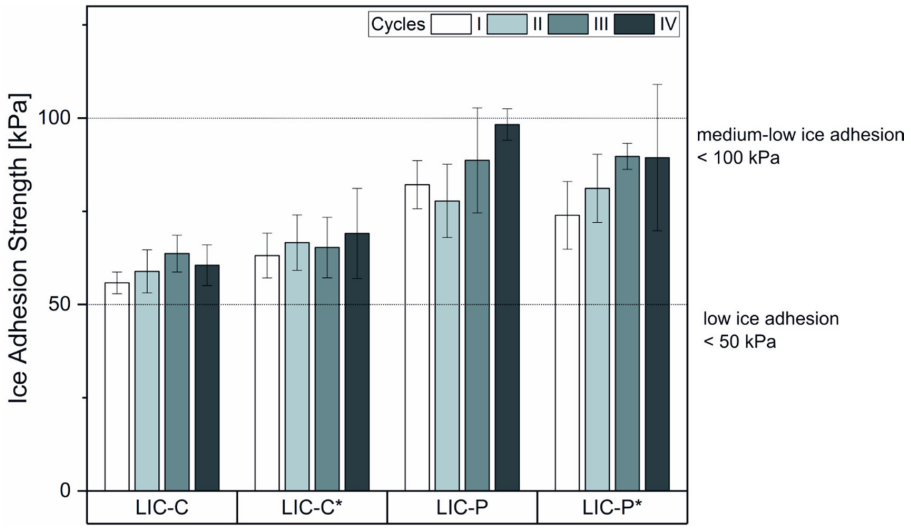

Figure 7. Ice adhesion results for lubricated icephobic coatings (LICs) under four icing/deicing cycles. Ice adhesion strength values at the first cycle were previously reported in Figure 6. C and P refer to fully hydrogenated cottonseed oil and paraffinic wax additives, respectively. The asterisk indicates the post-heating treatment by flame.

Ice adhesion strength values might vary over the cycles due to changes in surface morphologies and surface chemistry produced during icing/deicing cycles. Figure 8 shows the surface morphologies of all coatings before and after four icing/deicing cycles. The micrographs showed that scratches were visible on C-based coating surfaces, while no evident wear was produced on the polymeric surfaces of P-based coatings. Scratches were probably caused by cyclic shedding of mixed glaze ice via centrifugal forces during icing/deicing. Moreover, it cannot be excluded that a certain degree of surface damage could be produced during sample manipulation. Surface resistance to deicing improved for C-based coatings compared to our previous study, where the whole surfaces were scratched, and the icephobic behaviour significantly decreased over the cycles [36,37]. However, detected scratches did not strongly affect the icephobic behaviour in this study, which was stable over the cycles. Moreover, LIC-C and LIC-P samples showed minor surface cracks after the cycles. In our previous study, cracks were evidenced for some coatings, and these defects influenced the icephobic behaviour of coatings [37]. Here, the number of cracks was so small that they seemed to not affect the surface behaviour of coatings, which retained their icephobicity over the cycles. For additional discussion on the causes of cracks on LICs after cyclic icing/deicing tests, the authors refer to their previous study [37].

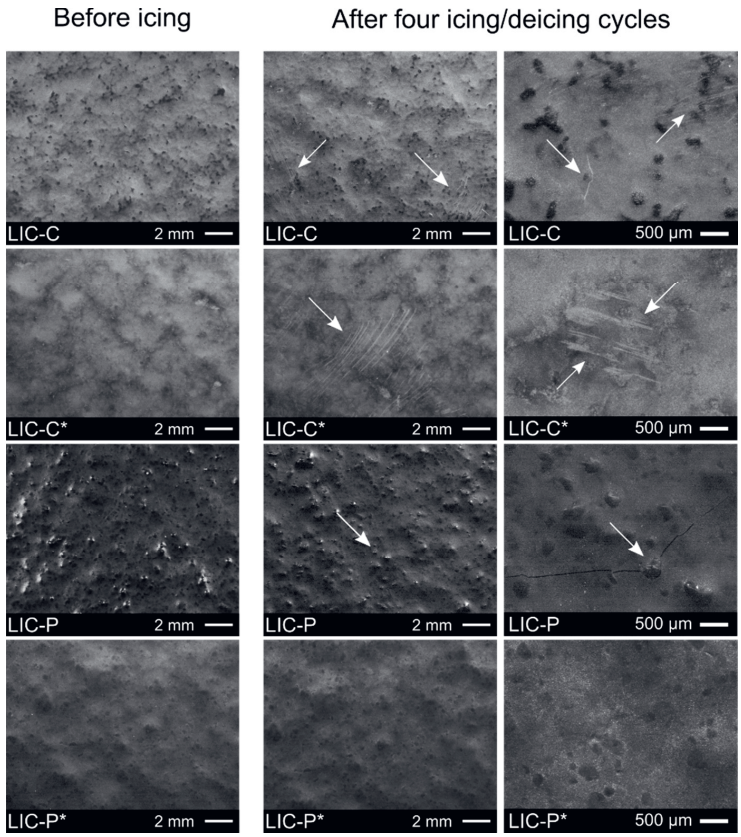

Figure 8. Surface morphologies of lubricated icephobic coatings (LICs) before and after four icing/deicing cycles at different magnification. C and P refer to fully hydrogenated cottonseed oil and paraffinic wax additives, respectively. The asterisk indicates the post-heating treatment by flame. White arrows indicate the presence of surface defects produced during the cyclic tests.

Figure 9 compares the variations in surface properties of LICs before and after four icing/deicing cycles. Figure 9a reports Sa and Sz parameters, and Figure 9b reports the apparent water contact angles. From the results on roughness, Sz values of LIC-C samples increased after the cycles. This rise could be justified by the mechanical damages produced on these surfaces, which increased surface roughness [18,37]. However, Sa and Sz mainly varied within the standard deviations for all other coatings. This result indicated that no significant changes in surface roughness were produced for the coatings during the cycles, thus justifying the stable icephobic behaviour of the coatings during the cyclic tests. From the results on wetting properties, only slight decrease in static water contact angle could be revealed for the coatings. This decrease could be related to surface damages produced during the cycles [15]. However, all surfaces retained their hydrophobicity after the cycles, and, in most cases, the variations fell within the standard deviation, similarly to roughness results. In contrast to static contact angle results, water mobility behaviour was affected after the cycles. No roll-off angles were revealed for LIC-C and LIC-C* coatings after the cycles, which initially showed values of approximately 73° and 49°, respectively. This result was due to water droplets pinned into the surface defects formed during the cyclic tests. From the results on surface chemistry, no chemical changes were revealed for the coatings after four icing/deicing cycles, as demonstrated by the FTIR spectra presented in Supplementary Figure S4.

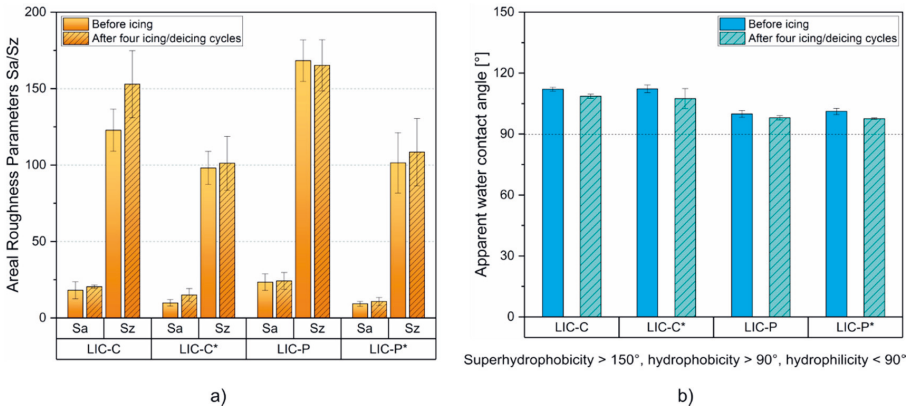

Figure 9. Comparison of surface properties before and after four icing/deicing cycles for LICs: (**a**) areal roughness parameters (Sa and Sz), and (**b**) apparent water contact angles.

In summary, LICs demonstrated good durability under repeated icing/deicing cycles, retaining their icephobicity below the medium-low ice adhesion limit of 100 kPa. Moreover, employed characterisation techniques revealed no significant changes in surface roughness, water contact angle, and surface chemistry. However, minor surface defects were evidenced for C-based coatings after the cyclic tests, which influenced the water mobility behaviour of surfaces.

The following sections of the manuscript will focus on the durability of LIC-C* and LIC-P* coatings, which showed no mechanical failure (cracks) after the icing/deicing tests. Coating durability in corrosive media and under UV irradiation exposure will be discussed.

3.5. Coating Performance in Acidic, Saline and Basic Environments

Icephobic coatings can contact several environments during their use in outdoor conditions. To simulate these environments and test their durability, three different corrosive media were selected, namely acidic, saline, and basic solutions, and immersion tests were performed. Figure 10 presents the variations of wetting properties after immersion.

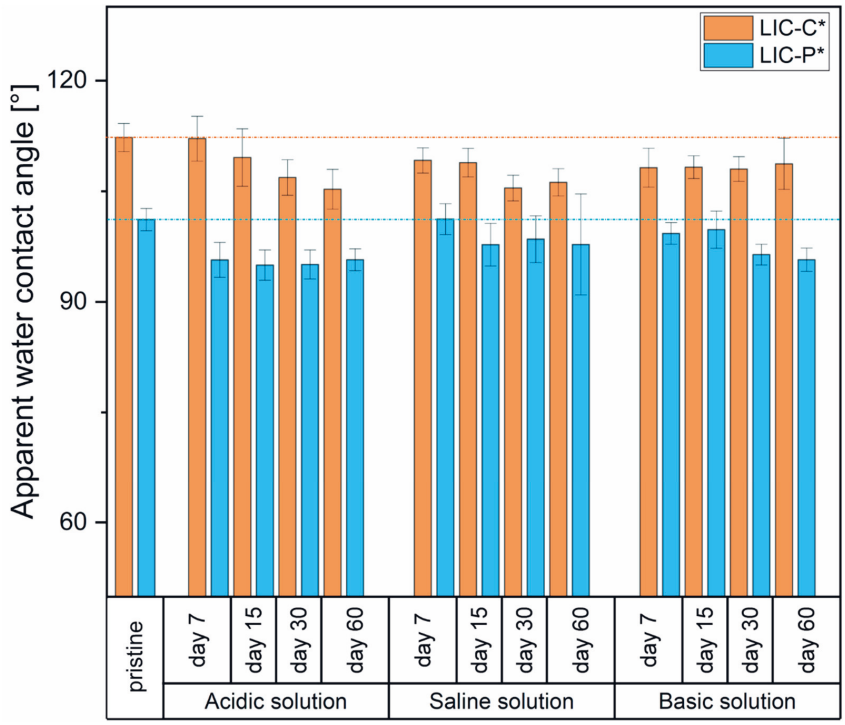

Figure 10. The apparent water contact angle of LIC-C* and LIC-P* samples before and after ageing in acidic, saline, and basic solutions.

Both LIC-C* and LIC-P* samples demonstrated a slight decrease in apparent water contact angles after immersion compared to the pristine ones. This decrease could indicate that variations in surface chemistry and/or surface morphology probably occurred during ageing. In acidic conditions, LIC-C* showed a slight decrease in hydrophobicity until 60 days of immersion. However, water contact angle of LIC-P* samples remained substantially steady from 7 to 60 days after an initial decrease. Conversely, in basic solution, LIC-C* samples demonstrated a better retainment of their wetting properties than LIC-P*, which showed a gradual decrease in hydrophobicity. In saline conditions, both surfaces slightly degraded, and their wetting properties seemed to stabilize after 30 days of immersion. The different behaviour probably derived from the chemical composition of the additives, their chemical resistance in various solutions, surface morphologies of the coatings, and different hydrolytic degradation of each polymer [12]. Besides the slight degradation of wetting properties, all surfaces maintained their hydrophobic character after the immersion tests.

Considering the water mobility properties of LIC-C* surfaces, water roll-off angles increased after 7 days of immersion in all tested conditions. In particular, the roll-off angle rose from $47° \pm 5°$ to $57° \pm 6°$ and $62° \pm 3°$ in saline and basic conditions, respectively. Droplet pinning behaviour was suddenly revealed for the surfaces immersed in acidic solutions after 7 days. No water mobility was detected for LIC-C* surfaces after 15 days of immersion in any of the different conditions. It is well known that water mobility properties are strongly affected by local surface hindrances and heterogeneities, both chemical and morphological, which are encountered by water droplets sliding onto surfaces [91–93]. Therefore, the increased roll-off angle value and consequent pinning into the surfaces could indicate the formation of defects on the coating surfaces. Furthermore, repeated cycles

of immersion, drying, wetting analyses, and samples manipulation could have produced surface damage, and these actions could influence the wetting results.

After 60 days of immersion in different conditions, surface chemical analyses were carried out for LIC-C* and LIC-P*. Figure 11 shows the FTIR spectra of the as-received coatings and after 60 days of immersion in different solutions.

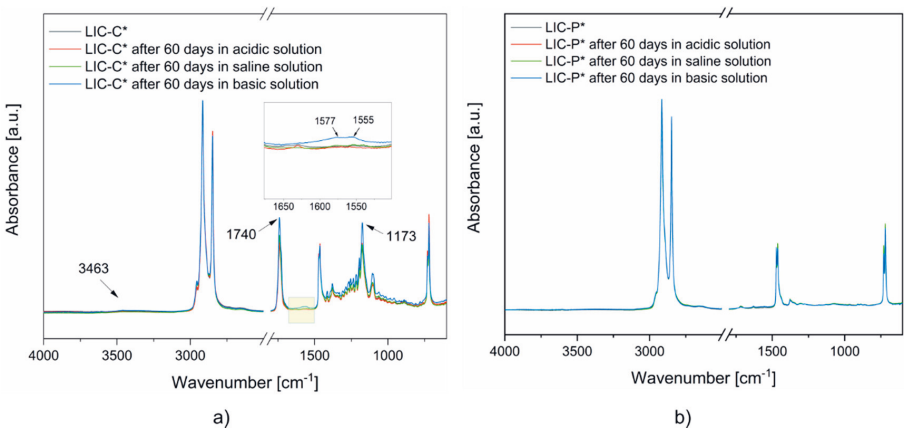

Figure 11. FTIR spectra of LICs surfaces after ageing in different environments: (**a**) LIC-C*, and (**b**) LIC-P*. The regions of the spectra are highlighted by yellow boxes when chemical modifications are detected.

The FTIR spectra of LIC-C* coatings (Figure 11a) demonstrated no relevant changes for the samples immersed in acidic and saline environments. However, minor variations in the chemical structure were evidenced for basic solutions experiments. Weak signals were present in the region between 1650 and 1500 cm^{-1}. These probably corresponded to the formation of alkene bonds [94,95]. Moreover, increased intensities were noticed for the signals related to the ester bonds at 1740 and 1173 cm^{-1}. Furthermore, a weak signal was present in the regions between 3700 and 3200 cm^{-1}. These probably corresponded to the formation of hydroxyl bonds [94,95]. Hydroxyl bonds and increased intensity of ester bonds could justify the presence of hydrolysis products of esters, which mainly consist of carboxylic acids [95].

Considering the FTIR spectra of LIC-P* coatings (Figure 11b), no significant chemical changes were revealed for the surfaces in contact with different solutions. Moreover, no absorbed water in the coating structures was detected from thermogravimetric experiments, as shown in Supplementary Figure S5. These results indicated that both surfaces demonstrated significant chemical resistance to water absorption in the tested environments. However, the TG curves related to LIC-C* samples showed some deviations from the pristine samples, which were not visible for the LIC-P* coatings. These deviations could indicate some degradation process for the polymers of LIC-C*, most probably for the additive C. However, further analyses are needed to support these results.

After 60 days of immersion, coating morphologies were further analysed at the microscale level to investigate their durability in the corrosive media. Figure 12 presents the surface morphologies of the coatings after 60 days in acidic, saline, and basic solutions.

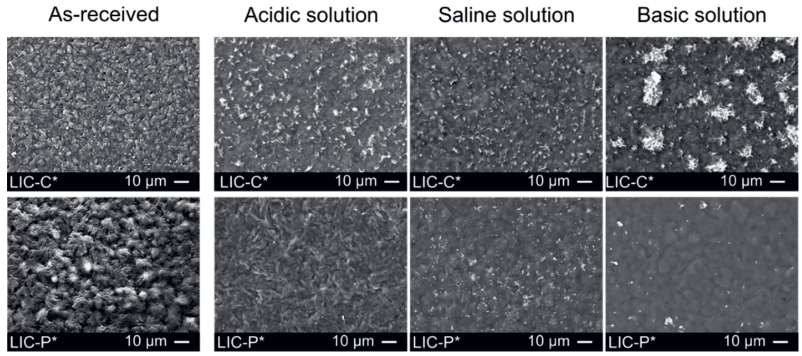

Figure 12. Micrographs of the surface morphologies of LICs after 60 days of immersion in acidic, saline, and basic solutions.

As can be seen from the micrographs, the surface morphologies of as-received coatings varied after immersion. Small protuberances characterised as-received surfaces. No similar features were revealed on the coating surfaces after immersion, and structural changes occurred for the surfaces in all solutions. Considering LIC-C* samples, surface morphologies revealed the presence of flake-like structures after immersion. These flakes probably derived from the hydrolytic degradation of C additive, which could be the most sensitive component to hydrolysis. Moreover, larger regions of flake-like structures were noticed for the samples immersed in basic solutions. Immersion tests produced surface morphologies and surface chemistry variations, which generally influence icephobicity [77,96,97]. In our study, the removal of wax from the coating surfaces might cause a decrease in icephobic properties for the aged coatings, as demonstrated for coatings with the lower amount of C additive in our previous studies [35,37]. However, further investigations are necessary to establish these correlations.

Considering LIC-P* samples, structural changes on the surfaces were noticed after immersion. Finer structures were produced after immersion in acidic solutions compared to saline and basic environments. These results could justify the reduced hydrophobicity of the coatings after immersion compared to the as-received ones. However, the wetting behaviour cannot be fully explained using the surface micrographs because these provide no information on the surface chemistry of coatings after immersion.

Degradation of polymers due to water, namely hydrolysis, can lead to cross-linking and porous structures on the exposed polymer surface, thus causing surface structural changes [12]. This phenomenon is enhanced if water-sensitive functional groups are present in the polymers [12,95]. Ester groups, typical of C additive, are more prone to hydrolysis than primary and secondary alkyl groups, which characterize both LDPE and P additive [12,94]. This aspect could justify the small hydroxyl signal evidenced for all aged LIC-C*, which was not revealed for LIC-P* surfaces. However, hydrolysis of esters occurs slowly, even in boiling water. If bases and acids are added to water, the reaction is slightly accelerated but still slow if conducted at room temperature [95]. Therefore, minor chemical degradation was justified considering the current experimental conditions.

Furthermore, other factors could influence hydrolysis, such as hydrophobicity, surface porosity, and mechanical stresses [12]. Concerning hydrophobicity, the tendency for hydrolysis decreases as the hydrophobicity of the surface increases [12]. Therefore, the higher water-repellent properties of LIC-C* samples could have contributed retarding the hydrolysis reaction, despite the presence of ester bonds.

In summary, samples demonstrated good durability in different corrosive environments. LIC-P* demonstrated better resistance in the selected conditions due to its chemical composition, being less affected by hydrolysis reactions. After immersion, structural

changes to surfaces were revealed for both samples, which could decrease coating hydrophobicity.

3.6. Coating Performance under Exposure to Ultraviolet (UV) Irradiation

Icephobic coatings are primarily used in outdoor conditions, where they are exposed to UV irradiation. Exposure to UV light causes polymers to degrade, thus decreasing their performance and shortening their lifetime [98]. Therefore, understanding the mechanism of polymer degradation under UV exposure is necessary to further improve the durability of icephobic coatings under these conditions.

Figure 13 compares the FTIR spectra of LIC-P* coatings at different times of UV exposure. According to the results, aged coating surfaces showed an increased signal in the region between 1850 and 1650 cm^{-1}. The signal gradually rose with the exposure time until 1000 h. This signal was attributed to the formation of carbonyl groups in the polymer structure. In particular, the broad peak with the highest intensity signal at 1713 cm^{-1} indicated the presence of several oxidation products, probably including carboxylic acid, carboxylic ester, and carboxylic anhydride [99]. These results are in accord with previous studies on the photodegradation of polyolefins [99–101].

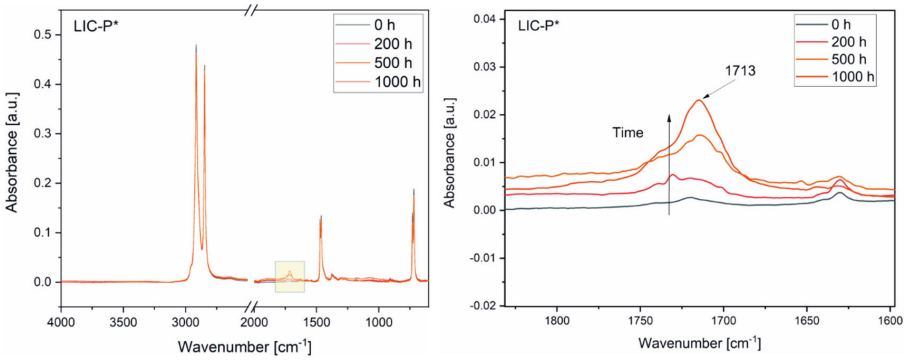

Figure 13. FTIR spectra of the coatings at different exposure times to UV irradiation: (**a**) LIC-P* spectra, (**b**) LIC-P* spectra enlarged in the region of interest. The spectra region is highlighted by a yellow box when chemical modifications are detected.

Figure 14 compares the FTIR spectra of LIC-C* coatings at different exposure times. From these spectra, the signal intensity gradually rose with exposure time. After 200 h, a slight increase was revealed in the peak intensity at 1737 cm^{-1} and 1173 cm^{-1}. This rise qualitatively corresponded to the increased stretching signal of the carbonyl bond (C=O) and the carbon–oxygen bond (C-O) of the ester group. After 500 h, the signal intensities of these bonds further increased. In particular, the peak at 1737 cm^{-1} shifted and divided into two peaks at 1740 and 1727 cm^{-1}. The first signal at 1740 cm^{-1} corresponded to increased carbonyl bonds, and the second signal at 1727 cm^{-1} represented the formation of carboxylic acids, as reported in a previous study [102]. These results indicated an increased amount of oxidation products due to photo-oxidation, as reported for natural and synthetic waxes in other studies [102–104]. Therefore, the photo-oxidation of LIC-C* coatings was mainly related to the degradation of C additive under UV exposure. After 1000 h, no new peaks were detected in the spectra compared to 500 h of exposure.

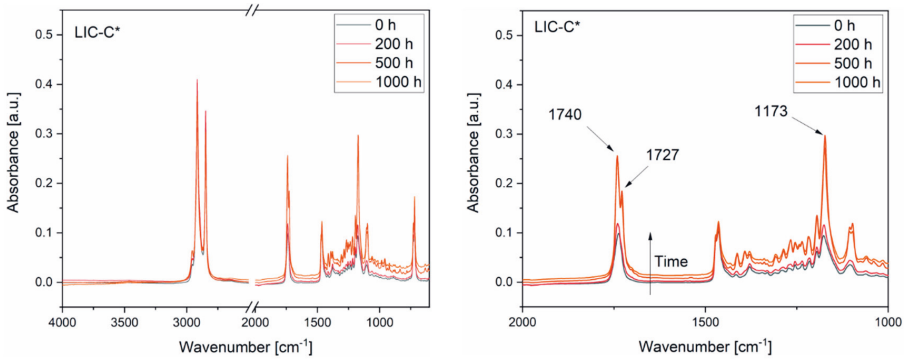

Figure 14. FTIR spectra of the coatings at different exposure times to UV irradiation: (**a**) LIC-C* spectra, (**b**) LIC-C* spectra enlarged in the region of interest.

Figure 15 compares the carbonyl indices of LIC-C* and LIC-P* coatings at different exposure times to UV irradiation. The carbonyl index represents one of the most used metrics in polymer chemical degradation studies, considering that carbonyl compounds generally constitute the main product of degradation reactions [52]. The carbonyl index of LIC-C* coatings rose with increasing exposure time. Similarly, the carbonyl index of LIC-P* gradually increased with exposure time, in accordance with FTIR analyses.

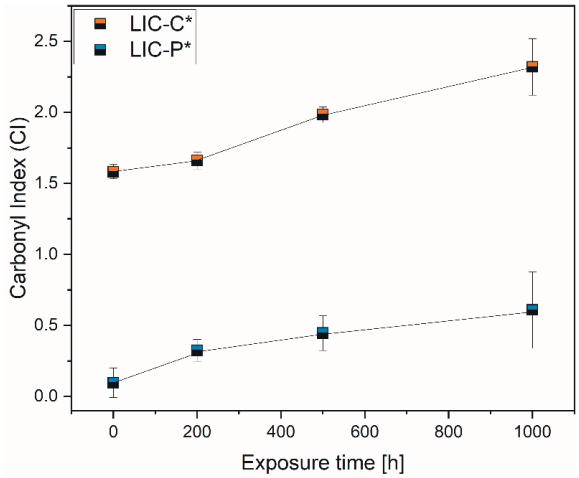

Figure 15. Comparison of carbonyl indices (CI) of LIC-C* and LIC-P* coatings calculated using the specified area under band (SAUB) methodology.

Moreover, photo-oxidation under UV irradiation produced colour changes in the coating surfaces. Visual inspection of the coatings detected no significant colour changes of the surfaces, probably because of the black colour of the main component, LDPE. Therefore, a chromameter was used for the analysis. Figure 16 compared the variation of colour, ΔE^*_{ab}, for the coatings at different times of exposure.

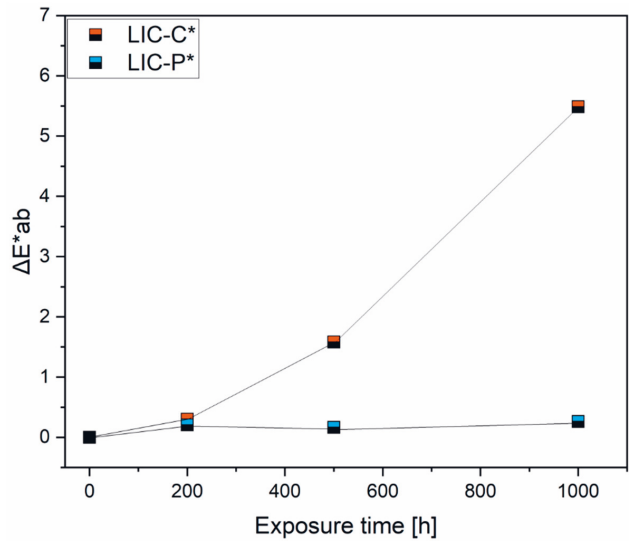

Figure 16. Comparison of colour changes for LIC-C* and LIC-P*coatings at different exposure times to UV irradiation.

Colour change value increased with exposure time for LIC-C* coatings compared to LIC-P* coatings, which demonstrated stable behaviour over the time of exposure. Similar results on colour change have been reported for aged polyethylene samples in other research [51]. Colour observations of aged samples correlated with the results of FTIR spectra. The more prominent colour variation was observed when a significant change was revealed in the FTIR spectra for LIC-C* and vice versa for LIC-P*. These results are in accordance with a previous study on weathered polymers and waxes [103].

Considering the sensitivity of chemical bonds to UV irradiation, carbonyl groups of ester bonds generally act as UV light-absorbing groups [94]. Moreover, ester bonds are more vulnerable to UV than primary and secondary alkyl groups typical of polyolefins [12]. As demonstrated by FTIR analyses, ester bonds characterised the chemical structure of fully hydrogenated cottonseed oil. Therefore, the presence of ester bonds could justify the higher tendency to photodegradation of C coatings compared to P coatings, although the presence of absorbent groups is not necessarily decisive for degradation [94,104]. Moreover, non-degraded, pure polyolefins should be photo-chemically resistant, considering that they theoretically do not absorb any UV light. However, UV light can be absorbed if any unsaturation or carbonyl groups are formed during manufacturing or additives are added [94]. Previous results presented in Figures 3 and 5b demonstrated the presence of weak signals at 1731 and 1630 cm^{-1}. These corresponded to possible carbonyl products in the feedstock material and alkenes after coating production in LIC-P*, respectively. Their presence could have accelerated the photodegradation reaction in LIC-P* coatings. However, LIC-P* samples better withstood degradation under UV irradiation than LIC-C* samples, and the latter showed better performances in icing conditions.

Surface photo-oxidation was evidenced for both coatings after UV irradiation, with C-based coatings more damaged than P-based coatings. Our previous study demonstrated that ice adhesion increased with surface oxidation for plain LDPE coatings [67]. The higher the oxidation degree of the surfaces, the greater the measured ice adhesion strength of coatings [67]. Moreover, a recent study demonstrated that UV ageing of polyurethane-based coatings negatively influenced their icephobic behaviour [10]. However, further investigations are needed to determine the influence of UV ageing on the icephobicity of these coatings.

4. Conclusions

Lubricated icephobic coatings (LICs) were fabricated using the flame spray method with hybrid feedstock injection. This one-step method allowed fast and scalable fabrication of LICs, which were composite polymer coatings made here of the main component, namely low-density polyethylene (LDPE), and two minor lubricating additives, namely fully hydrogenated cottonseed oil (C) and paraffinic wax (P). The choice of lubricants was based on chemical compatibility with the matrix material and surface free energy property. The latter property was considered to enhance the icephobic behaviour of flame-sprayed LDPE coatings. The first part of the study focused on characterising the properties and the icephobic behaviour of coatings. Employed process parameters and materials influenced the surface roughness and wetting behaviour of coatings. Post-heating reduced surface roughness, resulting in improved water droplet mobility. Little thermal degradation was revealed for P-based coatings after post-heating. Concerning icephobic behaviour, all LICs exhibited medium-low ice adhesion values at the first icing/deicing cycle. In general, slightly lower ice adhesion values were revealed for C-based coatings than for P-based coatings, according to the icephobicity of corresponding additive coatings. Moreover, all LICs showed stable icephobic behaviour over the cycles, maintaining their adhesion values below the low-medium limit of 100 kPa. Minor scratches were detected for C-based coatings, which lost their water mobility behaviour after the cycles. However, these surface damages caused no substantial changes in surface roughness, wettability, and icephobicity. Moreover, no chemical changes were produced for all surfaces after the cycles.

The second part of the study investigated the durability of selected coatings in acidic, saline, and basic environments and under exposure to ultraviolet (UV) irradiation. P-based coatings demonstrated excellent chemical resistance in selected corrosive environments, while C-based coatings experienced minor hydrolytic degradation, especially in basic solutions. However, wetting performance slightly decreased for all coatings due to surface structural changes revealed after immersion, but coating hydrophobicity was retained. Moreover, P-based coatings better withstood UV irradiation exposure compared to C-based coatings. The chemical structure of the C additive was characterised by ester bonds, which were more sensitive to UV irradiation. Carbonyl index and colour change measurements confirmed this result.

In summary, C-based coatings demonstrated better icephobicity and stability under repeated icing/deicing cycles compared to P-based coatings. However, the latter showed enhanced resistance to wear against ice shedding, immersion in selected corrosive media, and exposure to UV irradiation. Degradation under the studied environmental stresses mainly resulted in oxidation of the polymeric surfaces. These findings have significant implications in developing icephobic coatings for outdoor applications, thus highlighting the importance of material combinations in the coating structure. Future studies will investigate the effect of ageing in various environments on the icephobicity of coatings to further develop LICs.

Supplementary Materials: The following are available online at https://www.mdpi.com/article/10.3390/polym14020303/s1, Figure S1: Thermal properties of the matrix (LDPE) and lubricating additives (C and P) powders: (a) melting range with peak melting temperatures from the DSC analysis, and (b) onset decomposition temperatures (Tonset) from the TG curves and maximum degradation temperatures from the DTG curves; Figure S2: Curves obtained from the DSC experiments indicating the melting transitions related to (a) coatings LIC-C and LIC-C* and corresponding feedstock powders (LDPE and C), and (b) coatings LIC-P and LIC-P* and corresponding feedstock powders (LDPE and P); Figure S3: Curves obtained from the TG experiments indicating the mass percentage decrease as a function of temperature for (a) coatings LIC-C and LIC-C* and related feedstock powders (LDPE and C) and (c) coatings LIC-P and LIC-P* and related feedstock powders (LDPE and P). The degradation peaks evaluated from the first derivative of TG curves (DTG) are related to (b) LIC-C, LIC-C*, LDPE and C, and (d) LIC-P, LIC-P*, LDPE and P; Figure S4: The FTIR spectra of the coating surface before icing/deicing cycles (solid line) and after four icing/deicing cycles (dash line). The graphs correspond to samples LIC-C (a), LIC-C* (b), LIC-P (c), and LIC-P* (d); Figure S5:

Comparison of the thermogravimetric curves of the coatings before and after 60 days of immersion in acidic solution (a,b), in saline solutions (c,d), and basic solutions (e,f).

Author Contributions: Conceptualisation, V.D., H.K. and P.V.; methodology, V.D.; formal analysis, V.D.; investigation, V.D.; data curation, V.D.; writing—original draft preparation, V.D.; writing—review and editing, V.D., H.K., E.S. and P.V.; visualisation, V.D.; supervision, H.K., E.S. and P.V.; project administration, H.K. and P.V.; funding acquisition, H.K. and P.V. All authors have read and agreed to the published version of the manuscript.

Funding: This research was funded by the LubISS (Lubricant Impregnated Slippery Surfaces) project, which has received funding from the European Union's Horizon 2020 research and innovation programme under the Marie Sklodowska-Curie Grant Agreement No. 722497. In addition, V.D. acknowledges the Faculty of Engineering and Natural Sciences of Tampere University for the financial support. This work made use of Tampere Microscopy Center facilities at Tampere University (33014 Tampere, Finland).

Institutional Review Board Statement: Not applicable.

Informed Consent Statement: Not applicable.

Data Availability Statement: Data from this study are available upon request from the corresponding author.

Acknowledgments: Authors thank Anssi Metsähonkala and Jarkko Lehti, of Tampere University, for technical support in the flame spray process. Moreover, the authors acknowledge Matteo Orlandini, of Millidyne Oy, for the particle size analysis. Kaisa Kiuru and Niklas Kandelin, of Tampere University, are thanked for assisting with the icing testing.

Conflicts of Interest: The authors declare no conflict of interest.

References

1. Shen, Y.; Wu, X.; Tao, J.; Zhu, C.; Lai, Y.; Chen, Z. Icephobic Materials: Fundamentals, Performance Evaluation, and Applications. *Prog. Mater. Sci.* **2019**, *103*, 509–557. [CrossRef]
2. Shu, L.; Li, H.; Hu, Q.; Jiang, X.; Qiu, G.; McClure, G.; Yang, H. Study of Ice Accretion Feature and Power Characteristics of Wind Turbines at Natural Icing Environment. *Cold Reg. Sci. Technol.* **2018**, *147*, 45–54. [CrossRef]
3. Fillion, R.M.; Riahi, A.R.; Edrisy, A. A Review of Icing Prevention in Photovoltaic Devices by Surface Engineering. *Renew. Sustain. Energy Rev.* **2014**, *32*, 797–809. [CrossRef]
4. Shi, K.; Duan, X. A Review of Ice Protection Techniques for Structures in the Arctic and Offshore Harsh Environments. *J. Offshore Mech. Arct. Eng.* **2021**, *143*, 1–27. [CrossRef]
5. Luo, S.; Yang, X. Performance Evaluation of High-Elastic Asphalt Mixture Containing Deicing Agent Mafilon. *Constr. Build. Mater.* **2015**, *94*, 494–501. [CrossRef]
6. Habibi, H.; Edwards, G.; Sannassy, C.; Kappatos, V.; Lage, Y.; Stein, J.; Selcuk, C.; Gan, T.H. Modelling and Empirical Development of an Anti/de-Icing Approach for Wind Turbine Blades through Superposition of Different Types of Vibration. *Cold Reg. Sci. Technol.* **2016**, *128*, 1–12. [CrossRef]
7. Petrenko, V.F.; Sullivan, C.R.; Kozlyuk, V.; Petrenko, F.V.; Veerasamy, V. Pulse Electro-Thermal de-Icer (PETD). *Cold Reg. Sci. Technol.* **2011**, *65*, 70–78. [CrossRef]
8. Dalili, N.; Edrisy, A.; Carriveau, R. A Review of Surface Engineering Issues Critical to Wind Turbine Performance. *Renew. Sustain. Energy Rev.* **2009**, *13*, 428–438. [CrossRef]
9. Hochart, C.; Fortin, G.; Perron, J.; Ilinca, A. Wind Turbine Performance under Icing Conditions. *Wind Energy* **2008**, *11*, 319–333. [CrossRef]
10. Rehfeld, N.; Speckmann, B.; Schreiner, C.; Stenzel, V. Assessment of Icephobic Coatings—How Can We Monitor Performance Durability? *Coatings* **2021**, *11*, 614. [CrossRef]
11. Kulinich, S.A.; Masson, D.; Du, X.; Emelyanenko, A.M. Testing the Durability of Anti-Icing Coatings. In *Ice Adhesion: Mechanism, Measurement and Mitigation*; Mittal, K.L., Choi, C.-H., Eds.; Wiley: Hoboken, NJ, USA, 2020; pp. 495–520.
12. Hakimian, A.; Nazifi, S.; Ghasemi, H. Durability Assessment of Icephobic Coatings. In *Ice Adhesion: Mechanism, Measurement and Mitigation*; Mittal, K.L., Choi, C.-H., Eds.; Wiley: Hoboken, NJ, USA, 2020; pp. 521–545.
13. Golovin, K.; Kobaku, S.P.R.; Lee, D.H.; DiLoreto, E.T.; Mabry, J.M.; Tuteja, A. Designing Durable Icephobic Surfaces. *Sci. Adv.* **2016**, *2*, e1501496. [CrossRef]
14. Niemelä-Anttonen, H.; Koivuluoto, H.; Tuominen, M.; Teisala, H.; Juuti, P.; Haapanen, J.; Harra, J.; Stenroos, C.; Lahti, J.; Kuusipalo, J.; et al. Icephobicity of Slippery Liquid Infused Porous Surfaces under Multiple Freeze-Thaw and Ice Accretion-Detachment Cycles. *Adv. Mater. Interfaces* **2018**, *5*, 1800828. [CrossRef]

15. Asadollahi, S.; Farzaneh, M.; Stafford, L. On the Icephobic Behavior of Organosilicon-Based Surface Structures Developed Through Atmospheric Pressure Plasma Deposition in Nitrogen Plasma. *Coatings* **2019**, *9*, 679. [CrossRef]
16. Vercillo, V.; Cardoso, J.T.; Huerta-Murillo, D.; Tonnicchia, S.; Laroche, A.; Mayén Guillén, J.A.; Ocaña, J.L.; Lasagni, A.F.; Bonaccurso, E. Durability of Superhydrophobic Laser-Treated Metal Surfaces under Icing Conditions. *Mater. Lett. X* **2019**, *3*, 100021. [CrossRef]
17. Sharifi, N.; Dolatabadi, A.; Pugh, M.; Moreau, C. Anti-Icing Performance and Durability of Suspension Plasma Sprayed TiO2 Coatings. *Cold Reg. Sci. Technol.* **2019**, *159*, 1–12. [CrossRef]
18. Memon, H.; De Focatiis, D.S.A.; Choi, K.S.; Hou, X. Durability Enhancement of Low Ice Adhesion Polymeric Coatings. *Prog. Org. Coat.* **2021**, *151*, 106033. [CrossRef]
19. Veronesi, F.; Boveri, G.; Raimondo, M. Amphiphobic Nanostructured Coatings for Industrial Applications. *Materials* **2019**, *12*, 787. [CrossRef]
20. Wu, D.; Ma, L.; Zhang, F.; Qian, H.; Minhas, B.; Yang, Y.; Han, X.; Zhang, D. Durable Deicing Lubricant-Infused Surface with Photothermally Switchable Hydrophobic/Slippery Property. *Mater. Des.* **2020**, *185*, 108236. [CrossRef]
21. Balordi, M.; Santucci de Magistris, G.; Chemelli, C. A Novel Simple Anti-Ice Aluminum Coating: Synthesis and In-Lab Comparison with a Superhydrophobic Hierarchical Surface. *Coatings* **2020**, *10*, 111. [CrossRef]
22. Veronesi, F.; Guarini, G.; Corozzi, A.; Raimondo, M. Evaluation of the Durability of Slippery, Liquid-Infused Porous Surfaces in Different Aggressive Environments: Influence of the Chemical-Physical Properties of Lubricants. *Coatings* **2021**, *11*, 1170. [CrossRef]
23. Brown, S.; Lengaigne, J.; Sharifi, N.; Pugh, M.; Moreau, C.; Dolatabadi, A.; Martinu, L.; Klemberg-Sapieha, J.E. Durability of Superhydrophobic Duplex Coating Systems for Aerospace Applications. *Surf. Coat. Technol.* **2020**, *401*, 126249. [CrossRef]
24. Orlandini, M. Slippery Lubricant Infused Porous Surface Generated by Self-Assembly Mechanism of a Composite Organogel for Low Ice Adhesion. Ph.D. Thesis, Tampere University, Tampere, Finland, 2021.
25. Huang, X.; Tepylo, N.; Pommier-Budinger, V.; Budinger, M.; Bonaccurso, E.; Villedieu, P.; Bennani, L. A Survey of Icephobic Coatings and Their Potential Use in a Hybrid Coating/Active Ice Protection System for Aerospace Applications. *Prog. Aerosp. Sci.* **2019**, *105*, 74–97. [CrossRef]
26. Alamri, S.; Vercillo, V.; Aguilar-Morales, A.I.; Schell, F.; Wetterwald, M.; Lasagni, A.F.; Bonaccurso, E.; Kunze, T. Self-Limited Ice Formation and Efficient De-Icing on Superhydrophobic Micro-Structured Airfoils through Direct Laser Interference Patterning. *Adv. Mater. Interfaces* **2020**, *7*, 2001231. [CrossRef]
27. Bottone, D.; Donadei, V.; Niemelä, H.; Koivuluoto, H.; Seeger, S. Coral-like Silicone Nanofilament Coatings with Extremely Low Ice Adhesion. *Sci. Rep.* **2021**, *11*, 1–12. [CrossRef]
28. Wong, W.S.Y.; Hegner, K.I.; Donadei, V.; Hauer, L.; Naga, A.; Vollmer, D. Capillary Balancing: Designing Frost-Resistant Lubricant-Infused Surfaces. *Nano Lett.* **2020**, *20*, 8508–8515. [CrossRef] [PubMed]
29. Boinovich, L.; Emelyanenko, A.M.; Pashinin, A.S. Analysis of Long-Term Durability of Superhydrophobic Properties under Continuous Contact with Water. *ACS Appl. Mater. Interfaces* **2010**, *2*, 1754–1758. [CrossRef]
30. Boinovich, L.B.; Emelyanenko, A.M.; Ivanov, V.K.; Pashinin, A.S. Durable Icephobic Coating for Stainless Steel. *ACS Appl. Mater. Interfaces* **2013**, *5*, 2549–2554. [CrossRef] [PubMed]
31. Laroche, A.; Bottone, D.; Seeger, S.; Bonaccurso, E. Silicone Nanofilaments Grown on Aircraft Alloys for Low Ice Adhesion. *Surf. Coatings Technol.* **2021**, *410*, 126971. [CrossRef]
32. Farhadi, S.; Farzaneh, M.; Kulinich, S.A. Anti-Icing Performance of Superhydrophobic Surfaces. *Appl. Surf. Sci.* **2011**, *257*, 6264–6269. [CrossRef]
33. Koivuluoto, H.; Stenroos, C.; Kylmälahti, M.; Apostol, M.; Kiilakoski, J.; Vuoristo, P. Anti-Icing Behavior of Thermally Sprayed Polymer Coatings. *J. Therm. Spray Technol.* **2017**, *26*, 150–160. [CrossRef]
34. Janjua, Z.A.; Turnbull, B.; Choy, K.L.; Pandis, C.; Liu, J.; Hou, X.; Choi, K.S. Performance and Durability Tests of Smart Icephobic Coatings to Reduce Ice Adhesion. *Appl. Surf. Sci.* **2017**, *407*, 555–564. [CrossRef]
35. Donadei, V.; Koivuluoto, H.; Sarlin, E.; Vuoristo, P. Lubricated Icephobic Coatings Prepared by Flame Spraying with Hybrid Feedstock Injection. *Surf. Coatings Technol.* **2020**, *403*, 126396. [CrossRef]
36. Donadei, V.; Koivuluoto, H.; Sarlin, E.; Vuoristo, P. Durability of Lubricated Icephobic Coatings under Multiple Icing/Deicing Cycles. In Proceedings of the International Thermal Spray Conference (ITSC), Online, 24–28 May 2021; Azarmi, F., Chen, X., Cizek, J., Cojocaru, C., Jodoin, B., Koivuluoto, H., Lau, Y., Fernandez, R., Ozdemir, O., Salami Jazi, H., Eds.; ASM International: Anaheim, CA, USA; Quebec City, QC, Canada, 2021; pp. 473–481.
37. Donadei, V.; Koivuluoto, H.; Sarlin, E.; Niemelä-Anttonen, H.; Varis, T.; Vuoristo, P. The Effect of Mechanical and Thermal Stresses on the Performance of Lubricated Icephobic Coatings during Cyclic Icing/Deicing Tests. *Prog. Org. Coat.* **2021**, 106614. [CrossRef]
38. Tracton, A. *Coatings Technology Handbook*, 3rd ed.; Tracton, A.A., Ed.; CRC Press: Boca Raton, FL, USA, 2005; ISBN 9780429119644.
39. Mittal, K.; Lee, K. *Polymer Surfaces and Interfaces: Characterization, Modification and Application*; Mittal, K., Lee, K., Eds.; Springer Science & Business Media: Berlin/Heidelberg, Germany, 1997.
40. Novák, I.; Krupa, I.; Luyt, A.S. Modification of a Fischer-Tropsch Wax by Grafting with Maleic Anhydride. *J. Appl. Polym. Sci.* **2004**, *93*, 662–668. [CrossRef]
41. Ozbay, S.; Erbil, H.Y. On the Relationship between Surface Free Energy and Ice Adhesion of Flat Anti-Icing Surfaces. In *Ice Adhesion: Mechanism, Measurement and Mitigation*; Mittal, K.L., Choi, C.-H., Eds.; Wiley: Hoboken, NJ, USA, 2020; pp. 187–215.

42. ISO 4288:1996 Geometrical Product Specifications (GPS). Surface Texture: Profile Method for the Assessment of Surface Texture. Available online: https://www.iso.org/standard/2096.html (accessed on 20 October 2021).
43. ISO 25178-3:2012-Geometrical Product Specifications (GPS)—Surface Texture: Areal—Part 3: Specification Operators . Available online: https://www.iso.org/standard/42895.html (accessed on 2 June 2020).
44. Owens, D.K.; Wendt, R.C. Estimation of the Surface Free Energy of Polymers. *J. Appl. Polym. Sci.* **1969**, *13*, 1741–1747. [CrossRef]
45. Rabel, W. Einige Aspekte Der Benetzungstheorie Und Ihre Anwendung Auf Die Untersuchung Und Veränderung Der Oberflächeneigenschaften von Polymeren. *Farbe Lack* **1971**, *77*, 997–1005.
46. Fowkes, F.M. Attractive Forces at Interfaces. *Ind. Eng. Chem.* **1964**, *56*, 40–52. [CrossRef]
47. Kaelble, D.H. Dispersion-Polar Surface Tension Properties of Organic Solids. *J. Adhes.* **1970**, *2*, 66–81. [CrossRef]
48. Koivuluoto, H.; Stenroos, C.; Ruohomaa, R.; Bolelli, G.; Lusvarghi, L.; Vuoristo, P. Research on Icing Behavior and Ice Adhesion Testing of Icephobic Surfaces. In Proceedings of the International Workshop on Atmospheric Icing of Structures (IWAIS), Uppsala, Sweden, 28 June–3 July 2015; pp. 183–188.
49. Niemelä-Anttonen, H.; Kiilakoski, J.; Vuoristo, P.; Koivuluoto, H. Icephobic Performance of Different Surface Designs and Materials. In Proceedings of the International Workshop on Atmospheric Icing of Structures (IWAIS), Reykjavík, Iceland, 23–27 June 2019; pp. 1–5.
50. Likens, G.E.; Bormann, F.H. Acid Rain: A Serious Regional Environmental Problem. *Science* **1974**, *184*, 1176–1179. [CrossRef]
51. Fedor, G.R.; Brennan, P.J. Comparison between Natural Weathering and Fluorescent UV Exposures: UVA-340 Lamp Test Results. *ASTM Spec. Tech. Publ.* **1996**, *1294*, 91–105. [CrossRef]
52. Mylläri, V.; Ruoko, T.P.; Järvelä, P. The Effects of UV Irradiation to Polyetheretherketone Fibres - Characterization by Different Techniques. *Polym. Degrad. Stab.* **2014**, *109*, 278–284. [CrossRef]
53. Almond, J.; Sugumaar, P.; Wenzel, M.N.; Hill, G.; Wallis, C. Determination of the Carbonyl Index of Polyethylene and Polypropylene Using Specified Area under Band Methodology with ATR-FTIR Spectroscopy. *E-Polymers* **2020**, *20*, 369–381. [CrossRef]
54. Identifying Color Differences Using L*a*b* or L*C*H* Coordinates. Available online: https://sensing.konicaminolta.us/us/blog/identifying-color-differences-using-l-a-b-or-l-c-h-coordinates/ (accessed on 21 June 2021).
55. ISO/CIE 11664-4:2019-Colorimetry-Part 4: CIE 1976 L*a*b* Colour Space. Available online: https://www.iso.org/standard/74166.html (accessed on 25 October 2021).
56. Vasile, C.; Pascu, M. *Practical Guide to Polyethylene*; iSmithers Rapra Publishing: Shawbury, UK, 2005; ISBN 9783527680856.
57. Baglioni, M.; Poggi, G.; Ciolli, G.; Fratini, E.; Giorgi, R.; Baglioni, P. A Triton X-100-Based Microemulsion for the Removal of Hydrophobic Materials Fromworks of Art: SAXS Characterization and Application. *Materials* **2018**, *11*, 1144. [CrossRef]
58. Kühn, H. Detection and Identification of Waxes, Including Punic Wax, by Infra-Red Spectrography. *Stud. Conserv.* **1960**, *5*, 71–81. [CrossRef]
59. Masae, M.; Pitsuwan, P.; Sikong, L.; Kongsong, P.; Kooptarnond, K.; Phoempoon, P. Thermo- Physical Characterization of Paraffin and Beeswax on Cotton Fabric. *Thammasat Int. J. Sci. Technol.* **2014**, *19*, 69–77.
60. Varshney, D.; Ahmadi, M.; Guinel, M.J.-F.; Weiner, B.R.; Morell, G. Single-Step Route to Diamond-Nanotube Composite. *Nanoscale Res. Lett.* **2012**, *7*, 535. [CrossRef] [PubMed]
61. Albertsson, A.C.; Barenstedt, C.; Karlsson, S. Susceptibility of Enhanced Environmentally Degradable Polyethylene to Thermal and Photo-Oxidation. *Polym. Degrad. Stab.* **1992**, *37*, 163–171. [CrossRef]
62. Svečnjak, L.; Baranović, G.; Vinceković, M.; Prđun, S.; Bubalo, D.; Gajger, I.T. An Approach for Routine Analytical Detection of Beeswax Adulteration Using Ftir-Atr Spectroscopy. *J. Apic. Sci.* **2015**, *59*, 37–49. [CrossRef]
63. Ali, M.H.M.; Rakib, F.; Nischwitz, V.; Ullah, E.; Mall, R.; Shraim, A.M.; Ahmad, M.I.; Ghouri, Z.K.; McNaughton, D.; Küppers, S.; et al. Application of FTIR and LA-ICPMS Spectroscopies as a Possible Approach for Biochemical Analyses of Different Rat Brain Regions. *Appl. Sci.* **2018**, *8*, 2436. [CrossRef]
64. Uznanski, P.; Zakrzewska, J.; Favier, F.; Kazmierski, S.; Bryszewska, E. Synthesis and Characterization of Silver Nanoparticles from (Bis)Alkylamine Silver Carboxylate Precursors. *J. Nanoparticle Res.* **2017**, *19*, 121. [CrossRef]
65. Aykas, D.P.; Rodriguez-Saona, L.E. Assessing Potato Chip Oil Quality Using a Portable Infrared Spectrometer Combined with Pattern Recognition Analysis. *Anal. Methods* **2016**, *8*, 731–741. [CrossRef]
66. Imran, M.; Nadeem, M. Triacylglycerol Composition, Physico-Chemical Characteristics and Oxidative Stability of Interesterified Canola Oil and Fully Hydrogenated Cottonseed Oil Blends. *Lipids Health Dis.* **2015**, *14*, 138. [CrossRef]
67. Donadei, V.; Koivuluoto, H.; Sarlin, E.; Vuoristo, P. Icephobic Behaviour and Thermal Stability of Flame-Sprayed Polyethylene Coating: The Effect of Process Parameters. *J. Therm. Spray Technol.* **2020**, *29*, 241–254. [CrossRef]
68. Cui, W.; Jiang, Y.; Mielonen, K.; Pakkanen, T.A. The Verification of Icephobic Performance on Biomimetic Superhydrophobic Surfaces and the Effect of Wettability and Surface Energy. *Appl. Surf. Sci.* **2019**, *466*, 503–514. [CrossRef]
69. Chen, D.; Gelenter, M.D.; Hong, M.; Cohen, R.E.; Mckinley, G.H. Icephobic Surfaces Induced by Interfacial Nonfrozen Water. *ACS Appl. Mater. Interfaces* **2017**, *9*, 4202–4214. [CrossRef] [PubMed]
70. Bockhorn, H.; Hornung, A.; Hornung, U.; Schawaller, D. Kinetic Study on the Thermal Degradation of Polypropylene and Polyethylene. *J. Anal. Appl. Pyrolysis* **1999**, *48*, 93–109. [CrossRef]
71. Rønneberg, S.; Xiao, S.; He, J.; Zhang, Z. Nanoscale Correlations of Ice Adhesion Strength and Water Contact Angle. *Coatings* **2020**, *10*, 379. [CrossRef]

72. He, Z.; Vågenes, E.T.; Delabahan, C.; He, J.; Zhang, Z. Room Temperature Characteristics of Polymer-Based Low Ice Adhesion Surfaces. *Sci. Rep.* **2017**, *7*, 42181. [CrossRef]
73. Meuler, A.J.; Smith, J.D.; Varanasi, K.K.; Mabry, J.M.; McKinley, G.H.; Cohen, R.E. Relationships between Water Wettability and Ice Adhesion. *ACS Appl. Mater. Interfaces* **2010**, *2*, 3100–3110. [CrossRef]
74. Dotan, A.; Dodiuk, H.; Laforte, C.; Kenig, S. The Relationship between Water Wetting and Ice Adhesion. *J. Adhes. Sci. Technol.* **2009**, *23*, 1907–1915. [CrossRef]
75. Kreder, M.J.; Alvarenga, J.; Kim, P.; Aizenberg, J. Design of Anti-Icing Surfaces: Smooth, Textured or Slippery? *Nat. Rev. Mater.* **2016**, *1*, 15003. [CrossRef]
76. Koivuluoto, H.; Hartikainen, E.; Niemelä-Anttonen, H. Thermally Sprayed Coatings: Novel Surface Engineering Strategy towards Icephobic Solutions. *Materials* **2020**, *13*, 1434. [CrossRef]
77. Memon, H.; Liu, J.; De Focatiis, D.S.A.; Choi, K.S.; Hou, X. Intrinsic Dependence of Ice Adhesion Strength on Surface Roughness. *Surf. Coat. Technol.* **2020**, *385*, 125382. [CrossRef]
78. He, Z.; Xiao, S.; Gao, H.; He, J.; Zhang, Z. Multiscale Crack Initiator Promoted Super-Low Ice Adhesion Surfaces. *Soft Matter* **2017**, *13*, 6562–6568. [CrossRef] [PubMed]
79. Irajizad, P.; Al-Bayati, A.; Eslami, B.; Shafquat, T.; Nazari, M.; Jafari, P.; Kashyap, V.; Masoudi, A.; Araya, D.; Ghasemi, H. Stress-Localized Durable Icephobic Surfaces. *Mater. Horizons* **2019**, *6*, 758–766. [CrossRef]
80. Memon, H.; Mirshahidi, K.; Zarasvand, K.A.; Golovin, K.; De Focatiis, D.S.A.; Choi, K.S.; Hou, X. Comparative Study on the Influence of Surface Characteristics on De-Icing Evaluation. *J. Mater. Sci.* **2021**, *56*, 17337–17352. [CrossRef]
81. Makkonen, L. Ice Adhesion - Theory, Measurements and Countermeasures. *J. Adhes. Sci. Technol.* **2012**, *26*, 413–445. [CrossRef]
82. Zou, M.; Beckford, S.; Wei, R.; Ellis, C.; Hatton, G.; Miller, M.A. Effects of Surface Roughness and Energy on Ice Adhesion Strength. *Appl. Surf. Sci.* **2011**, *257*, 3786–3792. [CrossRef]
83. Fillion, R.M.; Riahi, A.R.; Edrisy, A. Design Factors for Reducing Ice Adhesion. *J. Adhes. Sci. Technol.* **2017**, *31*, 2271–2284. [CrossRef]
84. Varanasi, K.K.; Deng, T.; Smith, J.D.; Hsu, M.; Bhate, N. Frost Formation and Ice Adhesion on Superhydrophobic Surfaces. *Appl. Phys. Lett.* **2010**, *97*, 234102. [CrossRef]
85. Drelich, J.W. Contact Angles: From Past Mistakes to New Developments through Liquid-Solid Adhesion Measurements. *Adv. Colloid Interface Sci.* **2019**, *267*, 1–14. [CrossRef] [PubMed]
86. Tetteh, E.; Loth, E. Reducing Static and Impact Ice Adhesion with a Self-Lubricating Icephobic Coating (SLIC). *Coatings* **2020**, *10*, 262. [CrossRef]
87. Kim, P.; Wong, T.S.; Alvarenga, J.; Kreder, M.J.; Adorno-Martinez, W.E.; Aizenberg, J. Liquid-Infused Nanostructured Surfaces with Extreme Anti-Ice and Anti-Frost Performance. *ACS Nano* **2012**, *6*, 6569–6577. [CrossRef]
88. Boinovich, L.B.; Modin, E.B.; Sayfutdinova, A.R.; Emelyanenko, K.A.; Vasiliev, A.L.; Emelyanenko, A.M. Combination of Functional Nanoengineering and Nanosecond Laser Texturing for Design of Superhydrophobic Aluminum Alloy with Exceptional Mechanical and Chemical Properties. *ACS Nano* **2017**, *11*, 10113–10123. [CrossRef]
89. Yang, S.; Xia, Q.; Zhu, L.; Xue, J.; Wang, Q.; Chen, Q.M. Research on the Icephobic Properties of Fluoropolymer-Based Materials. *Appl. Surf. Sci.* **2011**, *257*, 4956–4962. [CrossRef]
90. Laforte, C.; Laforte, J.-L.J. Tensile, Torsional and Bending Strain at the Adhesive Rupture of an Iced Substrate. In Proceedings of the International Conference on Offshore Mechanics and Arctic Engineering-OMAE, ASME, Honolulu, HI, USA, 31 May–5 June 2009; Volume 5, pp. 79–86.
91. Yoshimitsu, Z.; Nakajima, A.; Watanabe, T.; Hashimoto, K. Effects of Surface Structure on the Hydrophobicity and Sliding Behavior of Water Droplets. *Langmuir* **2002**, *18*, 5818–5822. [CrossRef]
92. Ha, J.W.; Park, I.J.; Lee, S.B. Hydrophobicity and Sliding Behavior of Liquid Droplets on the Fluorinated Latex Films. *Macromolecules* **2005**, *38*, 736–744. [CrossRef]
93. Della Volpe, C.; Siboni, S.; Morra, M. Comments on Some Recent Papers on Interfacial Tension and Contact Angles. *Langmuir* **2002**, *18*, 1441–1444. [CrossRef]
94. Ehrenstein, G.W.; Pongratz, S. Resistance and Stability of Polymers. In *Resistance and Stability of Polymers*; Carl Hanser Verlag GmbH & Co. KG: München, Germany, 2013; ISBN 9781569904565.
95. Brown, W.H.; Poon, T. *Introduction to Organic Chemistry*, 5th ed.; John Wiley & Sons: Hoboken, NJ, USA, 2014; ISBN 9781118083383.
96. Kulinich, S.A.; Farzaneh, M. On Ice-Releasing Properties of Rough Hydrophobic Coatings. *Cold Reg. Sci. Technol.* **2011**, *65*, 60–64. [CrossRef]
97. Psarski, M.; Pawlak, D.; Grobelny, J.; Celichowski, G. Relationships between Surface Chemistry, Nanotopography, Wettability and Ice Adhesion in Epoxy and SU-8 Modified with Fluoroalkylsilanes from the Vapor Phase. *Appl. Surf. Sci.* **2019**, *479*, 489–498. [CrossRef]
98. White, J.R.; Turnbull, A. Weathering of Polymers: Mechanisms of Degradation and Stabilization, Testing Strategies and Modelling. *J. Mater. Sci.* **1994**, *29*, 584–613. [CrossRef]
99. Iring, M.; Tüdős, F. Thermal Oxidation of Polyethylene and Polypropylene: Effects of Chemical Structure and Reaction Conditions on the Oxidation Process. *Prog. Polym. Sci.* **1990**, *15*, 217–262. [CrossRef]
100. Sugimoto, M.; Shimada, A.; Kudoh, H.; Tamura, K.; Seguchi, T. Product Analysis for Polyethylene Degradation by Radiation and Thermal Ageing. *Radiat. Phys. Chem.* **2013**, *82*, 69–73. [CrossRef]

101. Kaczmarek, H.; Ołdak, D.; Podgórski, A. Photochemical Properties of Polyethylene Modified by Low-Molecular Organic Compounds. *Polym. J.* **2003**, *35*, 634–639. [CrossRef]
102. Kim, K.J.; Eom, T.J. Chemical Characteristics of Degraded Beeswax in the Waxed Volume of the Annals of King Sejong in the Joseon Dynasty. *J. Cult. Herit.* **2015**, *16*, 918–921. [CrossRef]
103. Lesar, B.; Pavlič, M.; Petrič, M.; Škapin, A.S.; Humar, M. Wax Treatment of Wood Slows Photodegradation. *Polym. Degrad. Stab.* **2011**, *96*, 1271–1278. [CrossRef]
104. Achhammer, G.B. Chemical Structure and Stability Relationships in Polymers. *Mod. Plast.* **1959**, *37*, 131–227.

PUBLICATION IV

The effect of mechanical and thermal stresses on the performance of lubricated icephobic coatings during cyclic icing/deicing tests

V. Donadei, H. Koivuluoto, E. Sarlin, H. Niemelä-Anttonen, T. Varis, and P. Vuoristo

Progress in Organic Coatings, 163 (2022), 106614
DOI: 10.1016/10.1016/j.porgcoat.2021.106614

Progress in Organic Coatings 163 (2022) 106614

Contents lists available at ScienceDirect

Progress in Organic Coatings

journal homepage: www.elsevier.com/locate/porgcoat

The effect of mechanical and thermal stresses on the performance of lubricated icephobic coatings during cyclic icing/deicing tests

Valentina Donadei *, Heli Koivuluoto, Essi Sarlin, Henna Niemelä-Anttonen, Tommi Varis, Petri Vuoristo

Tampere University, Faculty of Engineering and Natural Sciences, P.O. Box 589, FI-33014, Finland

ARTICLE INFO

Keywords:
Flame spraying
Ice adhesion
Icephobic coating
Polymer coating
Lubricated coating
Icing durability

ABSTRACT

Evaluating the performance of icephobic coatings interests various industries, such as aviation, maritime, energy, and transportation. Recent developments on icephobic coatings have consistently highlighted the need for durable icephobic surfaces in cold conditions. This study investigates the icing performance and durability of lubricated polymer coatings under cyclic icing/deicing tests. Coatings were made of polyethylene and a solid lubricant and manufactured using flame spray technology. Icing was performed by accreting ice in an icing wind tunnel. Deicing was conducted by removing ice with a centrifugal ice adhesion tester. Surface properties, such as surface morphology, roughness, wettability and chemical composition, were measured before and after the cyclic tests. The results showed stable icephobic behaviour for some coatings, while the performance of others decreased over the cycles. The cyclic tests caused mechanical damage to the surfaces, producing erosion, scratches and, for some coatings, surface cracks. These defects resulted in increased surface roughness and reduced hydrophobicity. However, no chemical changes were revealed for any of the surfaces. Moreover, the causes of cracks were attributed to the difference in thermal expansion behaviour of substrate and coating materials. This result highlights the importance of materials and process parameters selection in flame sprayed coatings designed for cold applications.

1. Introduction

Ice accretion and its accumulation on surfaces represent a significant problem for several industrial applications in cold regions. Ice can compromise the working operations of several applications and, in some cases, endanger human life [1]. For instance, aviation, maritime and ground transportation, renewable energy, and offshore platforms are affected by ice formation [2], leading to economic losses and catastrophic accidents. Due to the significant influence of icing in daily operations, the past decades have seen an increased interest in developing surface solutions to minimise icing problems [3–6]. Traditionally, active ice removal methods using various forms of energy (thermal, mechanical, or pneumatic) and chemicals have represented one strategy to ensure continuous and safe working operations [7]. However, active methods are time and energy-consuming, and their sustainability issues encourage developing alternative solutions. For this reason, passive methods, which passively repel ice or retard ice formation, have emerged as potential solutions for icing problems. Passive methods mainly consist of surface treatments or protective coatings, widely referred to as icephobic coatings [8,9]. Icephobic surfaces are expected to effectively reduce ice adhesion and spontaneously promote ice shedding from exposed surfaces.

Passive icephobic methods have been classified into three main surface designs, namely superhydrophobic surfaces (SHSs), slippery liquid-infused porous surfaces (SLIPSs) and smooth surfaces made of low surface free energy materials, commonly polymers [7]. Inspired by the surface microstructure of lotus leaves [10], SHSs have been fabricated using a large variety of technologies, combining several materials and surface modification treatments [11–14]. SHSs are characterised by a micro/nano hierarchical structure with high water repellency (water contact angle $>150°$ and water sliding angle $<10°$) [15]. Many researchers have hypothesised that their water repellency property would benefit surface icephobicity [16–18]. However, it was found that the long-lasting icephobic performance of superhydrophobic surfaces is limited. Several studies have shown a loss of icephobicity of SHSs, especially in environments with high humidity and sub-zero conditions

* Corresponding author at: Tampere University, Korkeakoulunkatu 6, P.O. Box 589, FI-33014 Tampere, Finland.
E-mail address: valentina.donadei@tuni.fi (V. Donadei).

https://doi.org/10.1016/j.porgcoat.2021.106614
Received 10 July 2021; Received in revised form 8 November 2021; Accepted 10 November 2021
Available online 19 November 2021

[19,20]. Moreover, mechanical damage of their hierarchical structure under consecutive icing/deicing cycles has been reported as another limitation of this surface design [13,21]. Another surface design widely tested for icephobic applications is represented by SLIPSs [7]. Inspired by the surface structure of Nepenthes pitcher plants [22], SLIPSs are characterised by a micro/nanostructure infused using various lubricating fluids based on fluorinated, silicone and hydrophilic liquids [7,23–25]. The presence of the lubricant layer ensures low surface roughness and slippery properties, which renders SLIPSs attractive for anti-icing applications. However, the instability of the lubricating layer in icing conditions represents a limitation for SLIPSs. Depletion of lubricant can lead to the degradation of icephobic properties and consequent environmental pollution [7,24,26,27]. Therefore, alternative surface designs with enhanced mechanical stability and icing durability are under consideration. An alternative surface design consists of smooth solid surfaces made of low surface free energy polymers [7]. Several polymers have been tested as potential anti-icing materials to produce smooth solid surfaces [28–33]. However, the mechanical weakness of polymeric materials may represent one challenge for this surface design [7]. Different strategies have been recently proposed to enhance the durability of polymer coatings, such as self-healing material solutions [34] or incorporation of various fillers [35]. Although smooth polymer surfaces can have less remarkable icephobic behaviour than SHSs and SLIPSs [36], their use in icephobic applications presents several advantages. In particular, polymeric coatings are cheaper and easier to prepare [36]. Moreover, they are expected to have enhanced durability over repeated icing/deicing cycles because of their more robust surface structure than the designs mentioned above [36]. Considering these advantages, the development of polymeric surfaces and assessment of their icing durability are strongly desirable. Furthermore, understanding the degradation mechanism of these surfaces in icing conditions is of fundamental importance to support future development aiming at improving their durability.

This study investigates the icing performance and durability of solid polymeric coatings under repeated icing/deicing cycles. Polymeric composite coatings were fabricated using a one-step coating method, termed flame spraying with hybrid feedstock injection in our previous work [37]. This versatile method was used to produce composite coatings consisting of two solid polymeric components: low-density polyethylene and fully hydrogenated cottonseed oil. The latter consists of a solid hydrophobic wax [38]. These coatings were named lubricated icephobic coatings (LICs) due to the lubricating additive in the coating structure [37]. The design was inspired by SLIPSs, aiming to enhance lubricant stability in icing environments [39]. Our previous work demonstrated the low ice adhesion behaviour of LICs in icing conditions. The behaviour indicates the potential of these coatings for low ice adhesion applications. Therefore, the present study aims at 1) Investigating the icing performance and durability of LICs under repeated icing/deicing cycles. 2) Understanding the effect of icing/deicing cycles on the coating surface properties, such as morphology, roughness, wettability and chemical composition, and establishing possible relationships. 3) Analysing the thermal and mechanical stresses involved in cyclic tests, which affect the coating durability, to better design coatings for cold applications.

2. Experimental procedure

2.1. Materials and coating fabrication

Commercially available low-density polyethylene powder (Plascoat LDPE, Plascoat Europe B.V., The Netherlands) and fully hydrogenated cottonseed oil powder (Lubritab® capsules, JRS PHARMA GmbH & Co. KG, Germany) were used as feedstock materials to produce composite coatings. LDPE represented the main component of the coatings, namely matrix material. Fully hydrogenated cottonseed oil constituted the minor component, namely lubricating additive. These coatings were named lubricated icephobic coatings (LICs) [37]. LICs were manufactured using flame spraying with hybrid feedstock injection, schematically represented in Fig. 1a. In this method, the matrix material was sprayed using an oxygen-acetylene flame spray gun (Castodyn DS 8000, Castolin Eutectic, Switzerland) with gas pressure for oxygen and acetylene of 4.2 bar and 0.7 bar, respectively. LDPE feedstock was fed using a powder feeder (Powder Feeder 1, Sulzer Metco 4MP, Oerlikon Metco, Switzerland) with compressed air as carrier gas. Simultaneously, the lubricating additive was sprayed externally from the gun using an injector. The injector was used to avoid direct interaction of the additive with flame and ensure its adequate feeding. The lubricant powder was fed with a second powder feeder (Powder Feeder 2, PT-10 Twin, Oerlikon Metco, Switzerland) with argon as carrier gas. Additional technical details are reported elsewhere [37]. Coatings were deposited on stainless steel substrates (EN 1.4301/2K (4N)), 30 mm × 60 mm × 1.5 mm in dimensions. Substrates were grit-blasted before spraying using aluminium oxide powder (grit size of Mesh 54). Fig. 1b summarises the sample designation together with employed process parameters.

For the coating production, process parameters, namely gun traverse speed and gun air pressure, were varied while gun spraying distance was kept constant at 250 mm. Gradual increase in gun traverse speed (from 500 to 900 mm/s) resulted in lower spraying time. However, the lower the spraying time, the lower the heat load transferred from the flame to the already deposited coating layer, thus resulting in rougher coating morphologies [33]. Similarly, the increased air pressure in the gun (from 0 to 4 bar) lowered the heat input from the flame to the powder during its flight, thus producing again rougher surfaces [37]. Additionally, post-heating of surfaces by flame was performed after coating deposition for a selected sample. Post-heating was carried out to obtain a smoother surface morphology [37].

2.2. Icephobicity and icing durability characterisation

The icephobic properties of lubricated coatings were studied using the icing test facilities at Tampere University [40]. An icing wind tunnel (IWiT) and a centrifugal ice adhesion tester (CAT) were used for the ice accretion process and the evaluation of ice adhesion strength, respectively. For these tests, the samples were placed in a climate-controlled room with monitored temperature and relative humidity (−10 °C ± 1 °C and 80% ± 5%). Once the samples reached the desired conditions, ice was accreted from supercooled water microdroplets on 30 mm × 30 mm coating areas in the IWiT. A mixed glaze type of ice was formed on the coating areas using laboratory-grade II+ water (Purelab Option-R 7/15, Elga, United Kingdom). After ice accretion, the iced samples rested in the cold room for approximately 16 h to ensure complete ice solidification. The ice was then detached from the sample surface using CAT, and ice adhesion was measured. Shear ice adhesion strength, τ_{ice} [kPa], is estimated according to Eq. 1, as the ratio of the centrifugal force F [N] at the moment of ice detachment, to the area of the iced surface A [m^2]:

$$\tau_{ice} = \frac{F}{A} = \frac{m_{ice} r \omega^2}{A} = \frac{m_{ice} r (\alpha t)^2}{A} \quad (1)$$

where m_{ice} [kg] is the known mass of the accreted ice on the specimen, r [m] is the radial spinning length at which the iced samples are spun. ω [rad/s] represents the rotational speed of the sample measured at the time t [s] of ice detachment, considering a constant angular acceleration α of 300 rpm/s. Once the ice adhesion was measured, the samples were stored at room temperature. Ice accretion and CAT testing were repeated four times to investigate icing performance and coating durability. During the cyclic icing/deicing tests, the samples experienced mechanical and thermal loads, from −10 °C to room temperature and vice versa. The ice adhesion strength was monitored at every cycle to record variations in icephobic behaviour. The ice adhesion strength was reported as the average and standard deviation of four parallel samples during each icing accretion event. A test reference surface (3M™ PTFE

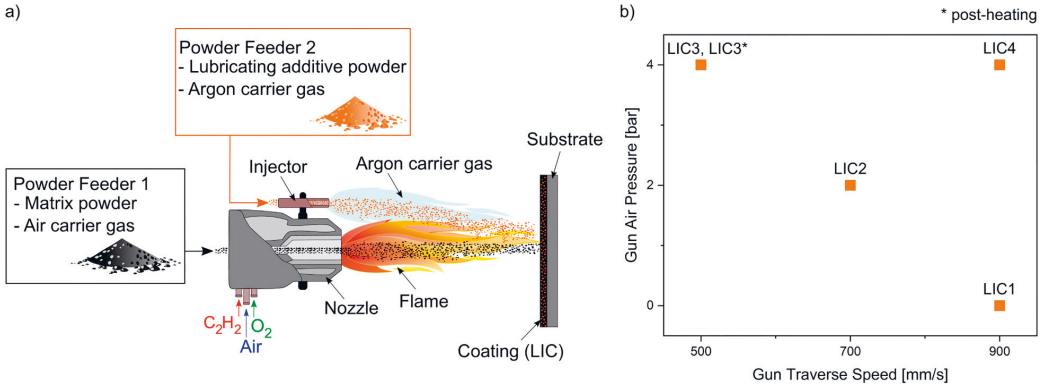

Fig. 1. Coating fabrication technique and employed process parameters. a) Schematisation of the flame spray process with hybrid feedstock injection to produce lubricated icephobic coatings (LICs), and b) summary of LIC samples studied in this work and corresponding process parameters.

Film Tape 5490, 3M, United States) was used to monitor the ice adhesion at each accretion event, considering possible variations in icing conditions [41,42].

2.3. Surface characterisation

Surface properties were investigated for as-sprayed coatings before and after the cyclic tests to analyse the effect of repeated icing/deicing. Variations in surface morphology were examined using a scanning electron microscope (SEM, Jeol, IT-500, Japan). The surface samples were cut using an automatic cut-off machine (Discotom-10, Struers ApS, Denmark). Before the analysis, the samples were dried in a desiccator and sputtered with a thin gold layer to enhance surface conductivity. An acceleration voltage of 15 keV was used to image the sample surfaces.

The surface topography was studied using an optical profilometer (contactless measuring instrument, Alicona Infinite Focus G5, Alicona Imaging GmbH, Austria). Areal roughness parameters, namely Sa, Sz and Sdr, were measured with 20× magnification objective on 2 mm × 2 mm areas at different surface locations, according to the standard ISO 25178-3 [43]. In particular, Sa represents the arithmetical mean height of the surface, Sz measures the maximum height of the surface, and Sdr signifies the developed interfacial area ratio, i.e. the percentage of additional surface area compared to an ideal plane with the size of the measurement region. Sdr value of 0% indicates a flat surface [44]. The areal roughness values were reported as the average and standard deviation of three measurements at different surface locations.

Variations in the chemical composition of surfaces were qualitatively analysed using a Fourier-transform infrared spectrometer (FTIR, Bruker Tensor 27 FT-IR spectrometer, Bruker, Sweden). The analysis was carried out using an attenuated total reflectance (ATR) sample holder (GladiATR, PIKE Technologies, United States) with a diamond crystal. Surfaces were directly placed in contact with the crystal for the analysis. The FTIR spectra were measured in the wavenumber range 4000 cm^{-1} to 600 cm^{-1} in the air at room temperature, recording 32 scans with a resolution of 4 cm^{-1}. In addition, variations in peak intensities and surface chemical composition were investigated by comparing the spectra of samples before and after the icing/deicing cycles.

Changes in wetting behaviour were analysed using a droplet shape analyser (DSA100, Krüss, Germany) in controlled conditions (22 °C ± 1 °C temperature and 60% ± 3% relative humidity). The static contact angle was measured by placing a 10 μL droplet of ultra-high purity water (MilliQ, Millipore Corporation, United States) onto the surface. The resulting apparent water contact angle was determined using the tangent method (polynomial fit of droplet shape). Tilting experiments were carried out by depositing 10 μL droplets on the surface and tilting the sample until water droplets rolled off. The roll-off angle was recorded when no droplet pinning was observed during the experiments. Both static contact angle and roll-off angle were reported as the average and standard deviation of at least five measurements on different locations of the sample surface. Moreover, the wetting behaviour in cold conditions was evaluated with a coating surface temperature of −10 °C using a temperature control chamber (Krüss TC40, Krüss, Germany). The selected temperature corresponds to our icing test temperature. The sample was placed on a Peltier stage, and the coating surface was gradually cooled from room temperature to −10 °C ± 1 °C. After the surface reached the desired temperature, the static contact angle and roll-off angle were measured. The results were reported as the average and standard deviation of at least three measurements. Further technical details on the test apparatus for sub-zero wetting experiments are described elsewhere [37].

2.4. Compositional and thermal characterisation

Thermal characterisation of coatings was carried out on as-received samples to investigate the possible effect of employed process parameters on their composition. Moreover, samples were characterised after the cyclic icing/deicing tests. Thermal analyses were performed using thermogravimetry (TG) (Netzsch TGA209F Tarsus, Netzsch, Germany) and differential scanning calorimetry (DSC) (Netzsch DSC214 Polyma, Netzsch, Germany). For TG analyses, specimens were weighted approximately 10 mg and placed in an open alumina pan. Dynamic heating was performed at 20 °C/min from 25 to 600 °C in an inert atmosphere (20 mL/min nitrogen flow). The mass change corresponding to the lubricating additive material was measured from the dynamic TG curve. For DSC analyses, specimens of approximately 10 mg were placed in a sealed concavus aluminium pans. Dynamic heating was performed from −30 °C to 150 °C at 20 °C/min in an inert atmosphere (40 mL/min nitrogen flow). The fusion enthalpies corresponding to lubricating additive and whole coating sample were measured from the dynamic curve. With this method, only the crystalline fraction of the coating is considered. The ratio between the two measured enthalpies gives a qualitative indication of the lubricating additive content in the coating. The results were reported as the average and standard deviation of at least three measurements. Additional details on the methods are described in the Supporting Information.

Coefficients of thermal expansion (CTEs) of feedstock materials, free-standing coatings, and substrate were evaluated using a dilatometer (DIL 402 Expedis® Select, Supreme, Netzsch, Germany) with a silica probe. This analysis was carried out to understand the behaviour of the coating structure (composite coating deposited on stainless steel

substrate) under repeated thermal loads experienced during icing/deicing tests. The samples were analysed from −15 °C to 35 °C with a heating rate of 1 °C/min in an inert atmosphere (50 mL/min helium flow). CTE values were reported as the average and standard deviation of at least three measurements in the range of −10 °C to 25 °C. The operating temperatures of the coatings were within this range during the icing/deicing cycles.

3. Results and discussion

3.1. Icephobic behaviour and icing durability

The tendency of a surface to repel ice is commonly defined as icephobicity [9]. However, different definitions of icephobicity have been considered in the literature. Some researchers note icephobicity as the distinctive characteristic of surfaces to weakly adhere to ice [5,45,46]. For this definition, the ice adhesion is measured using different ice adhesion tests [47,48]. The lower the measured ice adhesion, the higher the surface icephobicity. However, the employed test method, ice type, temperature, and other test variables strongly influence the obtained numerical adhesion values [42,45]. Other researchers consider icephobicity as the ability of surfaces to repel incoming cold water droplets and delay or inhibit ice nucleation [12,14,49]. For this definition, icephobicity is tested with impact droplet experiments on cold surfaces or freezing delay experiments. In this work, icephobicity was evaluated by measuring the shear ice adhesion strength of mixed glaze ice accreted in the IWiT. The ice adhesion was measured using CAT. For this specific test and ice type [24,29], ice adhesion values of 50 kPa and 100 kPa indicate the low and medium-low ice adhesion limit, respectively. Fig. 2a summarises the ice adhesion results at the first icing/deicing cycle and corresponding surface roughness values for all coatings and reference material. Fig. 2b shows the visual appearance of the ice block accreted on the coating surface at −10 °C.

At the first cycle, all lubricated coatings demonstrated low ice adhesion behaviour with values below 50 kPa. From the results, it was evident that the employed process parameters influenced the icephobic behaviour of coatings. Interestingly, the average ice adhesion value decreased with the increased gun air pressure during coating production (from LIC1 with no air to LIC3 with 4 bar air pressure), reaching the lowest value of 23 kPa ± 6 kPa for coating LIC3 (4 bar air pressure and 500 mm/s traverse speed). Moreover, if post-heating by flame was performed for LIC3, the ice adhesion increased approximately 61% (LIC3* compared to LIC3). If a faster traverse speed of the gun was employed, ice adhesion rose approximately 35% (LIC4 with 900 mm/s compared to LIC3 with 500 mm/s traverse speed). Surprisingly, ice adhesion decreased with increased surface roughness, passing from LIC1 to LIC3. Previous research demonstrated that the increased surface roughness promotes mechanical interlocking between ice and surface, thus resulting in enhanced ice adhesion [50]. Therefore, another factor could probably influence the icephobicity of these surfaces. However, this relationship was verified when an even rougher surface was produced, passing from LIC3 to LIC4, fabricated using the highest air pressure in the flame gun and traverse speed.

Coatings underwent repeated icing/deicing cycles, and changes in ice adhesion were monitored to assess the durability of LICs in icing conditions. Previous studies have reported the durability of surfaces tested under a few [24,46,51] until over 100 [5,52,53] icing/deicing cycles. In some studies, the icing procedure consists of forming ice by pouring water in a mould placed on the samples [30,54,55], while deicing comprises heating the sample until ice thaws [53,56]. Compared to methods where deicing occurs by applying shear or normal stresses to an adherent block of ice (accreted or moulded ice), these before mentioned deicing methods are significantly less severe for tested surfaces [46]. Therefore, the icing durability of surfaces should be carefully discussed when comparing different studies, considering employed icing/deicing methods, involved classes of materials and type of ice. Similarly significant, the number of performed cycles and their severity on the surface depends on employed icing test setups and icing/deicing methods. In our icing method, mixed glaze ice was accreted from accelerated supercooled microdroplets. These droplets penetrated the micro and macro-features of the surfaces, thus intimately anchoring the surface microstructure. Ice was then removed by centrifugal forces (shear stress distribution at the interface) and consecutively accreted and detached four times. Fig. 3 presents the ice adhesion values measured at each cycle.

From the first to the second cycle, an increase in ice adhesion was noticed for all coatings. This result indicated decreased surface icephobicity. Ice adhesion increase was probably due to changes in surface properties produced during the cyclic tests. Previous studies on the icing performance of polymeric coatings have reported a similar behaviour over the cycles using the CAT deicing method [46,57]. Both variations in surface chemistry and mechanical damage of surfaces have been considered the leading causes of reduced icephobic performances due to consecutive ice removal [21,46,51,56,58,59]. After the second cycle, a further increase in ice adhesion was observed for all coatings, except for LIC1, which showed a more stable icephobic behaviour. Similarly,

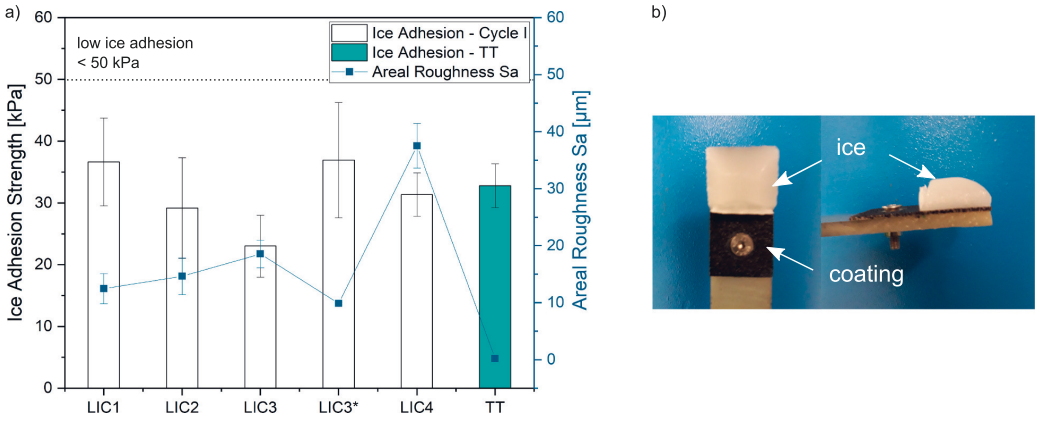

Fig. 2. Icephobic behaviour of lubricated icephobic coatings measured at −10 °C with mixed glaze ice. a) Ice adhesion strength and related surface roughness Sa values of LICs and Teflon tape (TT), which represents the reference material for the ice adhesion test, and b) accreted mixed glaze ice (white block) on a lubricated icephobic coating sample.

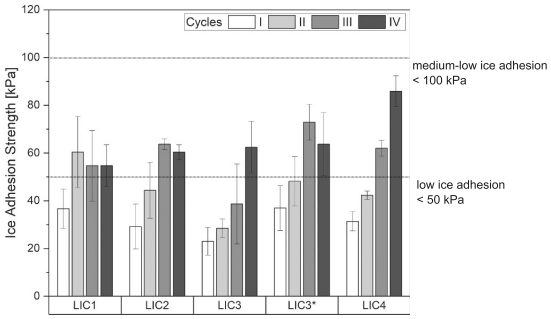

Fig. 3. Ice adhesion results for all LICs over four icing/deicing cycles.

coatings LIC2 and LIC3* seemed to stabilise their icephobicity after the third cycle. Conversely, coatings LIC3 and LIC4 showed gradual degradation until the fourth cycle. Due to the relevant variation in icephobic behaviour, four cycles were considered sufficient to evaluate the icing performance in this study. Despite degraded icephobic character over the cycles, all LICs maintained ice adhesion strength below the limit of 100 kPa, thus retaining their icephobicity within the medium-low ice adhesion level.

Differences in surface properties of LICs might have produced variations in ice adhesion values over the cycles. For example, LIC1 was characterised by a relatively smooth surface morphology compared to other coatings, as shown by the roughness values in Fig. 2a. Smooth surfaces reduce the possibility of mechanical interlocking of ice [50]. This property can be beneficial during repeated icing/deicing, resulting in lower surface damage by ice [60]. Moreover, coating composition could play a role in determining the icephobic behaviour over the cycles. The compositional analysis of LICs via thermal characterisation demonstrated a lower amount of lubricating additive for the coating LIC1 compared to all other coatings, as shown in supporting Fig. S3. This result was justified by the higher heat input employed in the processing of this coating (no additional air in the flame gun), which could reduce the deposition efficiency of the lubricating additive [37]. Furthermore, the lower amount of lubricating additive in the coating structure could increase the mechanical resistance of the coating to ice shedding during deicing. Therefore, the combination of both surface topography and content of lubricating additive could have determined the more stable icephobicity of LIC1. This result provides relevant information for further research in the design of LICs, aiming at enhancing icing performance and durability.

3.2. Effect of icing/deicing cycles on topography and coating morphology

Fig. 4 represents the surface topography and micrographs of all coatings before and after four icing/deicing cycles. Topographical representations of surfaces evidenced different morphologies depending on the employed process parameters. In general, for flame sprayed polymer coatings, the higher the heat input during the process, the higher the degree of melting of the feedstock powders and the lower the obtained surface roughness. In particular, unmelted particles were evident on LIC3 and LIC4 surfaces when low heat input of the flame (gun air pressure of 4 bar) was employed during spraying. The unmelted particles corresponded to the polyethylene matrix material, considering the lubricating additive completely melted with these specific process conditions [37]. Moreover, the micrographs visibly showed differences in coating surface morphologies before and after cyclic icing/deicing tests.

All coatings were mechanically damaged during the cyclic tests, which caused the wearing of polymeric surfaces. Micrographic analyses revealed different defects, such as surface erosion, surface scratches and cracks, as shown in Fig. 5. Surface defects, most commonly scratches, were produced for all coatings, and these were also visible from optical analyses, as shown in supporting Fig. S4. A few scratches were already evident before icing from the micrographs of LIC1 and LIC2, as shown in Fig. 4. These were also noticed in supporting Fig. S4. Therefore, a few scratches could have been formed during sample handling before the cycles and sample preparation procedure, considering the softness of the polymeric components and, particularly, of the lubricating additive. Moreover, cracking of the surfaces was detected between the unmelted particles for samples LIC3 and LIC4. The causes of cracking will be analysed and discussed in Section 3.4. However, cracking could be avoided for other coatings when lower air pressure was added to the flame gun (no air for LIC1 and 2 bar for LIC2), and post-heating was performed after coating deposition (LIC3*). From the results, mechanical damage of surfaces could represent one cause of the gradual increase in ice adhesion strength for LICs over the cycles (Fig. 3), according to previous studies [35,46,58,60].

Fig. 6 represents the variations in areal roughness parameters (Sa, Sz, Sdr) before and after the icing/deicing cycles. Fig. 6a reports variations in Sa and Sz parameters, and Fig. 6b the Sdr values. Supporting Table S1 collects the experimental data. From the results, the employed process parameters influenced the initial surface roughness of LICs. The lower the heat input of the flame gun, the rougher the surfaces (from LIC1 with no additional air to LIC3 and LIC4 with 4 bar). The lower heat input caused partial melting of the polymer particles, resulting in coatings with higher surface roughness and developed interfacial areas (LIC3 and LIC4 compared to other coatings). Post-heat treatment by flame produced remelting of polymers, reducing the coating surface roughness (LIC3* compared to LIC3). After the cycles, a slight increase in average height, Sa, and maximum height, Sz, was verified for all coatings. However, in most cases, the Sa and Sz values varied within the standard deviation. This slight rise can be justified by the produced mechanical damage, which increased the surface roughness [35]. A more significant difference was measured for the developed interfacial area value, Sdr. The increased area could promote mechanical interlocking between ice and surface features, thus probably justifying the increased ice adhesion strength over the cycles [50]. However, a relationship between the degree of increased interfacial area and the increased ice adhesion could not be systematically established in this study for LICs. Possibly, additional factors could influence icephobicity, and, therefore, further investigations are needed to establish correlations.

3.3. Effect of icing/deicing cycles on wettability and surface chemistry

Wettability of surfaces is commonly considered one of the critical properties to predict the icephobic behaviour of surfaces [30,31]. Moreover, wetting properties have helped to understand the variations in icing performance and durability of coatings under repeated icing/deicing cycles [36,46,57,61,62]. Fig. 7 shows the results of the wetting experiments before and after four icing/deicing cycles. Fig. 7a compares the apparent water contact angle (WCA) values obtained for room temperature experiments and Fig. 7b for cold temperature conditions. The latter was carried out to understand better the wetting behaviour of surfaces in conditions as similar as possible to the icing test environment [63,64].

From the wetting results before the cycles, LICs demonstrated different wetting behaviour. The different behaviour was more evident for the room temperature experiments than for the cold experiments. For room temperature experiments, the smoothest surfaces of this study, namely LIC1 and LIC3*, showed apparent water contact angles higher than 120°. It is well known that water contact angles never exceed 120° in a Wenzel wetting state for the most hydrophobic solids [65,66]. Therefore, these results suggested that the surfaces were partially wetted, and air pockets were probably trapped beneath the water droplets [67]. The wetting behaviour was better explained by the micrographs of surface morphologies presented in Fig. 8.

The micrographs showed that LIC1 and LIC3* were characterised by

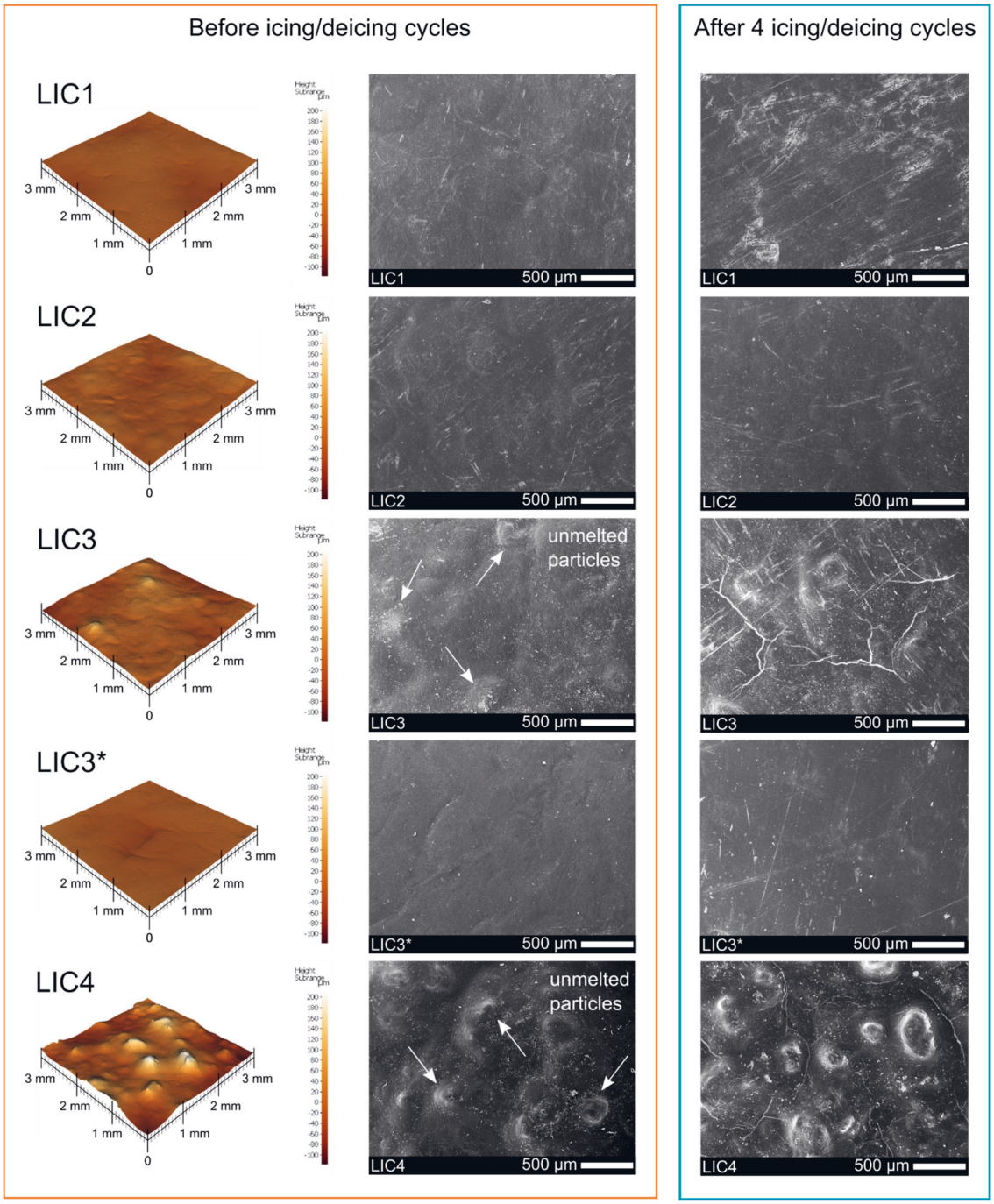

Fig. 4. Surface topographies and morphologies of the coatings before and after four icing/deicing cycles. Optical profilometer images of the surface areas before icing/deicing cycles (left). The colour scale in the images indicates the height of the surface: lighter colour for peaks and a darker colour for valleys. Electron microscope images of the coating surface before (middle) and after four icing/deicing cycles (right).

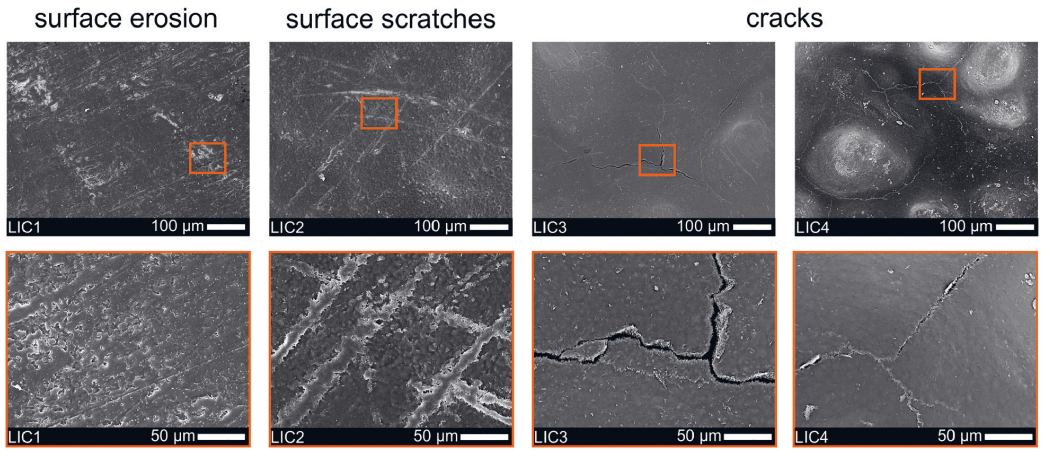

Fig. 5. Surface defects (indicated by orange squares) of LICs after four icing/deicing cycles at different magnifications. From left to right, the micrographs show surface erosion, surface scratches, and cracks.

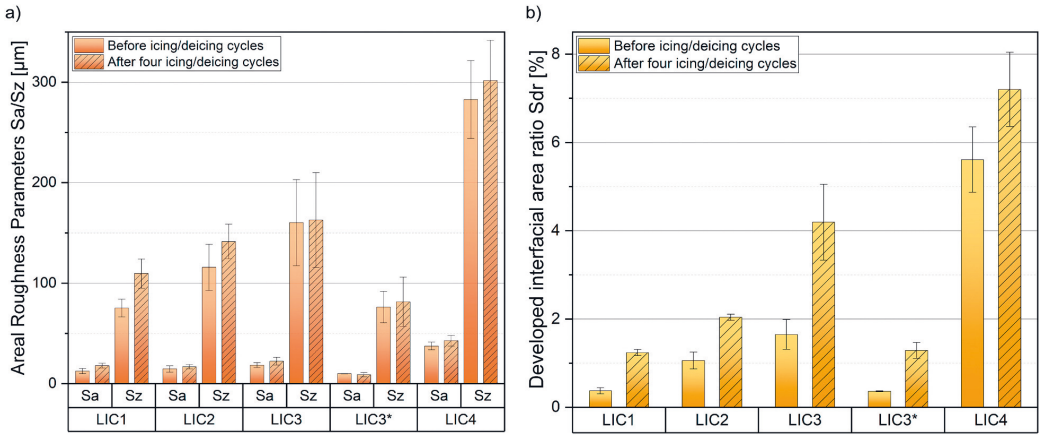

Fig. 6. Areal roughness parameters of LICs before and after four icing/deicing cycles. a) Areal roughness parameters (Sa and Sz), and b) developed interfacial area ratio (Sdr). No patterned columns and patterned columns indicate the parameters before and after four icing/deicing cycles.

finer surface features compared to all other coatings. These features were similar to small protuberances and resulted from the process parameters selected during coating production. Surface protuberances probably promoted the presence of air pockets trapped underneath water droplets in the wetting experiments. This resulted in a mixed Cassie-Wenzel wetting state with droplets showing contact angles higher than 120°. Moreover, the presence of air pockets was evidenced by the wetting results at cold temperature. A significant decrease in water contact angles was noticed in these conditions for LIC1 and LIC3* compared to room temperature experiments. Cold surfaces induce water condensation from the droplets to the surface microstructure. Condensation phenomena eliminate the trapped air pockets, thus reducing the measured water contact angle [63,68]. For more details on the wetting state of these coatings, the authors refer to their previous study [37]. From the results at room temperature, the surfaces retained their hydrophobic character after four icing/deicing cycles (apparent WCA > 90° for all coatings). A slight decrease of apparent WCA was revealed for all coatings, except for the rougher surface of this study (LIC4). However, in most cases, the values fall within the standard deviation of the measurements. Conversely, the decrease of WCA was more evident in the experiments performed in cold conditions. In these experiments, the water condensates onto the surface features, thus reducing the presence of possible air pockets beneath the drops [69]. This phenomenon results in decreased apparent WCA when passing from a mixed Cassie-Wenzel wetting state (room temperature experiments) to a Wenzel wetting state (cold temperature experiments) using the same volume of water droplets [37,65]. Moreover, roll-off angles were measured, but no droplet mobility was detected (water roll-off angle >90° for all surfaces). Considering the icephobic performance of LICs over the cycles, the wetting results supported the work of other studies linking the decrease of icephobicity with the decrease of surface hydrophobicity after icing/deicing cycles [13,46,57,58,61].

The decrease in surface hydrophobicity can depend on variations in surface roughness and chemistry [65]. In this study, variations in surface roughness were produced by mechanical damage during the cyclic tests. Moreover, mechanical damage could generate local modifications of surface chemistry due to possible material removal. In addition, the interaction of polymers with water, ice and humid environment can

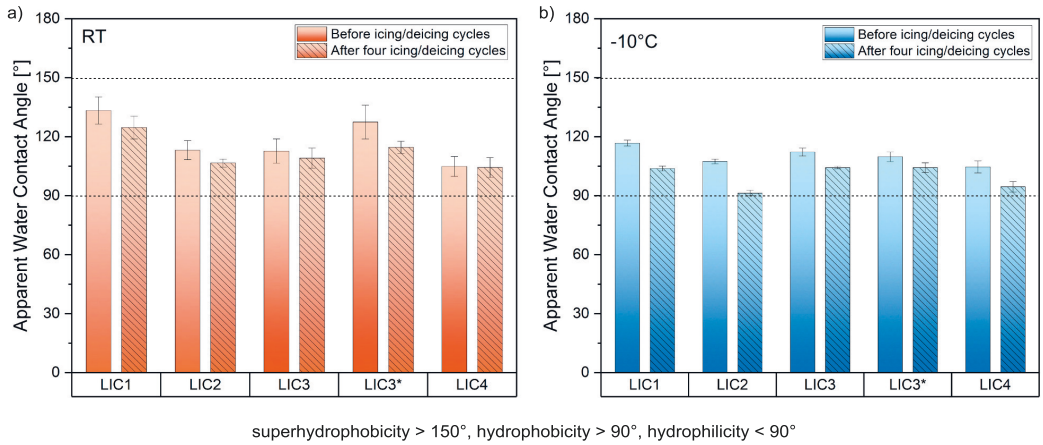

Fig. 7. Results of the wetting experiments before and after four icing/deicing cycles. Apparent WCA at a) room temperature, and b) −10 °C surface temperature, which corresponds to the icing test temperature.

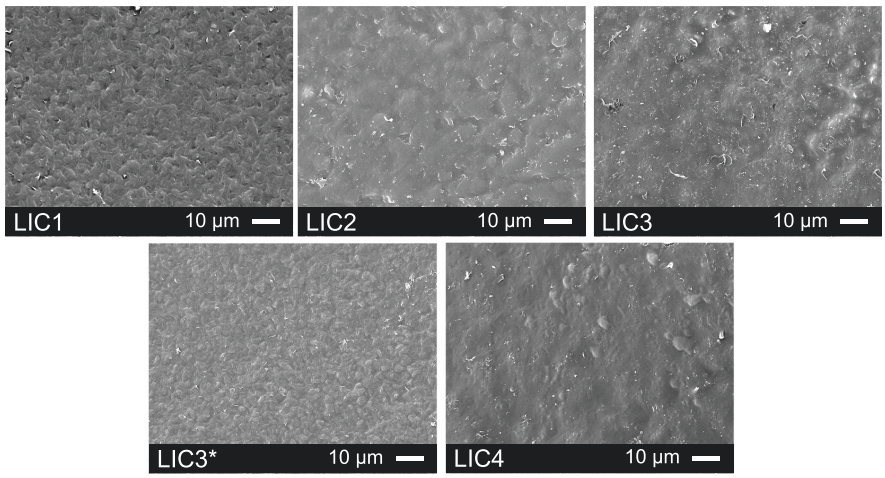

Fig. 8. Micrographs of the surface morphologies for all as-sprayed lubricated icephobic coatings.

cause chemical changes due to hydrolysis [70]. From the chemical analyses before and after the cycles, no variations in surface chemistry were revealed, as shown in the FTIR spectra of supporting Fig. S5. Therefore, the cause of the decreased hydrophobicity of surfaces was primarily related to mechanical damage. The soft additive, which has higher hydrophobicity than the matrix material [37], could have been locally removed from the surface during deicing. This local removal might contribute to the slight decrease in surface hydrophobicity. In conclusion, the results suggested that the decrement in icephobicity over the cycles was mainly due to mechanical damage, which produced variations of surface properties.

3.4. Effect of icing/deicing cycles on coating cracking behaviour

Surface cracking represents one of the possible mechanical failures of coatings [70] and can occur due to several factors. For example, cracks can form due to impact with objects, abrasion, degradation by ultraviolet irradiation, hydrolysis, contaminants on the substrate, and internal and external stresses [70]. In this study, micrographs in Fig. 4 and Fig. 5 revealed surface cracks between the unmelted matrix particles for coatings LIC3 and LIC4 after icing/deicing cycles. Presumably, the unmelted particles visible on the surfaces were surrounded by lubricant-rich regions.

During repeated icing/deicing tests, coatings experienced cyclic thermal and mechanical stresses, as schematically described at each test stage in Fig. 9. At the first stage, coatings (LICs on a stainless steel substrate) were cooled from room temperature to the icing test conditions (from 22 °C ± 3 °C and relative humidity of 20% ± 5% to −10 °C ± 1 °C and relative humidity of 80% ± 5%). During cooling, the coating and the substrate shrink depending on their coefficient of thermal expansion (CTE). If the coating has higher CTE than the substrate, the latter can constrain the coating from shrinking, thus inducing tensile stresses to the coating [70,71]. CTEs of 15.1 ± 0.1 × 10^{-6} °C^{-1} and 182.4 ± 1.7 × 10^{-6} °C^{-1} were measured for the stainless steel substrate and free-standing LIC3 coating, respectively. The experimental CTE data is reported in supporting Fig. S6 and Table S2. The results indicated a

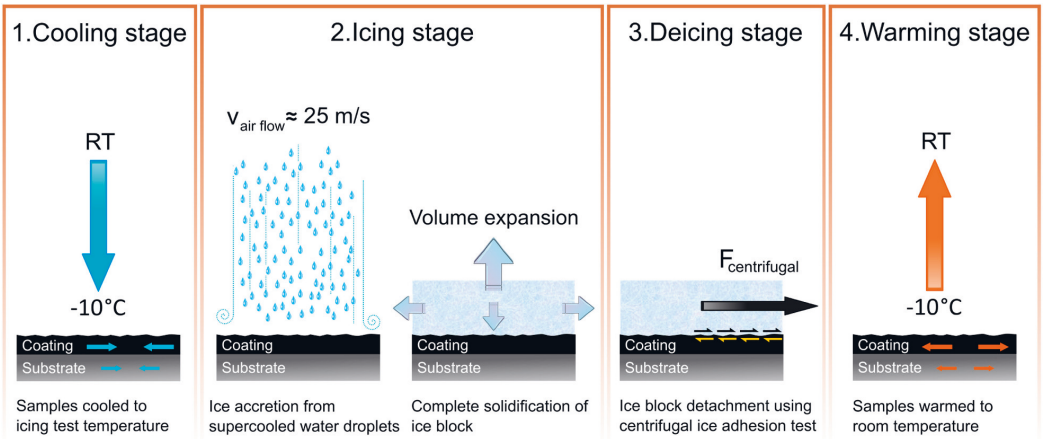

Fig. 9. Stages of the cyclic icing/deicing tests. 1) Cooling stage of the samples from room temperature to the icing test temperature. 2) Icing stage with the accretion of mixed glaze ice from supercooled water droplet in the icing wind tunnel and solidification of the ice block. 3) Deicing stage with the removal of the ice block using the centrifugal ice adhesion tester. 4) Warming stage with samples stored at room temperature.

significant mismatch between the CTEs. If induced tensile stresses exceed the fracture resistance of the coating, cracking can occur [72,73], especially considering the lower mechanical properties of the lubricant-rich regions. At the second stage, a cold wind flow accelerated the supercooled water microdroplets towards the coating surfaces placed in the icing wind tunnel. No stresses caused by water droplets impact on surfaces (possible peening stresses transferred to the coating surface due to impact) were considered in this analysis. A block of mixed glaze ice was then accreted from the continuous impact of supercooled micro-droplets. Immediately after accretion, the mixed glaze ice block comprised both fractions of liquid and solidified water. The block was rested to allow complete solidification, causing the liquid water to expand. Water expansion can cause some damage to the coating surface due to significant developed interfacial stresses [60]. At the third stage, a gradual centrifugal force was applied to the iced sample until ice detachment occurred, forming mechanical stresses (normal and shear stresses) at the ice-coating interface [40]. At the fourth stage, the samples were warmed to room temperature. The materials expanded and dried in this environment, and again mismatch of CTEs can induce stresses. The cycles were then repeated from the first stage.

To study more in detail the effect of the substrate material on cracking behaviour, LIC3 coating was sprayed on an LDPE substrate,

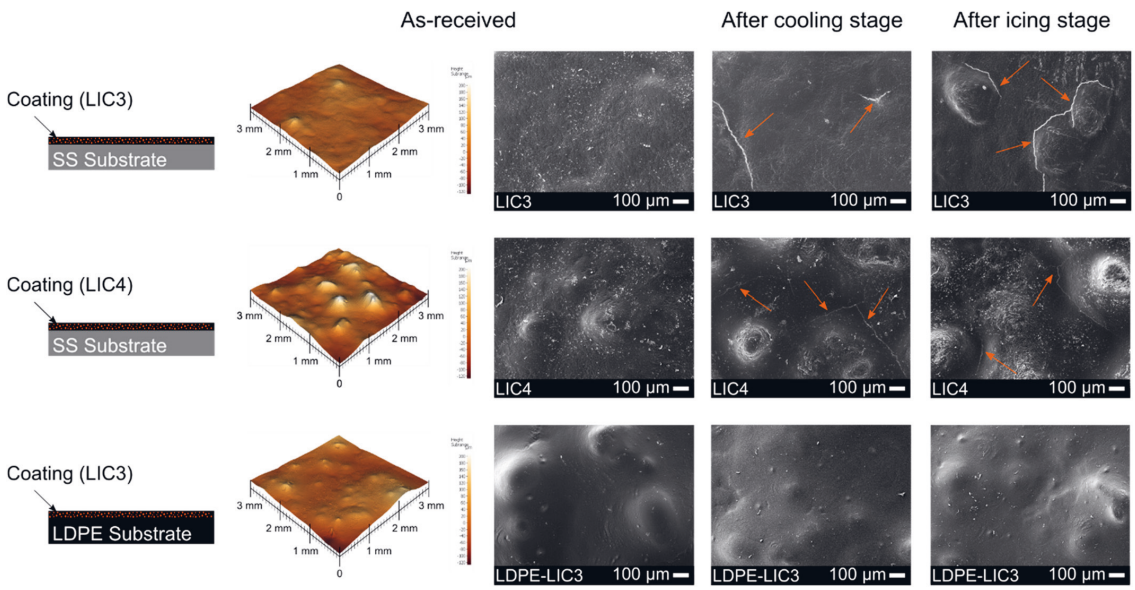

Fig. 10. Influence of the material substrate on the cracking behaviour of LICs. The schematisation of coating samples and related surface topographical images (left). Surface micrographs of the coatings at different stages of the icing/deicing cycles, such as as-received, after cooling stage, after icing/deicing stage (middle and right). Orange arrows indicate cracks.

which was prepared from the same grade as the matrix material of LICs. The CTE of the LDPE substrate was $188.3 \pm 1.4 \times 10^{-6}\ °C^{-1}$ and thus similar to the CTE of the coating. Icing/deicing cycles were performed as for the coatings sprayed on stainless steel substrate, and the surface morphologies were compared at every stage of the test. Fig. 10 shows the schematisation of the coating structures, their topography and surface morphology at different stages of the icing/deicing cycles.

It was noticed that cracking occurred already after the cooling stage of the icing/deicing tests for coatings sprayed on stainless steel substrates. This result indicated that cracking in the lubricant-rich regions was mainly induced by thermal stresses. The lubricant-rich regions presumably have lower mechanical properties than the matrix material. Therefore, these weaker regions of the coatings were probably more prone to cracking than others. However, cracking behaviour was prevented when the coating was sprayed on the LDPE substrate, which had thermal expansion properties similar to the coating material. Consequently, causes of cracking behaviour were considered to be directly related to the CTE mismatch and cohesive strength of the coating.

In addition, other hypotheses on the causes of cracking were considered. For example, residual tensile stresses could be present in the coating after its fabrication and solidification, thus further contributing to cracking [71]. Therefore, an annealing treatment was performed to relax possible residual stresses before cyclic icing/deicing tests. However, the coatings showed no change in cracking behaviour after annealing, as revealed in supporting Fig. S7, and the heat treatment was no beneficial to avoid crack formation. Another hypothesis on the causes of cracking was related to possible water absorption during the cyclic tests. Water absorption could then produce swelling of polymers and shrinking when drying occurs, thus inducing coating cracking [70]. However, this was not relevant in our study since cracking occurred during the first cooling stage for samples isolated (stored in sealed plastic containers) from possible contact with water, ice and humid environment. Furthermore, other coating properties could influence the formation of cracks, such as coating thickness, polymer properties in sub-zero conditions, Poissons's ratio and other variables [70,73]. Therefore, further studies, which consider these variables, should be considered. In conclusion, investigating possible causes of cracking was relevant for the design of flame-sprayed coatings for cold applications, thus highlighting the importance of selected materials (coating and substrate combination) and/or process parameters.

4. Conclusions

The study investigated the icing behaviour of flame sprayed lubricated icephobic coatings (LICs) and their durability under repeated icing/deicing cycles. LICs consisted of a matrix material made of low-density polyethylene and a lubricating additive made of solid fully hydrogenated cottonseed oil. Coatings were fabricated using flame spraying with hybrid feedstock injection. It was found that LICs exhibited low ice adhesion values at the first icing/deicing cycle. Over repeated cycles, some coatings (LIC1, LIC2, LIC3*) tended to stabilise their icephobic behaviour. In particular, LIC1 showed the most stable icephobic behaviour. This coating was characterised by a reduced amount of lubricating additive in its structure and relatively smooth morphology. Conversely, rougher coatings (LIC3, LIC4) showed a gradual decrease in their icephobicity over the cycles. However, all coatings retained their icephobicity after the cycles, residing below the low-medium ice adhesion limit of 100 kPa for this ice adhesion test. Repeated cycles caused mechanical damage to surfaces. This damage produced increased surface roughness and decreased hydrophobic character of the coatings. In addition, surface cracks were revealed in some coatings (LIC3, LIC4) after icing/deicing cycles. The causes of cracking behaviour were correlated to the significant difference in coefficients of thermal expansion between the coatings and the substrate material. It was demonstrated that cracking behaviour could be avoided using a substrate material with thermal expansion properties more similar to the coatings. These findings have significant implications in the development of coatings for cold applications, thus highlighting the importance of material combination and process parameters selection. Future studies will aim at further enhancing the durability of LICs in icing conditions. Moreover, their performance will be investigated under different environmental stresses.

CRediT authorship contribution statement

Valentina Donadei: Conceptualization, Methodology, Investigation, Visualization, Writing – original draft. **Heli Koivuluoto:** Conceptualization, Supervision, Funding acquisition, Resources, Writing – review & editing. **Essi Sarlin:** Supervision, Writing – review & editing. **Henna Niemelä-Anttonen:** Methodology, Writing – review & editing. **Tommi Varis:** Writing – review & editing. **Petri Vuoristo:** Supervision, Funding acquisition, Resources, Writing – review & editing.

Declaration of competing interest

The authors declare that they have no known competing financial interests or personal relationships that could have appeared to influence the work reported in this paper.

Acknowledgements

Authors thank the LubISS (Lubricant Impregnated Slippery Surfaces) project that received funding from the European Union's Horizon 2020 research and innovation programme under the Marie Sklodowska-Curie Grant Agreement No. 722497. V.D. acknowledges the Faculty of Engineering and Natural Sciences of Tampere University for the financial support. In addition, Mr. Anssi Metsähonkala and Mr. Jarkko Lehti from Tampere University are acknowledged for technical support in the flame spray process. M.Sc. Enni Hartikainen and Mr. Jarmo Laakso from Tampere University are thanked for assisting in icing testing and dilatometer experiments, respectively. This work made use of Tampere Microscopy Center facilities at Tampere University.

Appendix A. Supplementary data

Supplementary data to this article can be found online at https://doi.org/10.1016/j.porgcoat.2021.106614.

References

[1] M. Farzaneh, Atmospheric Icing of Power Networks, Springer Netherlands, Dordrecht, 2008, https://doi.org/10.1007/978-1-4020-8531-4.
[2] M. Grizen, M.K. Tiwari, Icephobic surfaces: features and challenges, in: K.L. Mittal, C.-H. Choi (Eds.), Ice Adhes. Mech. Meas. Mitig, Wiley, 2020, pp. 417–466, https://doi.org/10.1002/9781119640523.ch14.
[3] P. Irajizad, S. Nazifi, H. Ghasemi, Icephobic surfaces: definition and figures of merit, Adv. Colloid Interf. Sci. 269 (2019) 203–218, https://doi.org/10.1016/j.cis.2019.04.005.
[4] R. Menini, M. Farzaneh, Advanced icephobic coatings, J. Adhes. Sci. Technol. 25 (2011) 971–992, https://doi.org/10.1163/016942410X533372.
[5] K. Golovin, S.P.R. Kobaku, D.H. Lee, E.T. DiLoreto, J.M. Mabry, A. Tuteja, Designing durable icephobic surfaces, Sci. Adv. 2 (2016), e1501496, https://doi.org/10.1126/sciadv.1501496.
[6] T.M. Schutzius, S. Jung, T. Maitra, P. Eberle, C. Antonini, C. Stamatopoulos, D. Poulikakos, Physics of icing and rational design of surfaces with extraordinary icephobicity, Langmuir 31 (2015) 4807–4821, https://doi.org/10.1021/la502586a.
[7] S. Ozbay, H.Y. Erbil, On the relationship between surface free energy and ice adhesion of flat anti-icing surfaces, in: Ice Adhes, Wiley, 2020, pp. 187–215, https://doi.org/10.1002/9781119640523.ch7.
[8] M.J. Kreder, J. Alvarenga, P. Kim, J. Aizenberg, Design of anti-icing surfaces: smooth, textured or slippery? Nat. Rev. Mater. 1 (2016), 15003 https://doi.org/10.1038/natrevmats.2015.3.
[9] H. Sojoudi, M. Wang, N.D. Boscher, G.H. McKinley, K.K. Gleason, Durable and scalable icephobic surfaces: similarities and distinctions from superhydrophobic surfaces, Soft Matter 12 (2016) 1938–1963. https://doi.org/10.1039/C5SM02295A.

[10] C. Neinhuis, W. Barthlott, Characterization and distribution of water-repellent, self-cleaning plant surfaces, Ann. Bot. 79 (1997) 667–677, https://doi.org/10.1006/anbo.1997.0400.

[11] Y. Lin, H. Chen, G. Wang, A. Liu, Recent progress in preparation and anti-icing applications of superhydrophobic coatings, Coatings 8 (2018) 208, https://doi.org/10.3390/coatings8060208.

[12] L. Wang, Q. Gong, S. Zhan, L. Jiang, Y. Zheng, Robust anti-icing performance of a flexible superhydrophobic surface, Adv. Mater. 28 (2016) 7729–7735, https://doi.org/10.1002/adma.201602480.

[13] S. Farhadi, M. Farzaneh, S.A. Kulinich, Anti-icing performance of superhydrophobic surfaces, Appl. Surf. Sci. 257 (2011) 6264–6269, https://doi.org/10.1016/j.apsusc.2011.02.057.

[14] L. Cao, A.K. Jones, V.K. Sikka, J. Wu, D. Gao, Anti-icing superhydrophobic coatings, Langmuir 25 (2009) 12444–12448, https://doi.org/10.1021/la902882b.

[15] A. Nakajima, K. Hashimoto, T. Watanabe, Recent studies on super-hydrophobic films, in: Mol. Mater. Funct. Polym, Springer Vienna, Vienna, 2001, pp. 31–41, https://doi.org/10.1007/978-3-7091-6276-7_3.

[16] S. Zhang, J. Huang, Y. Cheng, H. Yang, Z. Chen, Y. Lai, Bioinspired Surfaces with superwettability for anti-icing and ice-phobic application: concept, mechanism, and design, Small 13 (2017), 1701867, https://doi.org/10.1002/smll.201701867.

[17] Q. Li, Z. Guo, Fundamentals of icing and common strategies for designing biomimetic anti-icing surfaces, J. Mater. Chem. A 6 (2018) 13549–13581, https://doi.org/10.1039/c8ta03259a.

[18] J. Lv, Y. Song, L. Jiang, J. Wang, Bio-inspired strategies for anti-icing, ACS Nano 8 (2014) 3152–3169, https://doi.org/10.1021/nn406522n.

[19] S. Jung, M. Dorrestijn, D. Raps, A. Das, C.M. Megaridis, D. Poulikakos, Are superhydrophobic surfaces best for icephobicity? Langmuir 27 (2011) 3059–3066, https://doi.org/10.1021/la104762g.

[20] L. Oberli, D. Caruso, C. Hall, M. Fabretto, P.J. Murphy, D. Evans, Condensation and freezing of droplets on superhydrophobic surfaces, Adv. Colloid Interf. Sci. 210 (2014) 47–57, https://doi.org/10.1016/j.cis.2013.10.018.

[21] S.A. Kulinich, S. Farhadi, K. Nose, X.W. Du, Superhydrophobic surfaces: are they really ice-repellent? Langmuir 27 (2011) 25–29, https://doi.org/10.1021/la104277q.

[22] T.S. Wong, S.H. Kang, S.K.Y. Tang, E.J. Smythe, B.D. Hatton, A. Grinthal, J. Aizenberg, Bioinspired self-repairing slippery surfaces with pressure-stable omniphobicity, Nature 477 (2011) 443–447, https://doi.org/10.1038/nature10447.

[23] M. Zhang, J. Yu, R. Chen, Q. Liu, J. Liu, D. Song, P. Liu, L. Gao, J. Wang, Highly transparent and robust slippery lubricant-infused porous surfaces with anti-icing and anti-fouling performances, J. Alloys Compd. 803 (2019) 51–60, https://doi.org/10.1016/j.jallcom.2019.06.241.

[24] H. Niemelä-Anttonen, H. Koivuluoto, M. Tuominen, H. Teisala, P. Juuti, J. Haapanen, J. Harra, C. Stenroos, J. Lahti, J. Kuusipalo, J.M. Mäkelä, P. Vuoristo, Icephobicity of slippery liquid infused porous surfaces under multiple freeze-thaw and ice accretion-detachment cycles, Adv. Mater. Interfaces 5 (2018), 1800828, https://doi.org/10.1002/admi.201800828.

[25] S. Ozbay, C. Yuceel, H.Y. Erbil, Improved icephobic properties on surfaces with a hydrophilic lubricating liquid, ACS Appl. Mater. Interfaces 7 (2015) 22067–22077, https://doi.org/10.1021/acsami.5b07265.

[26] H.Y. Erbil, Improvement of lubricant-infused surfaces for anti-icing applications, Surf. Innov. 4 (2016) 214–217, https://doi.org/10.1680/jsuin.16.00026.

[27] S.B. Subramanyam, K. Rykaczewski, K.K. Varanasi, Ice adhesion on lubricant-impregnated textured surfaces, Langmuir 29 (2013) 13414–13418, https://doi.org/10.1021/la402456c.

[28] S. Ozbay, H.Y. Erbil, Ice accretion by spraying supercooled droplets is not dependent on wettability and surface free energy of substrates, Colloids Surfaces A Physicochem. Eng. Asp. 504 (2016) 210–218, https://doi.org/10.1016/j.colsurfa.2016.05.065.

[29] H. Koivuluoto, E. Hartikainen, H. Niemelä-Anttonen, Thermally sprayed coatings: novel surface engineering strategy towards icephobic solutions, Materials 13 (2020), https://doi.org/10.3390/ma13061434. Basel.

[30] A.J. Meuler, J.D. Smith, K.K. Varanasi, J.M. Mabry, G.H. McKinley, R.E. Cohen, Relationships between water wettability and ice adhesion, ACS Appl. Mater. Interfaces 2 (2010) 3100–3110, https://doi.org/10.1021/am1006035.

[31] Z. He, E.T. Vågenes, C. Delabahan, J. He, Z. Zhang, Room temperature characteristics of polymer-based low ice adhesion surfaces, Sci. Rep. 7 (2017) 1–7, https://doi.org/10.1038/srep42181.

[32] H. Koivuluoto, C. Stenroos, M. Kylmälahti, M. Apostol, J. Kiilakoski, P. Vuoristo, Anti-icing behavior of thermally sprayed polymer coatings, J. Therm. Spray Technol. 26 (2017) 150–160, https://doi.org/10.1007/s11666-016-0501-x.

[33] V. Donadei, H. Koivuluoto, E. Sarlin, P. Vuoristo, Icephobic behaviour and thermal stability of flame-sprayed polyethylene coating: the effect of process parameters, J. Therm. Spray Technol. 29 (2020) 241–254, https://doi.org/10.1007/s11666-019-00947-0.

[34] Y. Zhuo, V. Håkonsen, Z. He, S. Xiao, J. He, Z. Zhang, Enhancing the mechanical durability of icephobic surfaces by Introducing autonomous self-healing function, ACS Appl. Mater. Interfaces 10 (2018) 11972–11978, https://doi.org/10.1021/acsami.8b01866.

[35] H. Memon, D.S.A. De Focatiis, K.S. Choi, X. Hou, Durability enhancement of low ice adhesion polymeric coatings, Prog. Org. Coat. 151 (2021) 106033, https://doi.org/10.1016/j.porgcoat.2020.106033.

[36] S.A. Kulinich, D. Masson, X. Du, A.M. Emelyanenko, K.L. Mittal, C.-H. Choi, Testing the durability of anti-icing coatings, in: Ice Adhes. Mech. Meas. Mitig, Wiley, 2020, pp. 495–520, https://doi.org/10.1002/9781119640523.ch16.

[37] V. Donadei, H. Koivuluoto, E. Sarlin, P. Vuoristo, Lubricated icephobic coatings prepared by flame spraying with hybrid feedstock injection, Surf. Coat. Technol. 403 (2020), 126396, https://doi.org/10.1016/j.surfcoat.2020.126396.

[38] V. Jannin, Y. Cuppok, Hot-melt coating with lipid excipients, Int. J. Pharm. 457 (2013) 480–487, https://doi.org/10.1016/j.ijpharm.2012.10.026.

[39] A. Sandhu, O.J. Walker, A. Nistal, K.L. Choy, A.J. Clancy, Perfluoroalkane wax infused gels for effective, regenerating, anti-icing surfaces, Chem. Commun. 55 (2019) 3215–3218, https://doi.org/10.1039/c8cc09818b.

[40] H. Koivuluoto, C. Stenroos, R. Ruohomaa, G. Bolelli, L. Lusvarghi, P. Vuoristo, Research on icing behavior and ice adhesion testing of icephobic surfaces, in: Proc. Int. Work. Atmos. Icing Struct., Uppsala, 2015, pp. 183–188.

[41] C. Stenroos, P. Vuoristo, H. Koivuluoto, Properties of Icephobic Surfaces in Different Icing Conditions, Mater Thesis, Tampere University of Technology, Tampere, FI, 2015.

[42] H. Niemelä-Anttonen, J. Kiilakoski, P. Vuoristo, H. Koivuluoto, Icephobic performance of different surface designs and materials, Proc. Int. Work. Atmos. Icing Struct. (2019) 1–5.

[43] ISO 25178-3:2012 - Geometrical product specifications (GPS) — Surface texture: Areal — Part 3: Specification operators. https://www.iso.org/standard/42895.html, 2012. (Accessed 6 February 2020).

[44] ISO 25178-2:2012 - Geometrical product specifications (GPS) — Surface texture: Areal — Part 2: Terms, definitions and surface texture parameters. https://www.iso.org/standard/42785.html, 2012. (Accessed 27 May 2021).

[45] S. Rønneberg, Y. Zhuo, C. Laforte, J. He, Z. Zhang, Interlaboratory study of ice adhesion using different techniques, Coatings 9 (2019) 678, https://doi.org/10.3390/coatings9100678.

[46] S. Asadollahi, M. Farzaneh, L. Stafford, On the icephobic behavior of organosilicon-based surface structures developed through atmospheric pressure plasma deposition in nitrogen plasma, Coatings 9 (2019) 679, https://doi.org/10.3390/coatings9100679.

[47] S. Rønneberg, J. He, Z. Zhang, The need for standards in low ice adhesion surface research: a critical review, J. Adhes. Sci. Technol. 34 (2020) 319–347, https://doi.org/10.1080/01694243.2019.1679523.

[48] A. Work, Y. Lian, A critical review of the measurement of ice adhesion to solid substrates, Prog. Aerosp. Sci. 98 (2018) 1–26, https://doi.org/10.1016/j.paerosci.2018.03.001.

[49] P. Eberle, M.K. Tiwari, T. Maitra, D. Poulikakos, Rational nanostructuring of surfaces for extraordinary icephobicity, Nanoscale 6 (2014) 4874–4881, https://doi.org/10.1039/c3nr06644d.

[50] J. Chen, J. Liu, M. He, K. Li, D. Cui, Q. Zhang, X. Zeng, Y. Zhang, J. Wang, Y. Song, Superhydrophobic surfaces cannot reduce ice adhesion, Appl. Phys. Lett. 101 (2012) 111603, https://doi.org/10.1063/1.4752436.

[51] M. Balordi, G. Santucci de Magistris, C. Chemelli, A novel simple anti-ice aluminum coating: synthesis and in-lab comparison with a superhydrophobic hierarchical surface, Coatings 10 (2020) 111, https://doi.org/10.3390/coatings10020111.

[52] L.B. Boinovich, E.B. Modin, A.R. Sayfutdinova, K.A. Emelyanenko, A.L. Vasiliev, A. M. Emelyanenko, Combination of functional nanoengineering and nanosecond laser texturing for design of superhydrophobic aluminum alloy with exceptional mechanical and chemical properties, ACS Nano 11 (2017) 10113–10123, https://doi.org/10.1021/acsnano.7b04634.

[53] L.B. Boinovich, A.M. Emelyanenko, V.K. Ivanov, A.S. Pashinin, Durable icephobic coating for stainless steel, ACS Appl. Mater. Interfaces 5 (2013) 2549–2554, https://doi.org/10.1021/am3031272.

[54] L. Makkonen, Ice adhesion - theory, measurements and countermeasures, J. Adhes. Sci. Technol. 26 (2012) 413–445, https://doi.org/10.1163/016942411X574583.

[55] J.H. Kim, M.J. Kim, B. Lee, J.M. Chun, V. Patil, Y.S. Kim, Durable ice-lubricating surfaces based on polydimethylsiloxane embedded silicone oil infused silica aerogel, Appl. Surf. Sci. 512 (2020) 145728, https://doi.org/10.1016/j.apsusc.2020.145728.

[56] S. Brown, J. Lengaigne, N. Sharifi, M. Pugh, C. Moreau, A. Dolatabadi, L. Martinu, J.E. Klemberg-Sapieha, Durability of superhydrophobic duplex coating systems for aerospace applications, Surf. Coat. Technol. 401 (2020), https://doi.org/10.1016/j.surfcoat.2020.126249.

[57] Z.A. Janjua, B. Turnbull, K.L. Choy, C. Pandis, J. Liu, X. Hou, K.S. Choi, Performance and durability tests of smart icephobic coatings to reduce ice adhesion, Appl. Surf. Sci. 407 (2017) 555–564, https://doi.org/10.1016/j.apsusc.2017.02.206.

[58] V. Vercillo, J.T. Cardoso, D. Huerta-Murillo, S. Tonnicchia, A. Laroche, J.A. Mayén Guillén, J.L. Ocaña, A.F. Lasagni, E. Bonaccurso, Durability of superhydrophobic laser-treated metal surfaces under icing conditions, Mater. Lett. X. 3 (2019), 100021, https://doi.org/10.1016/j.mlblux.2019.100021.

[59] V. Donadei, H. Koivuluoto, E. Sarlin, P. Vuoristo, Durability of lubricated icephobic coatings under multiple icing/deicing cycles, in: F. Azarmi, X. Chen, J. Cizek, C. Cojocaru, B. Jodoin, H. Koivuluoto, Y. Lau, R. Fernandez, O. Ozdemir, H. Salami Jazi, F.L. Toma (Eds.), Proc. from Int. Therm. Spray Conf, ASM International, Anaheim, CA, USA, Quebec City, 2021, pp. 473–481, https://doi.org/10.31399/asm.cp.itsc2021p0473.

[60] S.A. Kulinich, M. Farzaneh, On ice-releasing properties of rough hydrophobic coatings, Cold Reg. Sci. Technol. 65 (2011) 60–64, https://doi.org/10.1016/j.coldregions.2010.01.001.

[61] A. Laroche, D. Bottone, S. Seeger, E. Bonaccurso, Silicone nanofilaments grown on aircraft alloys for low ice adhesion, Surf. Coat. Technol. 410 (2021) 126971, https://doi.org/10.1016/j.surfcoat.2021.126971.

[62] N. Rehfeld, B. Speckmann, C. Schreiner, V. Stenzel, Assessment of icephobic coatings—how can we monitor performance durability? Coatings 11 (2021) 614, https://doi.org/10.3390/coatings11060614.

[63] Q. Fu, X. Wu, D. Kumar, J.W.C. Ho, P.D. Kanhere, N. Srikanth, E. Liu, P. Wilson, Z. Chen, Development of sol-gel icephobic coatings: effect of surface roughness and surface energy, ACS Appl. Mater. Interfaces 6 (2014) 20685–20692, https://doi.org/10.1021/am504348x.
[64] L. Mazzola, G. Bruno, Characterization of ice-phobic surfaces: improvements on contact angle measurements, Measurement 110 (2017) 202–210, https://doi.org/10.1016/j.measurement.2017.06.036.
[65] D. Quéré, Wetting and roughness, Annu. Rev. Mater. Res. 38 (2008) 71–99, https://doi.org/10.1146/annurev.matsci.38.060407.132434.
[66] E. Shafrin, W. Zisman, Upper limits to the contact angles of liquids on solids, in: R. F. Gou (Ed.), Contact Angle, Wettability Adhes. Adv. Chem. Ser, DC: Am. Chem. Soc., Washington, 1964, pp. 478–479, https://doi.org/10.1007/bf01150624.
[67] A. Lafuma, D. Quéré, Superhydrophobic states, Nat. Mater. 2 (2003) 457–460, https://doi.org/10.1038/nmat924.
[68] G. Momen, M. Farzaneh, R. Jafari, Wettability behaviour of RTV silicone rubber coated on nanostructured aluminium surface, Appl. Surf. Sci. 257 (2011) 6489–6493, https://doi.org/10.1016/j.apsusc.2011.02.049.
[69] T. Mouterde, G. Lehoucq, S. Xavier, A. Checco, C.T. Black, A. Rahman, T. Midavaine, C. Clanet, D. Quéré, Antifogging abilities of model nanotextures, Nat. Mater. 16 (2017) 658–663, https://doi.org/10.1038/nmat4868.
[70] A. Hakimian, S. Nazifi, H. Ghasemi, Durability assessment of icephobic coatings, in: Ice Adhes. Mech. Meas. Mitig, Wiley, 2020, pp. 521–545, https://doi.org/10.1002/9781119640523.ch17.
[71] A.A. Abubakar, A.F.M. Arif, K.S. Al-Athel, S.S. Akhtar, J. Mostaghimi, Modeling residual stress development in thermal spray coatings: current status and way forward, J. Therm. Spray Technol. 26 (2017) 1115–1145, https://doi.org/10.1007/s11666-017-0590-1.
[72] G. Montay, A. Cherouat, A. Nussair, J. Lu, Residual stresses in coating technology, J. Mater. Sci. Technol. 20 (2004) 81–84.
[73] M.E. Nichols, C.A. Darr, C.A. Smith, M.D. Thouless, E.R. Fischer, Fracture energy of automotive clearcoats - I. Experimental methods and mechanics, Polym. Degrad. Stab. 60 (1998) 291–299, https://doi.org/10.1016/s0141-3910(97)00081-5.